THESIS APPROVAL

GRADUATE SCHOOL, KASETSART UNIVERSITY

Doctor of Engineering (Civil Engineering)

DEGREE

Civil Engineering — **FIELD**

Civil Engineering — **DEPARTMENT**

TITLE: Stability Analysis of Excavated Slope Stabilized by DCM columns: Case Study and Parametric Analysis

NAME: Mr. Phermphorn Buathong

THIS THESIS HAS BEEN ACCEPTED BY

THESIS ADVISOR

(Associate Professor Warakorn Mairaing, Ph.D.)

THESIS CO-ADVISOR

(Associate Professor Suttisak Soralump, Ph.D.)

THESIS CO-ADVISOR

(Assistant Professor Barames Vardhanabhuti, Ph.D.)

THESIS CO-ADVISOR

(Mr. Pisit Kuntiwattanakul, D.Eng.)

DEPARTMENT HEAD

(Assistant Professor Wanchai Yodsudjai, D.Eng.)

APPROVED BY THE GRADUATE SCHOOL ON

DEAN

(Associate Professor Gunjana Theeragool, D.Agr.)

THESIS

STABILITY ANALYSIS OF EXCAVATED SLOPE STABILIZED BY DCM COLUMNS: CASE STUDY AND PARAMETRIC ANALYSIS

PHERMPHORN BUATHONG

A Thesis Submitted in Partial Fulfillment of
the Requirements for the Degree of
Doctor of Engineering (Civil Engineering)
Graduate School, Kasetsart University
2014

Phermphorn Buathong 2014: Stability Analysis of Excavated Slope Stabilized by DCM columns: Case Study and Parametric Analysis. Doctor of Engineering (Civil Engineering), Major Field: Civil Engineering, Department of Civil Engineering. Thesis Advisor: Associate Professor Warakorn Mairiang, Ph.D. 239 pages.

Recently, Deep Cement Mixing (DCM) columns have been used for permanent slope stabilization in several projects. However, the guideline for design and construction are not well developed. This research presents field observation, laboratory tests and numerical analysis.

Suvarnabhumi International Airport Drainage Canal project applied more than 300,000 DCM columns for stabilizing the canal slopes and roadway. The field observations showed that several failures occurred as the excavation of canal almost reached its proposed level.The failure modes were ranging from sudden failure, delay failure and creep type failure. The remedial solutions were additional DCM column, construction of counterweight berm, filling of surcharge water and arranging of construction sequences. The measured field lateral movements were used to determine elastic modulus of soil. The FEM back analysis indicated that the hardening soil model with $E_{50} = E_{oed} = 3{,}000\text{-}60{,}000$ kPa and $E_{ur}/E_{50} = 3$ resulting the lateral movement close to the field measurement. The Mohr-Coulomb model with $E_u/S_u = 300\text{-}1000$ can also give a reasonable prediction result. The numerical analysis of one row of DCM columns found that the $L_x/L = 0.29$ to 0.86 and $L_e/D_e = 3.6$ were effective to give maximum Factor of Safety (FS). The numerical analysis of multi-rows DCM column revealed that $L_e/D_e = 3$ can provide the maximum FS. For both types, the FS of slope increased with decreasing DCM column spacing. Therefore, the spacing design is depended on the required FS. The analysis revealed that the perfect tangential columns were quite effective to control lateral movement and provide high FS. The possible alternative DCM arrangements are also studied for the comparative designs and further recommendation.

_________________________ _________________________ ___ / ___ / ___

Student's signature Thesis Advisor's signature

ACKNOWLEDGEMENTS

I would like to grateful thank and deeply indebted to Assoc. Prof. Dr. Warakorn Mairaing my thesis advisor for advice, encouragement and valuable suggestion during my doctoral study. I would sincerely like to thank Assoc. Prof. Dr. Suttisak Soralump, Asst. Prof. Dr. Barames Vardhanabhuti and Dr. Pisit Kuntiwattanakul for their valuable comments and suggestion. I gratefully thank Assoc. Prof. Dr. Prasert Suwanvitaya serving as examination chairperson and also Dr. Gridsana Pensomboon serving as external examiner.

I would like to sincerely thank Assoc. Prof. Dr. Panich Voottipruex and Dr. Pitthaya Jansawang for suggestion and facilitation. The Funding sources for this research were supported by the Geotechnical Engineering Research and Development (GERD) at Kasetsart University.

I am especially appreciated my parents and brothers for their love, care and endless support.

Phermphorn Buathong

July, 2014

TABLE OF CONTENTS

LIST OF TABLES

LIST OF TABLES (Continued)

Table **Page**

Appendix Table

LIST OF FIGURES (Continued)

LIST OF FIGURES (Continued)

Figure **Page**

LIST OF FIGURES (Continued)

Figure **Page**

LIST OF FIGURES (Continued)

Figure **Page**

LIST OF FIGURES (Continued)

LIST OF FIGURES (Continued)

LIST OF FIGURES (Continued)

Figure **Page**

Appendix Figure

LIST OF FIGURES (Continued)

LIST OF ABBREVIATIONS

c	=	Cohesion
C_c	=	Compression index
C_r	=	Recompression index
C_v	=	Coefficient of consolidation
D	=	Diameter
DCM	=	Deep cement mixing
D_e	=	Excavated depth
e_0	=	Void ratio
E'	=	Drained elastic modulus
E_u	=	Undrained elastic modulus
E^{ref}_{50}	=	Secant stiffness in standard drained triaxial test
E^{ref}_{oed}	=	Tangential stiffness for primary oedometer loading
E^{ref}_{ur}	=	Unloading and reloading stiffness
FEM	=	Finite element method
FS	=	Factor of Safety
HS	=	Hardening soil
L	=	horizontal distance between the slope toe and slope crest
L_e	=	Embedded length
LI	=	Liquid index
LL	=	Liquid limit
L_x	=	horizontal distance between the slope toe and the column position
m	=	Power for stress-level dependency of stiffness
MC	=	Mohr-Coulomb
OCR	=	Over-consolidation ratio
PL	=	Plastic limit
PI	=	Plastic index
S	=	Spacing
S_u	=	Undrained shear strength
W_n	=	Natural water content

LIST OF ABBREVIATIONS (Continued)

q_u	=	Unconfined compressive strength
γ_t	=	Unit weight
τ	=	Shearing resistance
σ	=	Stress
ϕ	=	Friction angle

STABILITY ANALYSIS OF EXCAVATED SLOPE STABILIZED BY DCM COLUMNS: CASE STUDY AND PARAMETRIC ANALYSIS

INTRODUCTION

Soft clay is characterized by low shear strength and high compressibility. The construction of embankments frequently leads to large lateral movement, excessive settlements and slope instability (Abusharar *et al.,* 2009). A number of ground improvement techniques are available to solve these problems, such as reinforcement with geosynthetics, preloading, stage construction, excavation and replacement, light-weight fill, pre-fabricated vertical drains, reinforcement with piles (concrete piles, stone column or deep mixing columns), or conjugation of some aforementioned techniques (Abusharar *et al.*, 2009; Oliveira *et al.*, 2011). One of the effective ground improvement techniques for the soft Bangkok clay is in-situ deep mixing (Horpibulsuk *et al.*, 2011). The deep mixing method was first used in Japan and the Nordic countries in the mid-1970s, and then later spread to Thailand, China, the United States, the United Kingdom, Germany Poland and other countries (Coastal Development Institute of Technology (CDIT), 2002; Bhadriraju *et al*., 2008). Using this method, cement and/or lime additives in either slurry or powder is injected into the ground and mixed with the native soil by mixing blades that form a hard treated soil column**.** Cement is commonly used as an additive, since it is readily available at a reasonable cost in Thailand (Horpibulsuk *et al.*, 2011). When cement is used as a binder, this technique is called as “Deep Cement Mixing” (DCM) method.

In recent DCM columns can be used for other purposes than stabilization of embankment. Slope stabilization, railway vibration countermeasure and retaining wall are example. In Thailand, DCM columns for permanent slope stabilization in soft clay have been used in several infrastructure projects. Taesiri and Chantaranimi (2001) reported the use of DCM columns to improve stability of road embankments along canals. Petchgate and Petchgate (2006) used the DCM columns to increase stability of retention pound. Buathong and Mairaing (2010) investigated the behavior of canal and roadway construction stabilized by DCM columns. Although a number of success application of slope stabilization by mean of DCM columns have been reported in the literature, there are a lack of clear knowledge of the exact behaviour and potential failure mechanisms of these DCM columns. In order to effectively design and construct DCM columns used in slope stabilization, understanding the behaviour and potential failure mechanisms of DCM columns are very important.

Current design approach of DCM columns for slope stabilization is evaluation of stability of slope by using limit equilibrium methods. These methods only reflect the composite shearing through the DCM columns, and they do not reflect the more critical failure modes of DCM column, i.e. bending, rotation or a combination of these modes. In addition, the behaviour and potential failure mechanism of DCM column can be not addressed. For such problems, the numerical analysis such as Finite Element Method (FEM) can be utilized. DCM column-soil interaction is a complex three dimensional problem in nature, and therefore all the analyses presented in this thesis were carried out by using three dimensional finite element method incorporated in the PLAXIS 3D FOUNDATION software.

To develop an effective guideline for design and construction of DCM columns for slope stabilization, an actual case study is required. The Suvarnabhumi International Airport Drainage Canal Project selected as a case study is located at *Samutprakan* province, Thailand. The project consists of the canal, the pumping stations and the telemetering system. Moreover, a two-lane roadway is constructed on each bank of the canal for transportation. The project was constructed within the soft Bangkok clay area, which is well known as low strength and high compressibility. Ground improvement need to be undertaken, so that the serviceability of the infrastructure is assured throughout its service period. DCM columns are found to be the most suitable option. Several field trial tests during the construction were performed to evaluate the performance of DCM column and design assumption. The result of field trial tests were presented and discussed. Moreover, the geotechnical problems encountered with the design and construction were presented

OBJECTIVES

The objectives of this thesis are to:

1. Investigate the field behaviour of stabilized slope with DCM columns.

2. Characterize the strength and deformation behaviour of soft clay related to excavated slope.

3. Improved the understanding of the behaviour and potential failure of DCM columns for slope stabilization.

4. Provide a guideline in design and construction of DCM columns for slope stabilization.

LITERATURE REVIEW

Bangkok Clay

Formation of Bangkok clay

The Lower Central Plain or also known as Chao Phraya Basin begins at Chainat, where the Chao Phraya River flows southward through a flat and featureless plain. The river reaches the Gulf of Thailand at the Samutprakan province with the distance about 200 km. The width of the plain in an east-west direction is about 180 km and total area is approximately 36,000 km^2. Geological block faulting in Late Pliocene-Pleistocene formed deep horsts and grabens in the Lower Central Plain. This formation caused thick accumulation of Quaternary sediment overlain the basement rocks. The exact profile of bedrock is still unknown but rock surface in the Bangkok area is known to vary over the range of 550 to 2000 m. Figure 1 shows the cross-section of the basin on east-west direction, summarized by JICA (1999). The Quaternary sediments are classified into Pleistocene and Holocene deposits, described by Sinsakul *et al*. (2002).

Pleistocene deposit are mainly alluvium and fluvial, intercalated of gravels, sand, silt and clay. Generally, the upper sequence is stiff clay with orange and red mottles. Iron and manganese concretions are also found scattered in clay matrix. These sediments indicated the oxidizing environment, and the barren top surface of the Pleistocene deposit, within the depth of 10-20 meters from the present ground surface.

Holocene sediments of the Lower Chao Phraya plain were related with the sea-level change after the ice age of late Pleistocene epoch. The flat top terrain of the plain was affected by the transgression and regression of Holocene sea level, as shown in Figure 2. The accumulation of rapid sedimentary took place in the area where the Cho Phraya River flow to the sea produced the huge delta area so called

"Chao Phraya delta". Formation of the uppermost marine clay is known as "Bangkok clay", covering about 15,000 km^2 (Mairaing and Amonkul, 2010).

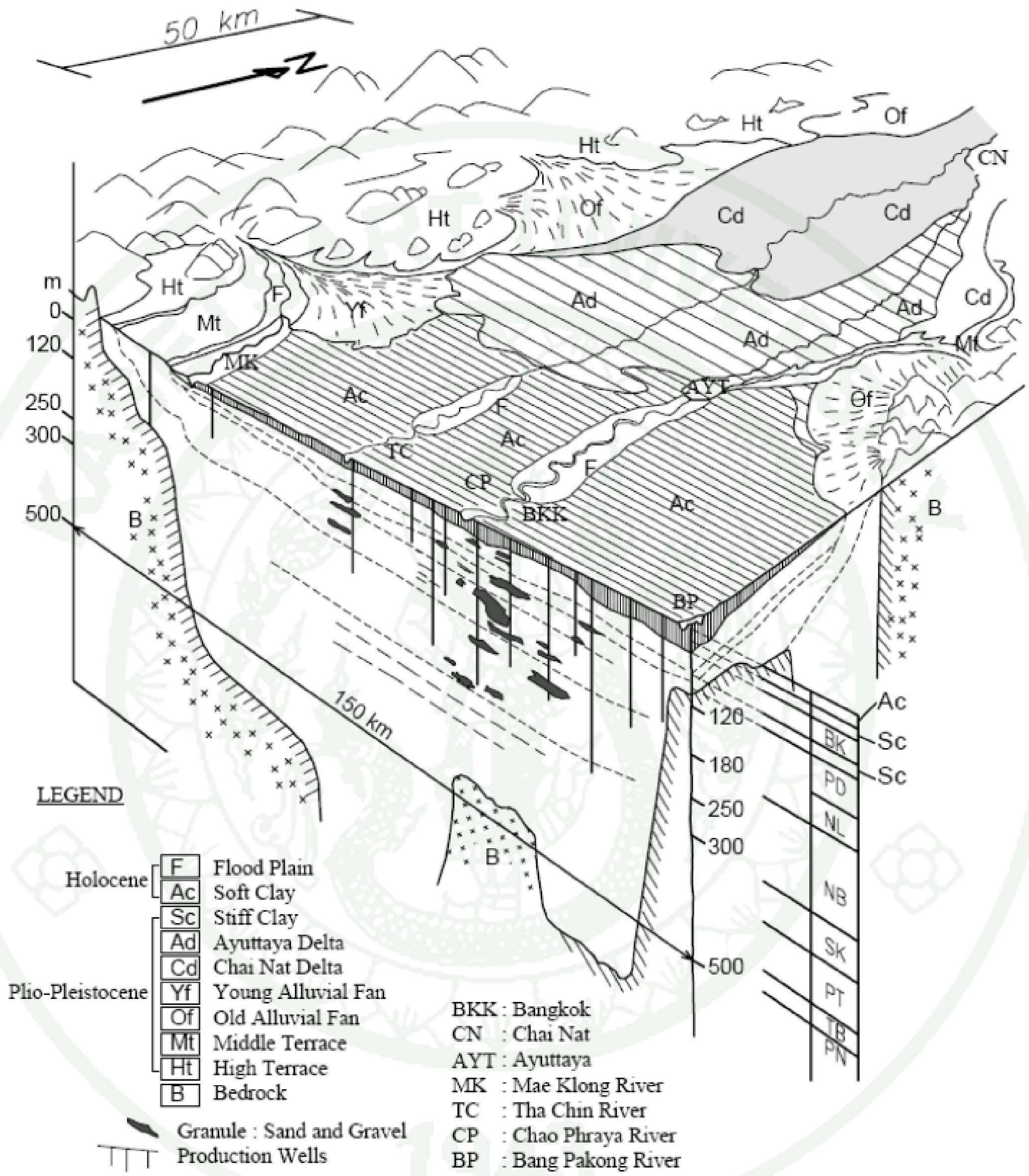

Figure 1 Schematic cross-section of lower Chao-Phraya Basin

Source: JICA (1999)

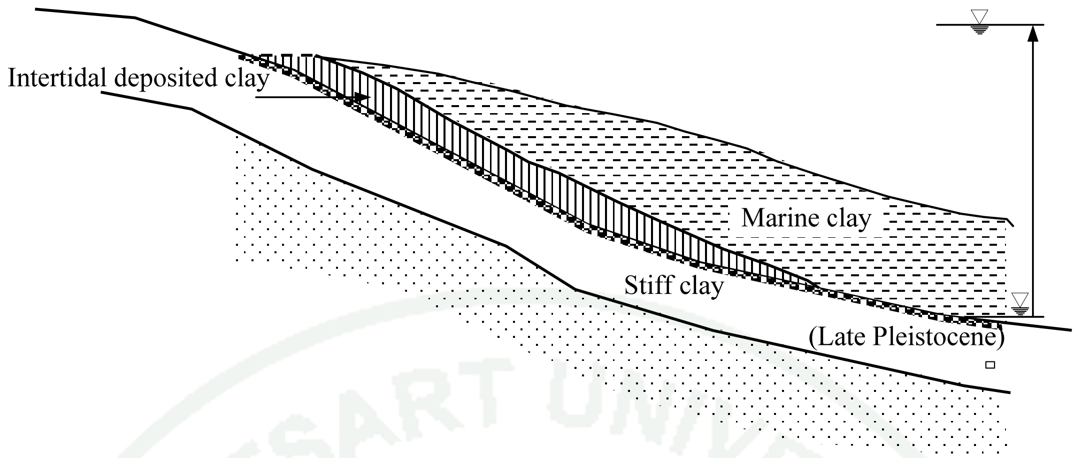

a) Transgression sediments

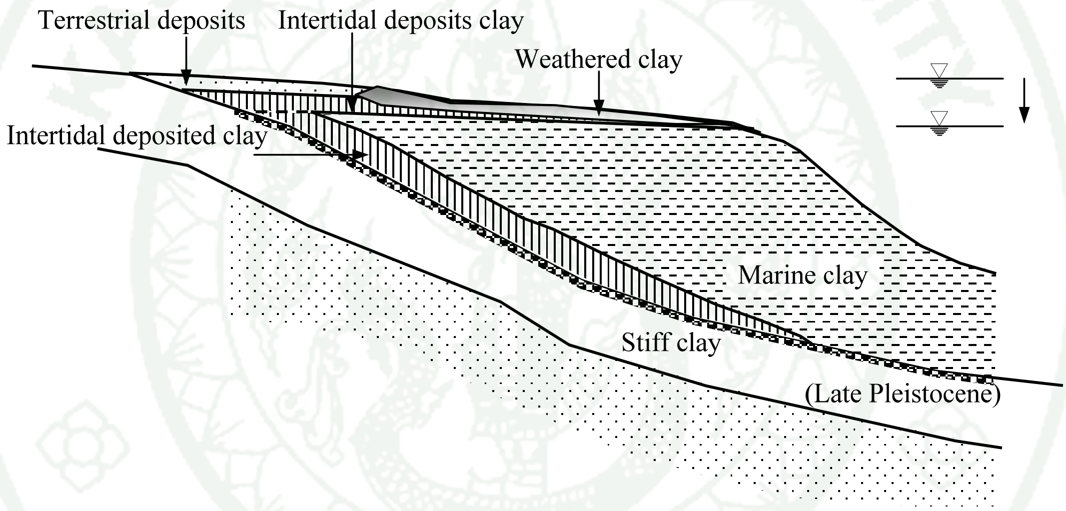

b) Regression sediments and Transgression sediments

Figure 2 Subsequent sedimentation of Bangkok clay

Source: EIT (2003)

For geotechnical engineering, the typical soil profile of Bangkok clay area from surface consists of (Mairaing and Amorkun, 2010):

1. Weathered clay: This weathered clay is hard and brown in color that varies considerably from 1 to 3 m. Hard clay is resulted from weathering and desiccation processes. The weathering process includes such features as fluctuation of ground

water level, leaching, ion exchange and precipitation of cementious materials due to drying and wetting during dry and wet seasons.

2. Compressible clay: This compressibility clay consists of very soft clay to medium stiff clay. The thickness of the soft clay varies from 10 to 20 m, which is well known as soft Bangkok clay. But in general, the thickness of soft clay is 15 m. The depth to the bottom of very soft to soft Bangkok clay is shown on Figure 3. The thickness is larger on the area close to the Gulf of Thailand with maximum depth to 25 m at Samut Prakan province. High compressibility and low strength are important properties of soft clay layer. Therefore, embankments construction on this layer frequently encounters the problems of slope instability and excessive settlement. The medium clay, which underlay the soft clay, has a thickness of 2 to 6 m.

3. Stiff clay: This stiff clay is hard in nature and the stiffness of this layer is caused by desiccation and to some extent in the past. In many places, it is mottled, fissured, with red and yellow colors indicating that it was exposed to sub-aerial processes of desiccation and chemical weathering before burial by the soft clay (Moh *et al*., 1969). Sub-aerial processes take place in the zone below ground level and above the groundwater table. There is also evidence that the first stiff clay has been weathered in places prior to deposition of soft clay on top. Thickness of the first stiff clay varies between 2 to 6 m, in central Bangkok. Low compressibility, high over-consolidation ratio (OCR) and low water content are some of its properties. This layer is light gray and yellow-brown in color.

4. Sand: This sand layer can be broadly divided into two part namely; 1) Medium dense sand of 2 to 6 m thick and 2) Dense to very dense sand of 0 to 6 m thick.

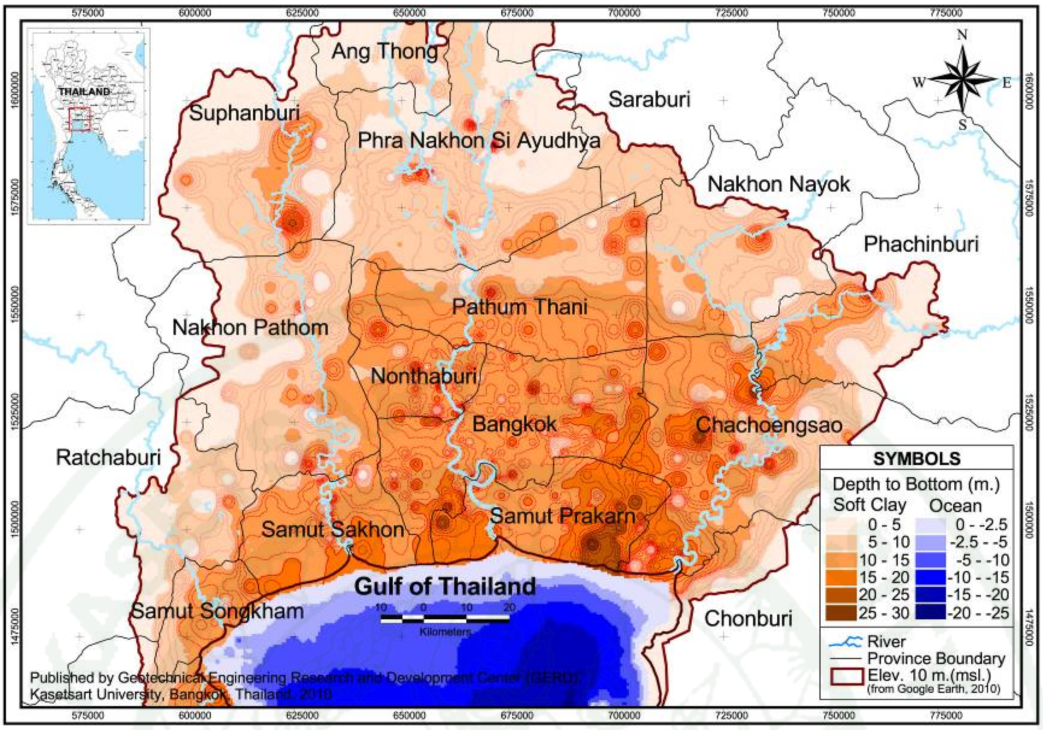

Figure 3 Depths to the bottom of soft clay

Source: Mairaing and Amorkun (2010)

Physical properties

Ohtsubo *et al.* (2000) investigated the mineralogy and pore water chemistry of Bangkok clay at a site that is 36 km east of Bang Na. The X-Ray Diffraction (XRD) patterns of the Mg-saturated clay fraction (<2 μm) show that the clay fraction contains montmorillonite as the principal clay mineral with the range of 54 to 74%, followed by kaolinite and mica. Based on the difference in the sediment volume between the Na- and Ca- clay fraction (<2 μm), the montmorillonite in Bangkok clay is classified as a high-swelling type. Cox (1968) mentioned that the presence of montmorillonite in Bangkok clay would characterize the high liquid limit (LL) and activity (I_a).

The physical properties of Bangkok clay such as the specific gravity, unit weight, water, and Atterberg's limits, are presented in Table 1.In general, the natural water content of soft Bangkok clay varies from 51.7% to 93.44 % while the liquid limit varies from 50.27 % to 96.77 %. It is noticed that the natural water content is close to liquid limit.

Compressibility properties

The compressibility properties of soft Bangkok clay are shown in Table 2. In general soft Bangkok clay is highly compressible, and it is lightly over-consolidated to normally consolidated. The Over-consolidated ratio (OCR) is about 1.87 due to aging. The compression index (C_c) ranges from 0.51 to 1.54 while the recompression index varies from 0.074 to 0.252. The coefficient of consolidation (C_v) from oedometer tests gives values varying from 2.93 to 19.09 m^2/year.

Table 1 Physical properties of Bangkok clay

Soil Layers	Depth(m)	w_n(%)	LL (%)	PL (%)	PI (%)	LI	γ_t (t/m^3)
Top Crust	2 - 3	-	-	-	-	-	-
Very Soft to Soft Clay	2 - 15	72.57±20.87	73.52±23.25	31.11±6.44	42.26±18.97	0.96±0.35	1.56±0.11
Medium Stiff Clay	15 - 17	53.71±17.69	67.11±17.51	28.13±5.36	38.83±14.14	0.64±0.38	1.68±0.14
Stiff Clay	17 - 19	30.70±10.06	56.38±16.02	24.48±5.41	31.80±12.13	0.23±0.29	1.90±0.14
Very Stiff Clay	19 - 22	24.51±6.47	49.83±14.07	22.53±4.85	27.10±10.69	0.11±0.25	1.99±0.12
Medium Dense Sand	22 - 25	19.16±4.52	-	-	-	-	1.94±0.15
Dense Sand	25 - 28	17.75±3.84	-	-	-	-	1.97±0.14
Very Dense Sand	28 - 32	17.14±3.90	-	-	-	-	1.99±0.16

Source: Amorkun (2010)

Table 2 Compressibility properties of soft Bangkok clay

Soil Layers	Depth (m)	e_0	C_c	C_r	OCR	C_{v_com}(m^2/year)
Very Soft to Soft Clay	2 - 15	2.120±0.794	1.028±0.515	0.163±0.089	1.874±1.042	8.077±11.012
Medium Stiff Clay	15 - 17	1.511±0.642	0.705±0.406	0.124±0.056	1.517±0.740	9.077±10.452
Stiff Clay	17 - 19	0.885±0.401	0.283±0.153	0.072±0.036	1.200±0.509	7.828±7.835
Very Stiff Clay	19 - 22	0.562±0.279	0.153±0.045	0.050±0.024	0.718±0.231	7.320±2.387

Source: Amorkun (2010)

Shear strength characteristics

The shearing resistance of a soil depends on many factors, represented by Equation 1 (Mitchel 1993):

$$\text{Shearing resistance} = F\,(e, \phi, C, \sigma', c, H, T, \varepsilon, \dot{\varepsilon}, S) \qquad (1)$$

Where e is the void ratio, ϕ is the angle of internal friction, C is the composition, σ' is the effective normal stress, c is the cohesion, H is the stress history, T is the temperature, ε is the strain, $\dot{\varepsilon}$ is the strain rate, and S is the structure. All these parameters may not be independent to each other; however, a functional form all the factors are not yet known. The Mohr-Coulomb equation for shearing resistance, which is a simplified form of Equation 2, is given by:

$$\tau = c + \sigma.\tan\phi \qquad (2)$$

Where τ is the shearing resistance of the soil. Equation 3may also be rewritten in terms effective soil parameters as:

$$\tau = c' + \sigma'.\tan\phi' \qquad (3)$$

Shear strength parameters used in geotechnical engineering is usually divided into two categories: undrained and drained shear strength.

The undrained shear strength plays an important role in calculating of the short term stability and bearing capacity. Also as an indicator for soil behavior correlates with other engineering properties, such as index parameters. The undrained shear strength of a soil is usually determined in laboratory from unconfined compression test (UC) or unconsolidated undrained (UU) triaxial test or consolidated undrained (CU) or laboratory shear vane. In the field, it can be obtained from field shear vane test, pressuremeter, cone penetrometer, etc.

Surarak (2010) summarized the undrained shear strength of Bangkok clay from the field vane shear and anisotrpically consolidated undrained triaxial compression tests (CK_0U), as shown in Figure 4. The average relations of the undrained shear strength-effective stress ratio (S_u/σ'_{vo}) for soft to medium stiff clay (3 m to 15 m depth) and stiff to hard clay (15 m to 50 m) were 0.33 and 0.2, respectively.

Amonkul (2010) assembled the data of undrained shear strength of Bangkok clay from unconfined compression and field vane shear tests. He found that the S_u/σ'_{vo}ratio for soft Bangkok clay was 0.47.

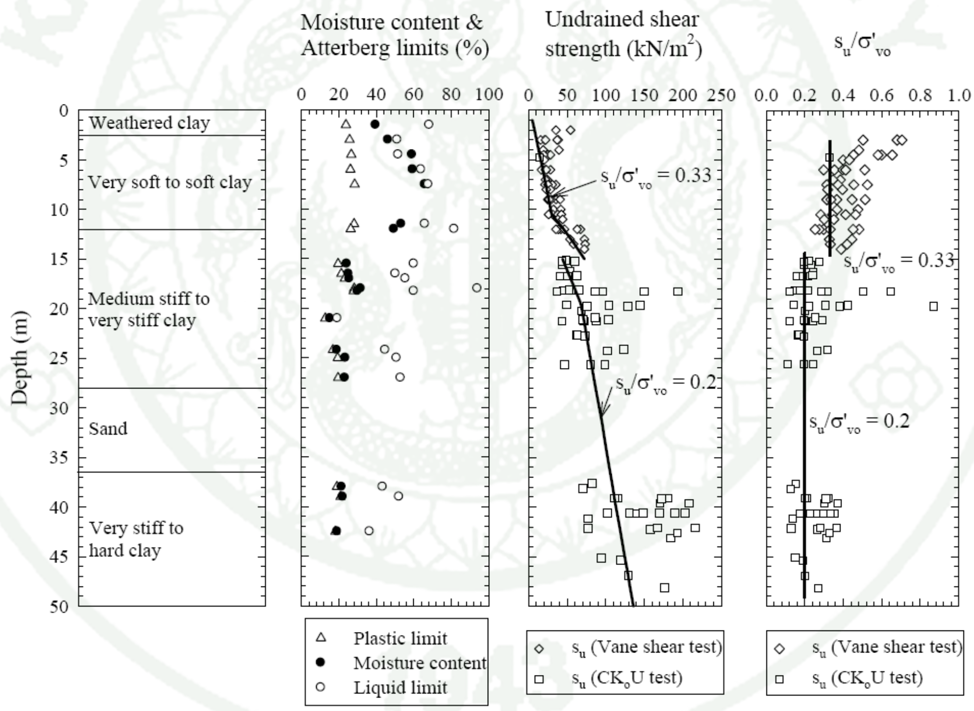

Figure 4 Undrained shear strength of Bangkok clays from vane shear and CK_0U tests

Source: Surarak (2010)

The drained shear strength is represented by the parameters c' (drained cohesion) and ϕ' (drained friction angle). It is used for long term analysis. Values of c' and ϕ' can be obtained from drained tests and undrained tests with measurements of pore water pressure during shear. In engineering practice, drained shear strength parameters are often determined from triaxial tests. The value of the c' is generally zero when the effective stress exceeds the critical or pre-consolidation pressure. If the effective stress does not exceed the critical pressure, the clay will behave as if it is over-consolidated and a cohesion intercept will exist. The notation for the triaxial tests identified in this literature review are explained in Table 3, and Table 4 presents a summary of the drained shear strength of Bangkok clays (i.e. weathered clay, soft clay, stiff clay and hard clay). The ϕ' of soft Bangkok clay varied in range between 22.2° and 34.8° while the c' was zero.

Table 3 Description for triaxial test notations

Notations	Description
CIU	Isotropically consolidated undrained triaxial compression test
CID	Isotropically consolidated drained triaxial compression test
CK_0U	Anisotropically (K_0) consolidated undrained triaxial compression test
CAU	Anisotropically consolidated undrained triaxial compression test
$CIUE_L$	Isotropically consolidated undrained triaxial extension test (Loading)
$CIUE_U$	Isotropically consolidated undrained triaxial extension test (Unloading)

Source: Surarak (2010)

Table 4 Summary of drained shear strength of Bangkok clay

Reference	Location	Depth (m)	Test type	ϕ' (degree)	c' (kPa)
Weathered clay					
Balasubramaniam and Chaudhry (1978)	Nong Ngoo Hao	2.5 to 3.0	CIU	22.2	0
			CID	23.5	0
Soft clay					
Wang (1969)	Nong NgooHao	8.83	CAU	34.8	0
Chaiyadhuma (1974)	AIT campus	5.5-6.0	CK_0U	27.1	0
		7.0-7.5		28.3	0
Chaudhry (1975)	-	6.0	CIU	27	0
Balasubramaniam and Chaudhry (1978)	Nong Ngoo Hao	5.5-6.0	CIU	26	0
Balasubramaniam *et al.* (1978)	Nong Ngoo Hao	5.5-6.0	CIU	24	0
Rahman (1980)	AIT campus	4.5	CK_0U	25.5	0
		5.5		23.6	0
		6.5		23.2	0
Kim (1991)	AIT campus	3.0-4.0	CIU	22.2	0
			CK_0U	23	0
Stiff clay					
Hassan (1976)	NongNgooHao	17.0 to 18.0	CIU	28.1	11.4
			CID	26.3	32.8
Surarak (2010)	MRT Blue Line Extension	15.0 to 25.0	CK_0U	26.1	26.9
Hard clay					
Surarak (2010)	MRT Blue Line Extension	39.0 to 43.0	CK_0U	23.4	41.9

Source: Modified from Surarak (2010)

There are many problems in the field correspond to stress change under extension condition where lateral stress is higher than the vertical stress. Excavation is an example. Table 5 presents the drained shear strength (c_e' and ϕ'_e) of soft Bangkok clay under extension conditions. The ϕ'_e was found to be in range between 14.1° to 33.5°. It is important to note that the high values of c_e' may be unrealistic. These high magnitudes of c_e' were in order of 32 kPa to 60 kPa. Surarak (2010) reported that the possible reasons of this were application of incorrect values of membrane correction. In addition, the pre-failure (i.e. necking failure) may be occurred during the extension test. Table 6 compares the results from triaxial compression and extension tests. The ϕ' obtained from compression test is usually smaller than that from the extension test. The ratio of ϕ'_c/ϕ'_e is in order of 0.70 to 1.10.

Table 5 Summary of drained shear strength of Bangkok clay under extension

Reference	Soil type	Depth (m)	Test type	c_e' (kPa)	ϕ_e'(degree)
Li (1975)	Soft clay	6.5-7.0	$CIUE_L$	47.1	19.60
			$CIUE_U$	59.8	21.10
Balasubramaniam *et al*. (1978)	Soft clay	5.5-6.0	$CIUE_L$	0	26.00
			$CIUE_U$	58.7	21.10
			$CIDE_L$	0	26.20
			$CIDE_U$	31.8	23.50
Tampubolon (1981)	Soft clay	6.0-6.5	$CIUE_U$	0	17.57
			$CIUE_L$	0	17.76
			$CAUE_U$	0	14.09
			$CAUE_L$	0	13.78
Kim (1991)	Soft clay	3.0-4.0	CK_0UE_U	0	33.10
			CK_0DE_U	16.5	33.50

Source: Modified from Surarak (2010)

Table 6 Summary of drained shear strength of Bangkok clay under extension conditions

Reference	Soil type	Consolidation stage	ϕ_c' (degree)	ϕ_e' (degree)	ϕ_c'/ϕ_e'
Parry (1960)	Weald clay	Isotropic	21	22.3	0.94
Duncan and seed (1966)	San Francisco bay mud	Anisotropic (K_0)	38	35	1.09
Parry and Nadarajah (1973)	Kaolin clay	Isotropic	22.6	20.5	1.10
		Anisotropic (K_0)	20.8	28.0	0.74
Balasubramaniam *et al*. (1978)	Weathered Bangkok clay	Isotropic	22.2	29.0	0.77
Atkinson *et al.* (1987)	Kaolin clay	Isotropic	24.0	27.0	0.89
		1-D then K_0	22.0	29.0	0.76
Kim (1991)	Soft Bangkok clay	Anisotropic (K_0)	23.0	33.1	0.70

Source: Modified from Surarak (2010)

Elastic parameters

The soil deformation during loading is one of important physical aspect in geotechnical problems. The material properties required for deformation analysis are four conventional constants used in the theory of elasticity, namely, Young's modulus (E), Poisson's ratio (ν), shear modulus (G) and bulk modulus (K). In generally, the shear modulus G and K can be written in terms of the Young' modulus E and Poisson's ratio ν as:

$$G = \frac{E}{2(1+\nu)} \tag{4}$$

$$K = \frac{E}{3(1+2\nu)} \tag{5}$$

There are two alternative definitions of the modulus of elasticity, namely, tangent modulus, and secant modulus, as illustrated in Figure 5. The tangent modulus (E_t) is the slope of the tangent to the any particular stress-strain point under consideration. The secant modulus (E_s) is the slope of the line joining the origin (0,0) to some desired stress-strain point such as 50% of maximum shear stress.

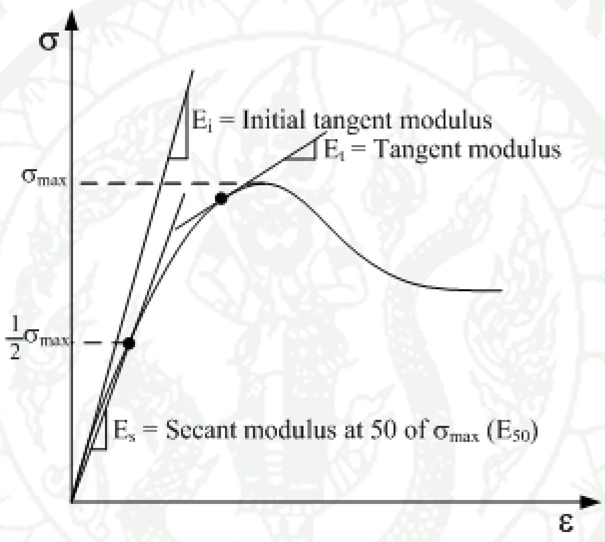

Figure 5 Definition of tangent and sevant modulus

Same as strength behavior, the E has to be distinguished between undrained and drained behavior of the deformation of soils. The value of E can be estimated from the results of laboratory tests, field tests and back-analysis on actual construction. The undrained modulus (E_u) for soft clay is commonly normalized by the undrained shear strength (S_u). Table 7 summarized the E_u of soft Bangkok clay. It can be seen that the E_u is varied within the range between $100S_u$ and $500S_u$. Most practical value of E_u for Bangkok clay is based on the correlation with OCR and plastic index (I_p) proposed by Duncan and Buchignani (1976), as shown in Figure 6. For soft Bangkok clay where OCR is approximate 1.5, E_u/S_u = 300-600.

For the long-term deformation analysis, the drained elastic modulus (E') is used instead of undrained modulus (E_u). Parnploy (1985) suggested the correlation between E_u and E' for soft Bangkok clay:

$$E' = 0.15E_u \text{ for very soft clay} \quad (6)$$

$$E' = 0.26E_u \text{ for soft clay} \quad (7)$$

Surarak (2010) analyzed the results of CIU and CID tests on soft Bangkok clay conducted by Chaudhry (1975). The confining pressure for both CIU and CID series ranges from 138 to 414 kPa. He found that the E_u and E' increased with confining pressure. For the CIU tests, the initial undrained modulus ($E_{u,i}$) and the undrained modulus at 50% of undrained shear strength ($E_{u,50}$) ranged from 10.5 to 40 MN/m^2 and 5.9 to 20.5 MN/m^2, respectively. For CID tests, the E'_i and and E'_u range from 2.0 to 6.6 MN/m^2 and 1.0 to 2.4 MN/m^2, respectively.

Table 7 Correlation between undrained elastic modulus and undrained shear strength

Equation	Reference	Remark
$E_u = 500S_u$	Cox (1973)	Embankment test on Thonburi-Pak Tor Road
$E_u = 131S_u$	Parnploy (1985)	S_u from field vane shear test
$E_u = 125\text{-}300S_u$	NAVFAC.DM.7.01 (1986)	Based on soft Bangkok clay properties (PI = 40-63%, OCR <3)
$E_u = 100\text{-}500S_u$	Duncan and Buchighani(1976)	Based on soft Bangkok clay properties (PI = 40-63%, OCR <3)
$E_u = 150S_u$	Bergado(1990)	Embankment test on Bangna-Bangpakong Road
$E_u = 500S_u$	Teparaksa (1999)	Back-analysis of deep braced excavation in Bangkok subsoil

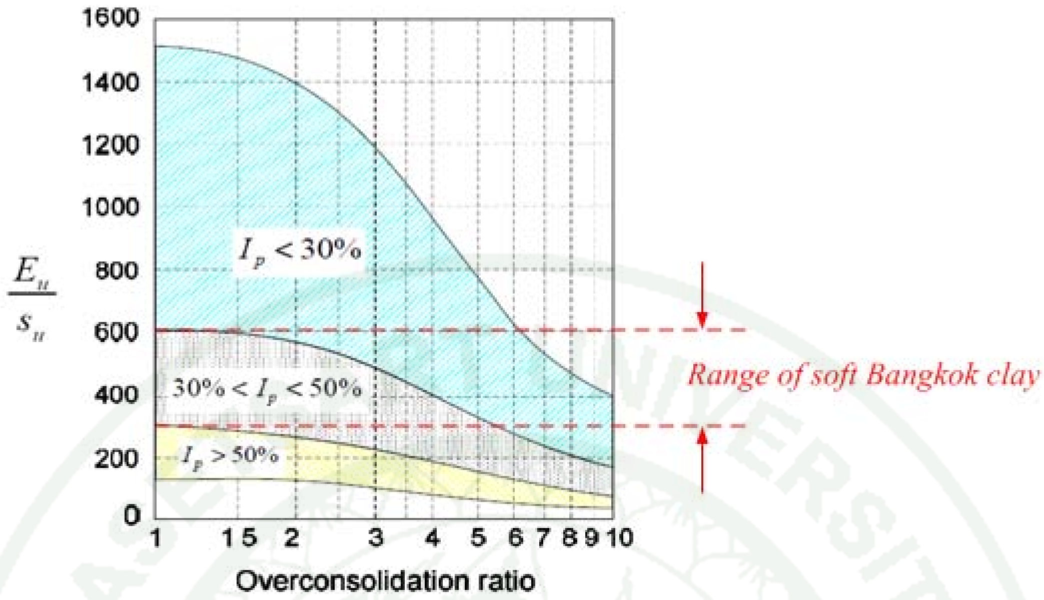

Figure 6 Empirical Young's modulus values

Source: Duncan and Buchignani (1976)

Creep Behavior

Soil is similar to other engineering materials which undergo time dependent deformation under sustained shearing stress. The time-dependent deformation is generally termed "creep". On low stress level, the creep may eventually appear to stop or continue at an imperceptible rate after large elapsed time. On the other hand, on the higher stress level, the creep rate may start to accelerate after a finite elapsed time and finally lead to creep rupture. This behaviour can result in excessive deformation leading to failure or collapse with time. These creep have been given the engineer many difficulties in the design of slopes, foundation and earth structures on clays.

A creep behavior can be subdivided into three stages based on strain-time curve, as shown in Figure 7. The primary stage is the stage which the strain rate is continuously decreasing. The secondary stage is the stage which the strain rate is nearly constant. The tertiary stage is the final stage which strain rate increases gradually leading to creep rupture (failure).

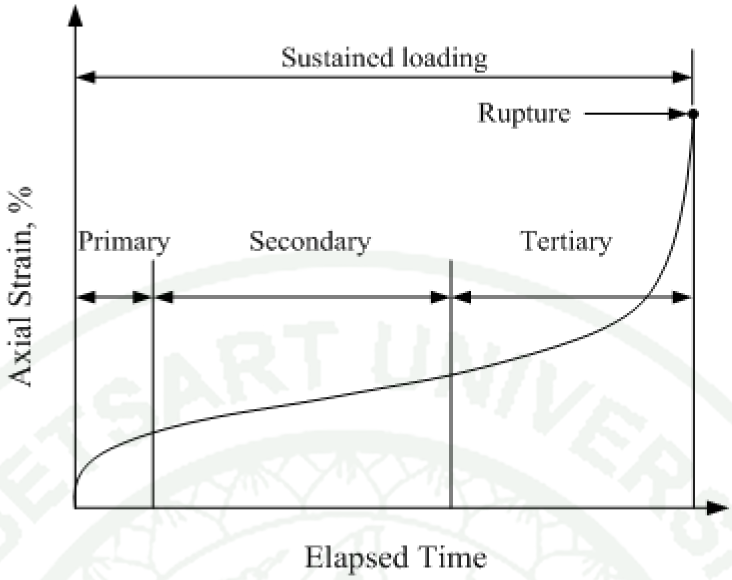

Figure 7 Typical creep curve

Snead (1970) performed a series of undrained creep test by varying sustained shearing stress on normally consolidated undisturbed clay, called Haney clay. The tests were conducted with conventional triaxial apparatus. He obtained the log-log plot of strain rate with time, as shown in Figure 8. For the deviator creep stress greater than 43.5 PSI, it was observed that initially the strain rate decreased, then reached a minimum and increased rapidly proceeding to rupture. The time to failure and time to reach minimum strain rate increase with the decrease in deviator stress. For the specimen with a deviator stress of 42.8 PSI, it continued parallel to the line of minimum strain rates. Therefore, it was predicted that the specimen should never fail under the imposed stresses. From the results, it was found that all points of minimum strain rate for a given failure stress lie on a straight line. The equation of minimum strain rate line was found to be:

$$\mathrm{Log}_{10}\, t = -0.412 - 1.15 \log_{10} \dot{\varepsilon}_m \pm 0.116 \quad (8)$$

where	t	=	elapsed time until the minimum strain rate in minutes
	$\dot{\varepsilon}_m$	=	minimum strain rate in percent per minute
	± 0.116	=	95% of the data points are considered

The results indicate that samples could fail under sustained shearing stress less than the strength determined from normal strength test. Once a minimum strain rate was reached, the strain rate began to increase, and the specimen was bound to fail. Snead (1970) used the existence of a minimum strain rate as a failure criterion.

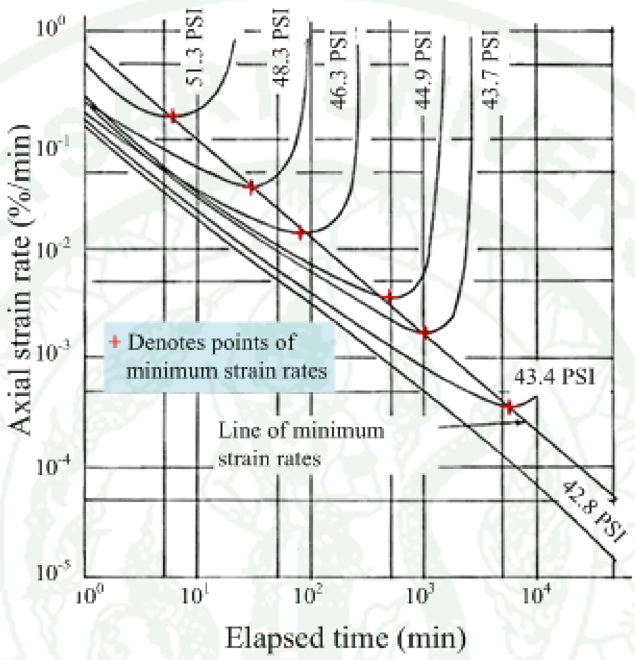

Figure 8 Creep rate behavior for normally consolidated undrained creep tests on Haney clay

Source: Snead (1970)

Arulanandan *et al.* (1971) studied creep behavior of coastal organic silty clay under undrained conditions at different isotropic consolidation pressure and stress level. For all consolidation pressures, the specimens subjected to creep loads of 30% and 50% showed only a small increase in strain after an initial deformation, whereas specimens subjected to creep loads of 70% and 90% led to failure. Figure 9 shows the example of creep behavior at consolidation pressure of 1 kg/cm^2.

Holzer *et al.* (1973) conducted a series of six consolidated isotropically undrained creep tests on San Francisco Bay mud by conventional triaxial apparatus. They found that the specimens tested at stress level of 80% and 90% of normal strength test attained axial strain of 15% in less than 2 weeks and were considered to fail, as shown in Figure 10.

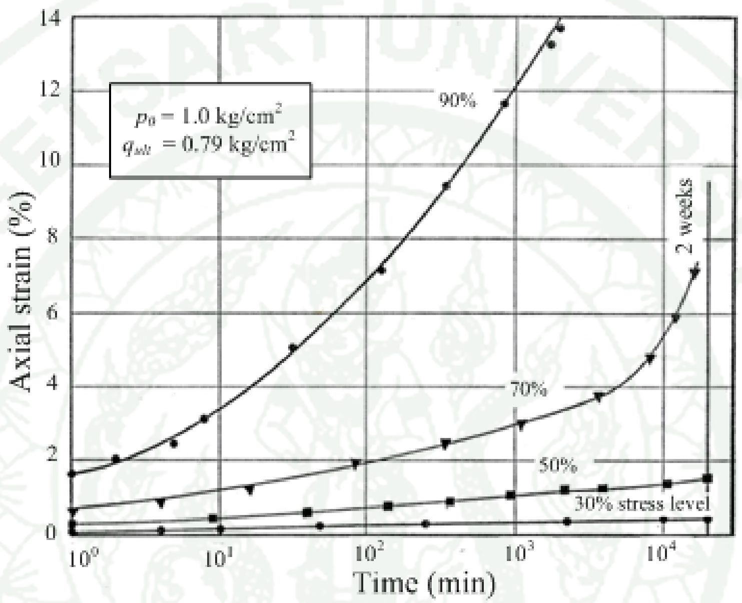

Figure 9 Axial strain versus log time at consolidation pressure of 1 kg/m^2

Source: Holzer *et al.* (1973)

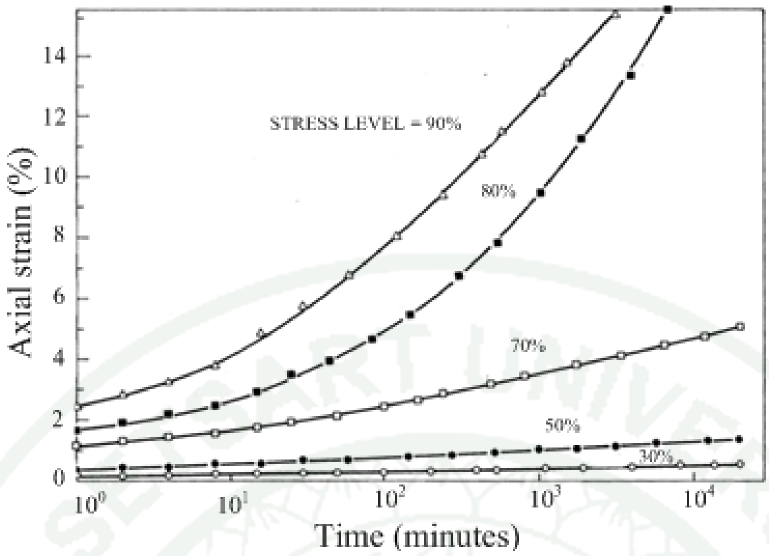

Figure 10 Axial strain behavior during undrained creep test

Source: Holzer *et al.* (1973)

Campanella and Vaid (1974) studied the undrained creep rupture characteristics for undisturbed normally consolidated sensitive clay, called Haney clay. A series of creep rupture tests was performed in each of the conventional triaxial, K_0 triaxial and plan strain apparatuses. The shape of the creep curve in each case is shown in Figure 11. The three distinct regions, namely, primary stage, secondary stage and tertiary stage can be recognized. It can be seen that the axial strain at creep rupture was not too different under K_0 triaxial and plan strain conditions. However, for the isotropic triaxial condition, the axial strain was larger than that obtained from plan strain condition approximately 4-5 times. They found the creep rate-time behavior in isotropic triaxial, K_0 triaxial and plan strain series was similar in shape, as shown in Figure 12. Under a given constant creep stress, the creep rate continuously decreased with elapsed time to a minimum value and thereafter increased until rupture. This indicated that the onset of an accelerating creep rate indicated impeding failure. They suggested that the elapsed time up to rupture was at least 2.5-3.5 times the elapsed time up to the point when the creep rate started accelerating.

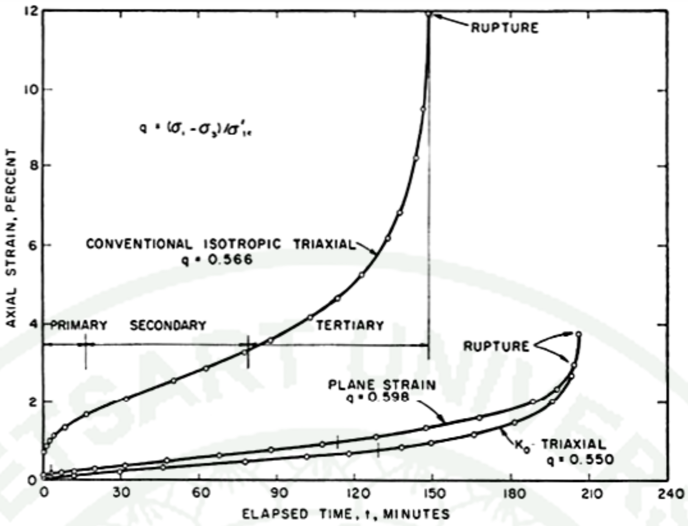

Figure 11 Typical creep curves for isotropically and K_0 consolidation triaxial and K_0 consolidation plane strain

Source: Campanella and Vaid (1974)

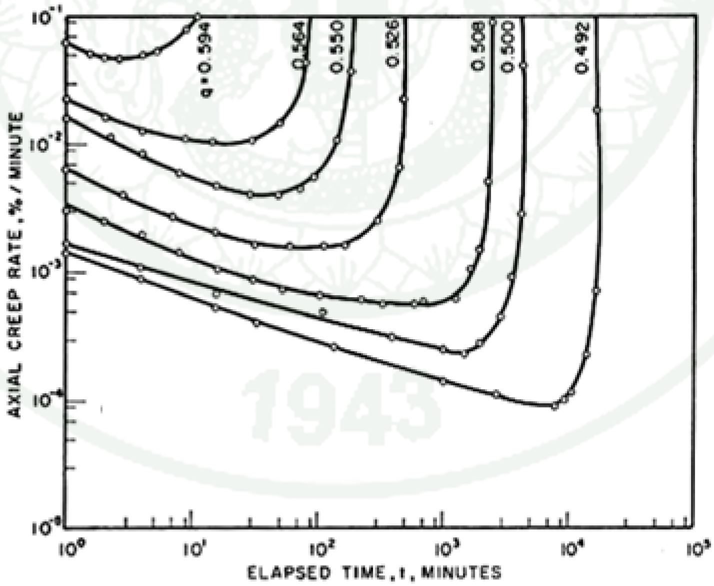

a) k_0 consolidated triaxial

Figure 12 Creep rate behavior for isotropically and K_0 consolidation triaxial and K_0 consolidation plane strain

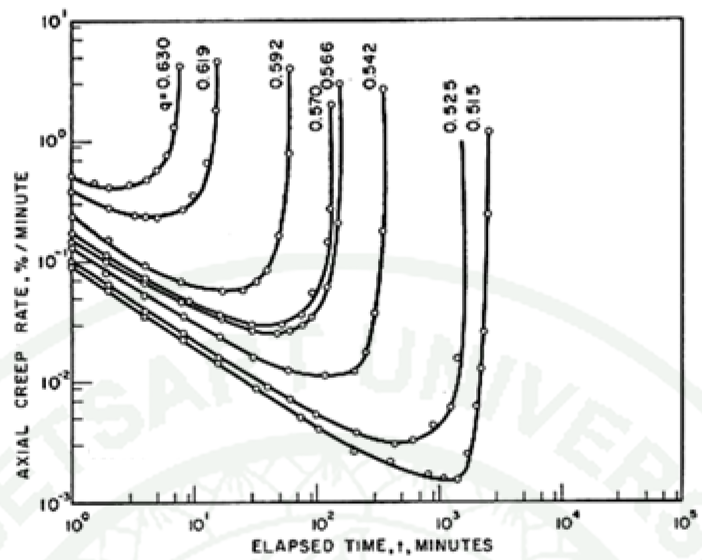

b) Isotropically consolidated triaxial

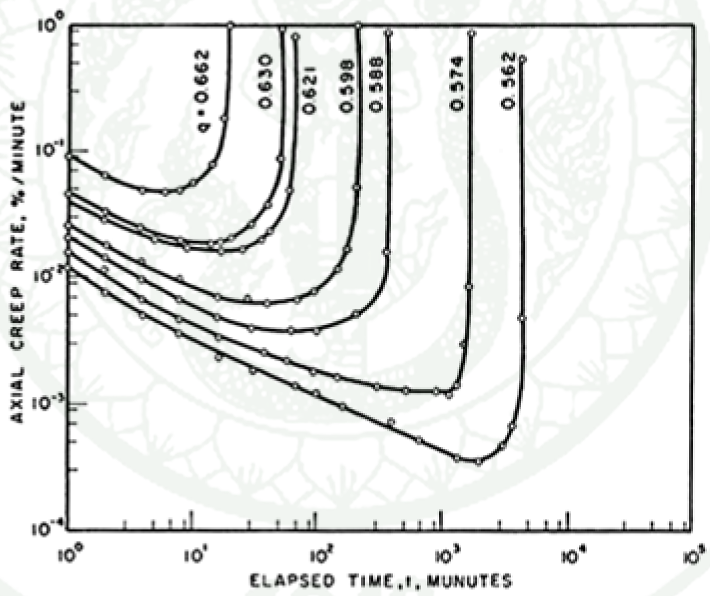

Figure 12 (Continued)

Source: Campanella and Vaid (1974)

Stress Paths Method

Definition of stress path

The Mohr circle is an excellent tool for analyzing the state of stress in a certain moment on a soil element. However, if the states of stress are changed, during a laboratory test or excavation, a diagram with many circles can be quite confusing. A more satisfactory agreement is to plot a series of stress points, and connect these points with a line or curve. Such a line or curve is called a stress path. Two different graphical techniques for stress paths are in common use: the MIT plot, originated at the Massachusetts Institute of Technology, USA (Lambe and Whitman, 1979) and the Cambridge plot, developed at the University of Cambridge, England (e.g., Atkinson and Bransby, 1978). In this section, the MIT plot, which is derived directly from Mohr's circle, was described.

Figure 13 illustrates the relationships between Mohr's circle and stress path. The stress point A represents the maximum value of shear stress while the stress point B denotes the maximum ratio of shear stress to normal stress, as shown in Figure 13a. The stress path method uses the point where the shear stress (τ) has its maximum value on point A. Figure 13b shows Mohr's circle and stress path for a stress change. In the stress path method, the stress path consists of a line drawn through points for the condition of maximum shear stress. An arrow head on a stress path denotes the direction of stress change. The stress path shown in Figure 13b represents a condition of loading followed by unloading.

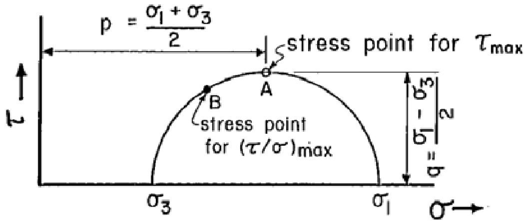

a) Mohr's circle

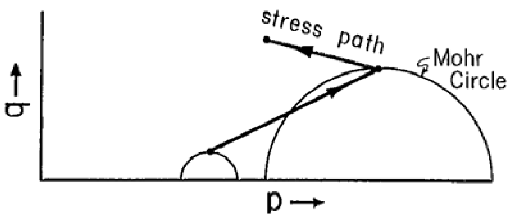

b) Stress path

Figure 13 Relationships between Mohr's circle and stress path

Source: Lambe *et al.* (1979)

The failure conditions used in stress path method are shown in Figure 14, which also shows the relationships with Mohr's Coulomb failure condition. For a cohesion soil, the K_f line which has a slope of α' and intercept on the vertical axis equal to a' for a cohesion soil, as shown in Figure 14a. For a soil without cohesion, the K_f line does not possess a cohesion intercept, as shown in Figure 14b.

Lambe *et al.* (1979) presented stress paths for four stress condition leading to failure, as shown in Figure 15. In each case the same starts from an initial isotropic stress state point I. It can be seen from the figure that reducing the value of p constitutes "unloading condition" while increasing the value of p constitutes "loading condition". The vertical compression and extension result in increasing and decreasing the value of q, respectively.

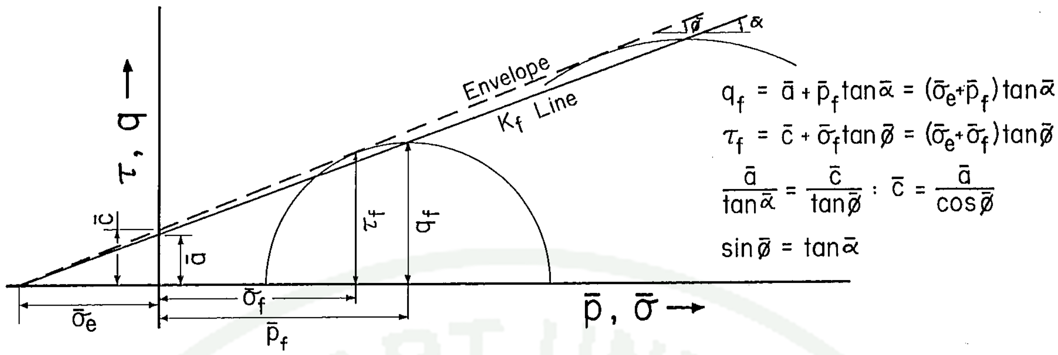

a) Cohesive soil

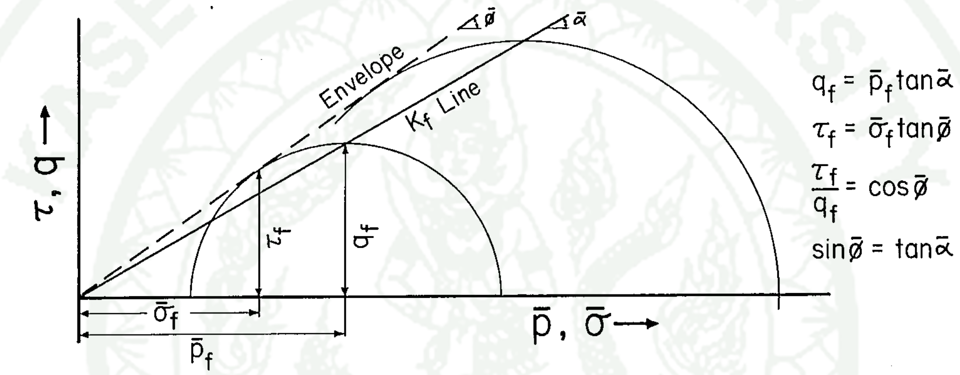

b) Cohesionless soil

Figure 14 Failure condition used in stress path method

Source: Lambe *et al.* (1979)

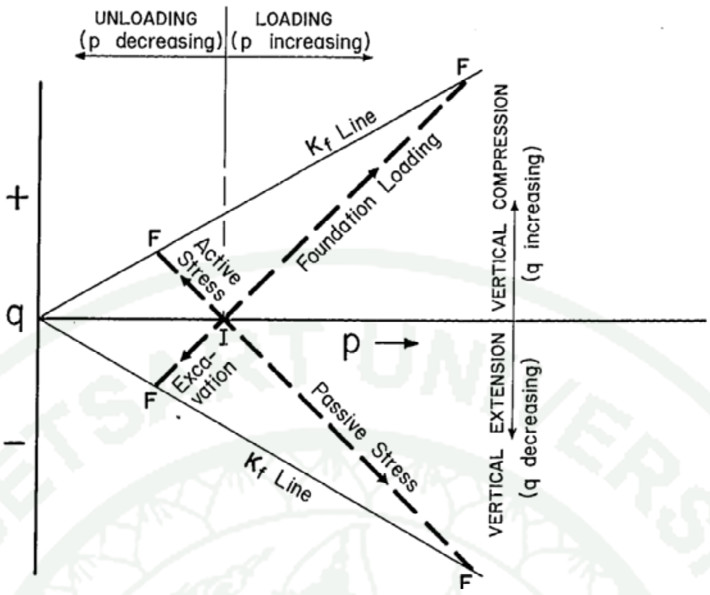

Figure 15 Stress paths under drained conditions

Source: Lambe *et al.* (1979)

Stress paths for an excavation

Stroh (1974) produced a diagram showing the zones of different stress paths in an excavation in Frankfurter overconsolidated clay supported by multiple ground anchors as shown in Figure 16.

Kempfert and Gebreselassie (2006) used finite element software to investigate the stress path at different locations of the supported excavation, shown in Figure 17. The effective and total stress paths at various points are presented in Figure 18. For the point B, C and D located at the passive side of the wall, the stress paths at theses points lie on the extension zone (below the K0-line). It can be seen that the stress paths at the point F, G, H, I and K located at the active side of the wall may not necessarily all lie within the compressive zone (above K0-line). The point E is located in a zone where maximum rotation of the principal stresses usually occurs. It can be proved by changing the total stress path.

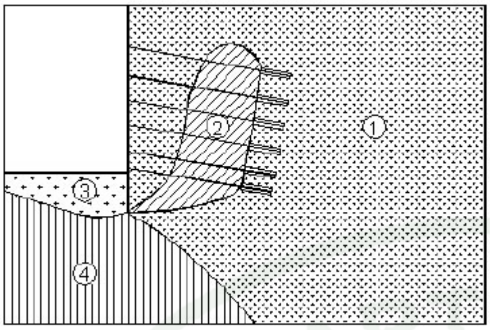

Zone-1: The vertical stress remains constant whereas the horizontal stress decreases during excavation.
Zone-2: The vertical stress remains almost constant whereas the horizontal stress increases due to anchor force.
Zone-3: The vertical stress decreases due to excavation and at the same time the horizontal stress increases due to wall displacement.
Zone-4: The vertical stress decreases due to excavation and the horizontal stress remain constant.

Figure 16 Stress paths in an anchored excavation

Source: Stroh (1974)

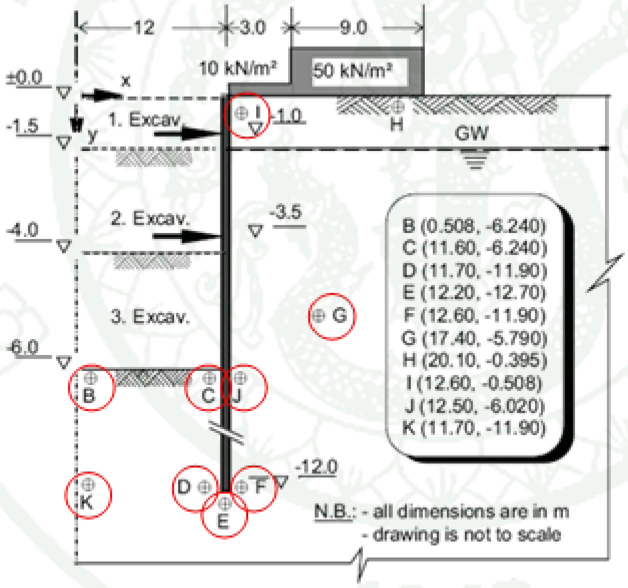

Figure 17 Idealized excavation problem with the location of the stress points

Source: Kempfert and Gebreselassie (2006)

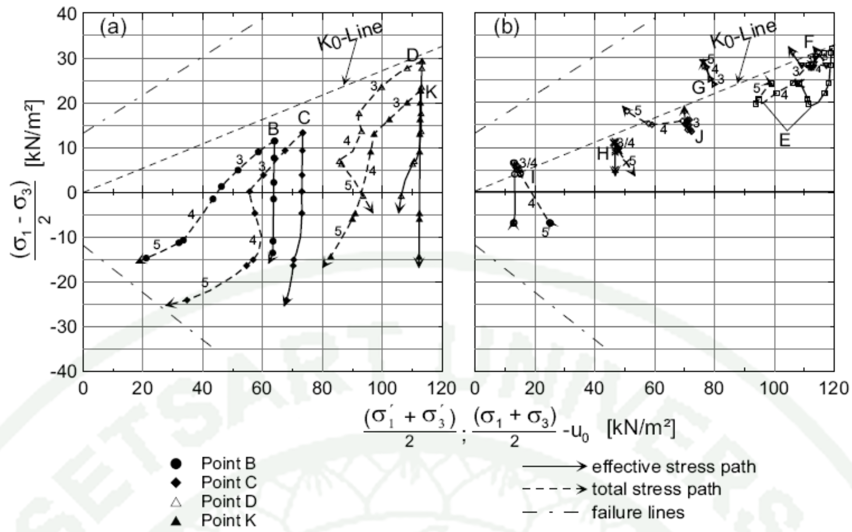

Figure 18 Effective and total stress paths at selected location in an excavation; (a) passive side and (b) active side

Source: Kempfert and Gebreselassie (2006)

Deep mixing method

The DMM was first used in Japan and the Nordic countries in the mid-1970s, and then later spread to Thailand, China, the United States, the United Kingdom, Germany Poland and other countries (Coastal Development Institute of Technology (CDIT), 2002; Bhadriraju *et al*., 2008). Using this method, cement and/or lime additives in either slurry or powder is injected into the ground and mixed with the native soil by mixing blades that form a hard treated soil column. Cement is commonly used as a additive, since it is readily available at a reasonable cost in Thailand (Horpibulsuk *et al.*, 2011). When cement is used as a binder, this technique is called as "Deep Cement Mixing" (DCM) method. Deep mixing technology has a variety of associated acronyms and terminology. Table 8 defines some current terms used in deep mixing industry and research project. Other phases include mixed-in-place piles, in-situ soil mixing, lime-cement columns and soil cement columns (Porbaha, 1998a, 1998b and Porbaha *et al.*, 2000).

Table 8 Deep Mixing Acronyms and Terminology

Acronym	Terminology
SMW	Soil mix wall
DSM	Deep soil mixing
DCM	Deep chemical mixing
DMM	Deep mixing method
CCP	Chemical churning pile
DCMM	Deep cement continuous method
DJM	Dry jet mixing
DLM	Deep lime mixing
SWING	Spreadable WING method
RM	Rectangular mixing method
JACSMAN	Jet and churning system management
DEMIC	Deep mixing improvement by cement stabilization

Source: After Porbaha (1998)

Basic mechanisms of cement treated clay

The cement types used as stabilizing agents are "Portland cement". There are two major chemical reactions of cement treated clay which are the primary hydration reaction and secondary pozzolanic reaction. The primary hydration reaction is reaction between cement and water. It leads to the initial gain in strength because of the formation of primary cementitious products and drying up of the soil-cement mix. The secondary pozzolanic reaction is reaction between the lime released by the cement and the clay minerals. It can be defined in term as solidification. In this reaction, the pore chemistry in soil system achieves a sufficiently alkaline condition. This occurs when sufficient concentration of OH^- ions is presented in the pore water due to the hydrolysis of the lime. The resulting alkalinity of the pore water promotes dissolution of silica and alumina from the clays, which then react with the Ca^{2+} ions, forming calcium silicate hydrate (CSH) and calcium aluminate hydrate (CAH), which are the secondary cementitious products. These compounds crystallize and harden with time; thereby enhancing the strength of the soil cement mixes (Xiao, and Lee, 2009). The reaction of the cement treated clay can be represented in the equation below.

$C_3S + H_2O$ = $C_3S_2H_x$(hydrated gel) + $Ca(OH)_2$ (9)
(*primary cementitious products*)

$Ca(OH)_2$ = $Ca^{++} + 2(OH)^-$ (10)

$Ca^{++} + 2(OH)^- + SiO_2$ (soil silica) = CSH
(*secondary cementitious product*) (11)

$Ca^{++} + 2(OH)^- + Al_2O_3$ (soil alumina) = CAH
(*secondary cementitious product*) (12)

When pH<12.6, then the following reaction occurs:

$C_3S_2H_x$ = $C_3S_2H_x$ (hydrated gel) + $Ca(OH)_2$ (13)

The rather complicated mechanism of cement treated clay is simplified and schematically illustrated in Figure 19 for the chemical reactions between clay, pore water and slag (Saitoh*et al*., 1985).

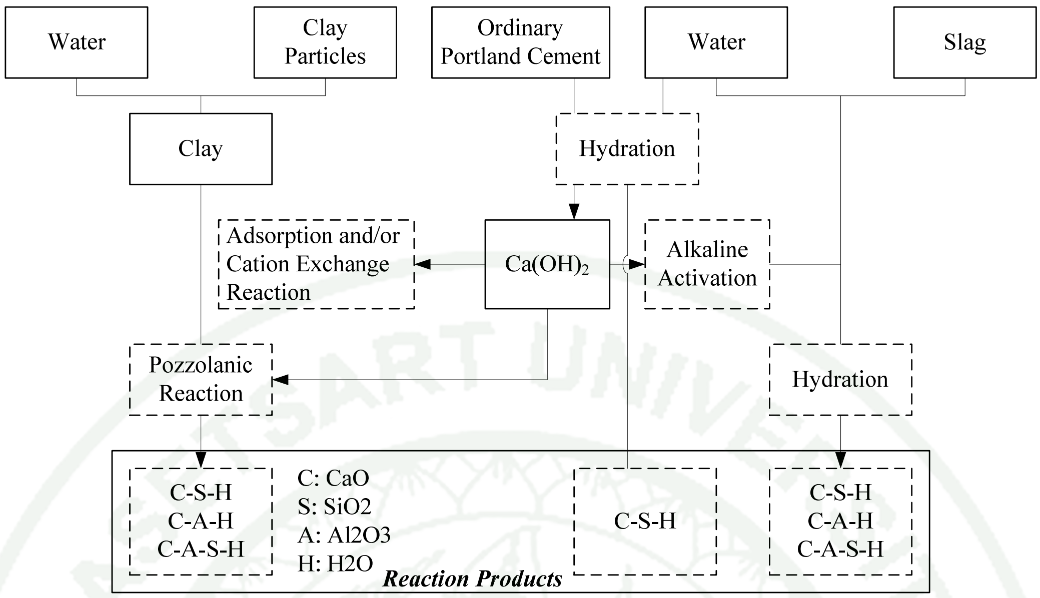

Figure 19 Chemical reaction between clay, cement, slag and water

Source: Saitoh *et al.* (1985)

Factor affecting strength increase

The strength of cement treated soil can be influenced by a number of many factors. Terashi (1997) summarized the factors that influence the strength of the improved soil into four categories: characteristics of stabilizing agent; characteristics and condition of soils; mixing condition; and curing conditions, as shown in Table 9.

Table 9 Factors affecting the strength increase

Factors	Details
I. Characteristic of stabilizing agent	1. Type of stabilizing agent 2. Quality 3. Mixing water and additives
II. Characteristics and conditions of soil(especially important for clays)	1. Physical chemical and mineralogical properties of soil 2. Organic content 3. pH of pore water 4. Water content
III. Mixing conditions	1. Degree of mixing 2. Timing of mixing/re-mixing 3. Quantity of stabilizing agent
IV. Curing conditions	1. Temperature 2. curing time 3. Humidity 4. Wetting and drying/freezing and thawing, etc.

Source: After Terashi (1997)

Engineering behaviors of DCM materials

1. Permeability

The permeability or hydraulic conductivity of cement treated soil is important for the design of cut-off wall where seepage needs to be suppressed. Terashi *et al.* (1983) found that the permeability of treated soil decreases with decreasing the water content and with increasing the amount of cement, as shown in Figure 20. From the accumulated test data on Japanese clay, the permeability of treated clays is equivalent to or lower than that of the untreated soft clay and whose order is 10^{-9} to 10^{-6} cm/sec. Kauschinger *et al.* (1992) indicated that the permeability of the cement-treated clay reduces with the increase of cement content and curing time. Porbaha *et al.* (2000) noted that the distribution of pore sizes inside the soil cement mix influences the coefficient of permeability of the treated soil. Win (1999) concluded that the permeability of cement treated soft Bangkok clay decreased with increasing cement. Its value varies in range between 8×10^{-8} and 30×10^{-8} cm/sec.

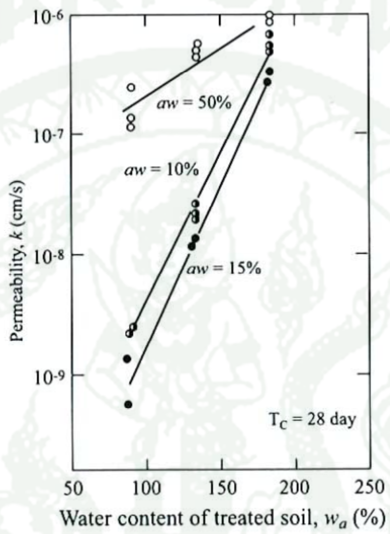

Figure 20 Permeability and water content of cement treated soils

Source: Terashi *et al.* (1983)

2. Compressibility

The compressibility behavior of cement treated clay is similar to the ordinary clay samples, as shown in Figure 21. The resistance to compression of cement treated samples prevails up to the pre-consolidation pressure, beyond which the samples exhibit a large compression. Hunag and Airey (1998) suggested that the effect of the bonding is only significantly for stress below a pre-consolidation pressure. Balasubramanian *et al*. (1998) reported that, at stresses much higher than the pre-consolidation pressure, the *e-log p′* relationship of the treated clay is almost parallel to the virgin compression line of the untreated clay. Horpibulsuk *et al.* (2005)

identified this stress level as the yield stress. It does not represent pre-consolidation or maximum part pressure since the cement treated clay was not being subjected to any stress history. Uddin *et al.* (1997) postulated that a certain amount of cement (>5%) is required to improve the compressibility of untreated clay. He also found that the compression index (C_c) reduces with the increase in cement content when cement content is lower than 15%. Kamruzzaman (2002) reported that compression index reduces with the increase in cement content and curing time. The some values of compression index and recompression index of cement treated soft Bangkok clay are present in Table 10.

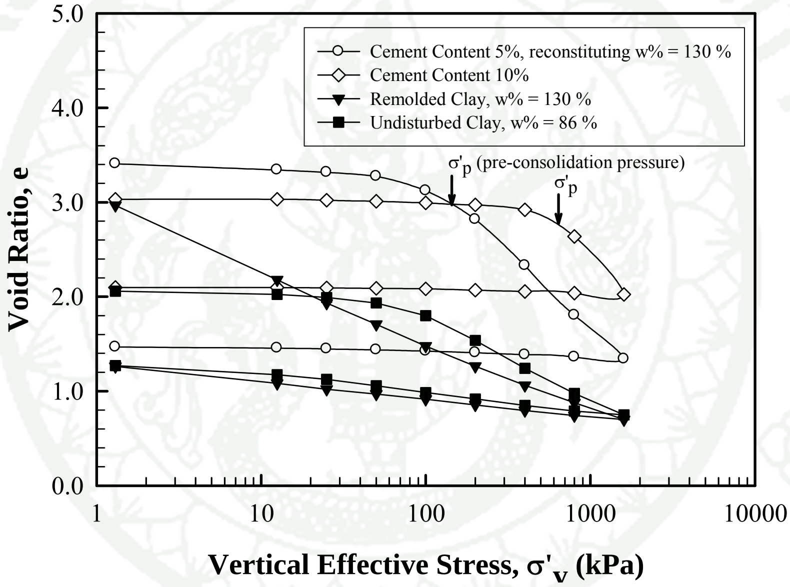

Figure 21 Effective stress versus void ratio of cement treated soft Bangkok clay

Source: Modified from Arnigo (2002)

Table 10 Compression and recompression index of cement treated soft Bangkok clay

Cement Content, kg/m^3	Compression Index,Cc	Recompression Index,Cr
0	0.970	0.060
125	1.760	0.023
150	1.260	0.033
200	1.190	0.030
250	0.760	0.029

Source: Win (1999)

3. Shear strength

Broms (1984) postulated that the two components of the strength, namely frictional resistance (ϕ') and cohesion intercept (c') increase via two processes. The frictional resistance increases due to the formation of significant amounts of particle interlocking in the clay-cement skeleton while the cohesion component increases due to the reduction of the thickness of the diffused doubled-layer of adsorbed water. Yin and Lai (1998) reported that, for Hong Kong marine deposit, the cohesion of the treated soil increase with increase in cement content and decrease in initial water content of the untreated soil. However, the internal friction angle decreases with the increase of cement content and decrease in initial water content. In contrast, Uddin *et al*. (1997) reported that, for soft Bangkok clay, both the cohesion and friction angle increase with the increase of cement content and curing time and reached asymptotic values at about 15% cement content. Horpibulsuk (2005) found that the cement content has a large effect on the cohesion intercept and little effect on the friction angle for soft Bangkok clay, as shown in Figure 22 and 23. Azman *et al*. (1994) classified the failure pattern of cement-treated clays into "friction-dominated" at very high confining stress, "cementation-plus-friction" at medium confining stress and "cementation-dominated" at low confining stress.

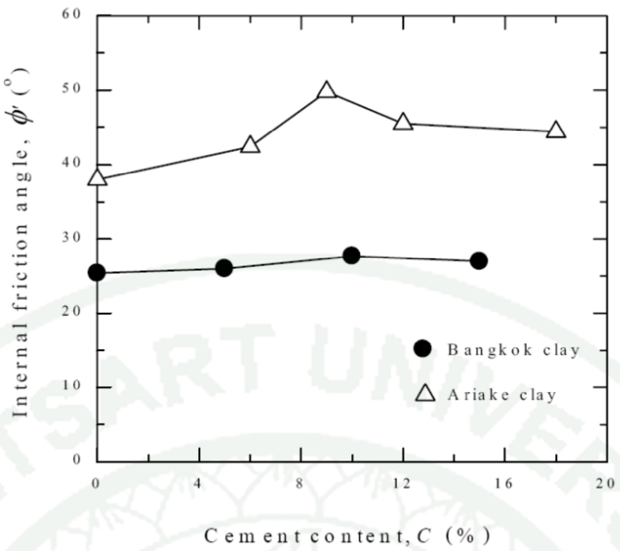

Figure 22 Friction angle and cement content of cemented Bangkok and Ariake clay

Source: Horpibulsuk (2005)

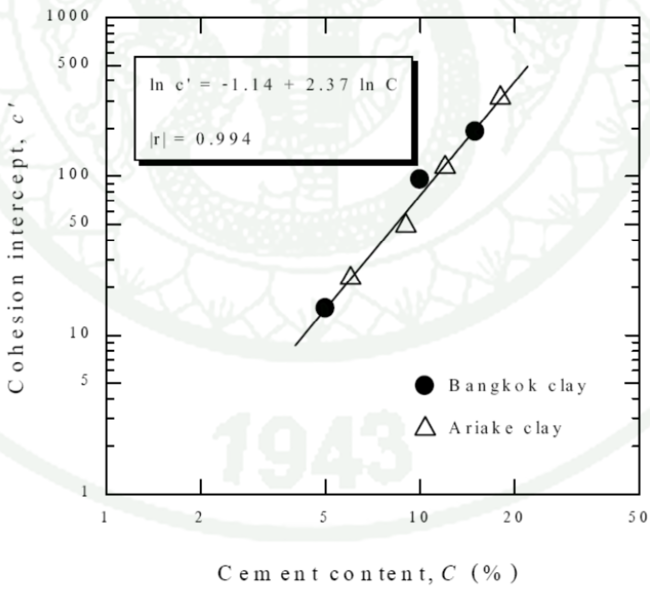

Figure 23 Cohesion and cement content of cemented Bangkok and Ariake clay

Source: Horpibulsuk (2005)

Lee (1999) studied the unconfined compressive strength of cement-treated Singapore marine clay with soil/cement/water ratios which are relevant to jet grouting. It was found that the strength was found to be dependent not only on the water/cement ratio but also the soil/cement ratio. Lorenzo and Bergado (2006) reported that the unconfined compressive strength increased with increasing cement content and curing time for certain remolding water content or mixing water content, as shown in Figure 24. Horpibulsuk *et al.* (2011) found that the average field to laboratory strength ratio (q_{uf}/q_{ul}) is about 0.7 and 1.0 for the dry and the wet mixing methods, respectively.

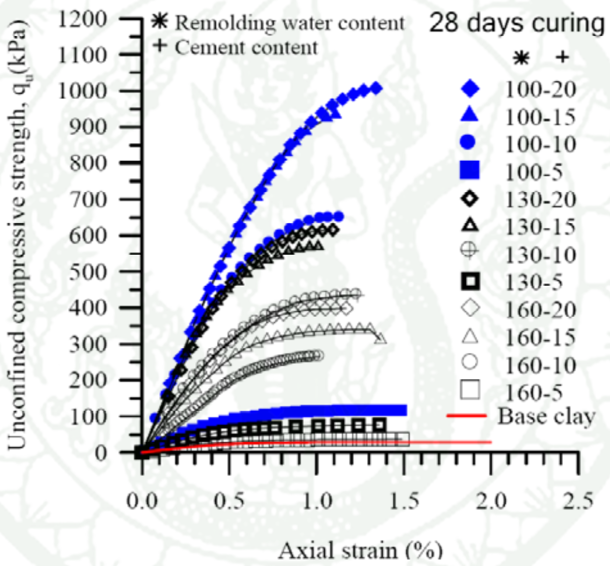

Figure 24 Stress-strain curve from UC tests of 28 day cured cement-admixed specimen

Source: Lorenzo and Bergado (2006)

4. Elastic modulus

The elastic modulus of cement treated soil is generally correlated with the unconfined compressive strength (q_u). The initial (E_i) and secant (E_{50}) moduli of cement treated Bangkok clay are shown in Figure 25. The figure indicated that the E_{50}

of cement treated Bangkok clay can be taken as $114q_u$-$150q_u$. Petchgate *et al*. 2003 found that the E_{50} of cement treated Bangkok clay ranged from $170q_{uf}$-$200q_{uf}$, where q_{uf} is the unconfined compressive strength of field coring specimen.

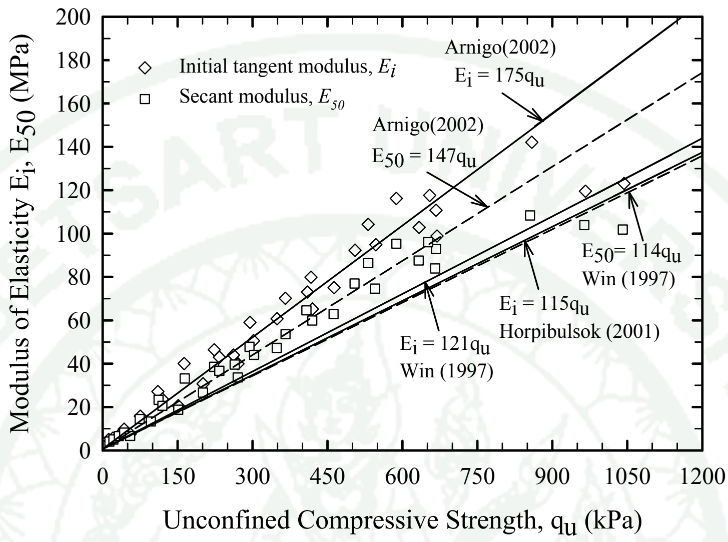

Figure 25 Modulus of elasticity versus unconfined compressive strength of cement-admixed Bangkok clay

Source: Arnigo (2002)

Tan *et al*. (2002) investigated the E_{50} of cement treated Singapore marine clay through unconfined compression test using external and internal strain measurement. The values of E_{50} both external and internal strain measurement are shown in Figure 26 and 27, respectively. For the external strain measurement, the range of $E_{50} = 150q_u$ to $400q_u$. While the E_{50} from the internal strain measurement varied between $350q_u$ and $800q_u$. Kamruzzaman (2002) found that the stiffness measured by local transducer is about 3.0 and 2.16 times of that by conventional method for unconfined compression and undrained triaxial test, respectively.

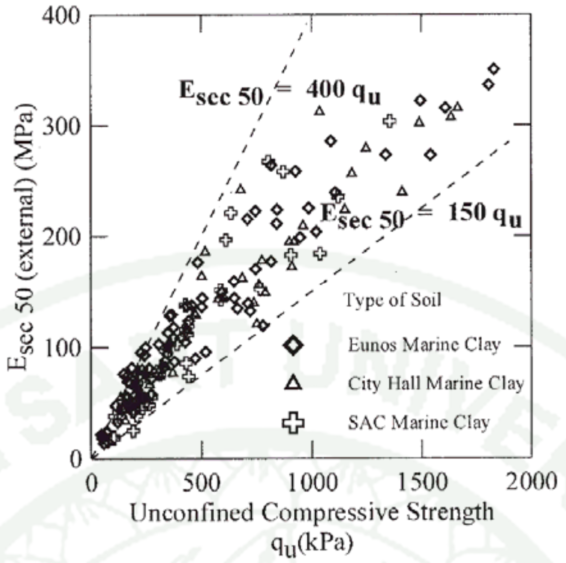

Figure 26 Correlation between E_{sec50} and q_u from external strain measurement

Source: Tan *et al*. (2002)

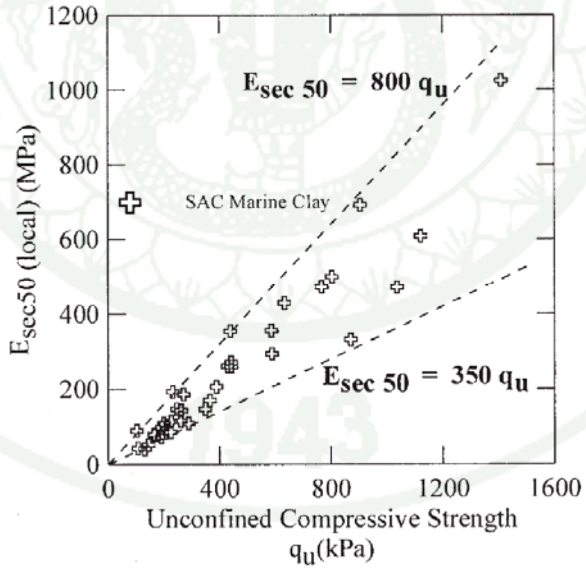

Figure 27 Correlation between E_{sec50} and q_u from local strain measurement method

Source: Tan *et al*. (2002)

Construction technique

The construction techniques for the Deep Cement Mixing (DCM) method can be divided into two groups, as illustrated in Figure 28.

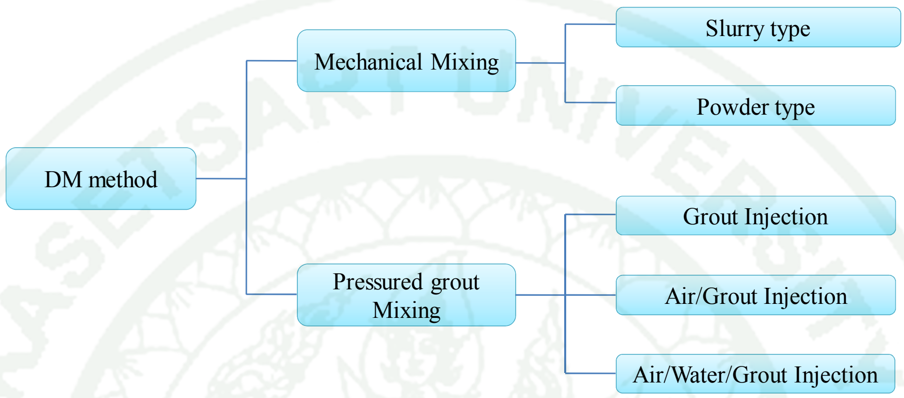

Figure 28 Classifications of Deep Mixing Methods

In mechanical Mixing method, DCM column is manufactured by mixing the chemical agents, which is either in a form of slurry (wet method) or power (dry method) of cement or lime, with in-situ soft soil by rotating mixing blades. The typical construction sequence of DCM column is shown in Figure 29, which is carried out from the left to right:

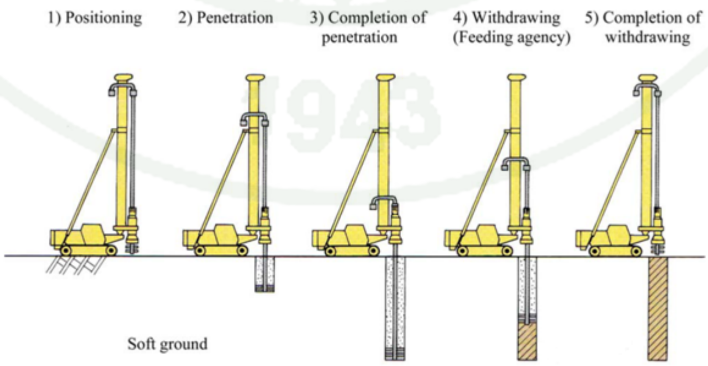

Figure 29 Construction sequence of Deep Mixing pile by mechanical mixing method

Source: Tateyama*et al.* (2006)

1. The position and verticality of the shaft is checked first.

2. Mixing shaft penetrated to the desired depth of treatment with simultaneous disaggregation of the soil by the mixing tool.

3. After reaching the desired depth, the shaft is withdrawn and at the same time, the binder in slurry or powder form is injected into the soil.

4. Mixing tool rotates in the horizontal plane and mixes the soil and the binder.

5. Completion of the treated pile.

In pressurized grout mixing method or sometimes called jet grouting; the typical construction process consists of breaking up the soil with a high pressure jet of fluid in a predrilled borehole and mixing the loosened soil with a self-hardening grout (slurry form) in order to form piles in the ground as shown in Figure 30.

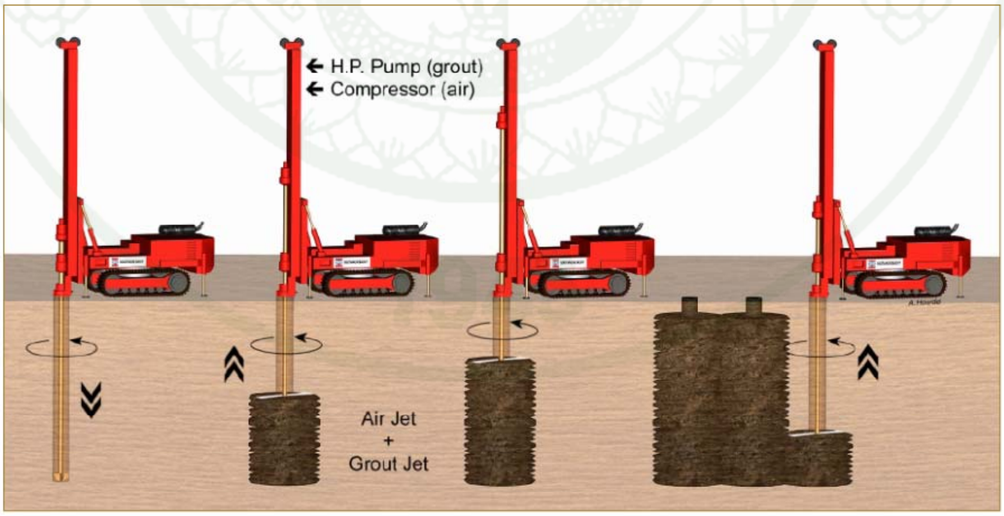

Figure 30 Construction sequence of Deep Mixing pile by jet grouting method

There are three basic jet grouting systems are currently used as shown in Figure 31.

Figure 31 Principal jet system: (1) single jet, (b) twin jet and (c) triple jet

1. Single jet: soil loosening and grout injection are performed by a jet of high pressure grout from nozzles at the bottom end of a drill rod. This method produces the most homogeneous soil-cement element with the highest strength and the least amount of grout spoil return.

2. Twin jet: soil loosening and grout injection are performed by a high pressure jet of grout shrouded by a concentric jet of air. The air reduces friction loss, allowing the grout to travel farther from the injection point, thereby producing greater column diameters. However, the presence of the air reduces the strength of the column as compared to the single jet and produces more spoil return.

3. Triple jet: soil loosening is performed by a jet of water shrouded by concentric jet of air. Grout injection is performed by a separate jet of grout.

Patterns of deep mixing installations and area of application

DCM column can be done to a replacement ratio of 100 per cent wherein all the soil inside a particular block is treated, as is usually the case for shallow mixing applications, or to a selected lower ratio, which is often practiced with DCM column. The chosen ratio reflects, of course, the mechanical capabilities and characteristics of the applied method. Depending on the purpose of DCM column works, specific conditions of the site, stability calculations and costs of treatment, different patterns of column installations are used to achieve the desired result by utilizing spaced or overlapping and single or combined columns. Typical patterns are presented in Figure 32.

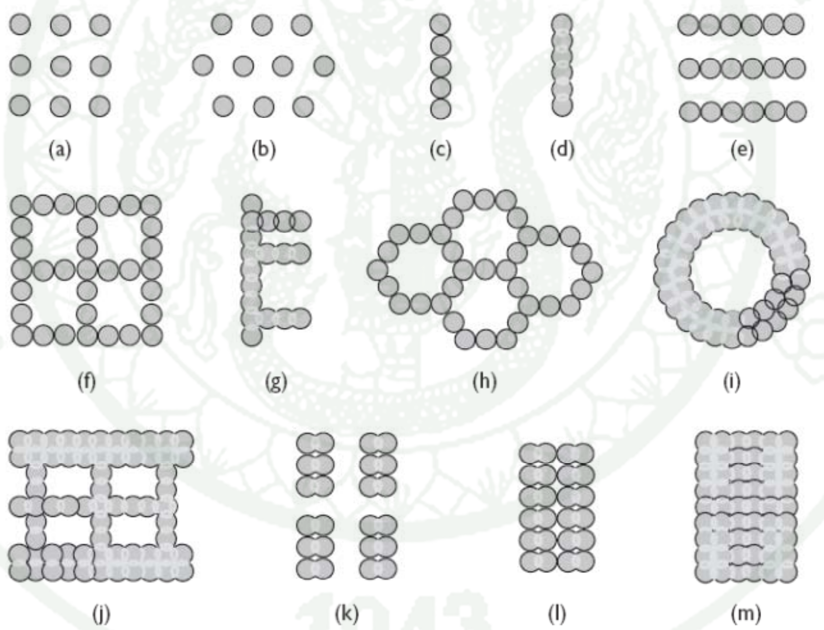

Figure 32 Examples of DCM column patterns: (a), (b) column-type (square and triangular arrangement); (c) tangent wall; (d) overlapped wall; (e) tangent walls; (f) tangent grid; (g) overlapped wall with buttresses; (h) tangent cells; (i) ring; (j) lattice; (k) group columns; (l) group columns in-contact; (m) block

Source: Moseley and Kirsch (2004)

Stability analysis of embankments supported on deep mixing columns

The current Swedish design method considers the stabilized soil as a composite material (SGF, 2000; Vägverket, 2009). The peaks shear strength of the DCM columns is assumed to mobilize at the same time as the peak shear strength of the unstabilized soil between the columns (Figure 33). This means that there is full interaction between the soil and the DCM columns. Failure is assumed to occur along a slip surface through the DCM columns and the surrounding soil.

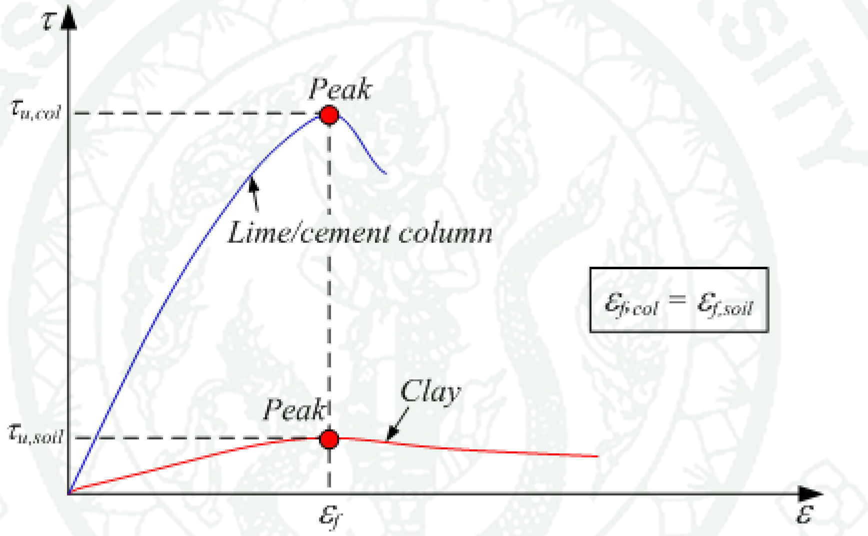

Figure 33 Assumed strains in the calculation of weighted average shear strength

A weight average undrained shear strength of the stabilized soil is used to estimate the stability of the embankment on improve soil.

$$\tau_u = \tau_{u,col}.a_s+\tau_{u,soil}.(1-a_s) \quad (14)$$

$$\tau_{u,col} = c_{u,col}.a_s+\sigma_n.\tan\phi_{u,col} \quad (15)$$

$$\tau_{u,soil} = c_{u,\ soil}.a_s+\sigma_n.\tan\phi_{u,soil} \quad (16)$$

where: τ_u = average undrained shear strength of the stabilized soil

$\tau_{u,col}$ = undrained shear strength of the DCM column

a_s = area replacement ratio

$\tau_{u,soil}$ = undrained shear strength of the soil

If $\phi_{u,col} = \phi_{u,soil} = 0$, as commonly used by many practitioners and researchers for DCM columns, then $\tau_{u,soil}$ is equal to $c_{u,soil}$, and $\tau_{u,col}$ is equal to $c_{u,col}$. When these simplifications are made, the equation for average undrained shear strength of ground improved with DCM columns takes the form of Equation 14.

$$\tau_u = c_{u,col}.a_s+c_{u,soil}.(1-a_s) \tag{17}$$

The area replacement ratio (a_s) is represented as the percentage of the sectional area of the DCM column to the ground occupied by the DCM column; it is calculated by equation 9. DCM column is usually arranged either rectangular or staggered pattern, as shown in Figure 34.

$$a_s= \frac{A_p}{d_1 x\ d_2} \tag{18}$$

where: a_s = improvement ratio

A_p = sectional area of DCM column

d_1, d_2 = interval between DCM columns

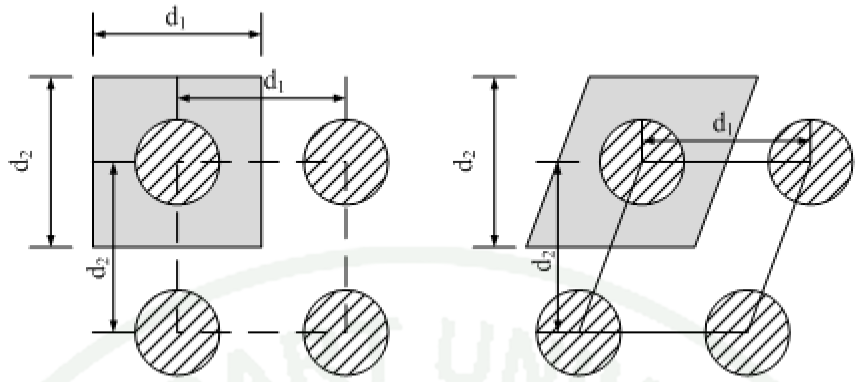

Figure 34 Arrangement of DCM column

Source: CDIT (2002)

The design method in Japan (CDIT, 2002) is similar to Swedish design. It considers the stabilized soil as a composite material. However, unlike the Swedish practice, it assumes that the shear strengths of the DCM columns and the unstabilized soil between the DCM columns are not mobilized at the same time, as shown Figure 35. Therefore, in the method used in Japan, a factor, k, is applied to account for the difference in strain at failure between DCM columns and surrounding soil. The average undrained shear strength of ground improved with DCM columns is:

$$\tau_u = c_{u,col}.a_s+k.c_{u,soil}.(1-a_s) \quad (19)$$

where: k = coefficient factor for soft soil strength = $\tau_{u,mob}/\tau_{u,soil}$

$\tau_{u,mob}$ = shear strength of soft soil mobilized at the peak of the shear strength of treated soil

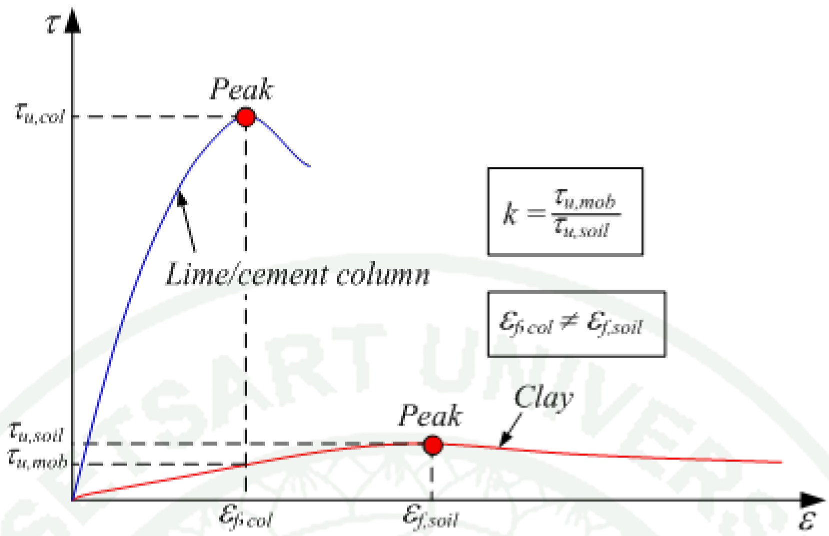

Figure 35 Mobilized shear strength of stabilized soil

Limit equilibrium methods (LEM) have been commonly adopted for analyzing slope stability of embankments over deep mixed foundations. By this method, soil and DCM column are assumed to behave as an elastic perfectly plastic material, and the failure surface takes a certain shape. Despite the simplicity of LEM methods, they may overestimate the safety of the embankment constructed on DCM foundations. This is probably due to the adopted assumptions and the possibility of more than one failure mode occurring in the columns at failure. More important point, the stress-strain behavior of materials is not considered.

In recent years, numerical methods have been increasingly used for analyzing slope stability including the computation of its factor of safety. Numerical methods are more rather powerful than limit equilibrium slope analyses because they are able to include other failure modes than shear mode, namely bending, rotation, tension or a combination of these modes.

Broms (1999) illustrated the possible failure modes of columns under the embankment as shown in Figure 36. There exist flexural and tension failure depending on the locations of the columns. He also indicated that horizontal forces from the embankment would reduce the bearing capacity of DM columns.

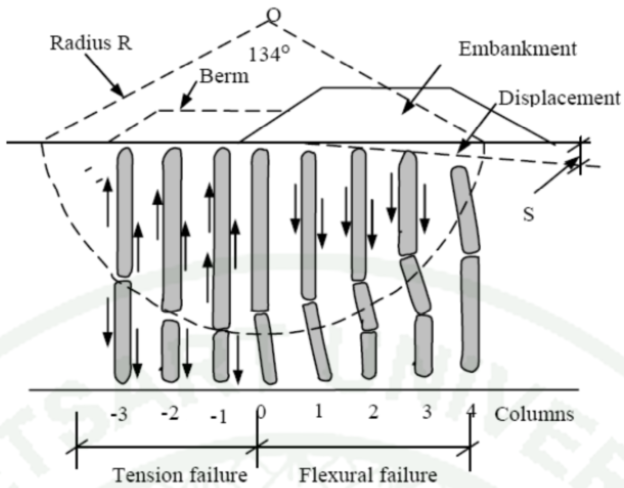

Figure 36 Possible failure modes of columns

Source: Broms (1999)

Han *et al*. (2005) investigated the influence factors on the deep-seated failure of the embankment over DCM columns by finite difference program FLAC 2D (Fast Lagrangian Analysis of Continua) and Bishop's method included in the software-ReSSA. They varied several parameters such as the size and strength of the DCM columns, the spacing and the thickness of the soft soil underneath. A series of comparisons demonstrate that the calculated factors of safety using Bishop's simplified method are higher than those calculated using the FLAC. They also concluded that the modes of failure for DCM columns include shearing, bending, or rotation, tension failure, or a combination of these four modes depending on soil conditions, DCM column strength, and design configurations. Kitazume *et al.* (2005, 2007) studied external and internal stability of DCM columns embankment by using centrifuge model tests. For the external stability, DCM columns did not fail with a sliding failure pattern but rather with a collapse failure pattern where the columns tilt like dominos, as show in Figure 37. The example of failure patterns of DCM columns for the internal stability is shown in Figure 38. Their study revealed that the DCM columns did not fail simultaneously but fails one by one by bending failure mode. Moreover, they found that the location of bending failure is shallower in the low strength DCM column than the higher one.

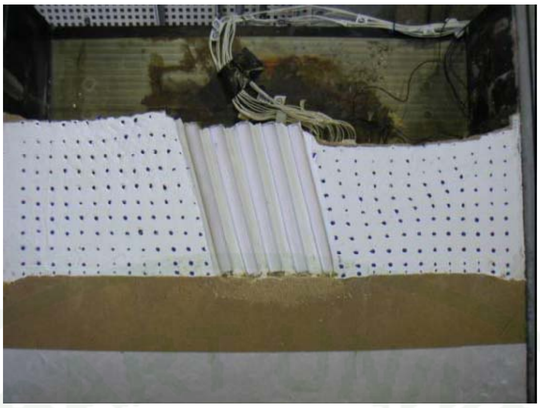

Figure 37 Collapse failure pattern of DCM columns

Source: Kitazume *et al.* (2005)

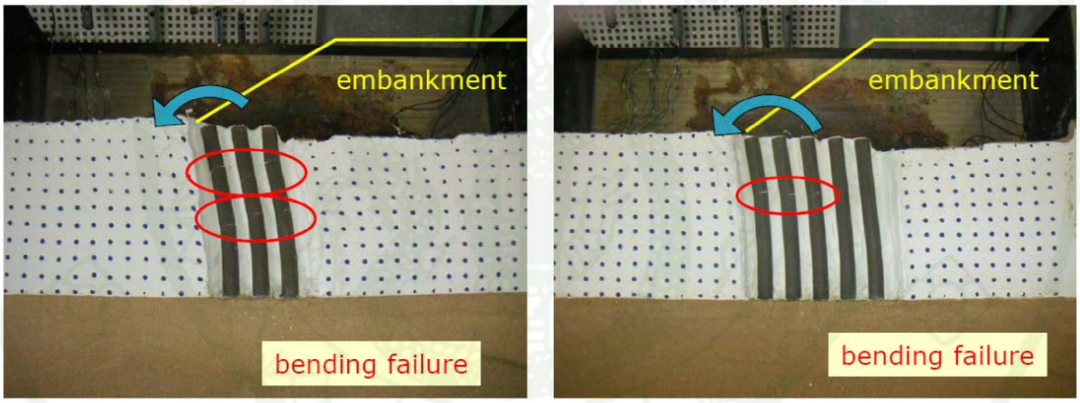

Figure 38 DCM Column failures

Source: Kitazume *et al.* (2007)

Adams *et al.* (2009) used the finite difference program FLAC to study the internal stability (failure of the columns under embankment load) of single columns and shear walls. Several important conclusions can be drawn:

a. Numerical analyses give a lower factor of safety than limit equilibrium slope analyses. This means that considering solely shear failure overestimates the embankment stability (the classical methods tend to be risky).

b. Single DCM columns fail with a bending mode failure. This behavior is proposed by KivelÖ (1998) and confirmed by the tests performed by Larsson (1999, 2008) and Larsson and Broms (2000).

c. DCM shear walls are more effective than single columns at the same area replacement ratio, i.e. about the same cost for raw material. The same conclusion was drawn by Larsson (2008).

d. The failure modes of shear walls are greatly influenced by the interaction between the overlapping columns. If the interaction is assumed to be perfect (that is, the compressive strength of the material between two columns is equal to the compressive strength of the columns), then the shear wall fails by sliding and shearing. In reality the mixing process of the columns leads to weaker joints between the overlapping columns. When the vertical joint efficiency is below 30% of the strength of the columns, the shear walls fail by racking. The same behavior is indicated by the test performed by Larsson (2008), where the overlapping distance between the columns was varied.

Possible failure modes of DCM column

The possible behavior of lime-cement columns has been investigated by KivelÖ (1998). He pointed out that individual lime-cement columns may fail at different patterns along the potential slip surface, as shown in Figure 39. Failure modes a, b and c represent column bending, d represents flow of soil around the column, and e, f, g and h represent column tilting, column translation, shearing through the column and compression failure in the column, respectively. He has also derived the expressions for evaluating the shear resistance of the columns along assumed slip surfaces for each failure mode. It has been shown that the failure of relatively high-strength columns can occur by exceeding the moment capacity of the columns (i.e. failure modes a, b and c) or the lateral resistance of the soft soil around the columns (i.e. failure modes d, e and f). Failure of low-strength columns can be caused by shear failure along a slip surface (i.e. failure mode g) or when the compressive strength of the columns is exceeded (i.e. failure mode h). The low-strength column is defined as the columns that possesses shear strength equal to or lower than 150 kPa (Brom, 2004). It should be noted that the proposed failure modes has not been verified by load tests and has therefore not yet been applied in practice.

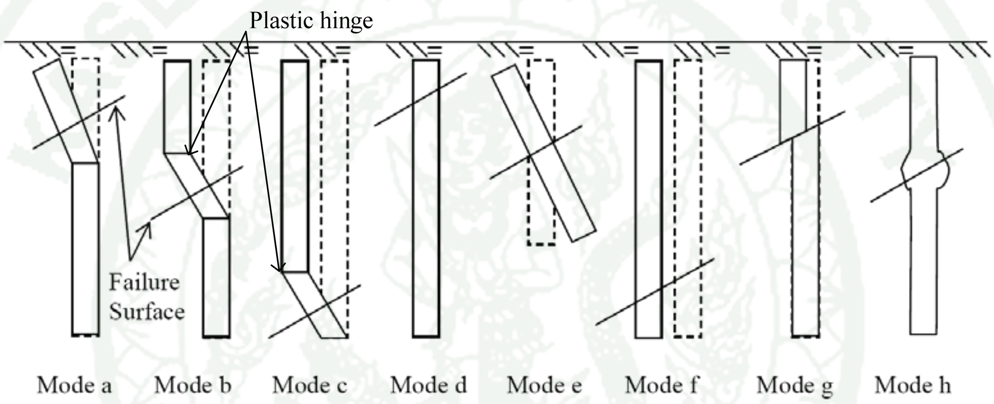

Figure 39 Failure modes of single DCM columns

Source: Modified from KivelÖ (1998)

Possible failure modes of DCM column row were illustrated by Moseley and Kirsch (2004), as shown in Figure 40. The unstabilized soil is extruded between the column walls (Figure 40a) when the slip surface is located close to the top of the column row. A DCM column row fails by overturning (Figure 40b) when the toe resistance is high. The wall is displaced laterally (Figure 40c) together with the unstabilized soil above the slip surface. The shear resistance depends on the penetration depth of the DCM columns into the hard or stiff layer below the wall (Figures 40d and 40e). The DCM column wall could also fail when the bearing capacity of the DCM columns is exceeded (Figure 40f).

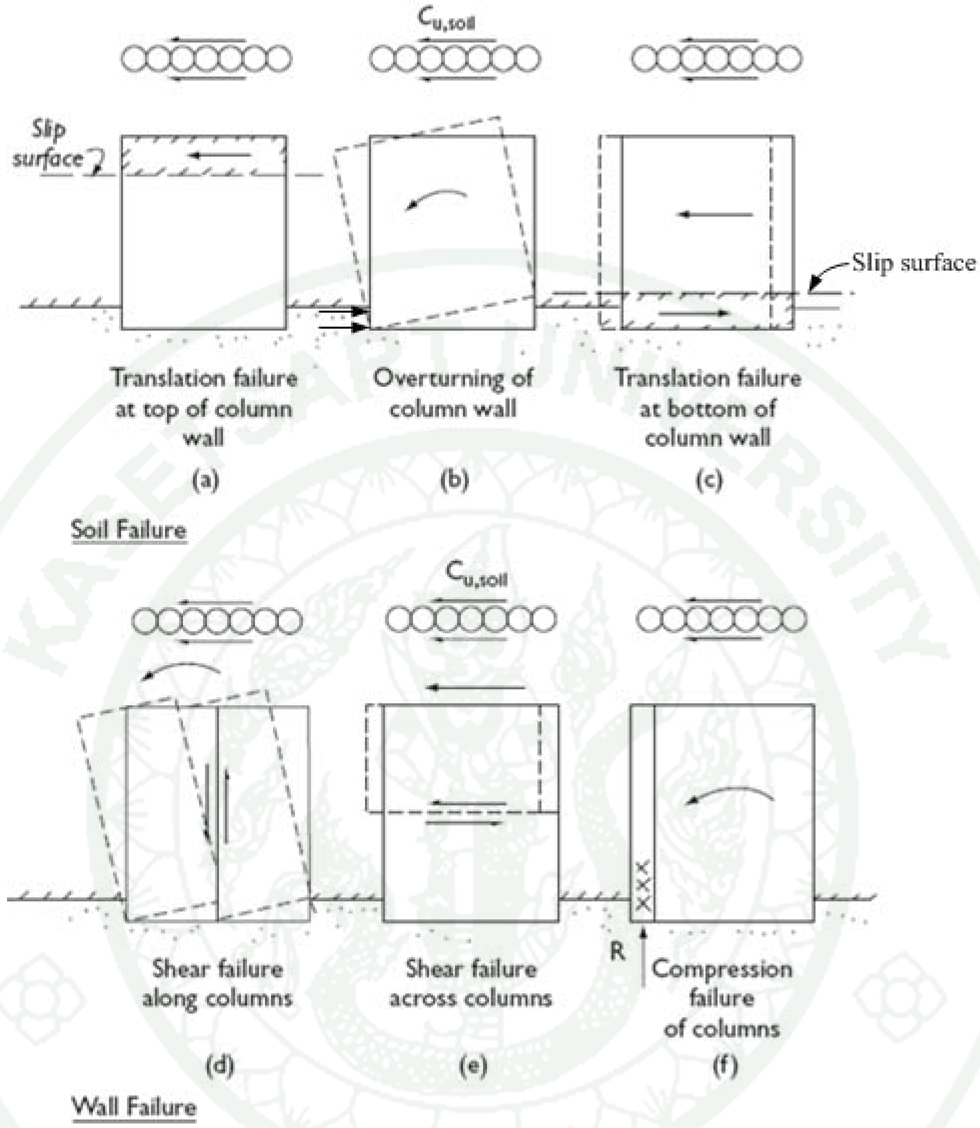

Figure 40 Failure modes of DCM column walls

Source: Moseley and Kirsch (2004)

Case histories and previous research in slope stabilized by DCM columns

Presently, the DCM columns can be used for other purposes than stabilization of embankment; slope stabilization is an example. There was a few papers related to slope stabilized by DCM columns have been published. The available researches related with this topic are presented below.

Watn *et al.* (1999) observed behaviour of lime-cement columns for slope stabilization in Norway. The configuration of lime-cement columns for stabilization of slope is illustrated in Figure 41. They found that there were several incidents of deformations and failures of slopes during the construction, as shown in Figure 42. They reported that typical sources for failure were:

1. Inhomogeneous of lime-cement columns resulting in lower strength than assumed in design;

2. Temporary cut at toe of slope for drainage trenches;

3. Insufficient transition zone between rib and bed rock;

4. Deformation in remolded clay above rib;

5. Water runoff from upstream the slope;

6. Water fill cracks on the clay surface;

7. Surface deformation due to swelling of the clay.

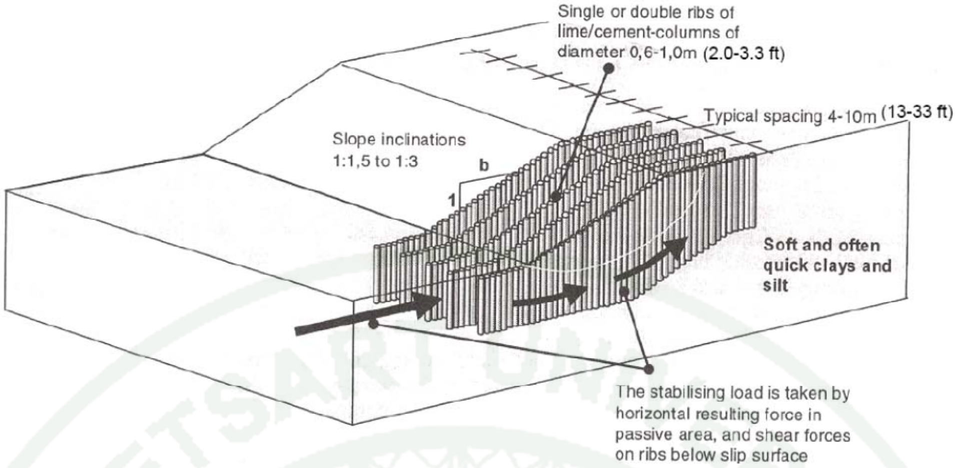

Figure 41 Configuration of lime-cement columns for stabilization of slope

Source: Watn *et al*. (1999)

(a) Slope failure

(b) Outfall of clay

Figure 42 Failures during the construction

Source: Watn *et al*. (1999)

Priol *et al.* (2007) used the Three-Dimension Finite Element Method, incorporated in Plaxis 3D Tunnel, in order to investigate the influence factors on the stability of slope. The geometry of model is presented in Figure 43, which was simplified from Figure 41. The factors varied were spacing of columns rib, cohesion and friction of soft clay. The important conclusions can be drawn:

1. The safety factor of slope decreased when spacing had increased, as shown in Figure 44. Two different modes were observed when the spacing had been varied, as shown in Figure 45 and 46. It was observed a modification of the mode of failure between the 4 m spaced ribs showing a block failure and 6 m spaced ribs exhibiting a rotational failure. After the failure mode changing from block failure to slip on soil between column ribs, the change of FS is similar to virgin soil.

2. When the cohesion of soft clay had increased, the safety factor increased. However, it observed that the rate of increase in the safety factor was not the same for each spacing value, as shown in Figure 47. The transition between the block and rotational failures was separated by the dot line.

3. The rate of increase in the safety factor of stabilized slope was greater than the virgin slope once the friction angle of soft clay had increased, as shown in Figure 48.

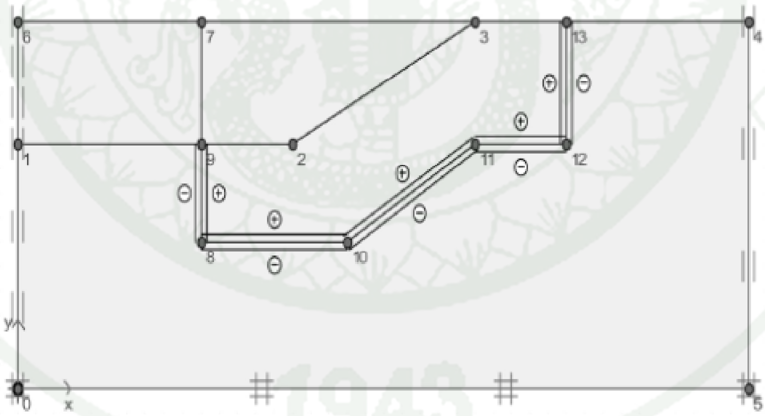

Figure 43 Cross section of the 3D model

Source: Priol*et al.* (2007)

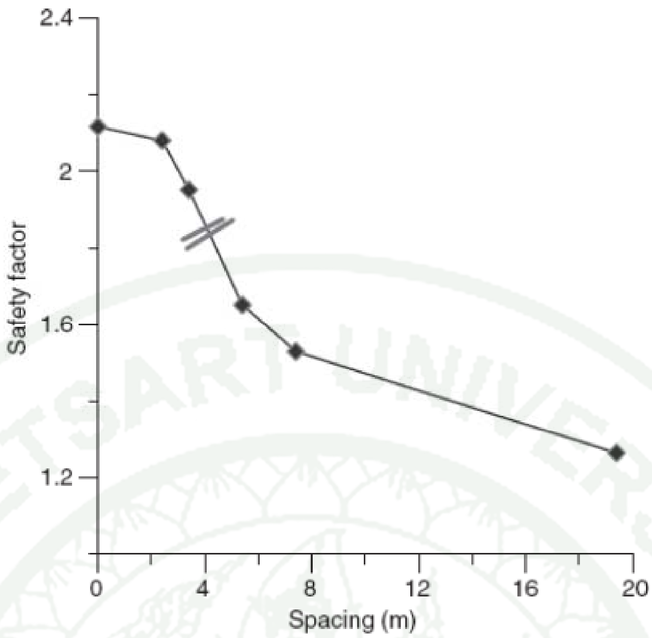

Figure 44 Effects of the spacing on the safety factor

Source: Priol *et al.* (2007)

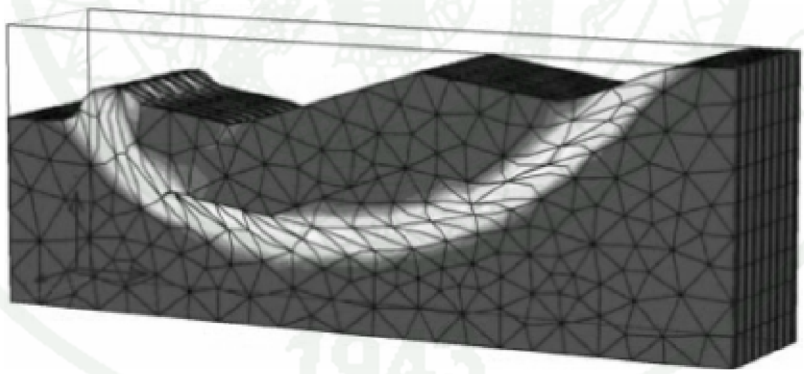

Figure 45 Block failure: rotational failure (S = 4)

Source: Priol *et al.* (2007)

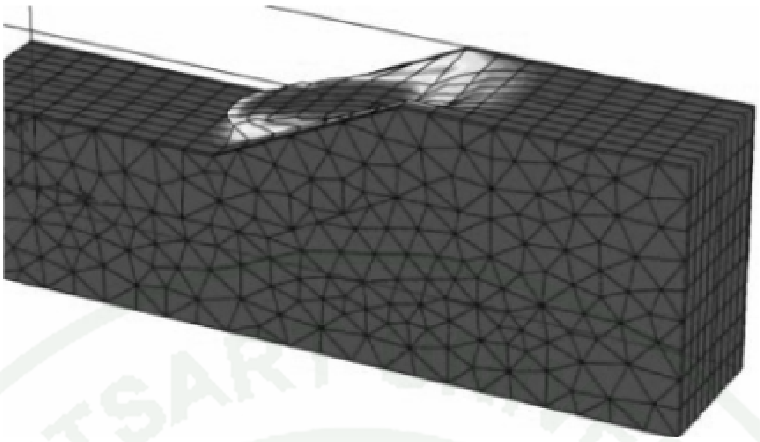

Figure 46 Rotational sliding: "banana" type of failure of the soil in between the ribs (S = 6)

Source: Priol *et al.* (2007)

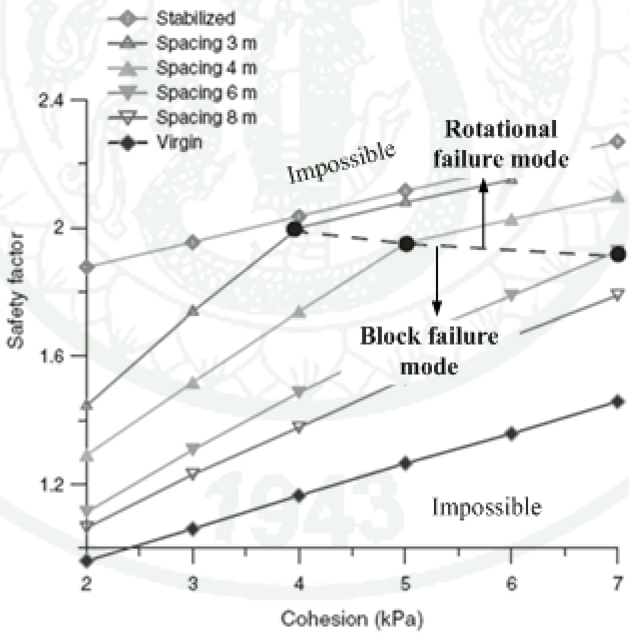

Figure 47 Effects of the cohesion on the safety factor

Source: Priol *et al.* (2007)

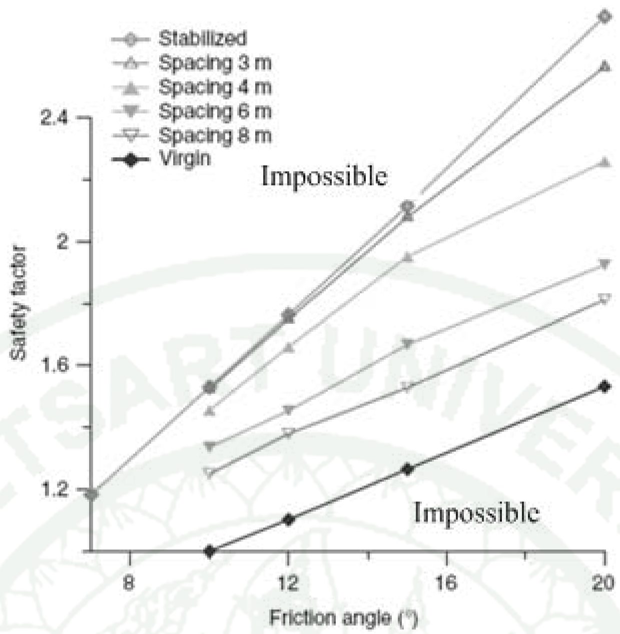

Figure 48 Effects of the internal friction angle on the safety factor

Source: Priol *et al.* (2007)

Taesiri and Chantaranimi (2001) reported the use of DCM columns for improving stability of road embankments along canals. The diameter of each DCM column was 0.6 m and the length of the DCM columns, depending on the soil profile, varied from 13 m to 20 m. The DCM columns were arranged in form of a wall type aligning parallel to the road, as shown in Figure 49.

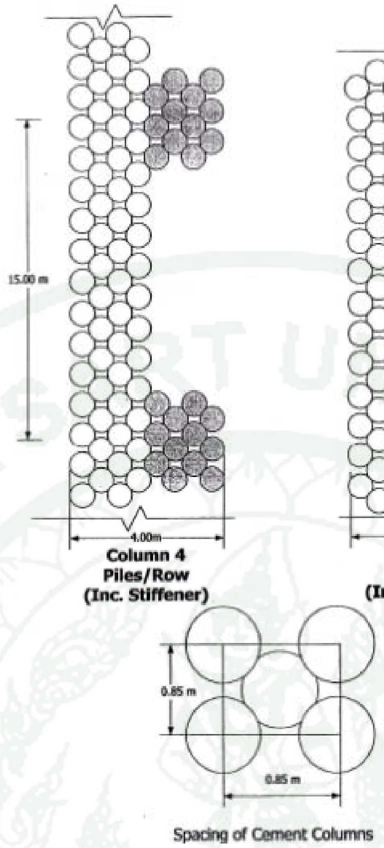

Figure 49 DCM column arrangements

Source: Taesiri and Chantaranimi (2001)

Stabilization of Slope Using Piles

Stabilization of slopes by placing spaced rows of piles is a widely accepted. The piles used in slope stabilization are in passive stage, because they are usually subjected to lateral force arising from the horizontal movements of the sliding mass. Chen (1994) introduced the typical situation of a pile undergoing lateral soil movement, as shown in Figure 50. The pile in the upper part is subjected to lateral soil movement and is referred as a “passive” portion. Where the pile in the lower part is subjected to lateral loading transmitted from the upper pile portion, and it is referred as an “active” portion. It can be seen that the soil surrounding the pile at any depth is at equilibrium under the initial stress state before the soil starts moving. When the soil begins to move, the stress surrounding the pile will change from the initial state to a new equilibrium state.

Some of successful applications of such techniques have been reported by Esu and D'Elia (1974), Ito and Matsui (1975), Sommer (1977), Wang *et al*. (1979), Ito *et. al*. (1982), Nethero (1982) and Reese *et al* (1992). Driven timber piles have been used to reinforced the slope stability of very soft clays in Sweden, while cast-in-place reinforced concrete piles as large as 1.5m diameter have been used in Europe and the United States to stabilize active landslides in stiff clays (Bulley, 1965 and Offenberger, 1981). In Japan, steel tubes piles of 300mm diameter have been used to stabilize active landslides areas. Taniguchi (1967) and Fukouka (1977) presented three real-life cases in Kanogawa Dam, Hokuriku Expressway in Fukue Prefecture and Higashitono where steel piles were used to improve the factor of safety of landslides.

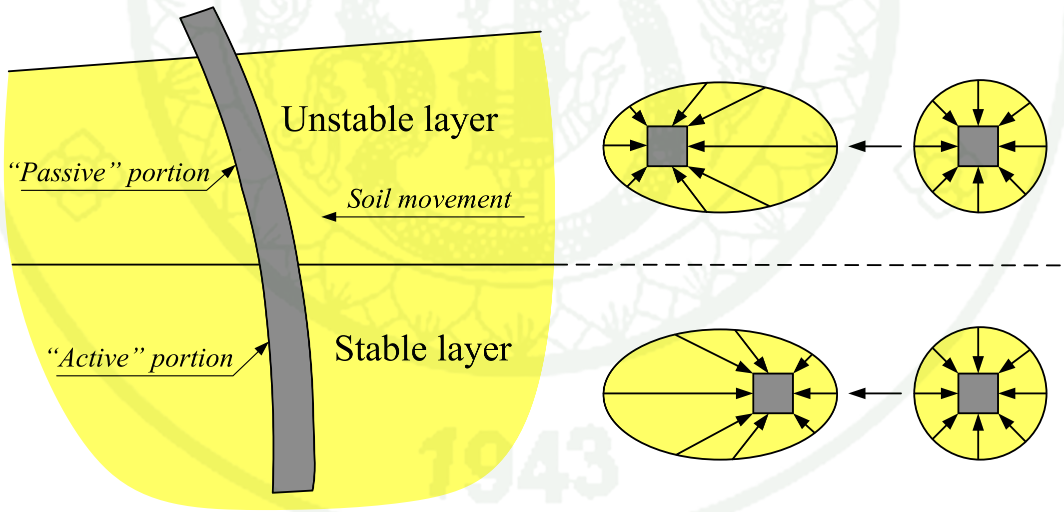

(a) A deflected pile (b) Stress state

Figure 50 Pile loaded by lateral soil movement

Source: Modified from Chen (1994)

Methods for analyses

A number of methods have been proposed to analyze stabilizing piles. The four main categories of analysis have been classified as (Pradel *et al*., 2010):

a. Limit Equilibrium Method: Methods for the design of stabilizing piles using limit equilibrium method have been proposed by many researchers in the past decades (Ito *et al.*, 1975; Poulos, 1995; Lee *et al.*, 1995; Hassiotis *et al.*, 1997). In practical design, the limit equilibrium method is used most often in analysis due to its simplicity. The design methods based on limit equilibrium generally obtain an equivalent force, which piles must be capable of resisting. The basic concept to determine the factor of safety is as shown in Equation 20. This equation is based on the resisting moment M_{rs} of the soil, and the driving moment, M_d of the sliding mass. After placing a reinforcing pile in an unstable slope, the pile is considered to provide an additional resistance and will increase the overall resistance. In the calculation, a limiting resistance force per unit width, F_r which is provided at the sliding surface by reinforcing pile is added to the internal forces of the intersecting slice. The additional resistance provided by the pile is included in the equilibrium equations to satisfy the static equilibrium. The resisting moment by the pile, M_{rp} can be determined. The equation of the factor of safety can be written as Equation 21. However, the present design for pile-stabilized slopes using limit equilibrium methods is unable to take the pile-soil interaction into account. The piles are assumed to only provide reinforcing resistance.

$$FS = \frac{M_{rs}}{M_d} \tag{20}$$

$$FS = \frac{M_{rs} + M_{rp}}{M_d} \tag{21}$$

b. Pressure Based Method: This method is based on the analysis of the passive pile subjected to the lateral soil pressure. Generally, the lateral soil pressure on the piles in a row is estimated based on plastic theory developed by Ito and Matsui (1975). The main assumption is that the soil is soft and able to deform plastically around the piles. The other assumptions are; the plies are rigid, the frictional forces between pile and soil are neglected, the active earth pressure acts on inner distance between pile faces, two sliding surfaces occur marking an angle of (45+ϕ/2) with soil movement direction (Figure 51). This model may not represent the actual piles in the field, because it does not take account for the finite flexibility of the pile, soil arching and saturated soft clayey soil, etc (Jeong *et al.*, 2003).

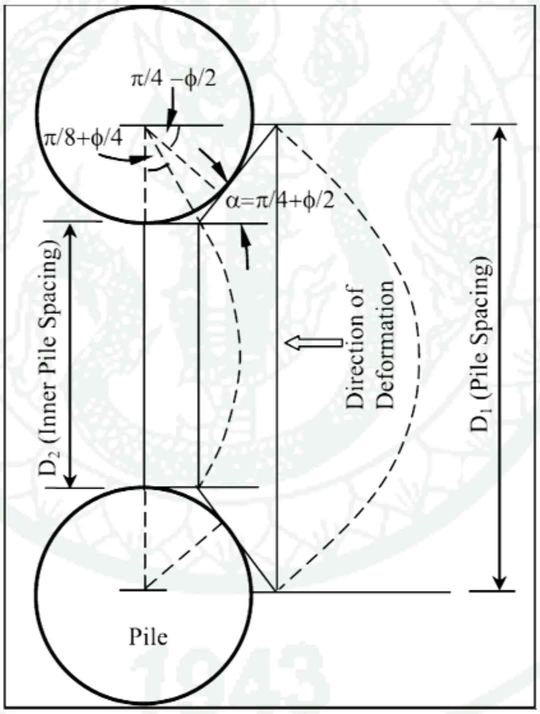

Figure 51 Stage of plastic deformation in the ground just around piles

Source: Ito and Matsui (1975)

c. Displacement Based Method: This method considers the relative displacement between the soil and pile. The soil movement can be measured directly from inclinometer data or calculated by the finite element approach. Poulos (1973) mentioned a boundary element method to analyze a single pile subjected to lateral soil movements. The soil was assumed to be elastic; the parameters of elastic modulus and yield pressure were allowed to vary with depth. The method required an input of the magnitude of the free field soil movement at each depth, and the ultimate soil pressure acting on the pile. Based on comparisons between the method predictions and the measured data, the author concluded that it was quite agreement with the measurements. This method is used for analyzing the single pile as well as the pile group. Later, this was modified by Hull *et al*. (1991). He raised different failure modes which were identified for the pile-soil interaction when the pile was subjected to lateral soil movements. The modified method was considered to be good practical applications. However this method still depends on an input of both soil movement and ultimate soil pressure.

d. Numerical Solution Method: The Finite Element Method (FEM) or Finite Difference Method (FDM) are normally used. It provides coupled solution for the pile response, and slope stability simultaneously. Cai and Ugai (2000) used the 3D-FEM with shear strength reduction method to study the effect of stabilizing piles on the stability of a slope. They varied parameters such as the pile spacing, pile head conditions, bending stiffness, and pile positions. Jeong *et al*. (2003) used finite element program, ABAQUS, to study the influence of the one row pile groups on the stability of the weathered slope. Goh and Wong (1997) presented a simplified numerical method for analyzing the response of single piles to lateral soil movements. In their method, the pile is modeled as beam element, and the pile-soil interaction as the hyperbolic soil springs.

Parameters affecting the stability of slope

There are several parameters that could affect the stability of slope with pile. Some of these parameters are the pile position, pile depth and pile spacing. The previous researches on pile stabilizing slope were reviewed in this section.

1. Effect of pile location

The pile location within a slope is very important to the increase in the slope stability. Numerous studies performed to determine the optimal location of piles within a slope were summarized by Ho (2009):

Lee *et al*. (1995) using the simplified Bishop's slip circle approach, found out that the most effective pile positions are at the toe and crest of the slope for homogeneous cohesive soil slopes. And for the slope on soft clay layer underlain by stiff clay, the pile positions are between mid point to the crest of slope.

Poulos (1995) pointed out that the row of piles should be located in the vicinity of the center of the critical failure wedge to avoid merely relocating the failure surface behind or in front of the piles.

Hassiotis *et al.* (1997) used the extended friction and Ito's approach to analyze slopes reinforced with one row of piles. They concluded that for a maximum factor of safety, the piles must be placed in the upper middle part of the slope. When the slope steeper, pile have to be placed closer to the top.

Cai and Ugai (2000) compared the results obtained by using shear strength reduction finite element and Bishop's simplified methods, as shown in Figure 52. The L_x is horizontal distance between the slope toe to the pile position. The L is horizontal distance between the slope toe and the slope shoulder. In finite element analysis, the pile should be located in the middle of the slope to achieve the maximum safety factor. While in Bishop's simplified method, the largest factor of safety occurred once the pile was placed in the upper middle part of the slope. The pile behavior for various pile position are shown in Figure 53. When the piles were placed in the lower and middle portion of the slopes, the pressure on the piles is larger, and the soil-pile interface is sufficiently mobilized. On the other hand, the soil-pile interface is not sufficiently mobilized when the piles were installed in the upper portion of the slopes.

They concluded that the pile behavior characteristics were significantly influenced by the positions of the piles.

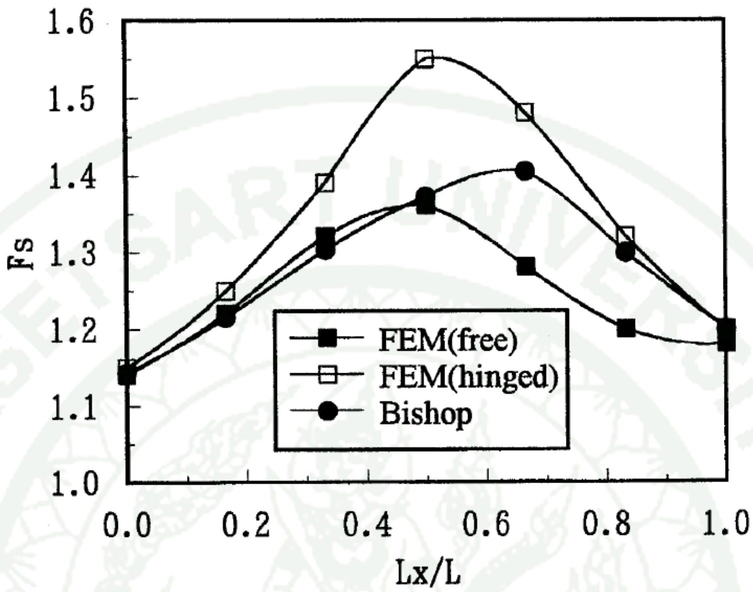

Figure 52 Effect of pile position on safety factor

Source: Cai and Ugai (2000)

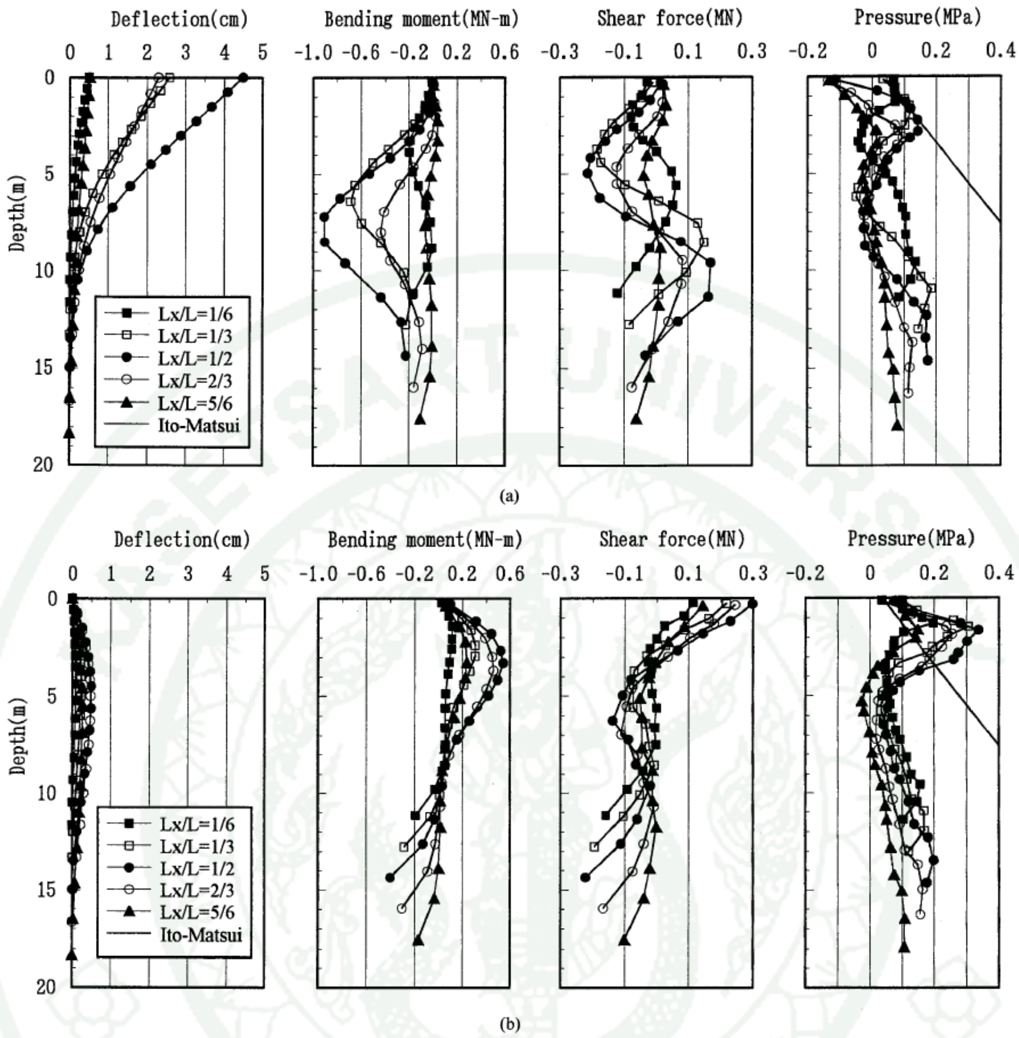

Figure 53 Pile behavior characteristics for various pile position (a) free head and (b) fixed head

Source: Cai and Ugai (2000)

Ausilio *et al.* (2001) developed an analysis for stabilizing of slopes reinforced with piles using the kinematic approach of limit analysis. According to their studies, the optimal location of the piles within the slope is near the toe of the slope where the stabilizing force needed to increase the safety factor to the desired value takes a minimum value. They also found out that piles also appear to be very effective when they are installed in the region from the middle to the toe of the slope.

Jeong *et al*. (2003) used finite element program, ABAQUS, to study the influence of the one-row pile groups on the stability of the weathered slope. The result between coupled and uncoupled analysis were compared. In uncoupled analysis, the pile response and slope stability are considered separately. While in coupled analysis, the pile response and slope stability are considered simultaneously. Their results show in Figure 54. For the coupled analysis, the safety factor was largest when the piles were installed in the middle of the slope. However, uncoupled analysis showed that the piles should be placed slightly closed to the top of the slope for largest safety factor. They gave the reason that when the piles were placed at the middle portion of the slope, the soil-pile interaction was sufficiently mobilized. In other word, the pressure action on the piles installed at the middle portion of the slope was larger than that on the piles in the upper portion.

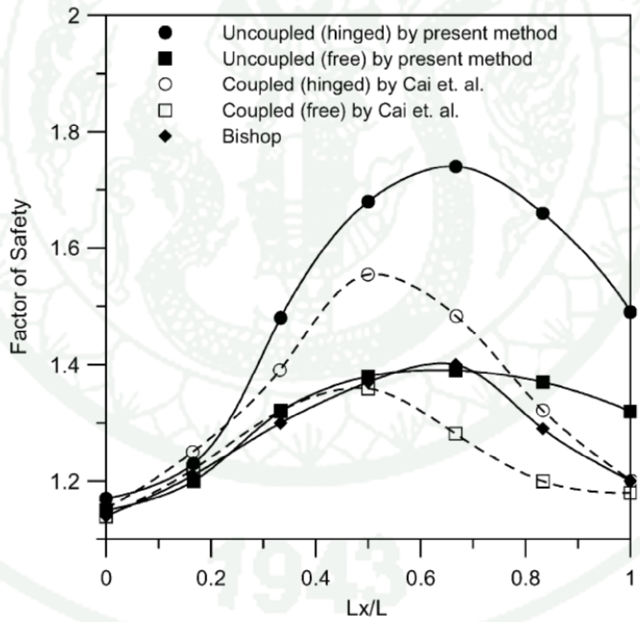

Figure 54 Effect of pile position on safety factor

Source: Jeong*et al*. (2003)

Nian *et al*. (2008), using limit analysis, concluded that the optimal location of the piles is near the toe of the slope where the force needed to increase the slope stability to the design safety factor has the lowest value.

Wei and Cheng (2009), also using FLAC3D, considered the problem of slope reinforced with one row ofpiles. Their numerical results showed that the optimal pileposition lies between the middle of slope and the middle of the critical slip surface of the slope with no pile.

The results from researchers described above were summarized in Table 11. The optimal location is rather different. It depends on many factors such as soil type and analytical model.

Table 11 Summary of recommended optimum pile position

Reference	Soil type	Failure type	Recommended location	Case histories or analytical model	Comment
Lee *et al.* (1995)	Purely Cohesive slope	Circular	Toe and Crest	Uncoupled formulation	Different soil distributions govern the optimal pile location
	Upper soft lower stiff	Circular	Between middle and Crest	Pile response-boundary element	-
	Upper Stiff lower soft	Circular	Toe and crest	Slope stability - simplified Bishop slip circle approach	-
Poulos (1995)	Clay, Clay stone and Silt stone	Circular	Middle	Highway 23, Newcastle AU Use program ERCAP derive from Ito & Matui's Equation	Analyzed the response of pile placed in the middle

Table 11 (Continued)

Reference	Soil type	Failure type	Recommended location	Case histories or analytical model	Comment
Hassiots *et al*. (1997)	Cohesive soils	Circular	Upper to top	Friction circle method incorporate the reaction force derived from plasticity theory	Plane Strain conditions
Cai and Ugai (2000)	c = 10 kPa ϕ= 20°	Circular	Middle	3D FEM Shear Reduction finite element method	Compared different pile head conditions Hinged pile condition is recommended
			Top	Modified Bishop Method	Did not consider the influence of pile head

Table 11 (Continued)

Reference	Soil type	Failure type	Recommended location	Case histories or analytical model	Comment
Ausilio *et al.* (2001)	c = 4.7 kPa ϕ= 25°	Circular	Toe	Kinematic approach limit Analysis	-
Joeng *et al.* (2003)	c = 10 kPa, ϕ= 20°	Circular	Middle	ABAQUS Finite element modeling	Uncoupled analysis
Nian *et al.* (2008)	Anisotropic and non-homogeneous	Log-spiral	Toe	Kinematic Limit analysis combined with strength reduction method	-
Wei and Cheng (2009)	c = 10 kPa ϕ = 20°	-	Middle of slope and the middle of the critical slip surface of the slope with no pile	FLAC 3D	-

Source: Ho (2009)

2. Effect of pile length

The pile length for a stabilization of slope is generally penetrated beyond the potential slip surface in order to provide adequate fixity condition and utilize the full pile resistance. There is no absolutely appropriate pile length to be used because it is dependent on the dimension of the slope, the depth of potential slip surface and location of pile within the slope. Several papers related to numerical analysis of slope stabilized with piles usually assumed that the piles are embedded and fixed into the bedrock or a stable layer. There are a few papers study the effect of pile length for stabilizing slope.

Griffiths *et al*. (2010) investigated the effect of pile length on the factor of safety of slope by using finite element method. The slope model used in their study is shown in Figure 55. They found that the influence of pile length depended on its position, as shown in Figure 56. If the pile was driven at the slope vertex or toe, its length has little effect on the factor of safety. For the pile at the optimum location, the factor of safety increased almost linearly with increasing pile length until reaching a stable depth. Beyond 16 m depth, the factor of safety remains constant, as shown in Figure 57.

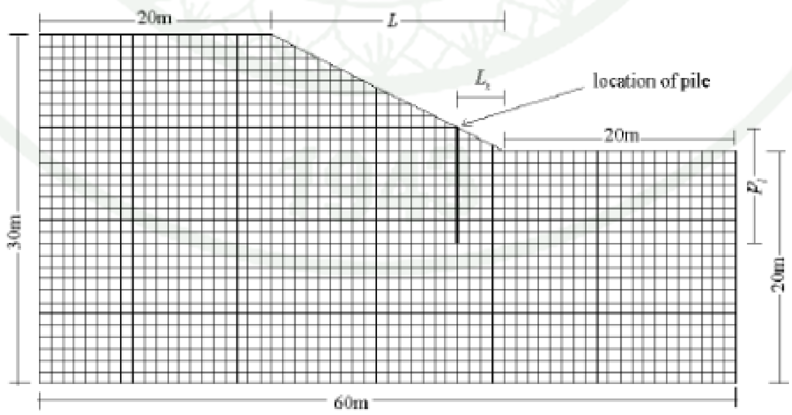

Figure 55 Slope model used in the study of effect of pile length

Source: Griffiths *et al*. (2010)

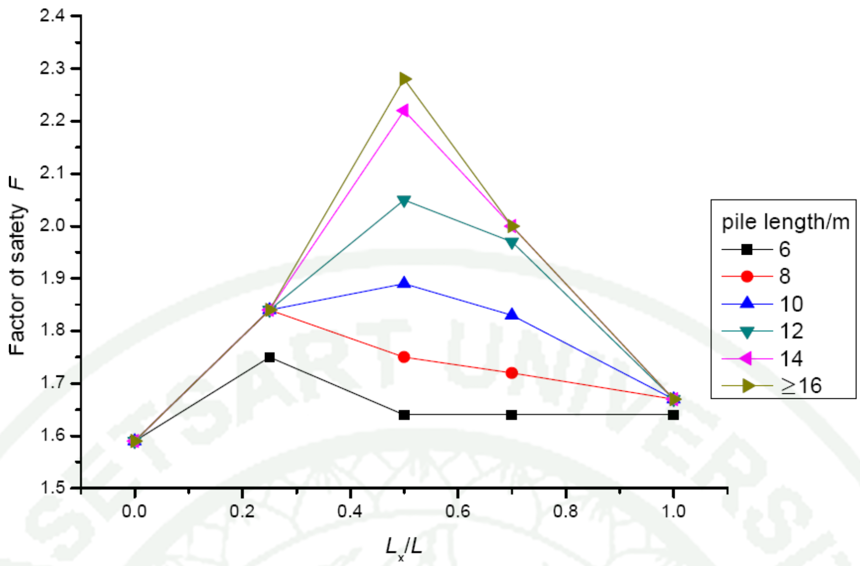

Figure 56 Effect of pile location and length on the factor of safety of slope

Source: Griffiths *et al*. (2010)

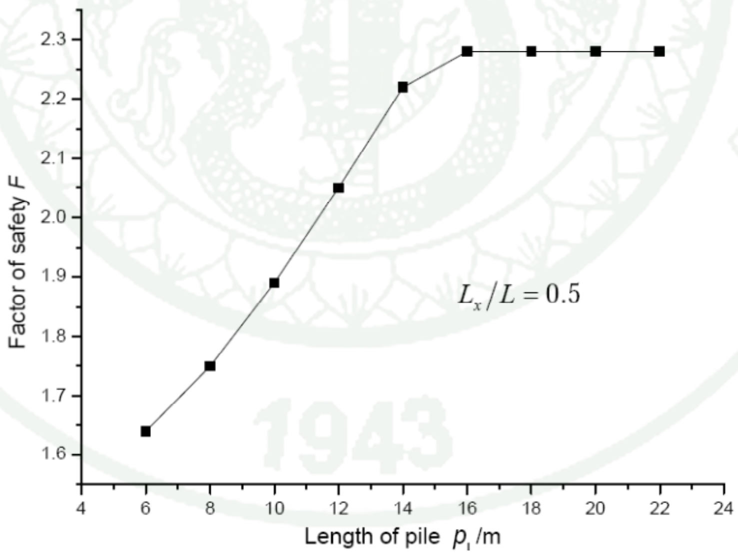

Figure 57 Relationship between factor of safety of slope and pile length

Source: Griffiths *et al*. (2010)

Yang *et al*. (2011) used three-dimensional elastoplastic shear strength reduction method to study the effect of embedded length on the stability of slope. The slope model used in their study is shown in Figure 58. Their results showed that the factor of safety of slope increased with increasing length of piles, as shown in Figure 59. It can be seen that when the embedded pile length exceeded the critical embedded length, the factor of safety approached a constant. However, this length is significantly dependent on the pile spacing and pile head conditions. In addition, they observed the pile behavior for various embedded lengths of pile, as shown in Figure 60. The deflection, bending moment shear stress and pressure of pile increased with increasing pile length. However, they come to be a steady distribution when the pile length is greater than a critical length.

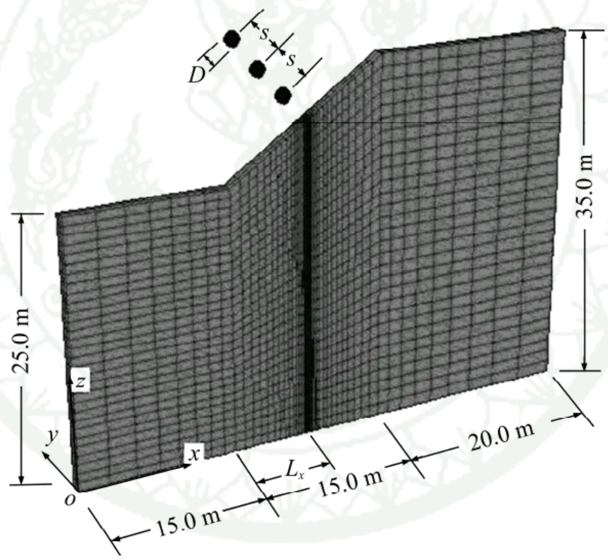

Figure 58 Model of slope and finite element

Source: Yang *et al*. (2011)

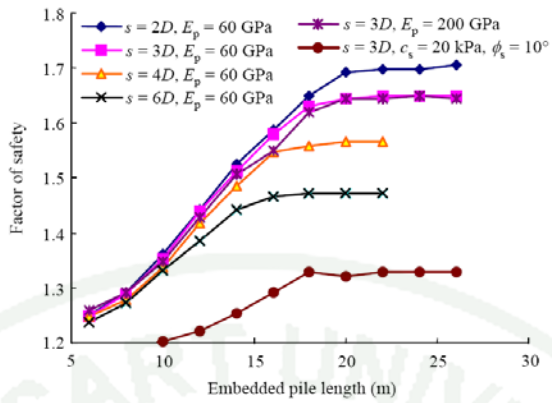

Figure 59 Factor of safety for various pile lengths (Free head condition)

Source: Yang *et al*. (2011)

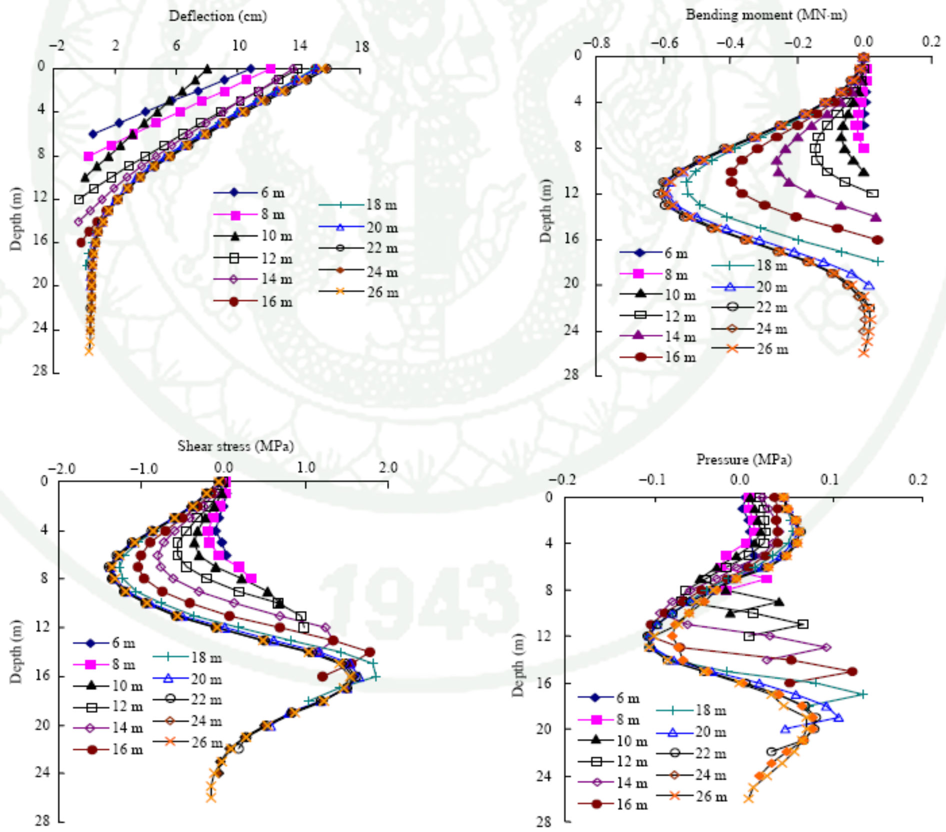

Figure 60 Pile behaviour for free head condition

Source: Yang *et al*. (2011)

Kourkoulis *et al.* (2011) used a hybrid method for analysis slope stabilized with piles. The slope model used in their study is shown in Figure 61. They found that for small embedment length ($L_e = 0.7H_u$), the pile behave as rigid-body rotation without substantial flexural distortion. This similar to the short pile failure mode described by Poulos's (1999). They proposed that the critical embedment depth (L_e) of pile in the stable soil layer should be at least equal to unstable soil depth (H_u).

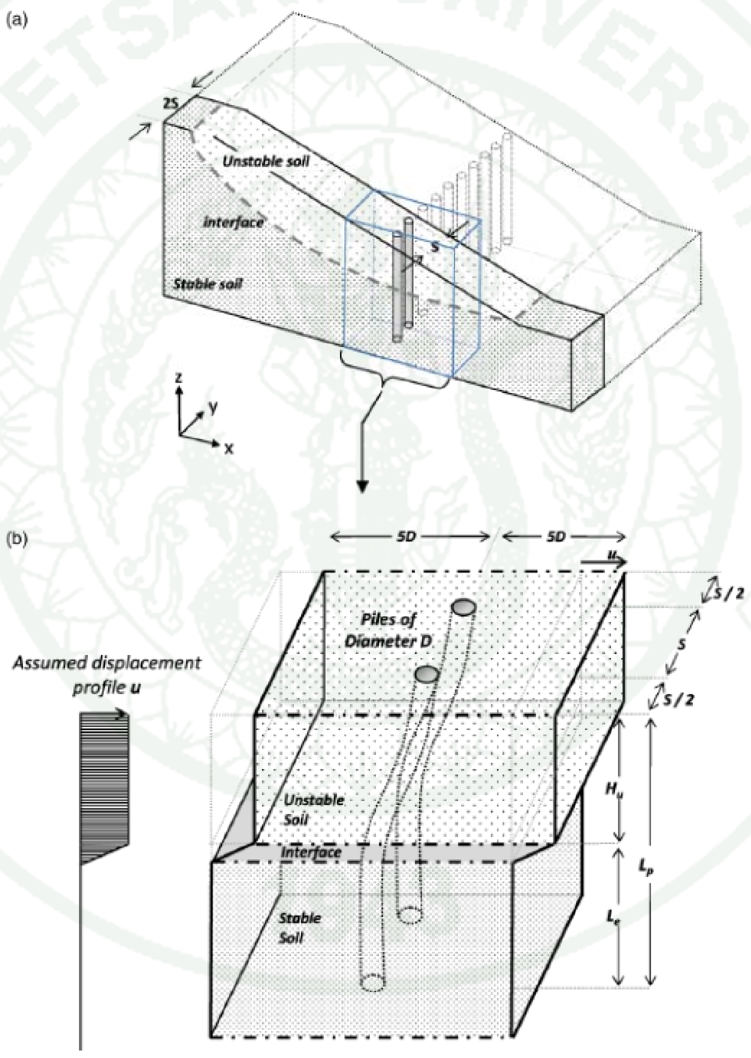

Figure 61 Slope model: (a) slope-soil-pile system; (b) simplified model

Source: Kourkoulis *et al.* (2011)

3. Effect of pile spacing

Wang and Yen (1974) analytically investigated the behavior of piles in a rigid-plastic infinite soil slope. They concluded that there is a critical pile spacing value in both sandy and clayey slopes beyond which almost no aching develops. The arching originates from the stress transfer from the soil to the piles through the mobilization of shear strength (Kourkoulis *et al*., 2011). The stress is transferred from a yielding mass of soil to the adjoining stationary part of the soil (Terzaghi, 1936).

Cai and Uai (2000) studied the effect of pile spacing on the safety factor of slope by using shear strength reduction finite element and Bishop's simplified method. Their results showed that the safety factor increased with decreasing the pile spacing, as shown in Figure 62. They gave the reason that when the pile spacing decreases, the pile become more like a continuous barrier and the influence of soil arching becomes more pronounced. Therefore, the soil does not reach the limit state until the soil is deformed greatly. It can be indicated by the pile deflection in Figure 63, which also shows the bending moment, shear force and pressure acting on the pile.

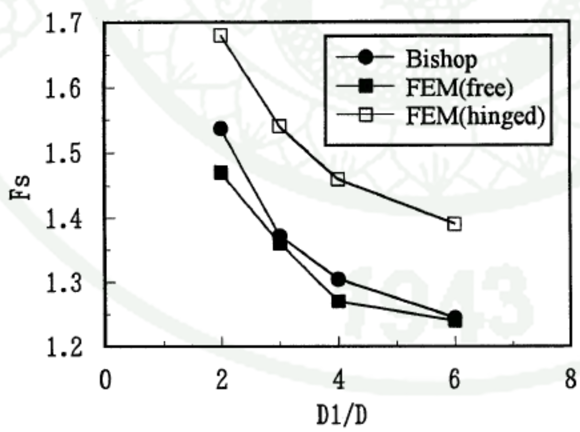

Figure 62 Effect of pile spacing on factor safety: D = pile diameter and D1 center to center spacing

Source: Cai and Uai (2000)

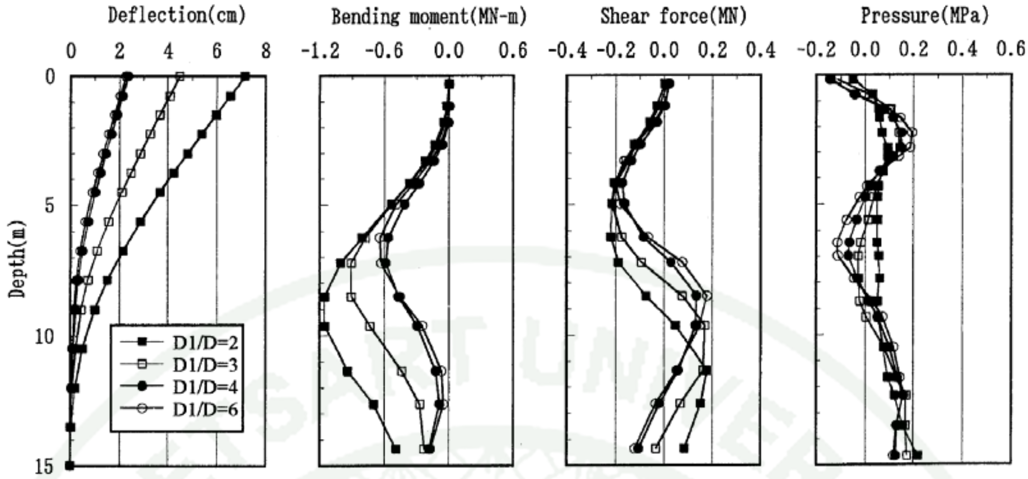

Figure 63 Pile behaviours of free head condition for various pile spacing

Source: Cai and Uai (2000)

Jeong *et al*. (2003) used ABAQUS to study the effect of pile spacing on the safety factor for pile head assumed to be free, unrotated, and hinged condition. The effect of pile spacing on safety factor is shown in Figure 64. The figure showed that the safety factor with hinged head piles was larger than with free head. They suggested that, a restrained pile head is recommended (hinged or fixed), and the free head condition should be avoided.

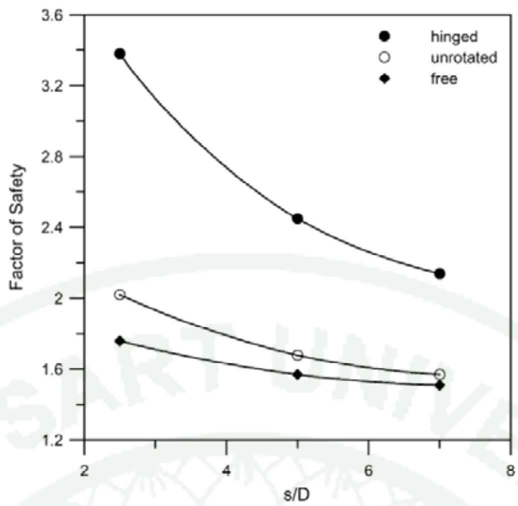

Figure 64 Effect of pile spacing on safety factor

Source: Jeong*et al*. (2003)

Won *et al*. (2005) used FLAC 3D to investigated the effect of pile spacing on the safety factor of the slope for two different pile head conditions. Their results showed that the safety factor increases significantly as the pile spacing decrease (Figure 65). They explained that the lateral soil movement between the piles was more resisted by the piles as the spacing becomes closer. In addition, the pile head conditions have more influence on the safety factor of the slope.

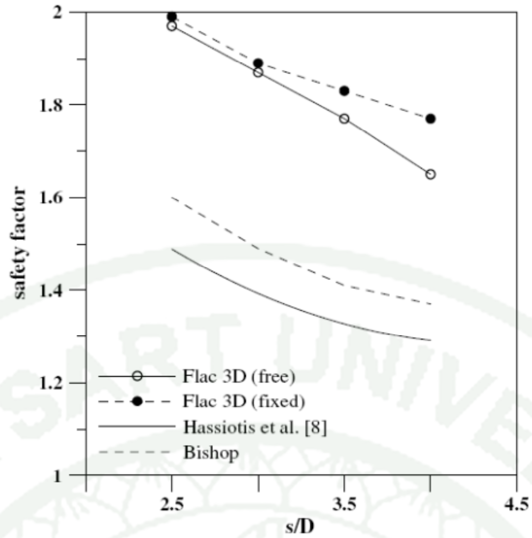

Figure 65 Effect of pile spacing on safety factor at the middle of slope

Source: Won *et al.* (2005)

Yang *et al.* (2011) investigated the effect of pile spacing on the safety factor of slope by using three-dimensional elastoplastic shear strength reduction method. Their results is similar to previous studies that discussed above (Cai and Uai, 2000; Jeong *et al.*, 2003; Won *et al*., 2005). Their results showed that when the pile spacing decreases, the pile become more like a continuous pile wall and integrity of soil and piles becomes larger. Therefore, the lateral bearing capacity of reinforced slope had greatly improved. They explained their assumption by the pile behavior for various pile spacing, as shown in Figure 66. As the pile spacing increased, the bearing capacity of single pile increased. This was because the loading zone by the lateral soil movement of single pile increased.

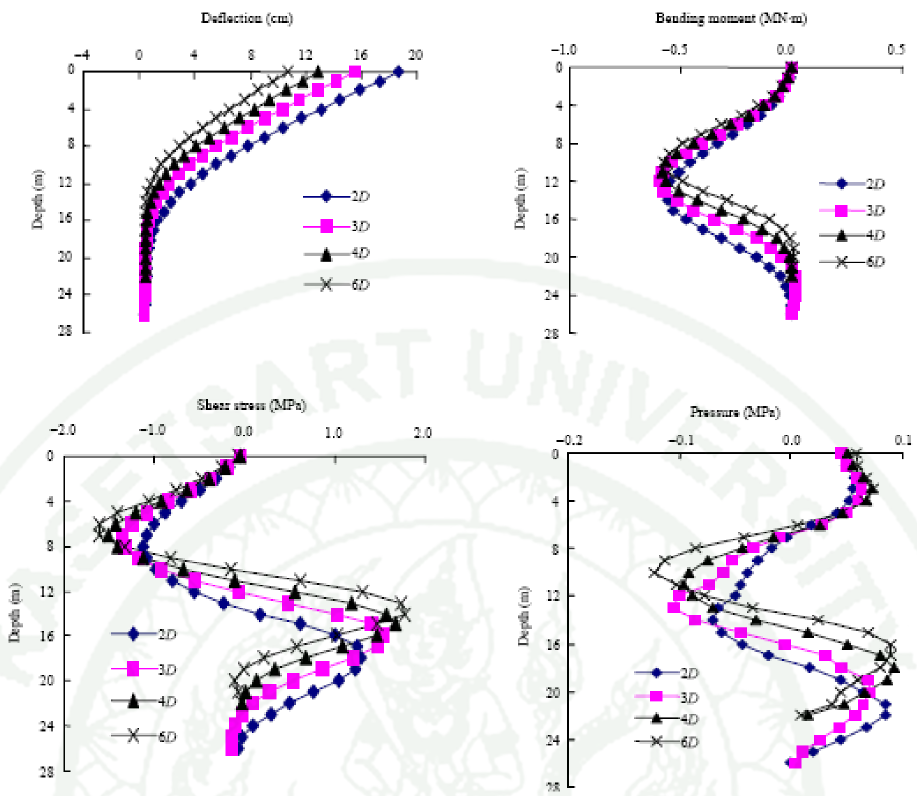

Figure 66 Pile behaviour for free head condition

Source: Yang *et al.* (2011).

Kourkoulis *et al.* (2011) used finite element model to determine the effective pile spacing for stabilized slope with piles. They found that the pile spacing of 4 diameters ($S = 4D$) was the most cost-effective pile spacing, because it was the largest spacing that can still generate soil arching between the piles. While the pile spacing was greater than 5 diameters ($S \geq 5D$), the pile behaved almost as single isolated piles, and the soil can flow between them. Figure 67 illustrated comparison between two extreme cases: a very dense configuration in which pile spacing is S = 2D, where soil arching was guaranteed. And a configuration with large spacing S = 7D, where the piles were so far that soil flowed between them (i.e., no arching develops).

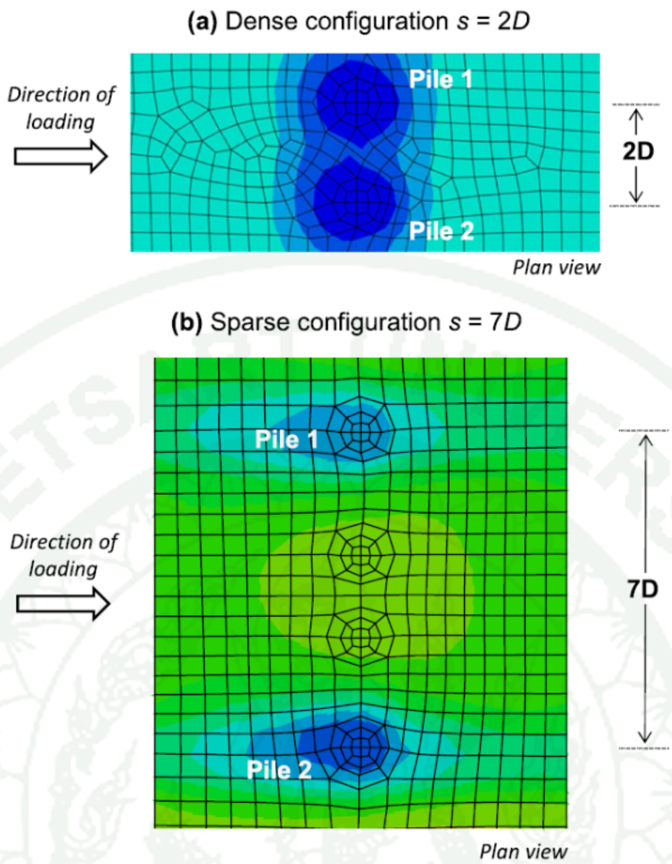

Figure 67 Soil arching between piles: contour of horizontal displacement

Source: Kourkoulis *et al.* (2011)

Hayward *et al.* (2000) carried out a series of centrifuge tests, shown in Figure 68, to investigate the use of discrete piles for slope stabilization. A slope without piles, and with piles spaced at about 3, 4and 6 pile diameters (*d*) were modeled, and the long term behavior was then investigated. Their results showed that the slope without piles and with piles spaced at 6*d* failed while others did not. Figure 69 shows the plan view of displacement vector at the end of test for the pile spacing at 3d and 6d. It is found that soil flow between pile spacing of 6d was more than of 3d spacing. They explained that when the spacing between piles increased to a certain distance then pile behaves like a single isolated pile with piles interaction. The increase in the pile spacing also increase the bending moment developed on the piles, as shown in

Figure 70. This is because when the piles are installed at a large spacing, each pile has to resist a wider strip of the lateral load.

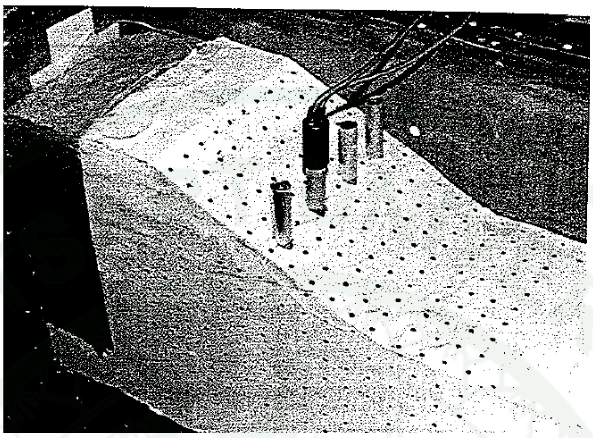

Figure 68 Photograph taken at end of test where piles were spaced at 3 d center-to-center spacing

Source: Hayward *et al.* (2000)

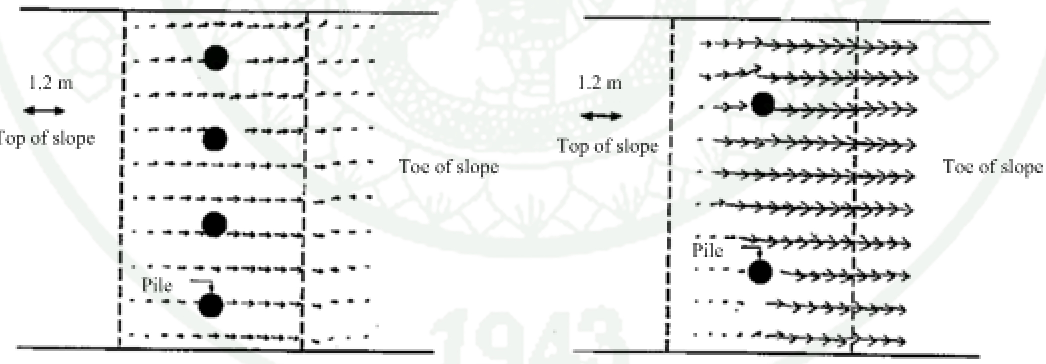

(a) 3d (b) 6d

Figure 69 Plan view of displacement vectors measured in centrifuge tests for piles spaced at 3d and 6d

Source: Hayward *et al*. (2000)

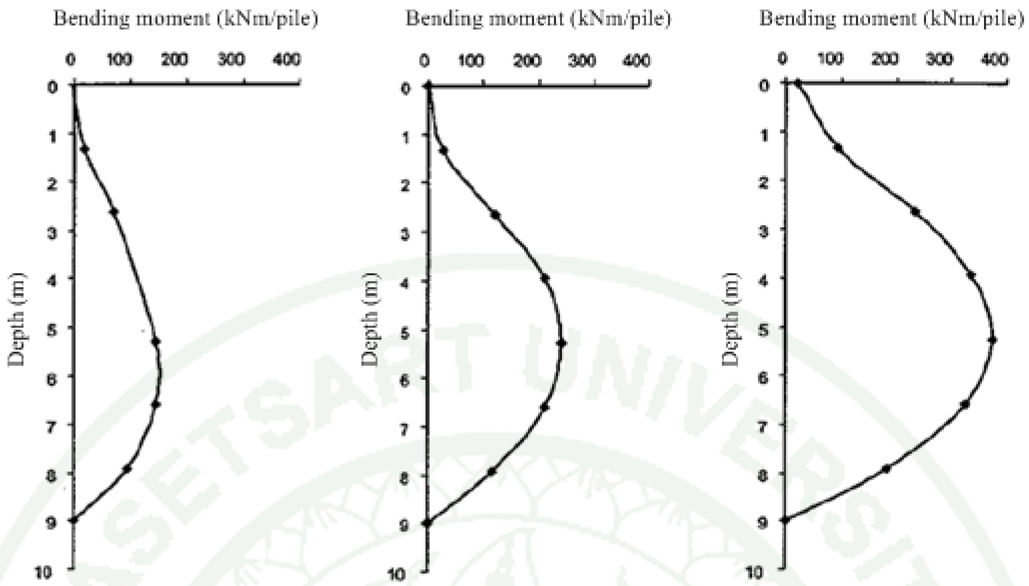

(a) 3d (b) 4d (c) 6d

Figure 70 Measured bending moment profiles of piles spaced at 3d, 4d and 6d

Source: Hayward *et al*. (2000)

Potential failure mechanism of laterally loaded piles

The resisting force which each pile can provide against the sliding soil mass depends on several factors including the diameter, length and stiffness of the pile, the length of pile embedded into the firm layer, the size and extent of the slipping mass and the stiffness of the soil layer (Kanagasabai, 2010). There are two main types of potential failure mechanism for laterally loaded piles classified by Kanagasabai (2010), as shown in Figure 71. The first group involves a flow of soil around the pile associated with failure of the soil if the pile can be designed with sufficient bending capacity (Figure 71a and b). The second group concerns with the formation of one or more plastic hinges in the pile (Figure 71c). The plastic hinges will form at the points where maximum bending moments occur.

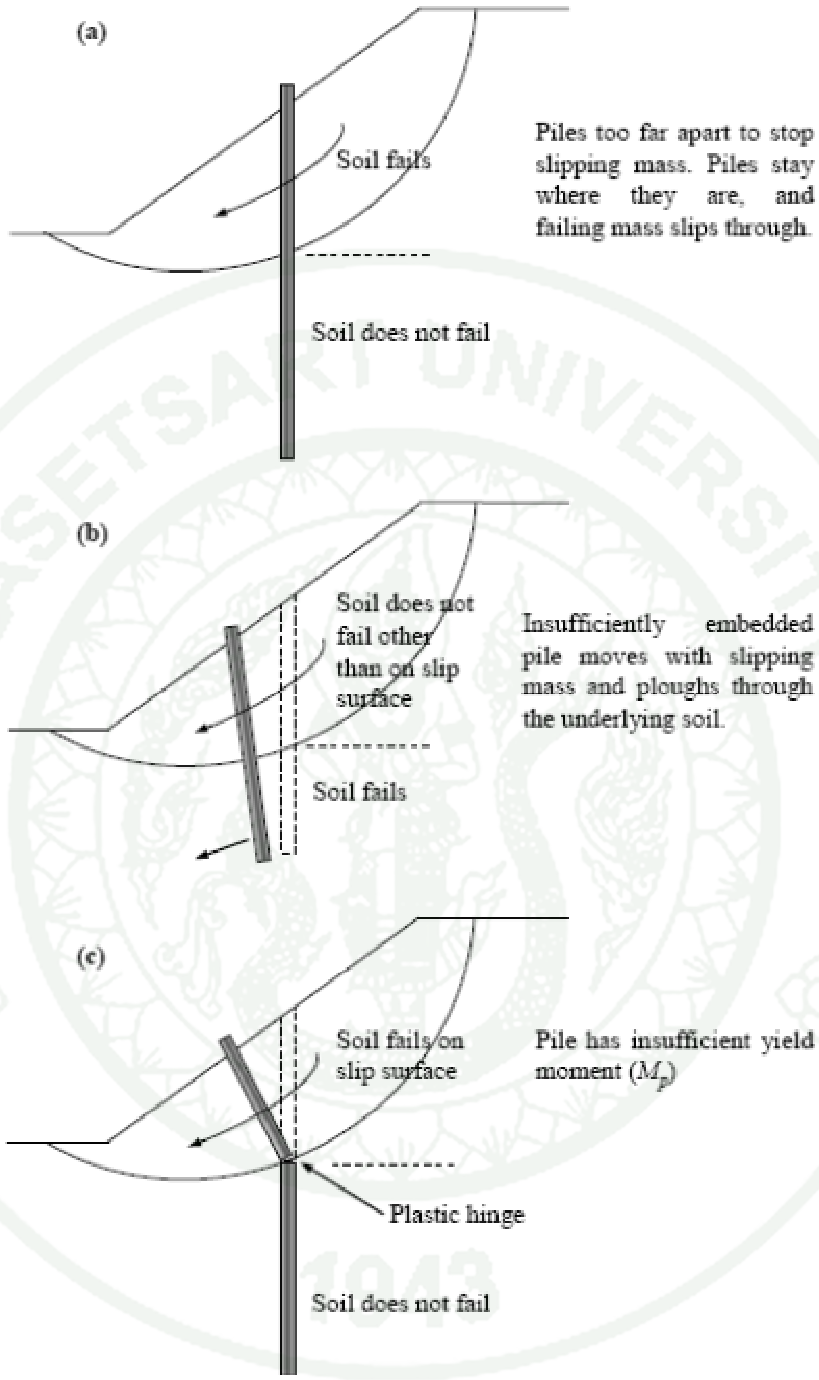

Figure 71 Potential failure mechanisms in the laterally loaded piles

Source: Kanagasabai (2010)

Poulos (1995) carried out a number of simplified boundary element analyses using a computer program, *ERCAP* (CPI, 1992), to present an approach for design of slope stabilizing piles by assessing their response to lateral ground movement. He reported three different failure modes of slope stabilizing piles (Figure 72).

1. Flow mode: when the depth of the slip plane is shallow, the unstable soil becomes plastic and flows around the stationary pile (Figure 72a).

2. Intermediate mode: when the soil strength in both the unstable and stable soil is mobilized along the pile length (Figure 72b).

3. Short pile mode: when the slip plane is relatively deep and the length of the pile in the stable soil is relatively shallow, the unstable sliding soil carries the pile through the stable soil layer (Figure 72c).

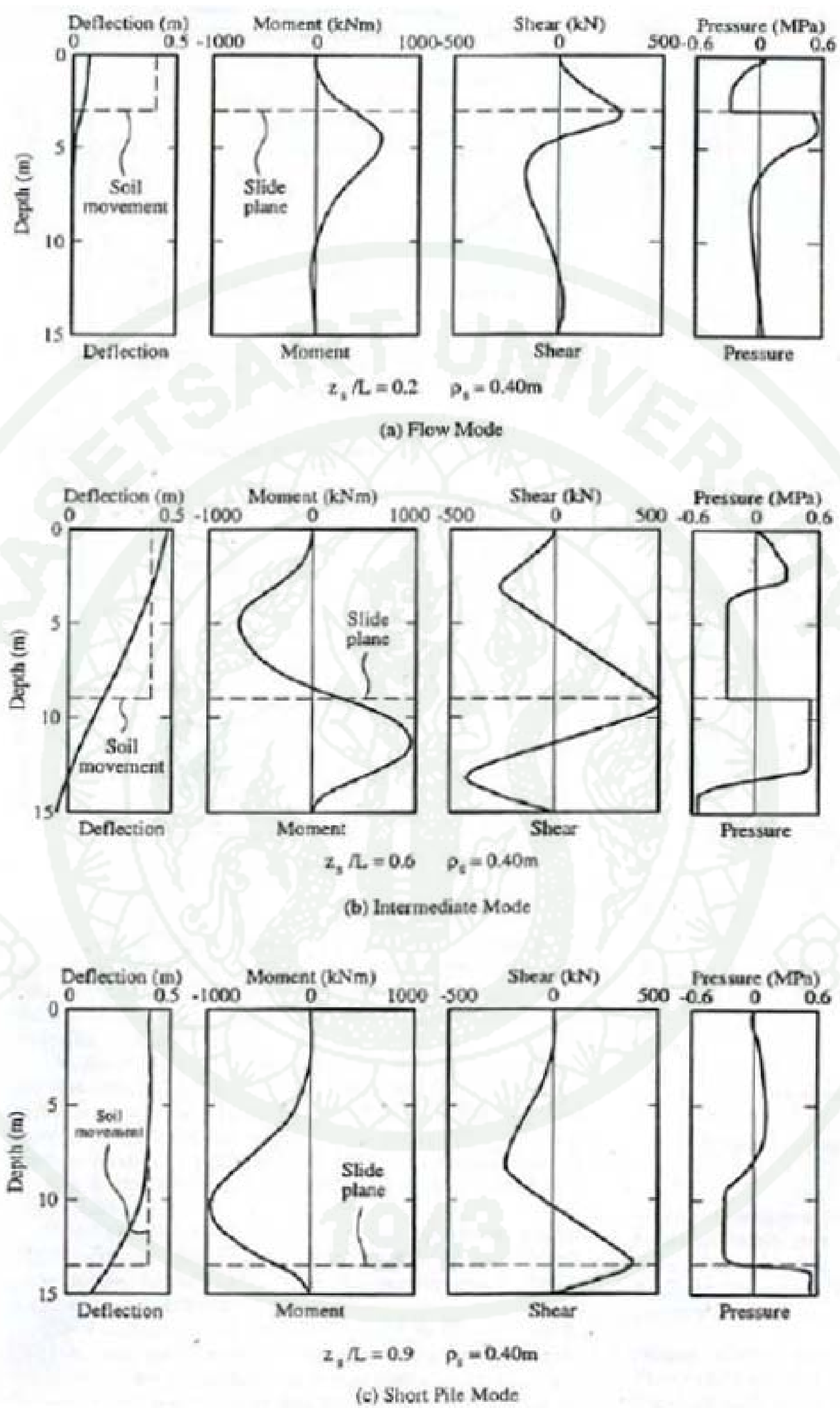

Figure 72 Pile behavior characteristics at ultimate loading state

Source: Poulos (1995)

Three Dimensional Finite Element Analysis

Over the last few decades, the finite element analyses (FEA) have been increasingly used in the design and analysis of geotechnical systems. FEA can provide information on stability and displacements over time and, in many situations. The PLAXIS 3D FOUNDATION software is a reasonably new finite element program for geotechnical applications in which various soil models can be used to simulate soil behavior in three dimensions. This program consists of three main parts which is Model, Calculation and Output mode.

1. Model mode:

In the model mode, the boundary condition, problem geometry and materials are defined. The geometry is defined by vertical "boreholes" and horizontal "work planes". The boreholes are used to define the soil stratigraphy, ground surface level and pore water pressure distribution. Soil layers and ground surface may be non-horizontal by using several boreholes at different location. And the work planes are used to define geometry points, geometry lines, clusters, loads, boundary conditions and structures. After creating the 2D geometry model in a work plane, the 2D mesh is first generated. Then, the 3D mesh is created by vertical mesh that connects the work plane meshes together, with taking account in to the soil profiled.

2. Calculation:

A number of calculation phases can be defined in the calculation mode. Different load cases and geometries are set to simulate a realistic construction sequences. For every step, different groundwater conditions can be set, and construction elements could be activated or deactivated. The calculation mode must be defined including *plastic*, *consolidation* or *phi/c reduction*. The *plastic* calculation is used to analyze the elastic-plastic deformations according to small deformation theory. The *consolidation* analysis is used when modeling time dependent behaviours such as development and dissipation of excess pore pressures and settlement calculation when creep deformations are requested. The result is depending on the choice of material model.

The *phi/c reduction* is a safety analysis that will calculate the global factor of safety and is executed by stepwise reduction of the strength parameters of the soil. This iteration process proceeds until failure occur somewhere in the model. The safety factor, M_{sf}, is then calculated by the relation between the input strength parameters and the stepwise reduced strength parameters when failure occurs, see Equation 22. Note that *phi/c reduction* will not reduce the strength parameters of the structural elements such as plates and anchors.

$$\Sigma M_{sf} = \frac{tan\phi_{input}}{tan\phi_{reduced}} = \frac{c_{input}}{c_{reduced}} \qquad (22)$$

3. Output mode

In the third main part of PLAXIS is the output mode and is used for post processing of the calculation result. Deformations, strains and pore-pressures are visualized for every phase of the calculation and for construction elements bending moments and shear forces can be studied.

Mesh Generation

To perform finite element calculations, the geometry has to be divided into elements. A composition of finite elements is called a finite element mesh. When the geometry model is fully defined and material properties have been assigned to all soil layers and structural objects, it is recommended to first generate a 2D mesh of work planes. The 2D mesh should be made fully satisfactory before proceeding to the 3D mesh generation. If the 2D mesh is satisfactory, 3D mesh generation can be performed. The 3D mesh generation process will take the information from the work planes at different levels as well as the soil stratigraphy from the boreholes into account. The 3D FOUNDATION program allows for a fully automatic generation of 2D and 3D finite element meshes.

Element

The basic soil elements of a 3D finite element mesh are the 15-node wedge elements, as shown in Figure 73. These elements are generated from the 6-node triangular elements as generated in a PLAXIS 2D mesh. Due to the presence of non-horizontal soil layers, some 15-node wedge elements may degenerate to 13-node pyramid elements or even to 10-node tetrahedral elements. The 15-node wedge element is composed of 6-node triangles in horizontal direction and 8-node quadrilaterals in vertical direction. The accuracy of the 15-node wedge element and the compatible structural elements are comparable with the 6-node triangular element and compatible structural elements in a 2D PLAXIS analysis.

The soil elements, special types of elements are used to model structural behavior. For beams, 3-node line elements are used, which are compatible with the 3-noded sides of a soil element. In addition, 6-node and 8-node plate elements are used to simulate the behavior of walls and floors. Moreover, 12-node and 16-node interface elements are used to simulate soil-structure interaction.

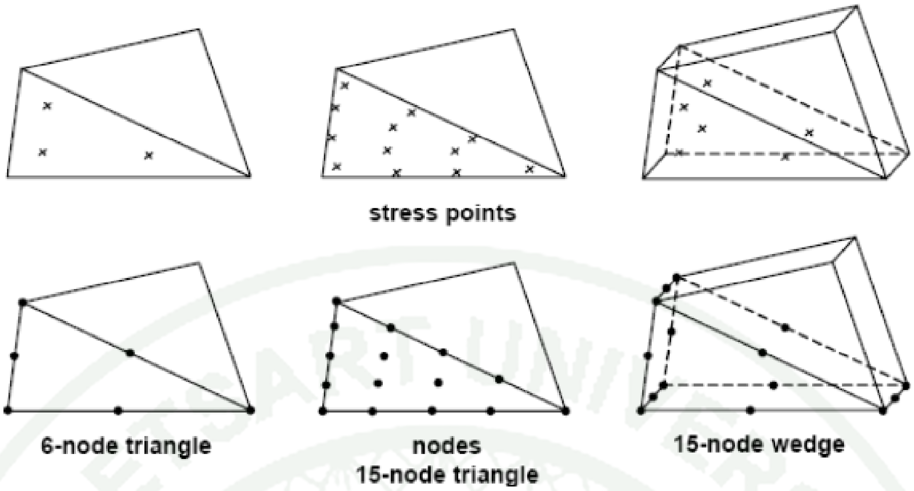

Figure 73 Comparison of 2D and 3D soil element

Source: Brinkgreve and Swolfs (2007)

Volume pile elements

The geometry of the volume piles is defined vertically by specifying two work planes, between which, the piles should be drawn. The piles are then defined horizontally by choosing a cross section. There are five different cross section types available; massive circular pile, circular tube pile, massive square pile, square tube pile and user-defined pile shape. The tube piles (i.e. hollow piles) are composed of wall elements and the massive piles are composed of volume elements. The material properties are subsequently assigned to the piles. All pile types have interface elements (optional), which are placed at the periphery of the piles. These are implemented to model the interaction between the piles and the surrounding soil, such as the shaft resistance.

Modeling of soil behavior

Three major soil models are available in PLAXIS 3D FOUNDATION; Mohr-Coulomb model (MC), Hardening Soil model (HS) and Soft Soil Creep model (SSC). The MC model is generally recommended for first analysis of complex geotechnical problems or the basic for numerical analysis when soil parameters are not well known with great certainty. The basic principle of this model is explained below.

The MC model is a linear elastic perfectly plastic model. It is assumed that the soil resistance increases linearly with displacement, until the failure criterion is reached. This model describes material behavior as elastic within a certain defined area and outside of it plastic, as shown in Figure 74.

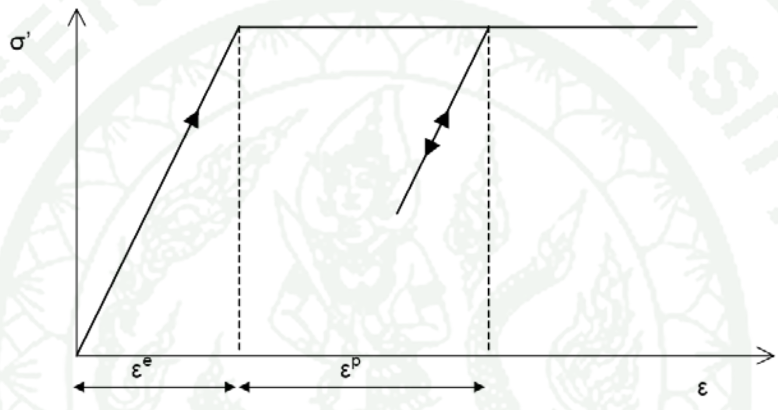

Figure 74 Basic idea of an elastic perfectly plastic model

Source: Brinkgreve and Swolfs (2007)

The model requires five basic input parameters, namely a Young's modulus (E), a Poisson's ratio (v), a cohesion (c), a friction angle (□), and a dilatancy angle (ψ). To understand the five basic model parameters, typical stress-strain curve for dense sand or over-consolidated clays as obtained from standard drained triaxial test are compared with the MC model, illustrated in Figure 74. The figure gives an indication of the meaning and influence of the five basic model parameters.

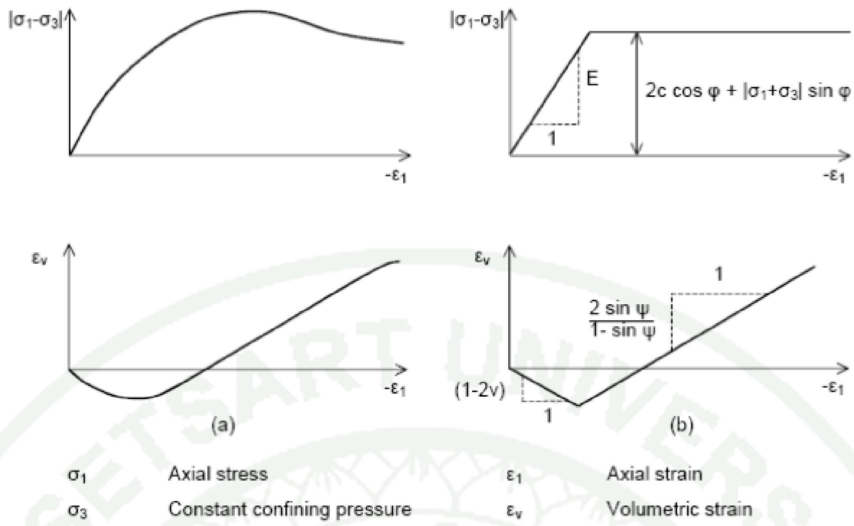

Figure 75 Drained triaxial test of dense sand or over-consolidated clay (a) Results from standard drained triaxial tests and (b) elastic-plastic model

Source: Brinkgreve and Swolfs (2007)

Type of material behavior (Material type)

In principle, all model parameters in PLAXIS are meant to represent the effective soil response, i.e. the relation between the stresses and strains associated with the soil skeleton. An important feature of soil is the presence of pore water. Pore pressures significantly influence the soil response. To enable incorporation of the water-skeleton interaction in the soil response PLAXIS offers for each soil model a choice of three types of behavior:

Drained behavior

Using this setting no excess pore pressures are generated. This is clearly the case for dry soils and also for full drainage due to a high permeability (sands) and/or a low rate of loading. This option may also be used to simulate long-term soil behavior without the need to model the precise history of undrained loading and consolidation.

Undrained behavior

This setting is used for a full development of excess pore pressures. Flow of pore water can sometimes be neglected due to a low permeability (clays) and/or a high rate of loading. All clusters that are specified as undrained will indeed behave undrained, even if the cluster or a part of the cluster is located above the phreatic level. The input soil parameter can be divided into two ways. The first is by adopting effective parameters i.e. E', ν', c', ϕ'. The second is by adopting undrained parameter, i.e. E_u, ν_u, c_u (s_u), ϕ_u. The latter option is used for this research.

Non-porous behavior

Using this setting neither initial nor excess pore pressures will be taken into account in clusters of this type. Applications may be found in the modeling of concrete or structural behavior. Non-porous behavior is often used in combination with the linear elastic model. The input of a saturated weight is not relevant for non-porous materials.

Suvarnabhumi Drainage Canal Project: A Case Study

September 29, 2005, was opening date ceremony for Suvarnabhumi International Airport. The area surrounding airport locates in the eastern part of the lower Chao Phraya River basin which is the low lying plain area. Therefore, the flooding problem often occurs during the rainy season influencing the airport. The Royal Irrigation Department contacted three education institutions, the Faculty of Engineering Kasetsart University, the Asia Institute of Technology, and Thammasart University, to carry out survey and design for drainage canal at the tender design level. The immediate action plan requires the digging of a new canal from the Samrong Canal to the sea, the building of pumping stations and the installation of a telemetry system, as shown in Figure 76. Moreover, a two-lane roadway is constructed on each of the canal for transportation. Water from the vicinity of the airport will be drained to the sea through this new canal, as shown in Figure 77, which also shows the location of project.

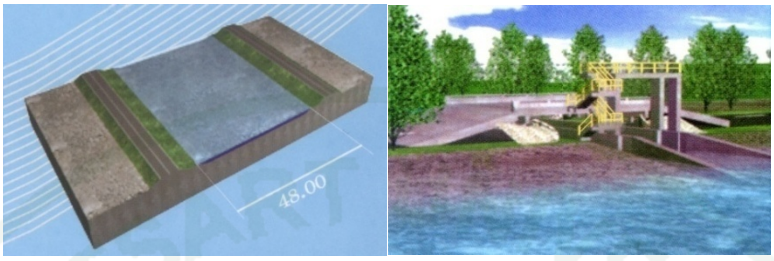

(a) drainage canal and roadway b) Floodgate

(c) Pumping station (d) Water bridge

Figure 76 Constructions in the Suvarnabhumi Drainage Canal Project

Figure 77 Project location

The project, called as "Suvarnabhumi Drainage Canal Project", located at Samutprakan province, Thailand (Figure 77).The project is divided into three sections with different contractors, illustrated in Figure 78:

Section I consists of the digging of drainage canal and the roadway from 0+000 to 5+000 km.

Section II consists of the digging of drainage canal and the roadway from 5+000 to 10+000 km.

Section III consists of the digging of drainage canal, the roadway, pumping station as well as water bridge from 10.00 to 12+650 km.

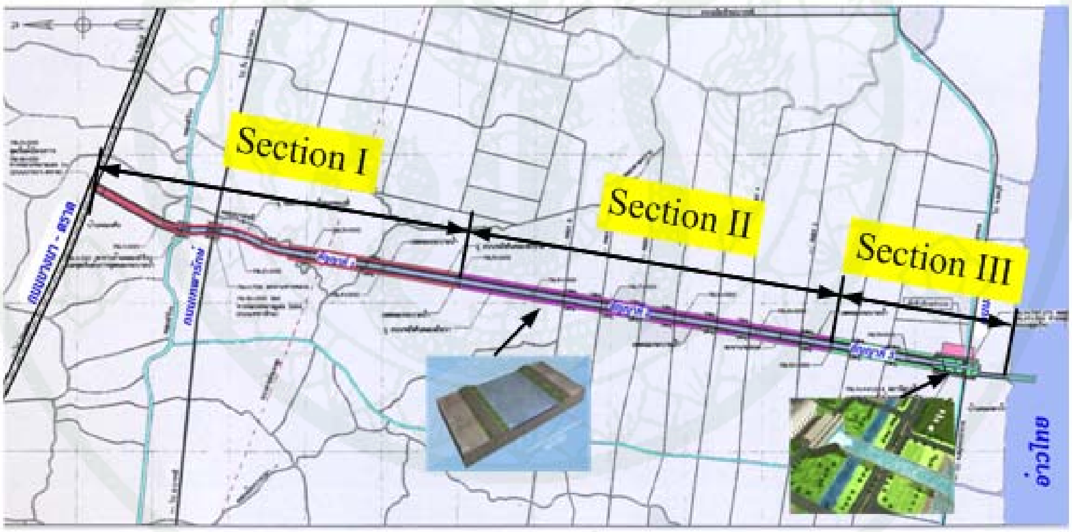

Figure 78 Divide of section for construction

Source: Rojkansadarn (2009)

Soil profiles and their properties along the project

Figure 79 shows the subsoil profile as interpreted by Rojkansadarn (2009) from 50 boreholes close to the project and the position of borehole drilled at the project. The general soil profile consisted of the deltaic sediment of approximately 12 m to 18 m of soft normally consolidated clay, which is highly compressible clay. This sediment was underlain by medium stiff clay of thickness 2 to 7 m, followed by stiff clay and sand.

The properties of soil from the 8 boreholes drilled in the project are shown in Figure 80. The natural water content approximately close to liquid limit and high water content is noted in depth range 3 to 8 m (80% to 140 %), followed by lower water content for deeper layer. The shear strength typically increases with depth, and the low shear strength is encountered in the depth range of 3 to 8 m, corresponding to the high natural water content.

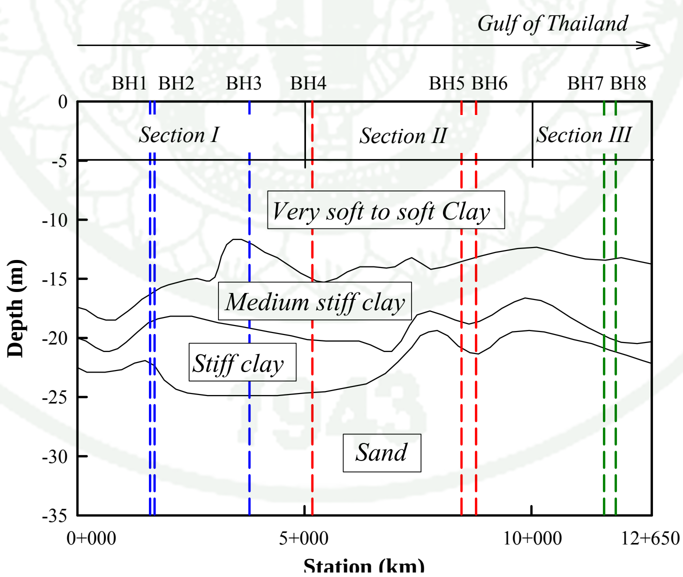

Figure 79 Soil profiles along the project

Source: Rojkansadarn (2009)

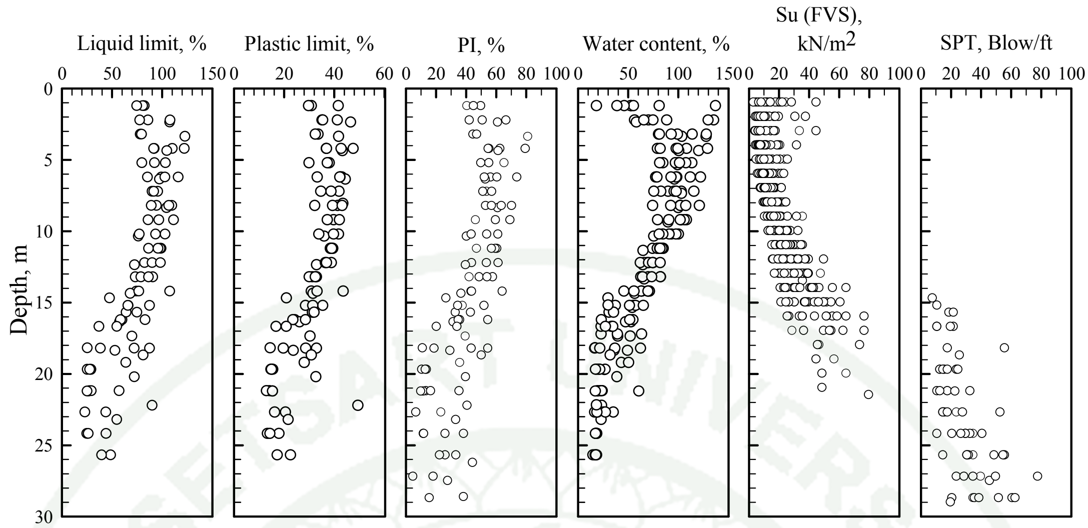

Figure 80 Physical properties, water content, vane shear strength, and standard penetration test

Source: Rojkansadarn (2009)

Original Design of DCM columns

The design criterion of this project is given in Table 12. To provide the safety factor of 1.3 during the construction period and 1.5 during the serviceability, a ground improvement technique by deep mixing (DCM) method was used for stabilizing soil foundation. The typical cross-section of canal in each section is presented in Figure 81 and 82. The DCM columns under the roadway (which are called the bearing DCM columns) were 0.6 m in diameter and were installed in a rectangular pattern at 1.50 X 1.75 m spacing. Seven tangential DCM columns (which are called the tangential DCM columns) were installed in a row pattern at the canal slope with a spacing of 1.50 m. It is noted that the DCM column row of the Section II and III is designed to be 1.0 m from the canal edge.

The construction plan was divided into four stages: first the DCM columns were installed; second, the roadway with a height of 1.2 m was constructed using silty sand fill material; third, the canal was constructed with a depth of 3.0 m; finally, the roadway was built to a full height of 2.4 m.

Table 12 Design criterion for Suvarnabhumi Drainage Canal project

Criteria	Construction period	Service period
Live Load	20 kPa	10 kPa
Factor of Safety	1.30	1.50
Allowable Settlement of Roadway	<0.30 m. in 20 years	

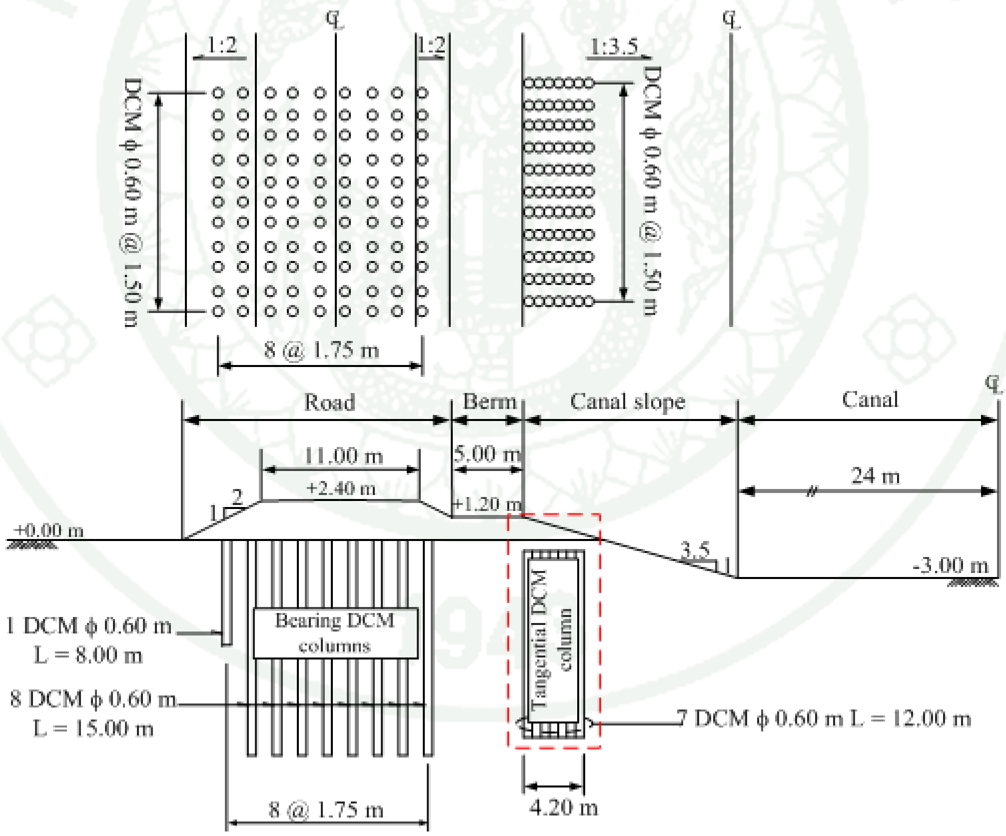

Figure 81 Typical cross-section of canal at Section I

Source: Rojkansadarn (2009)

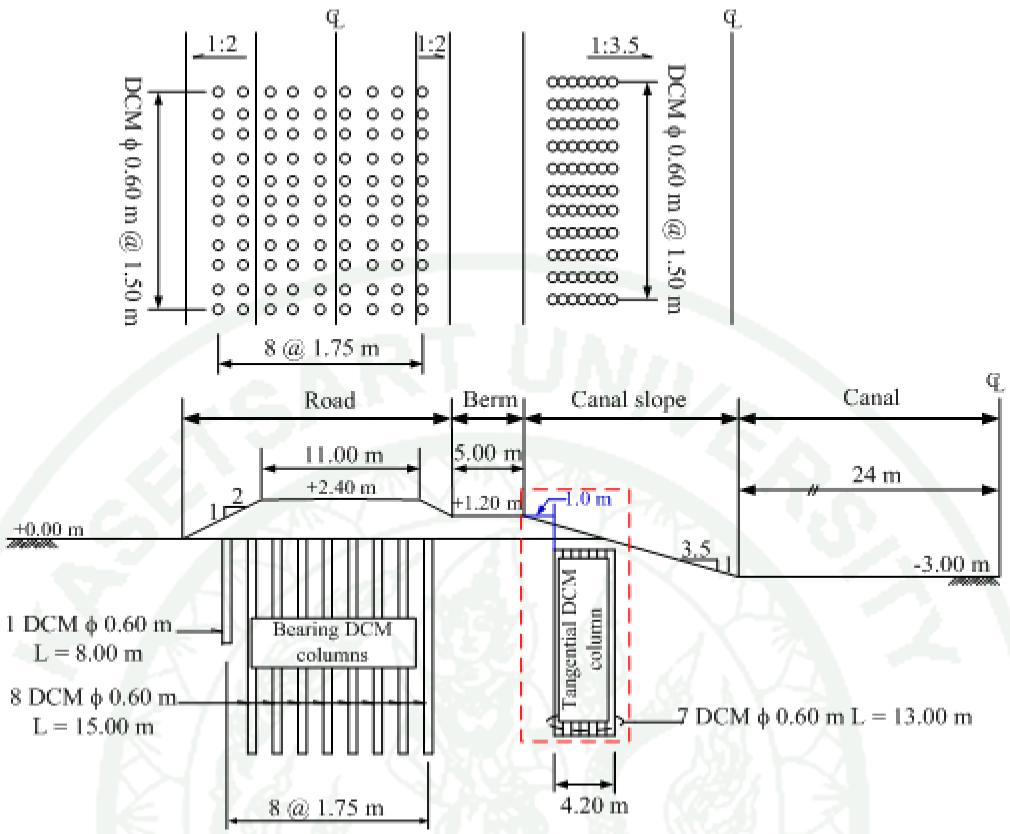

Figure 82 Typical cross-section of canal at Section II and III

Source: Rojkansadarn (2009)

Installation of DCM columns

Four techniques of DCM installation were proposed in this project namely: low pressure mechanical mixing (Section I), jet grouting and modified dry mixing (Section II) and high pressure mechanical mixing (Section III). The required compressive strength of DCM pile is 600 and 1000 kN/m^2 for bearing DM columns and row DM columns, respectively. To reach the required compressive strength, 220 kg/m^3 of cement is used. Because the low strength and non-homogeneous of columns from traditional dry mixing method occurred during a field trial, the modified dry mixing method was employed. The principles of the system are shown in Figure 83. The dry binder is fed pneumatically during installation. At the same time, water is added through separate injection ports on the mixing tool.

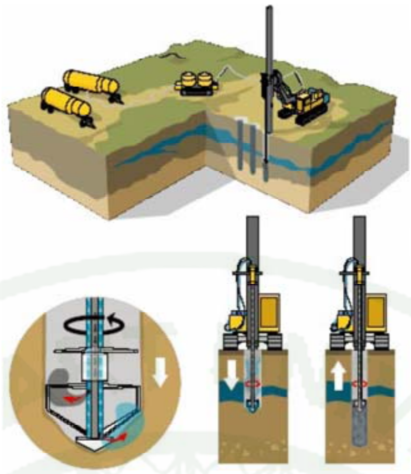

Figure 83 Principles of modified dry mixing method

Source: Eriksson *et al.* (2005)

Field strength and elastic modulus of DCM column

Rojkansadarn (2009) collected the strength and elastic modulus data of DCM columns obtained from field specimens and performed statistical analysis. Table 13 presented the average undrained shear strength in each mixing method. The average undrained shear strength was found to ranges from632to 1047kN/m^2. The highest average undrained shear strength is encountered in the modified dry mixing method. He concluded that the mixing method and natural water content significantly affect on the undrained shear strength of DCM columns. As for average elastic modulus (at 50% of q_u), which shown in the Table 14, it varies between 229,790 and 314,010 kN/m^2. The modified dry mixing method gives the highest value of average elastic modulus. He also evaluated the correlation between elastic modulus and undrained shear strength, as given in Table 15 based on the Coefficient of Determination (r^2) more than 0.40.

Table 13 Variation of undrained shear strength of DM columns by different methods

Section	Method	N	Undrained Shear Strength, (kN/m^2)			
			Max	Min	Mean	SD
1	Low Pressure	524	1470.00	270.00	630.22	23.79
2	Low Pressure	463	1680.00	310.00	760.74	27.19
2	Jet Grouting	226	2090.00	310.00	870.58	44.55
2	Modified Dry Mixing	116	2290.00	180.00	1040.73	32.82
3	High Pressure	492	1470.00	130.00	710.95	25.35

Source: Rojkansadarn (2009)

Table 14 Variation of elastic modulus of DCM columns by different methods

Section	Method	N	Modulus of Elasticity, (kN/m^2)			
			Max	Min	Mean	SD
1	Low Pressure	564	1957550	29260	229790	14905
2	Low Pressure	463	782040	60940	262110	10860
2	Jet Grouting	226	753000	85710	302090	15312
2	Modified Dry Mixing	131	956660	100000	314010	12931
3	High Pressure	547	1451000	25830	161940	14771

Source: Rojkansadarn (2009)

Table 15 Correlation between elastic modulus and undrained shear strength of DCM column (r^2>0.4)

Method	Correlation	r^2	N
Low Pressure	E_{50} = 319 S_u	0.613	1974
Jet Grouting	E_{50} = 320 S_u	0.419	452
Modified Dry Mixing	E_{50} = 281 S_u	0.734	232

Source: Rojkansadarn (2009)

METHODOLOGY

To achieve the objective of providing guideline for design and construction of stabilized slope with DCM columns, a systematic procedure was followed in Figure 84.

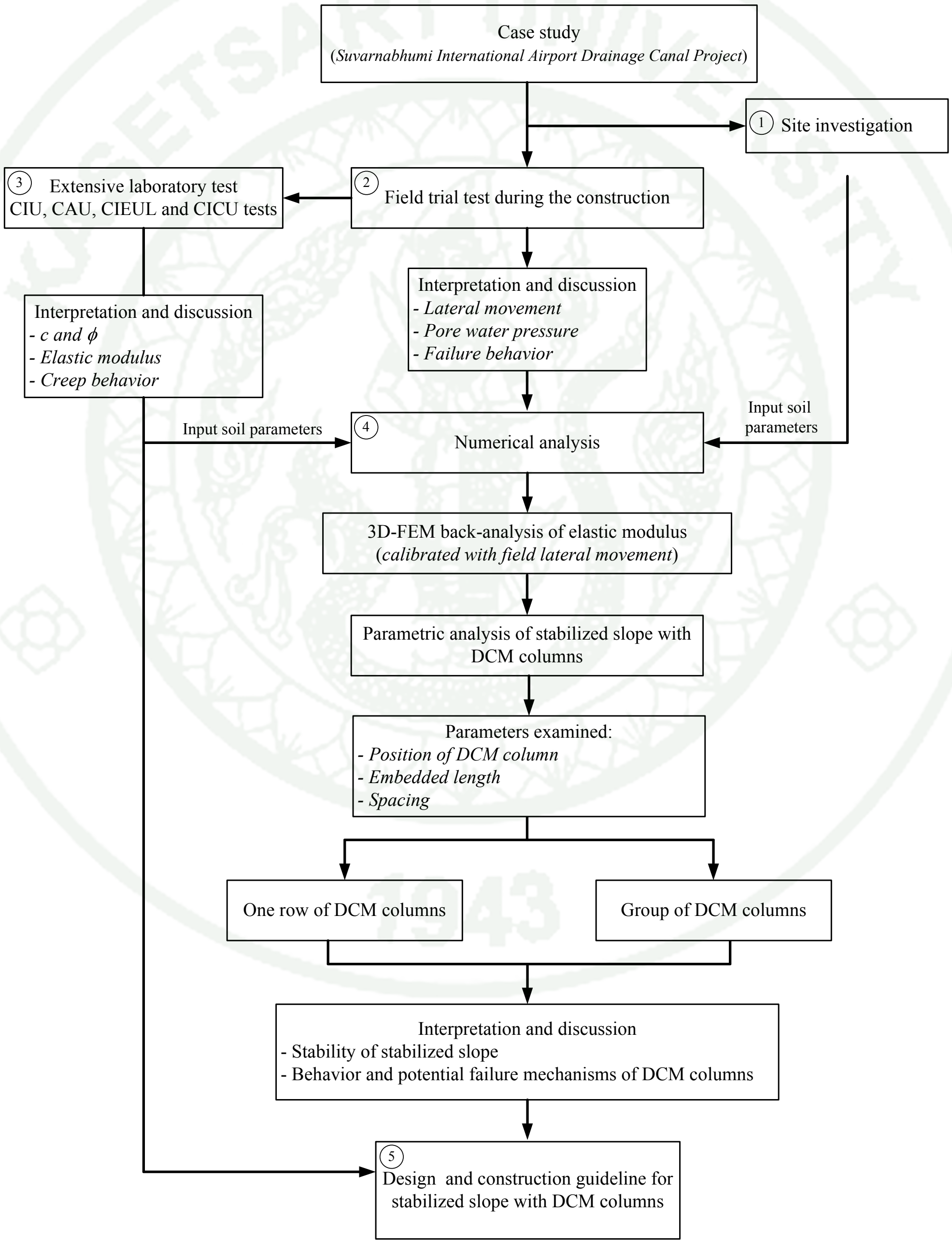

Figure 84 Flowchart of methodology

Site investigation

Field and laboratory testing results close to the field trial tests were collected to investigate the geotechnical properties of soils and provide input soil parameter for finite element analysis. The field testing data include standard penetration tests (SPT) and field vane shear test. The laboratory testing data consists of that standard classification and tests involved in determining the engineering properties of soils.

Field trials during the construction

The field trial tests at the Section I and II selected as a case study in this research. The field data were interpreted on the lateral movement and excess pore water pressures. From the lateral movement measurements, field value of soil stiffness was evaluated. The geotechnical problems and solutions encountered during the construction were also reported.

Laboratory tests

Extensive laboratory tests related to the field behaviour were carried out to characterize the undrained strength and deformation behavior of soft clay. The test results were then used for numerical analysis. The testing program consists of undrained triaxial test under compression, extension and creep test. The notation and details of all tests are summarized in Table 16 and 17, respectively. The result from laboratory tests was compared with the previous researches on Bangkok clay and other clays.

Table 16 Description for triaxial test notations

Notations	Descriptions	No. of test
CIU	Isotropically consolidated undrained triaxial compression test	3
CAU	Anisotropically consolidated undrained triaxial compression test	3
$CIUE_U$	Isotropically consolidated undrained triaxial extension test (unloading)	3
CIUC	Isotropically consolidated undrained triaxial creep test	3
CAUC	Anisotropically consolidated undrained triaxial creep test	3

Table 17 Summary of undrained triaxial tests

Test series	Depth (m)	K_0	σ'_3	σ'_1
			kPa	kPa
CIU-I			50.00	50.00
CIU-II	3.0	1	80.00	80.00
CIU-III			100.00	100.00
CAU-I			37.5	62.5
CAU-II	3.0-4.0	0.6	75	125
CAU-III			100.00	166.67
CIUE-I			50.00	50.00
CIUE -II	3.0-4.0	1	80.00	80.00
CIUE -III			100.00	100.00

Table 17 (Continued)

Test series	Depth (m)	Stress level	σ'_3	σ'_1
CIUC-I		50%		
CIUC-II	3.0-4.0	70%	50.00	50.00
CIUC-III		85%		
CAUC-I		50%		
CAUC-II	3.0-4.0	70%	50.00	50.00
CAUC-III		85%		

Numerical analysis

The field trial test was reproduced by three-dimensional finite element method to improve understanding of stabilized slope and roadway with DCM columns. To ensure reasonableness of the results, the back-analysis of soil stiffness with measured field lateral movements was performed.

To effectively establish a guideline for design, the influential factors on stability of slope and DCM column behaviours are needed to be understood. Three-dimensional shear strength reduction finite element method was used for analyses. The stabilized slope with one row of DCM column was firstly desirable to study prior to multi-rows of DCM columns. The behaviour of DCM column was interpreted in term of displacement, shear force and bending moment.

Suggested guideline for design and construction of DCM column on excavated slope and roadway

Based on the result from field trial tests, laboratory tests, and numerical analyses, design and construction guideline were established. The guideline included laboratory tests, field tests, and stability analysis, construction techniques and remedial work.

RESULTS AND DISCUSSION

Field Trial Tests

Prior to the actual construction, the field trial tests were performed to verify the design assumption and construction process. The first field trial tests were conducted according to the initial design of DCM columns. The failures occurred after the end of construction. The additional DCM columns were considered as remedial solution. The second field trial tests were carried out again with lateral movement and pore water pressure measurements.

Integrity of DCM column

1. Tangential DCM columns

DCM column located in the canal slope is designed to resist lateral force by its flexural resistance. Due to low flexural resistance of a single DCM column, tangential DCM columns were used. To confirm the design assumption, the construction of tangential DCM column needs to be perfectly contacted to each other. Figure 85 provides an illustrative comparison between two cases of the constructed tangential DCM columns by jet grouting method. It can be seen from Figure 85a that the contacts of tangential DCM columns are relatively well. However, on some of tangential DCM columns is not good quality; there are small gaps in between. Figure 85b shows the worse condition of constructed tangential DCM column. The tangential DCM column is not well in alignment and contact. Moreover, the overlapping column leading to reduce in improvement area can be observed. In construction, the constructed tangential DCM column in Figure 85a can be considered as a satisfactory condition. While constructed tangential DCM column on Figure 85b leads to the weakness on flexural resistance.

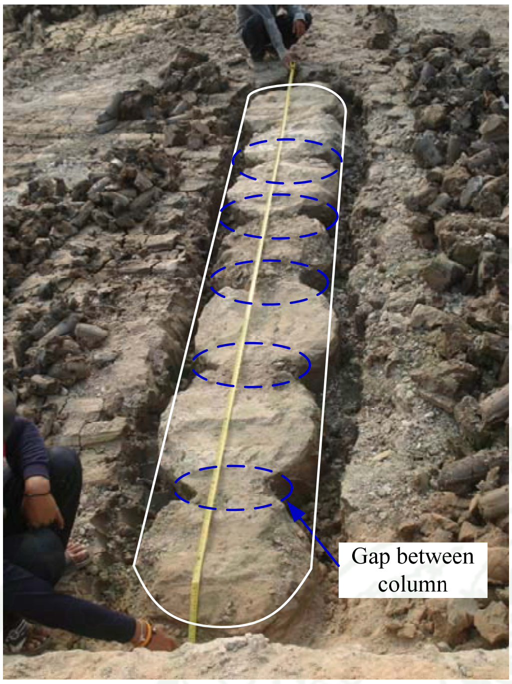

(a) Satisfying condition

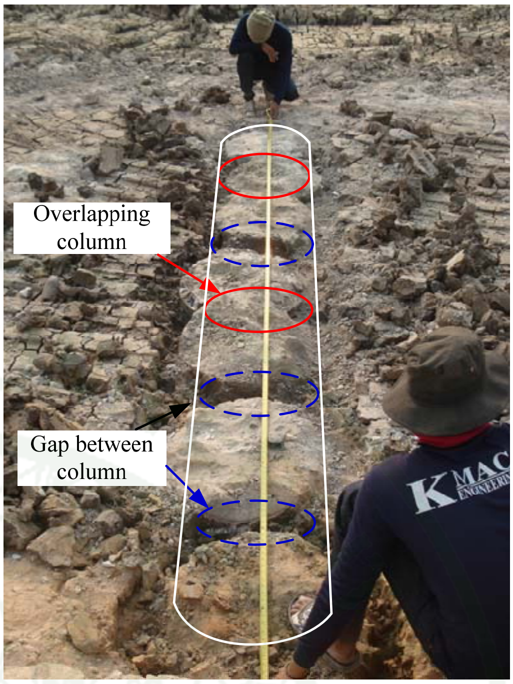

(b) Worse condition

Figure 85 Integrity of DCM column row

2. Pull out test

Pullout test was also conducted to extract the whole column for visual inspection, including homogeneity of material and DCM column size. The procedure of pullout test and inspection of DCM column are presented in Figure 86. An 80 cm steel casing with flap door at the bottom was then lowered to enclose the DCM column until the tip of casing was approximate 1 m below the DCM column tip. A vibro-hammer was employed to ease the driving of casing. The flap door was closed at the bottom of the casing to capture the DCM column, and the casing was then pulled out from the ground. The DCM column in the casing was pulled out, and the covering soil of the DCM column was removed. The recovered DCM column was cut into several sections and split apart for investigating homogeneity and size. If the recovered DCM column has a perimeter smaller than 15% or larger than 20% of designed perimeter, then the construction process of DCM column is adjusted (i.e. mixing time, binder, injection energy, etc.)

Figure 86 Procedure of pullout test and inspection of DCM column

First field trial tests

1. Construction of field trials

The cross-section of canal of the first field trial at the Section I and II is shown in Figure 87 and 88.The DCM columns under the roadway (which are called the bearing DCM columns) were 0.6 m in diameter, and were installed in a rectangular pattern at 1.50 X 1.75 m spacing. Seven tangential DCM columns (which are called the tangential DCM column) were installed in a row pattern at the canal slope with a spacing of 1.50 m. For the Section II (Figure 88), the tangential DCM column was installed 1.0 m from the canal edge. Low pressure mechanical and jet grouting methods are used for construction of DCM columns at the field trial Section I and II, respectively.

The construction stages were performed as follows. First, the DCM columns were installed according to designed configuration. Next, the roadway was built to +1.2 m high equal to one half of the final elevation. Then, the canal was excavated to a depth of -3.0 m with 1:3.5 slope. The final stage was roadway construction to the final elevation at +2.4 m. There were no measurement devices installed at this stage.

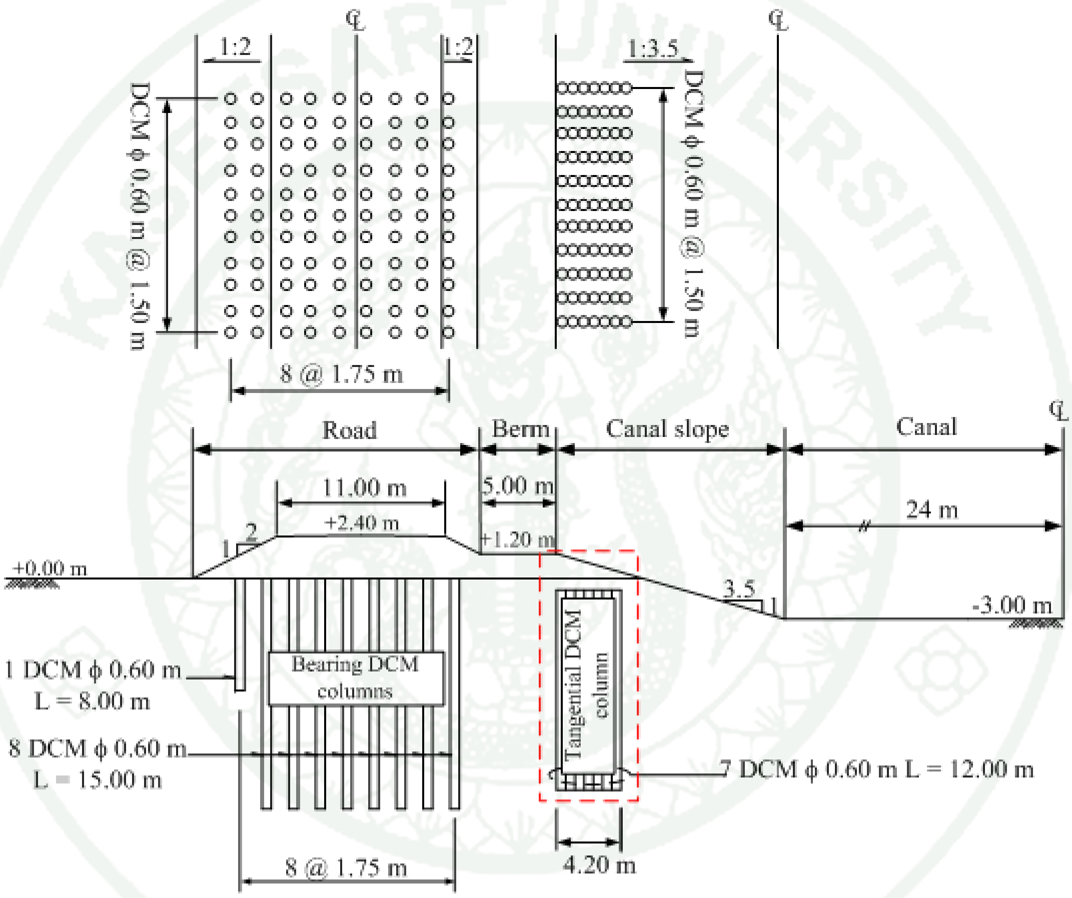

Figure 87 Cross-section of canal at the Section I

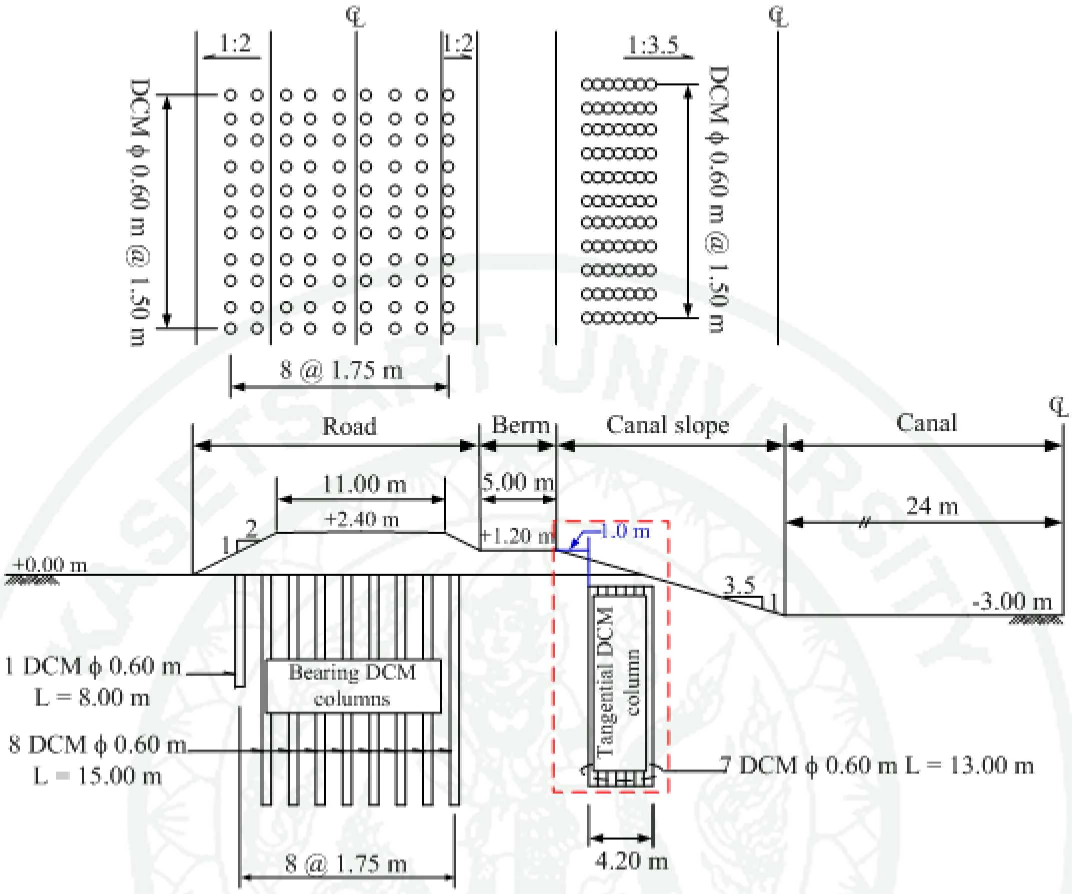

Figure 88 Cross-section of canal at Section II

2. Field trial test at the Section I

The failure occurred when the excavation reached to 3.0 m deep, as shown in Figure 89. The scarp of failure extended approximately 5.0 m to the top of canal, throughout the berm area where no DCM column. Based on geometry of failure, the settlement of berm area approximate 0.6 m was observed. The head of tangential DCM columns tilted toward the canal side approximately 1.0 m from its original position while the base of canal heaved up. It indicates that the tangential DCM columns cannot resist the active force.

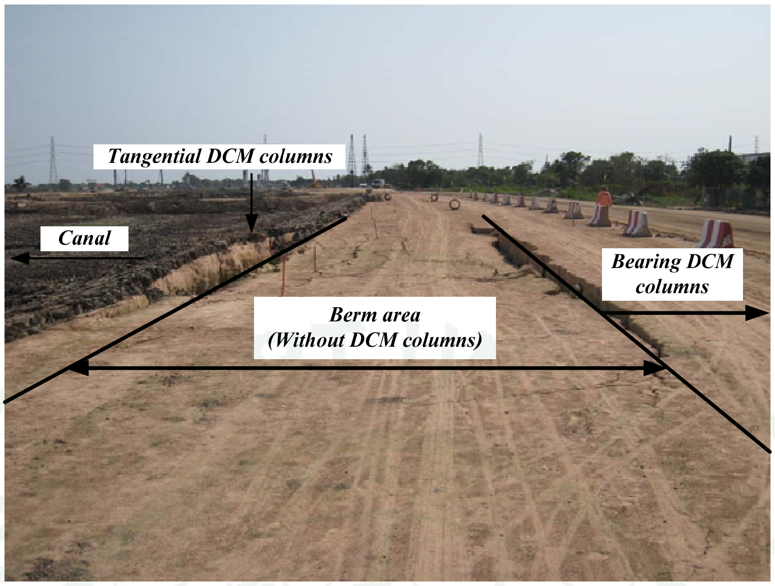

Figure 89 Failure of canal at the Section I for the first field trial

3. Field trial test at the Section II

The failure also occurred in this field trial test, as shown in Figure 90. The failure mode was similar to the field trial test at Section I. After the failure, the geometry of tangential DCM column was investigated. The DCM columns in row separate and move toward the canal side, as shown in Figure 91.

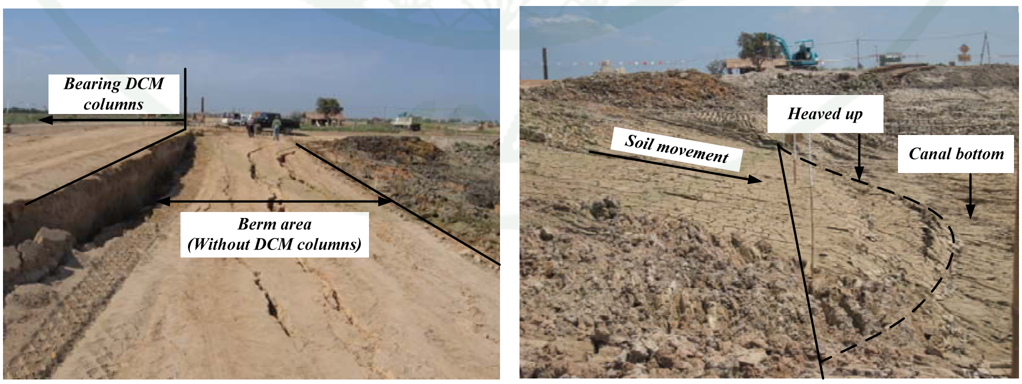

(a) Canal failure (b) Soil movement

Figure 90 Failure of canal at the Section II for the first field trial

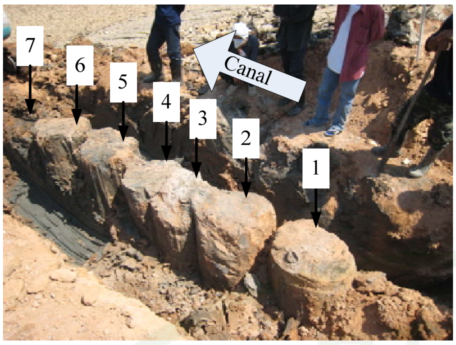

(a) Excavation of surrounding soil

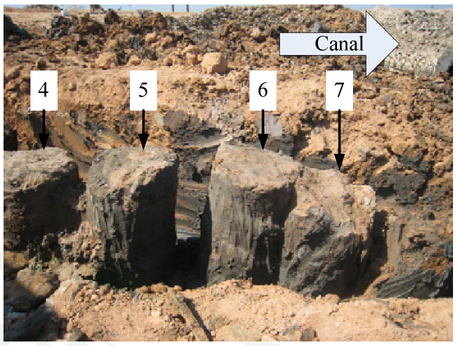

(b) Separation of DCM columns

Figure 91 Failure of tangential DCM columns

Buathong *et al.* (2010) undertook Two-Dimensional Finite Element Method (2D-FEM) of the field trial test at Section II. Figure 92 shows the potential failure surface at the end of excavation. The potential failure surface was close to the top of tangential DCM columns, and extended to the top of canal. It can be seen that the potential failure surface from the FEM coincided with the field failure behavior.

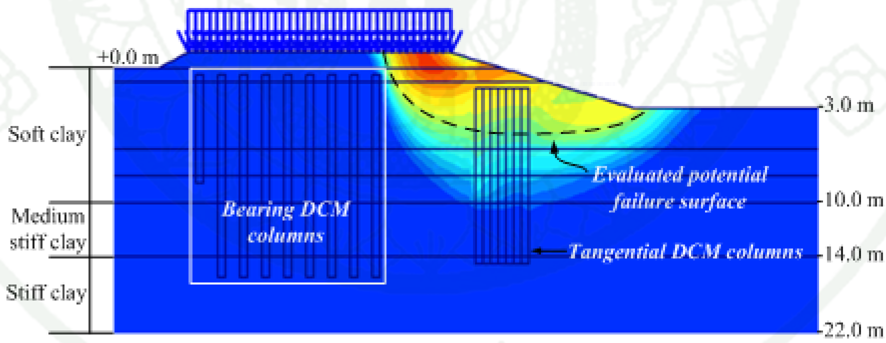

Figure 92 Potential failure surface at the end of excavation

Source: Modified from Buathong *et al.* 2011

4. Possible failure mode of canal and tangential DCM columns

Based on the observed geometry of failure and FEM result, the possible failure mode was illustrated in Figure 93. The scrap of failure extends to the top of canal throughout the berm area, where no DCM column. The tangential DCM columns are considered to fail by bending. The plastic hinge where maximum bending moment exceeds moment capacity of DCM column is expected to develop at the upper portion of tangential DCM columns. This is because the potential failure surface obtained from the FEM was close to the upper portion of DCM columns.

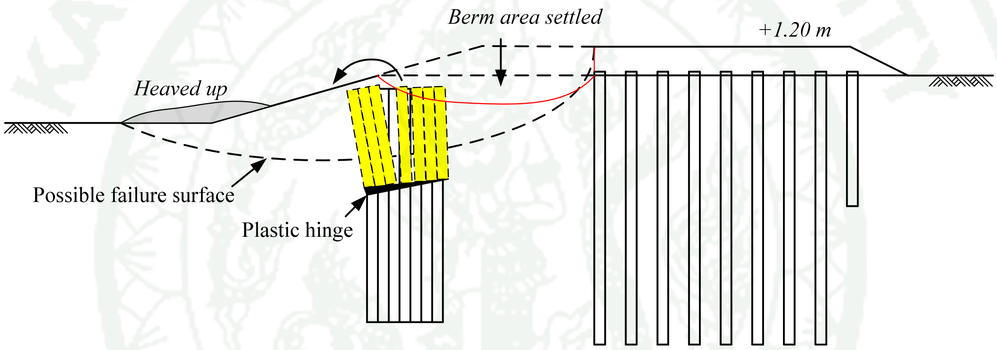

Figure 93 Possible mode of canal failure

Remedial solution

After the first failure cases, several remedial solutions were proposed by the contractors. However, the additional DCM columns were generally used for the solution. There were two positions of additional DCM column (i.e. Group I and II) were considered for the remedial solution, as shown in Figure 94. The berm area was considered as a primary area for additional DCM columns to reduce the active force on the tangential DCM column and also support the future roadway widening. Due to relative low soil strength in some area, the extra additional DCM columns were required to increase passive force. The guideline for selection of additional DCM column position was proposed by consultant of the project based on in-situ soil strength, as described below.

1. If the shear strength of in-situ soil is higher than 7 kPa, defined as "normal soft clay", only Group-I of additional DCM columns was installed.

2. If the shear strength of in-situ soil is lower than 7 kPa, defined as “very soft clay”, the Group-I and II of additional DCM columns were installed.

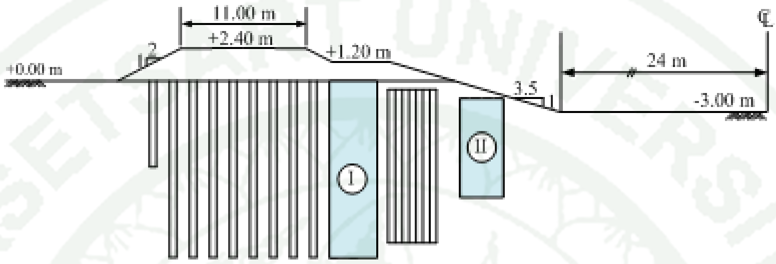

Figure 94 Typical cross-section of DCM columns for the remedial solution

Not only the additional DCM columns were used to increase the stability of canal, but also the lateral movement were closely controlled and kept within allowable values. Operation of heavy machines is recommended to move in the canal rather than on the canal bank. The lateral movement during the various stages of construction was also monitored by a series of inclinometers. In addition, piezometer was installed as part of research to measure the change of pore water pressure during the excavation.

Second field trials tests at Section I

1. Location of field trial and configuration of DCM columns

Two locations at the Section I were selected to perform the field trial test, as shown in Figure 95. The first location was constructed on the natural canal crossing, named as F1-1. The shear strength of soil was found to be lower than 7 kPa (i.e. very soft clay condition); therefore, the additional DCM columns at the canal slope and berm area were installed, as shown in Figure 96. Three additional DCM columns with a length of 15 m were installed at the berm area, and four DCM columns with a length of 8 m were placed at the canal slope in front of the tangential DCM column. The second location was built on the natural ground where the shear strength of soil was higher than 7 kPa (i.e. normal soft clay condition). Thus, the additional DCM columns with a length of 15 m at berm area were installed, as shown in Figure 97.

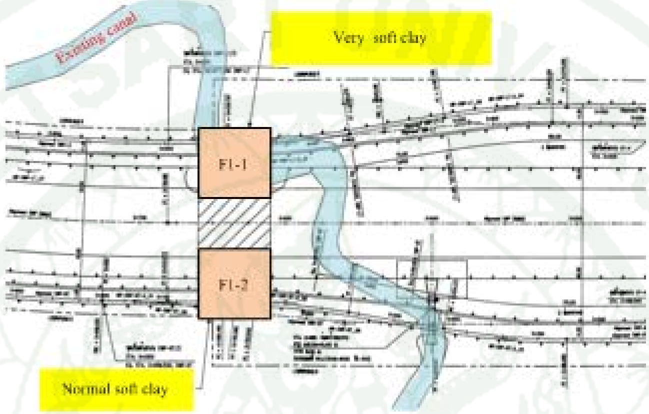

Figure 95 Location of field trials at the Section I

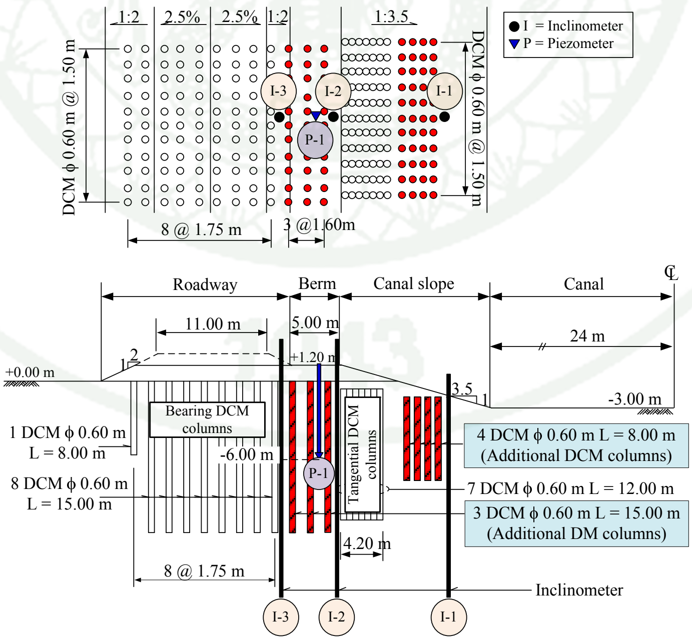

Figure 96 Cross-section of canal at the field trial test F1-1

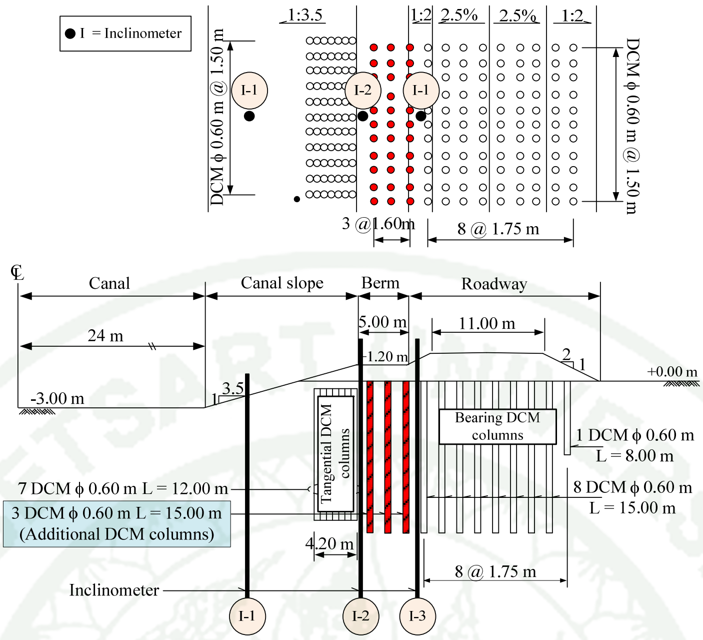

Figure 97 Cross-section of canal at the field trial test F1-2

2. Instrumentation

The lateral movement during the various stages of constructions were monitored by a series of inclinometers installed prior to the excavation works. The layout of inclinometers is shown in Figure 96 and 97. For the field trial F1-1, the variation of pore water pressure throughout the construction was monitored by piezometer (KU type) installed as part of research. The pore water pressure data were recorded every 30 minute.

3. Field trial test F1-1

The lateral movement profiles with depths measured from the inclinometers at the end of excavation are shown in Figure 98. The lateral movement of the inclinometer I-1 moved backward to the canal slope due to the effect of machine operation. The data obtained from inclinometer I-2 and I-3 indicated that the maximum lateral movement was 13.85 mm.

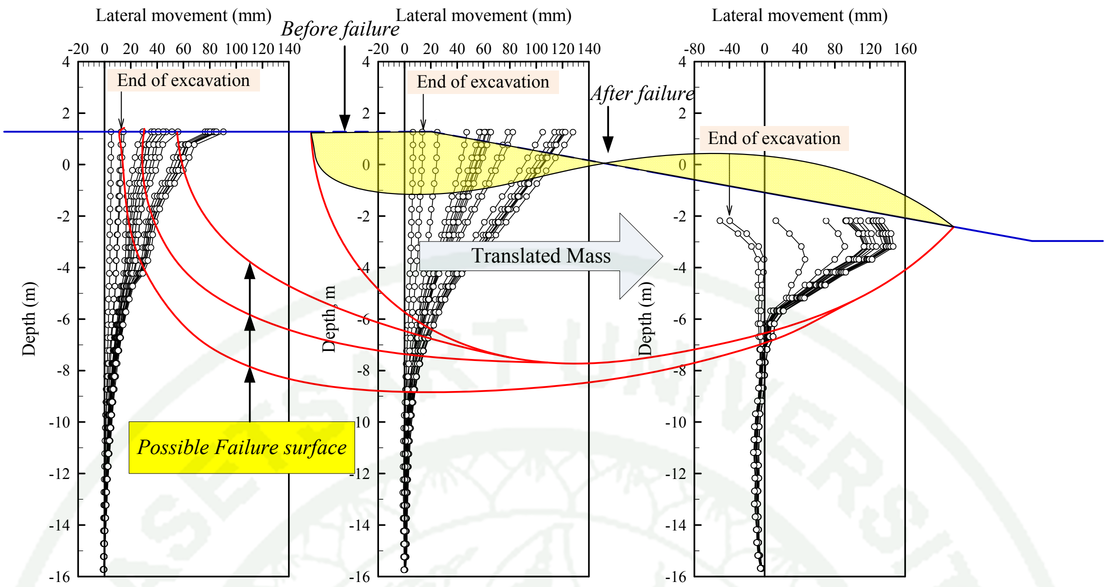

Figure 98 Lateral movement profiles at the field trial F1-1

After the end of excavation following the rainfall, longitudinal surface cracks were observed on the top of roadway, as shown in Figure 99. Moreover, the lateral movement indicated continuous increase with time. The cracking is considered to have an effect on the abrupt change of lateral movement. To prevent progressive failure, the soil was filled back at the slope toe. Based on the lateral movement profiles, the potential failure surfaces can be interpreted as shown in Figure 98.

Figure 99 Longitudinal surface cracks at the field trial F1-1

The variations of pore water pressure (i.e. hydrostatic plus excess pore water pressure) at the depth of 6 m throughout the excavation are shown in Figure 100. The pore water pressure before the excavation is higher than the hydrostatic pore water pressure. This excess pore water pressure may be generated during the installation process of DCM column (Phanumart *et al.*, 2007) and first stage of roadway construction. As the excavation commenced, the pore water pressure reduced as a result of stress relief. It found that the pore water pressure indicated rapid reduction which coincided with the significant increase of lateral movement. It is considered that the increase of pore water pressure is associated with the shear stress developed in the vicinity of piezometer.

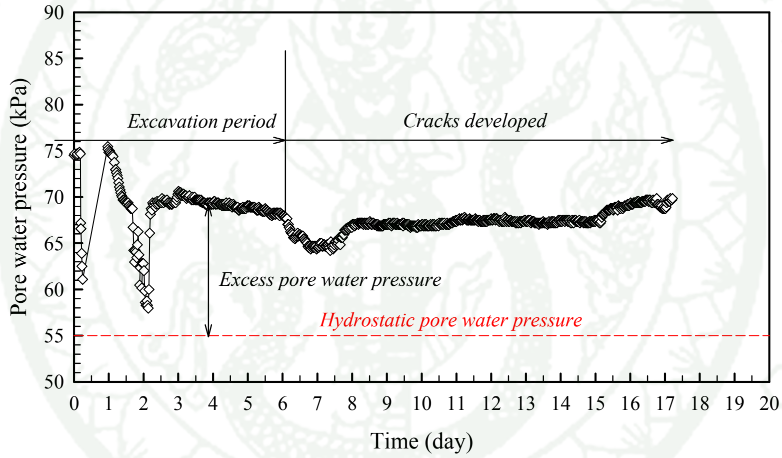

Figure 100 Variation of pore water pressure during the excavation of F1-1

4. Field trial test F1-2

The canal and roadway were successfully constructed at this field trial test. However, the failure occurred after the completion of roadway construction at about 10 days. Figure 101 shows the lateral movement profiles with depths during and post construction. The inclinometer data revealed that the maximum lateral movement after the end of excavation was 5.33 mm, less than the field trial test F1-1. As the roadway had reached to the finial elevation, the maximum lateral movement was 41.46 mm.

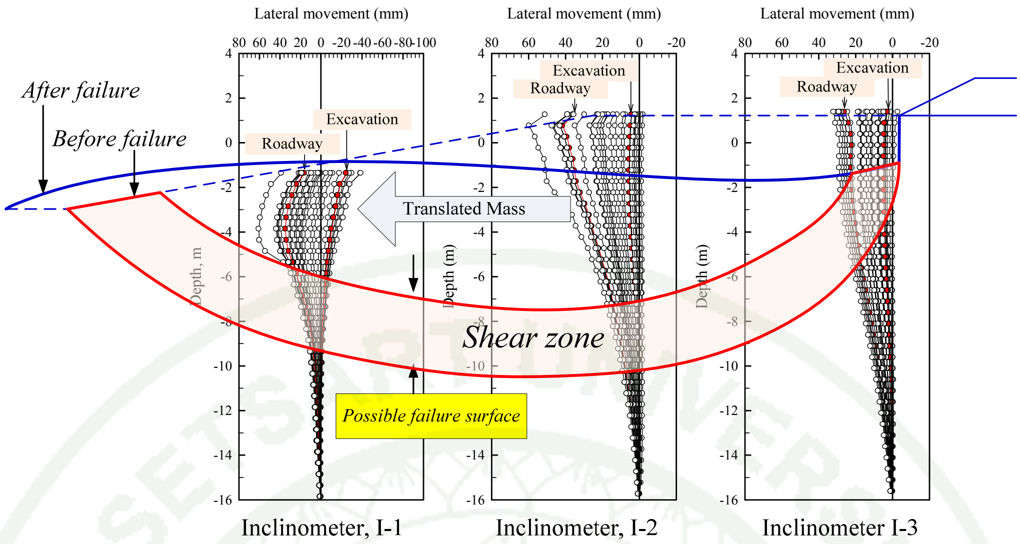

Figure 101 Lateral movement profiles at the field trial F1-2

The lateral movements indicated continuous to increase with time until eventual failure, as shown in Figure 102. The scrap of failure was extended throughout the berm area while the base of canal heaved. The tangential and additional DCM columns also tilted toward the canal. The failure behavior is similar to that found in the first field trial tests. Based on the lateral movement profiles, the potential failure surfaces are illustrated in Figure 101. The translation soil mass dominated down to 7.5 m deep. The lateral movement obtained from the inclinometer I-1 clearly indicates that development of shear zone occurs at the depth from 5.0 m to 9.0 m.

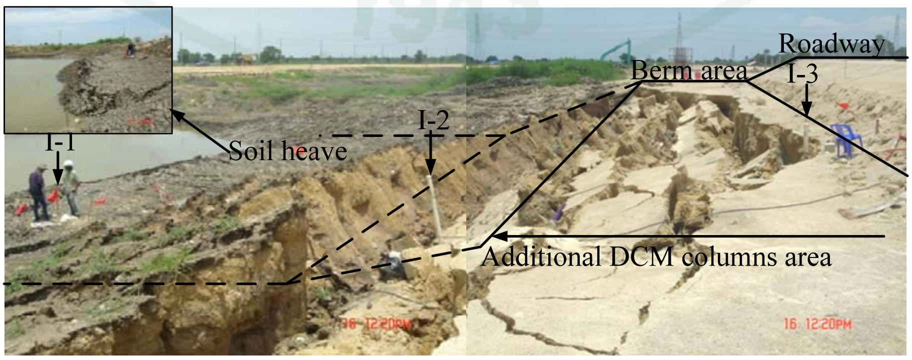

Figure 102 Failure of field trial test F1-2

The increase of lateral movements with time is resulted by the coupling process of swelling and undrained creep. Figure 103 plots the lateral movement with time at the 3.0 m deep after the end of roadway construction. The lateral movement behavior is similar to that of undrained creep behavior (Snead, 1970; Arulanandan *et al.,* 1971), which is divided into three stages (i.e. primary, secondary and tertiary stages). It can be seen from the inclinometer I-1 that the rate of lateral movement in secondary stage is constant prior to reach the failure condition. Therefore, the remedial measures should be applied in the secondary region to prevent the failure.

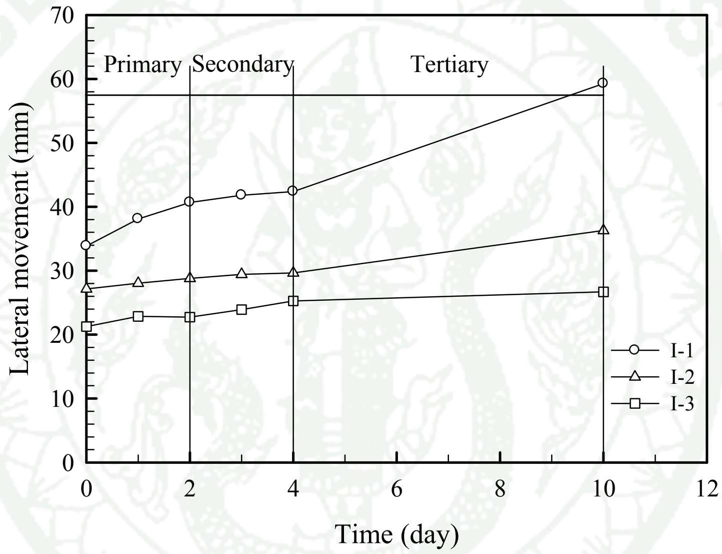

Figure 103 Lateral movement at depth of 3 m after the end of construction

Second field trials test at Section II

1. Additional remedial solution

The field trial tests at the Section I indicated that the lateral movement increased with time after the end of construction leading to eventual failure condition. Toe berm and canal water were considered to provide additional resistance force. The toe berm has a width of 6.0 m and a height of 1.0 m. The water at least 1.0 m was filled at the canal bottom. The purpose of this field trial test is to assess the performance of the toe berm and canal water.

2. Cross-section of canal and layout of instrumentation

Figure 104 shows the cross-section of canal and layout of instrumentation. The additional DCM columns with a length of 15.0 m were installed only at the berm area. The lateral movements were closely monitored by a series of inclinometers. The change of pore water pressure was monitored by piezometers installed at various depths. The interpretation of instrumentation was emphasized at the excavation stage.

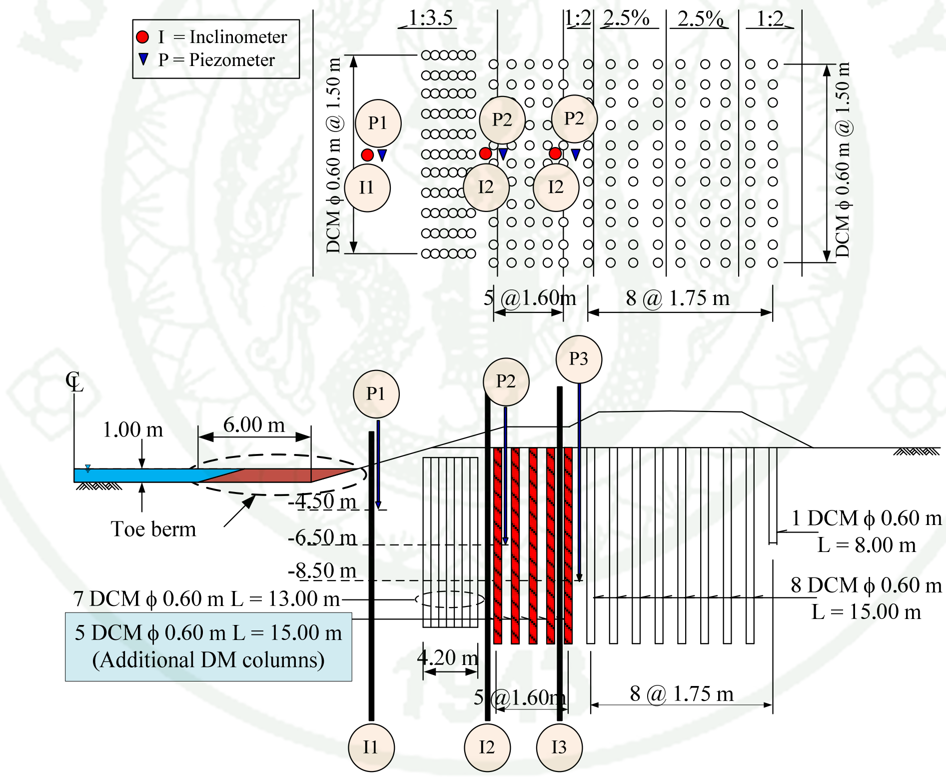

Figure 104 Configuration of DM columns at the Section II

3. Lateral movement

During the excavation, the fine longitudinal surface cracks were observed at the top of canal approximately 1.0 cm to 2.0 cm width. The lateral movement profiles with depths measured from the inclinometers during the excavation are shown in Figure 105. The inclinometer I-1 indicated partial disturbance from the machine operation in the early stage of excavation, similar to the previous field trial tests. The data from inclinometers reveal that the maximum lateral movement was 20.2 mm, greater than the field trial at Section I. The lateral movements show the increase with time after the end of excavation. However, it is approach a constant due to effect of toe berm and canal water.

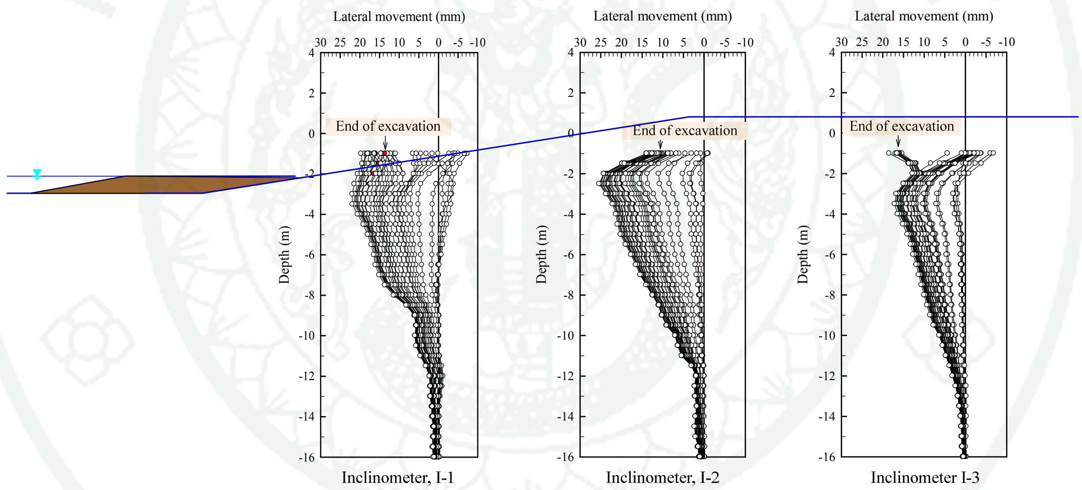

Figure 105 Lateral movement profiles of field trial at Section II

Figure 106 shows the lateral movements at 3.0 m depth after the end of excavation. The rate of increase in lateral movements is significant in the early stage of toe berm construction. The reduction in the rate of lateral movement is coincident with the time that the toe berm is completely constructed, and the canal water is started to apply. This indicates that the toe berm and canal water are effective to remedy the lateral movement after the end of excavation. Unfortunately, the lateral movements during the roadway construction were not monitored.

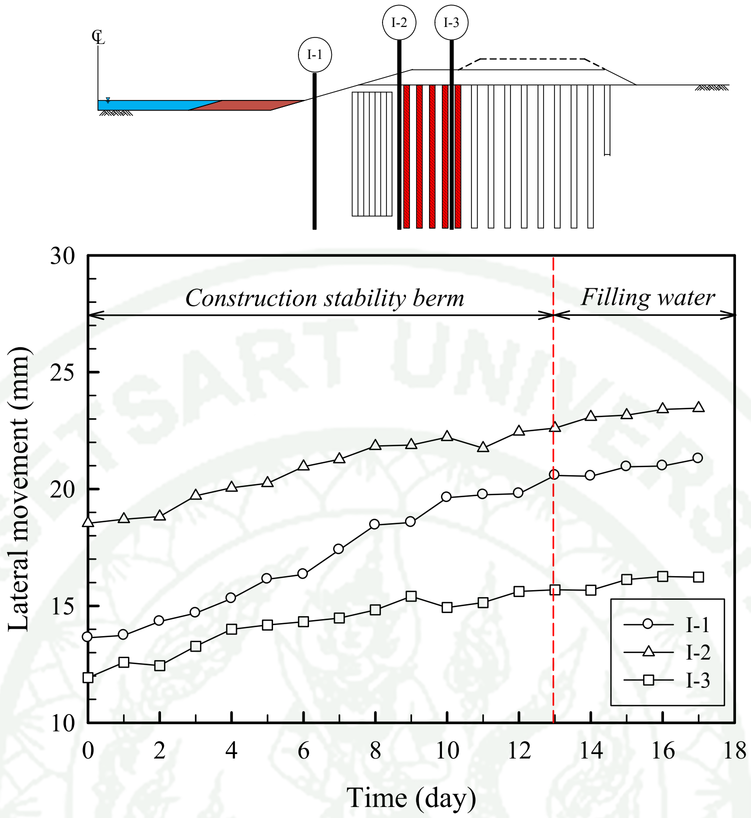

Figure 106 Lateral movements after the end of excavation at 3.0 m depth

4. Pore water pressure

Figure 107 shows the variation of pore water pressures (i.e. hydrostatic plus excess pore water pressure) at the depth of 4.5 m, 6.5 m and 8.5 m during the canal and roadway construction. It is noted that the initial pore water pressures prior to the excavation were higher than the hydrostatic pore water pressures, as found at the field trial F1-1. As the excavation commenced, the pore water pressures reduced as a result of stress relief. The piezometer P-1, located at the canal slope, indicated the fluctuation of pore water pressure during construction of the toe berm and canal water. While the Piezometer P-2 and P-3 continued to decrease at a relatively steady rate. This is coincident with the reduction rate of increase in lateral movement. The piezometer P-3, located on the top of canal, shows obviously increase in pore water pressure during the roadway construction. The increase of pore water pressure is then stable as the roadway reached to its final level. The pore water pressure of piezometer

P-1 and P-2 show slightly increase of pore water pressure in the early stage of roadway construction.

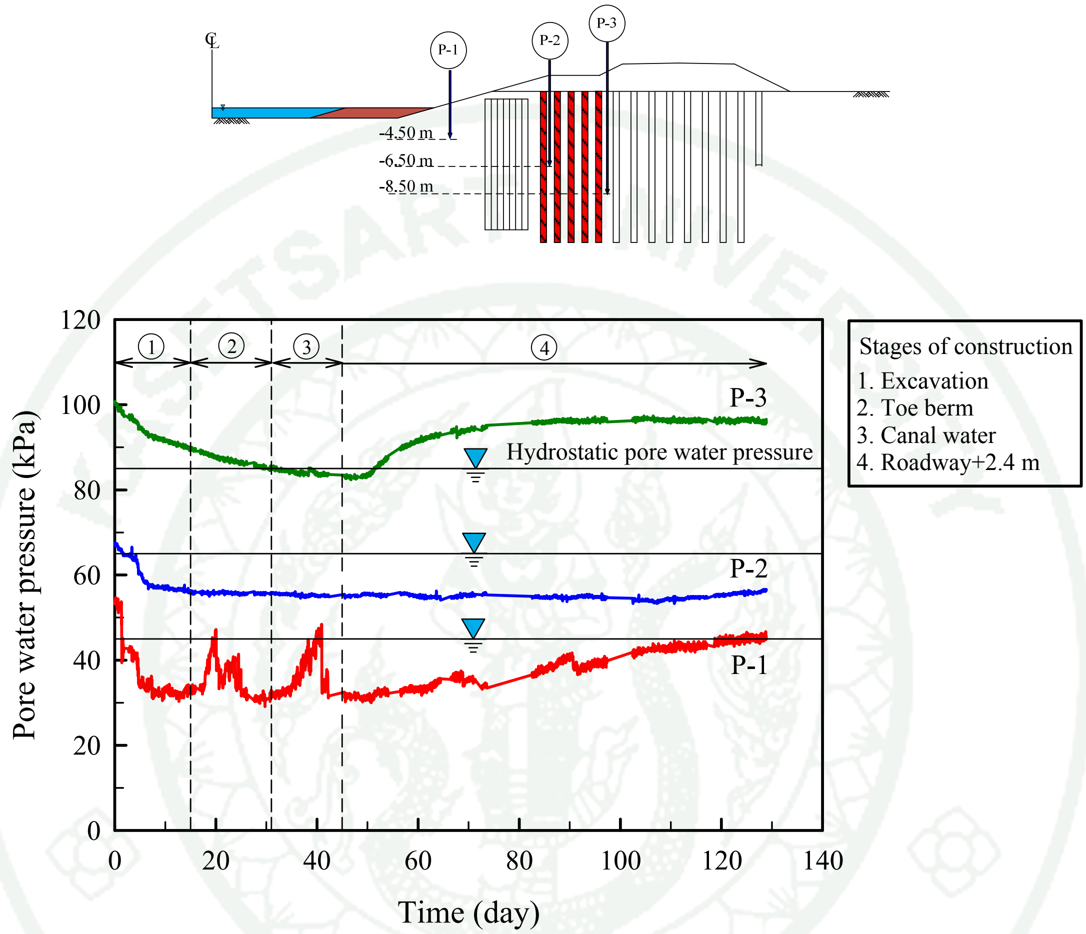

Figure 107 Variation of pore water pressure during the construction of field trial at Section II

Numerical Back-Analysis of Field Trial Test

The input soil parameters are primary factor that affects the reliability of the results. Several approaches are available for determining soil parameters. For simplicity, soil parameters can be indentified on the basic of laboratory tests. However, using these parameters from the laboratory tests may not always give results that are representative to the actual field behavior. Sometimes, the soil parameters from the literature and empirical values can be used. Generally, this method can be considered as imprecise. For these reason, soil engineers often perform the full scale test in the field or proceed the back-analysis using measured data (such as lateral movement, etc.). The numerical back-analysis is an approach that widely used in geotechnical engineering to estimate the soil parameters, because it is economical as compared with the full scale test.

This section examined the soil stiffness for a stabilized canal and roadway with Deep Cement Mixing (DCM) columns. The measured lateral movements at the field trial test F1-1 were used to back-analyze soil stiffness. Mohr-Coulomb (MC) and Hardening Soil (HS) model, as implemented in finite element software PLAXIS 3D Foundation, were employed in this study.

Soil and DCM properties

Figure 108 shows soil characteristics and DCM properties with the depths. The soil profiles consist of four layers as follows: 5.5 m of soft clay 1; 9.5 m of soft clay 2; 4.2 m of medium clay; and 1.6 m of stiff clay. The natural water content (W_n) of soft clay is approximately close to liquid limit (LL). The undrained shear strength (S_u) obtained from field vane shear (FVS) test typically increases with depth.

The unconfined compressive strength (q_u) of Deep Cement Mixing (DCM) column obtained from the field specimens ranged from 1,000 kPa to 2,600 kPa. While the undrained elastic modulus (E_u) ranged from 200,000 kPa to 900,000 kPa, indicating empirical $E_u = 200q_u$ to $350q_u$.

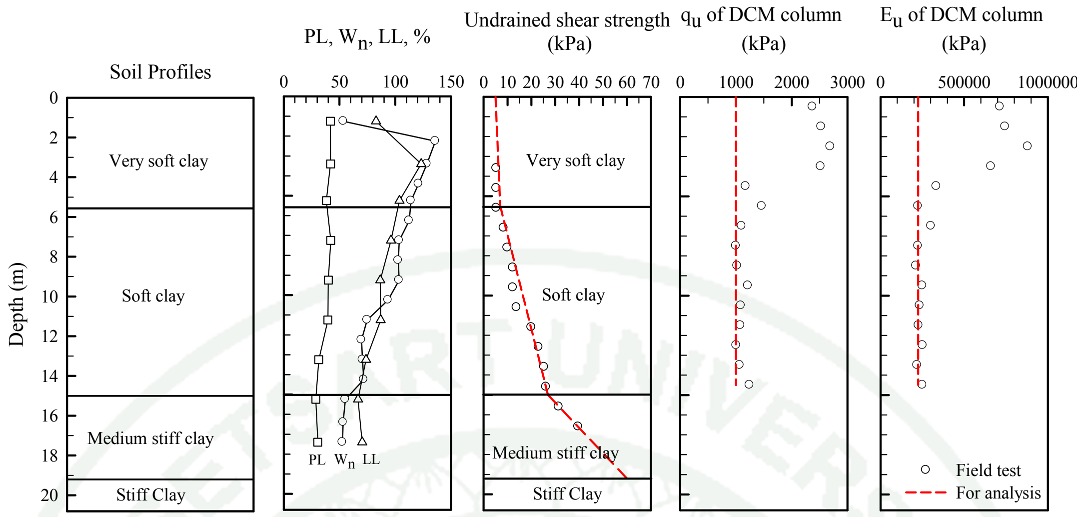

Figure 108 Soil and DCM column properties with the depths

Finite element modeling

The stabilized canal and roadway with DCM columns is truly three-dimensional as each column is not continuous in the out-of-plane direction. Therefore, three-dimensional finite element software, PLAXIS 3D FOUNDATION V2.2, was adopted. The total stress analysis was used in corresponding with rate of construction.

The field trial test of F1-1was reproduced by finite element modeling, which is shown in Figure 109. The 3D-FEM mesh has a size of 4.5 m wide x 80 m long x 20.8 m deep. The boundary conditions are; restrained horizontal displacement and free vertical displacement on the side of boundaries. Both horizontal and vertical displacements are also restrained at the bottom of boundary.

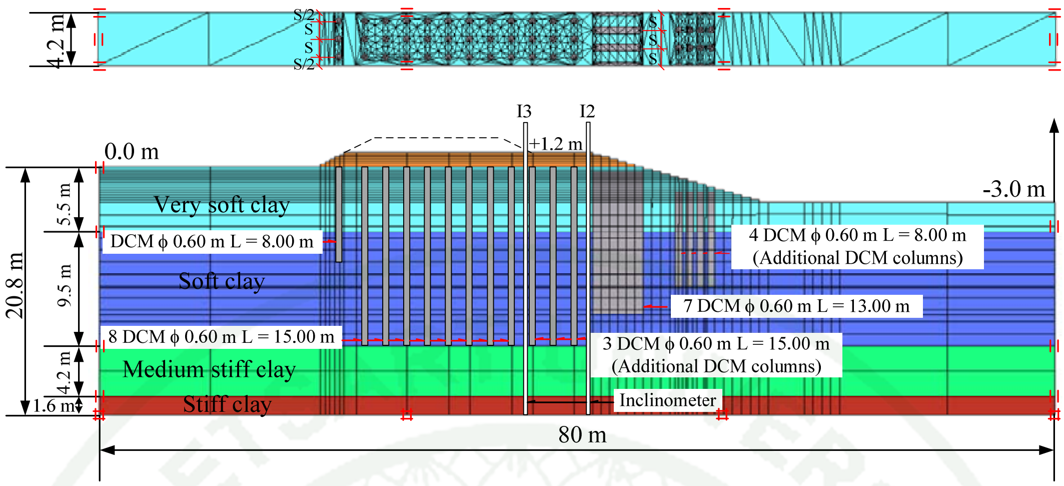

Note | | Restrained horizontal displacement

⌗ Fixed horizontal and vertical displacement

Figure 109 Finite element mesh for numerical back-analysis of field trial F1-1

Construction stages that were used in the numerical analysis correspond to those in the actual construction as follows:

1. Generation of initial stresses according to Jaky's formula (K_0 = 1-sinϕ');

2. Activation of DCM columns;

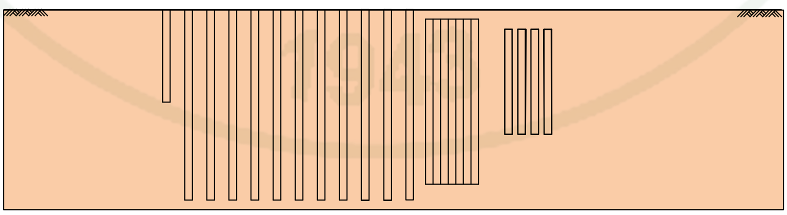

3. Construction of Roadway of 1.2 m (half of final level);

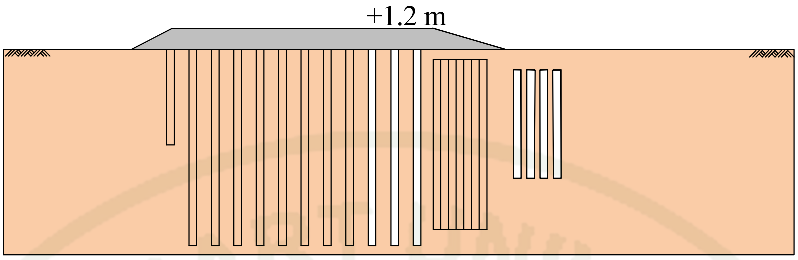

4. Excavation of 1.5 m deep and installation of inclinometers;

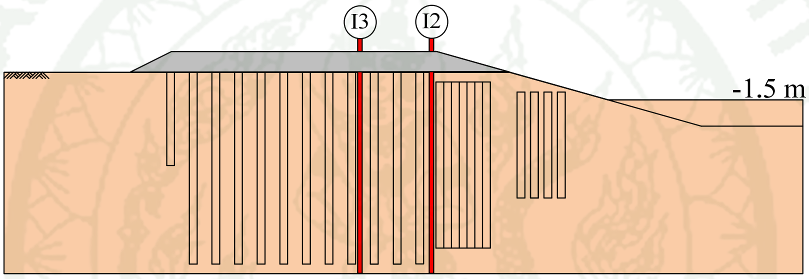

5. Excavation of 3.0 m deep

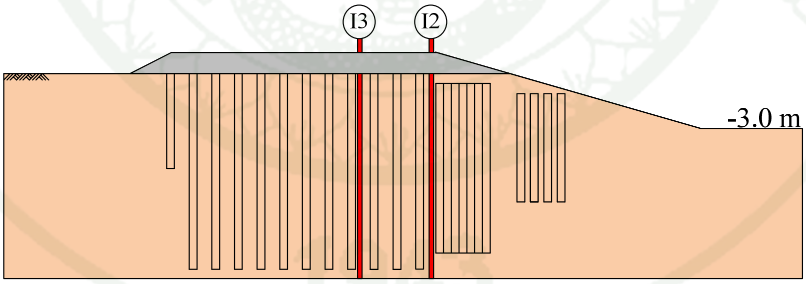

Constitutive model and parameters

The behaviour of DCM columns and roadway were usually simulated by using Mohr-Coulomb (MC) model, linear elastic-perfectly plastic model (Han *et al*., 2007; Huang and Han, 2009; Huang and Han, 2010; Abusharar *et al.*, 2009). An unconfined compressive strength q_u of 1,000 kN/m^2 and an undrained elastic modulus E_u of 225,000 kN/m^2 indicating the empirical relation $E_u = 225q_u$ were used in the analyses (Figure 108). Terashi *et al.* (1980) conducted a series of flexural strength tests on Kawasaki clay stabilized either by quicklime or Portland cement. They found that the flexural strength was around 0.1 to 0.6 of unconfined compressive strength. For soft Bangkok clay, the flexural strength of soft Bangkok clay was 0.16 of unconfined compressive strength (Jamswang *et al.*, 2010). To indicate the failure criteria of the DCM columns due to the bending mode, the flexural strength of 0.16qu was applied. The DCM column and roadway parameters used in analysis are shown in Table 18.

Table 18 DCM columns and roadway parameters for numerical back-analysis

Material	Material behaviour	γ (kN/m^3)	ν_u	E' (kPa)	c' (kPa)	ϕ' (°)	σ_t (kPa)
DCM	Undrained	15	0.33	E_u = 225,000	S_u = 500	0	$0.16q_u$
Roadway	Drained	20	0.33	7,500	8	29	

Two constitutive models of soil, Mohr-Coulomb (MC) model and Hardening Soil (HS) model, were selected to evaluate the performance of model. The MC model is considered the most widely used model among practicing engineers. Many researchers have used this model to simulate the behavior of soft clay as a first-order approximation of real soil behavior (Hossain *et al*., 2006; Huang *et al*., 2006; Madhyannapu *et al*., 2006; Han *et al.* 2005, Chen *et al.*, 2006). This model is assumed that the soil resistance increases linearly with displacement, until the failure criterion is reached. The stiffness is estimated to be constant. In this model, the undrained Poisson's ratio (ν_u) of soils is assumed to be 0.495. The cohesion intercept is equal to undrained shear strength, i.e. $c = S_u$, and friction angle is equal to 0. The undrained shear strength from the field vane shear test (Figure 108) is adopted for the analysis.

The HS model is an advanced hyperbolic soil model formulated in the framework of hardening plasticity. The main difference with the MC model is stiffness approach. The HS model utilizes four basic stiffness parameters: the secant stiffness in standard drained triaxial tests (E^{ref}_{50}), the tangential stiffness for primary oedometer loading (E^{ref}_{oed}), the unloading and reloading stiffness (E^{ref}_{ur}). The strength parameters of very soft clay and soft clay were obtained from a series of undrained triaxial test performed. The medium stiff clay and stiff clay were selected from the previous analyses on Bangkok clay.

Back-analysis results

In back-analysis, the stiffness of soils was adjusted so that the measured lateral movements were matched by the analyzed lateral movement. Initially the typical values of the soil stiffness were used. Then, a trial-and-error procedure was employed to obtain the best fit between the field measurements and the finite element simulation results. Figure 110 shows the analysis results that used the Mohr-Coulomb (MC) and Hardening Soil (HS) model. The final set of soil parameters used in the HS model is shown in Table 19. The value of $E^{ref}_{50} = E^{ref}_{oed}$ was 3000, 15000, 30000 and 60000 for very soft, soft, medium stiff and stiff clay, respectively. The ratio of $E^{ref}_{ur}/ E^{ref}_{50} = 3$ for all soils.   At the location of inclinometer I-2, the lateral movement analyzed from the HS model is generally close to the measured lateral movement but larger than the field measurement for a depth below 4.0 m from the ground surface. While the analyzed lateral movement at the location of inclinometer I-3 is quite close to the measured lateral movement at a depth below 8.0 m.

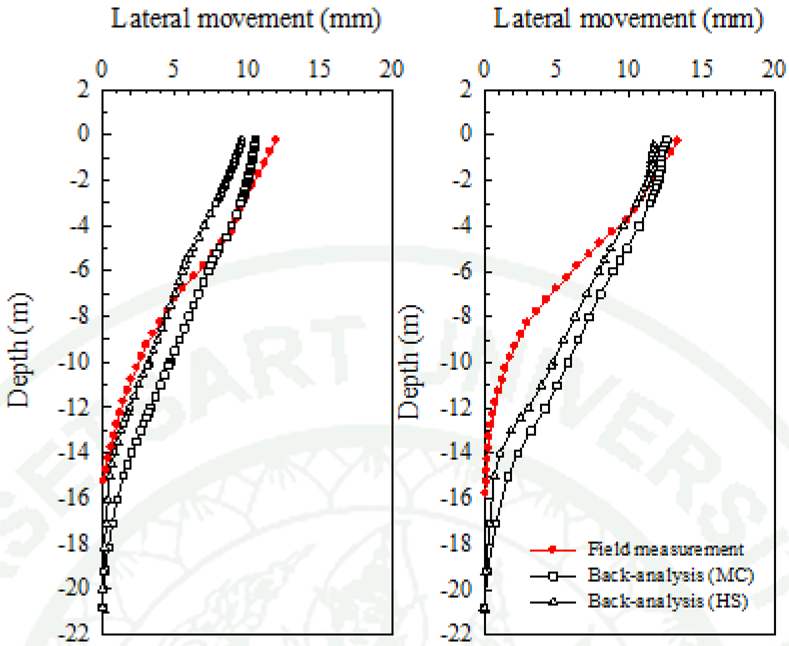

a) Inclinometer I-3 b) Inclinometer I-2

Figure 110 Comparison between FEM results and field measurement data after excavation completed

Table 20 presents the final set of soil parameters used in the MC model. The values of E_u/S_u = 300, 600, 1000 and 1000 for very soft, soft, medium stiff, and stiff clay, respectively. The back-analyzed values of E_u/S_u are in good agreement with the empirical correlation proposed by Duncan and Buchigani (1976) based on PI and OCR. It can be seen that the analyses of lateral movement using the adjustment of soil stiffness are generally good agreement with the HS model. As long as the maximum lateral movement is concerned, the use of MC model seems to give a reasonable lateral movement with the field measurement.

The investigation of model performance revealed that rather than using complex model (HS model), a simple model (MC model) with carefully selected soil stiffness produced reasonable prediction of lateral movements for the investigated case. However, the use of MC model may not be sufficient for complex geotechnical problems due to its limitation (i.e. constant stiffness). For this reason, the HS model was selected for further studies in this paper.

Table 19 Final set HS model Parameters used for numerical back-analysis

Materials	Very soft clay	Soft clay	Medium clay	Stiff clay
Depth (m)	0.0- 5.5	5.5-15.0	15.0-19.2	19.2-20.8
Model	HS	HS	HS	HS
Material behavior	Undrained	Undrained	Undrained	Undrained
E^{ref}_{50} (kPa)	3,000	15,000	30,000	60,000
E^{ref}_{oed} (kPa)	3,000	15,000	30,000	60,000
E^{ref}_{ur} (kPa)	9,000	45,000	90,000	180,000
γ (kN/m^2)	14	15	17	19
υ'	0.33	0.33	0.33	0.33
m	1	1	1	1
c' (kPa)	0	0	10	30
ϕ (°)	26.5	26.5	25.0	26.0

Note HS = Hardening Soil

E^{ref}_{50} = Secant stiffness in standard drained triaxial test

E^{ref}_{oed} = Tangent stiffness for primary oedometer loading

E^{ref}_{ur} = Unloading/reloading stiffness

m = Power for stress-level dependency of stiffness

υ' = Effective Poisson's ratio

Table 20 Final set of MC model parameters used for numerical back-analysis

Materials	Very soft clay	Soft Clay	Medium stiff Clay	Stiff Clay
Depth (m)	0.0- 5.5	5.5-15.0	15.0-19.2	19.2-20.8
Model	MC	MC	MC	MC
Material behaviour	Undrained	Undrained	Undrained	Undrained
E_u(kPa)	$300S_u$	$600S_u$	$1000S_u$	$1000S_u$
γ (kN/m^3)	15.5	15.5	17	18
ν_u	0.495	0.495	0.495	0.495
ϕ (°)	-	-	-	-
S_u (kPa)	5^*	7^*	27^*	132.5

Note MCM = Mohr-Coulomb model
DCM = Deep Cement Mixing
S_u = Undrained shear strength
E_u = Undrained elastic modulus
ν_u = Undrained Poisson's ratio
* = Strength increase with depth according to Figure 108

Multi-stage behaviours

For this field trial, there are no detailed field measurements of lateral movement and pore water pressure after the excavation completed. Therefore, the finite element analysis with the HS model was performed in order to examine the behaviours. The cases analyzed correspond to the actual construction and service period as follows: 1) Construction of second stage of roadway with a height of 1.2 m, 2) Filling water in the canal with a height of 3.0 m, 3) Performing of consolidation process 1 year and 4) Lowering of water in the canal to represent dry season. Figure

111 shows the location of lateral movement and pore water pressure that were investigated.

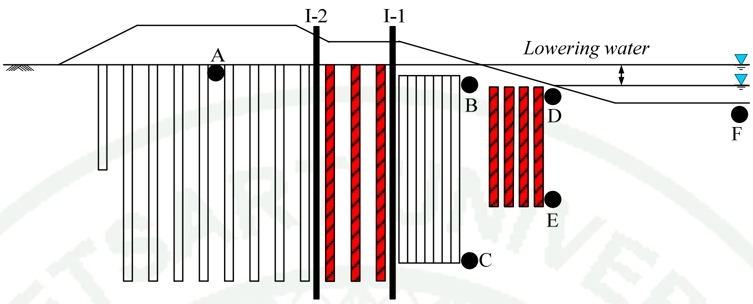

Figure 111 Location of investigated lateral movement and pore water pressure

Figure 112 illustrated the variation of excess pore water pressure throughout the construction. As expected, the excess pore water pressure at the point A increased during the first stage of roadway construction. The increase in the excess pore water pressure also was observed at the point C and E. This is probably due to the result of load transfer from roadway to DCM columns. As the excavation commenced, the excess pore water pressures on the excavation side (point B, C, D and F) reduced to the negative values, as a result of stress relief. The point A showed a small decrease of excess pore water pressure. At the second stage of roadway construction, the point A indicated significantly increase in the excess pore water pressure. While the other points slightly changed in excess pore water pressure. The water was assumed to fill immediately after the roadway construction complete. It can be seen on the excavation side at point B, C, D and E that the negative pore water pressures decreased, and tended to reach equilibrium condition due to the effect of water in the canal. It is noted that the positive excess pore water pressure was developed at the point E after the filling of water in canal. This means that the soil element is compressed due to the load from the water.

Figure 113 illustrates the dissipation of excess pore water pressure after the filling of water. Generally the dissipation of excess pore water pressures was completed approximately 120 days. However, the negative excess pore water pressure at point B and D still remained. The rapid drawdown during dry season was carried out by lowering of water in the canal immediately (i.e. undrained condition). There was no change of pore water after the lowering of water in the canal from 3.0 m to 1.0 m. However, the analysis result revealed that the instability of canal is shown when the water in the canal reduced from 3.0 m to 2.0 m.

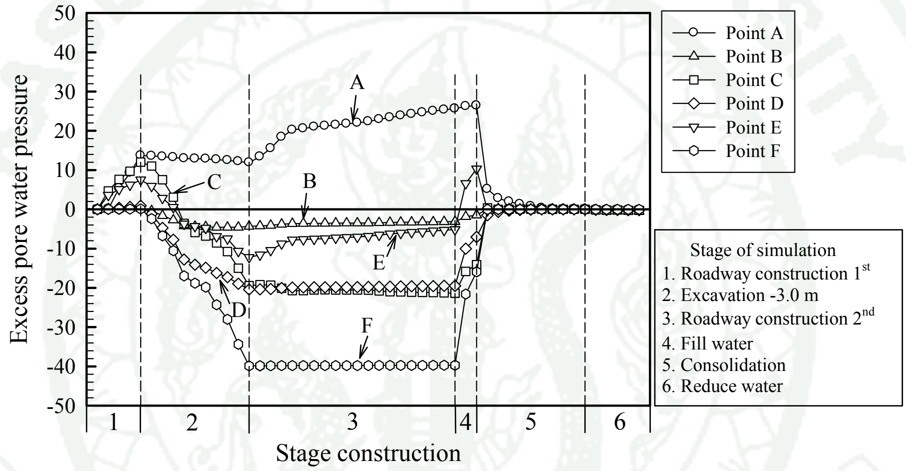

Figure 112 Excess pore water pressure throughout the construction

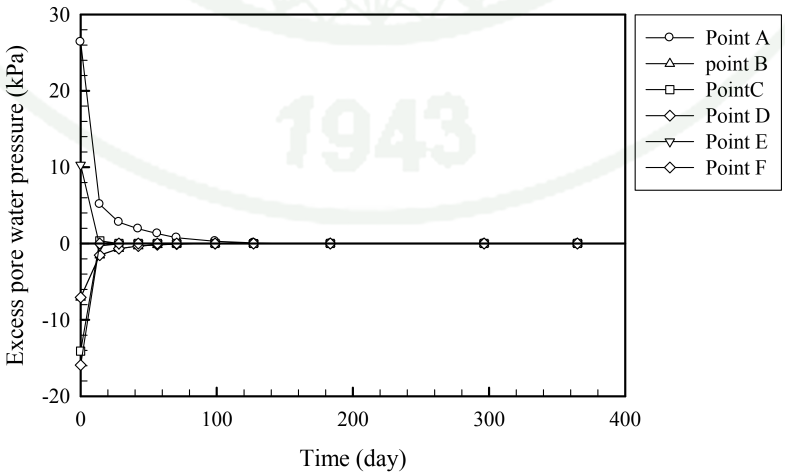

Figure 113 Dissipation of excess pore water pressure after the end of filling water

Figure 114 shows the development of excess pore water along the canal and roadway. It is clear that the negative excess pore water pressures were generally generated at the canal side as a result of vertical stress relief. While the positive excess water pore pressures were commonly developed under the roadway. The filling of water in the canal led to the reduction of negative excess pore water pressure at the canal side. After the consolidation process of 1 year, the excess pore water was nearly close to zero. The slight negative excess pore water pressures were observed at the canal slope.

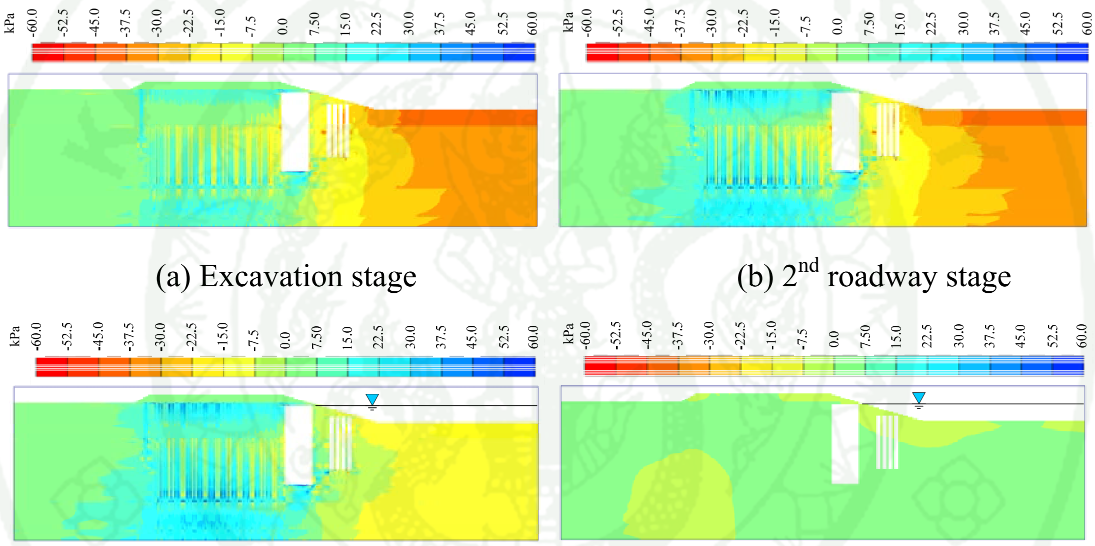

(a) Excavation stage (b) 2nd roadway stage

(c) Filling water stage (d) Consolidation stage

Figure 114 Shading contours of excess pore water pressures

Figure 115 shows the lateral movements after the end of roadway construction. The maximum lateral movements of inclinometer I-2 and I-3 at the end of roadway construction was 36.59 mm and 42.38 mm, respectively. It was also found that the large lateral movement occurred at the outside slope of roadway instead of the canal side, as shown in Figure 116. The DCM column at the outside slope of roadway also indicated the tension failure from bending mode. This behaviour coincides with the analysis of Navin (2005). He recommended using the shear wall pattern of DCM columns at the side slope of roadway to improve bending strength of column. After the filling water in the canal completed, the decreased of lateral movement was shown. This is because the lateral pressure from the water in the canal compressed the soil element in concurrence with the relief of negative pore water pressure. The lateral movements continued to decrease due to the relief of negative and positive excess pore water pressure from consolidation process. When the water in the canal reduced from 3.0 to 2.0 m high, the lateral movement showed slight increase. The analysis result indicated that the failure of canal occurred as the water in the canal sudden reduced from 2.0 to 3.0 m high.

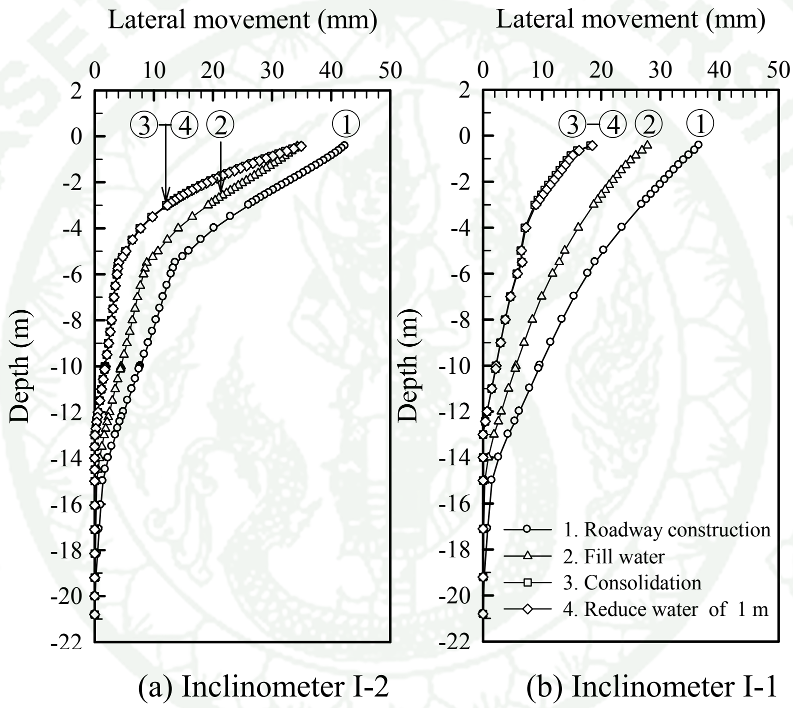

Figure 115 Predicted lateral movement at different stage of construction

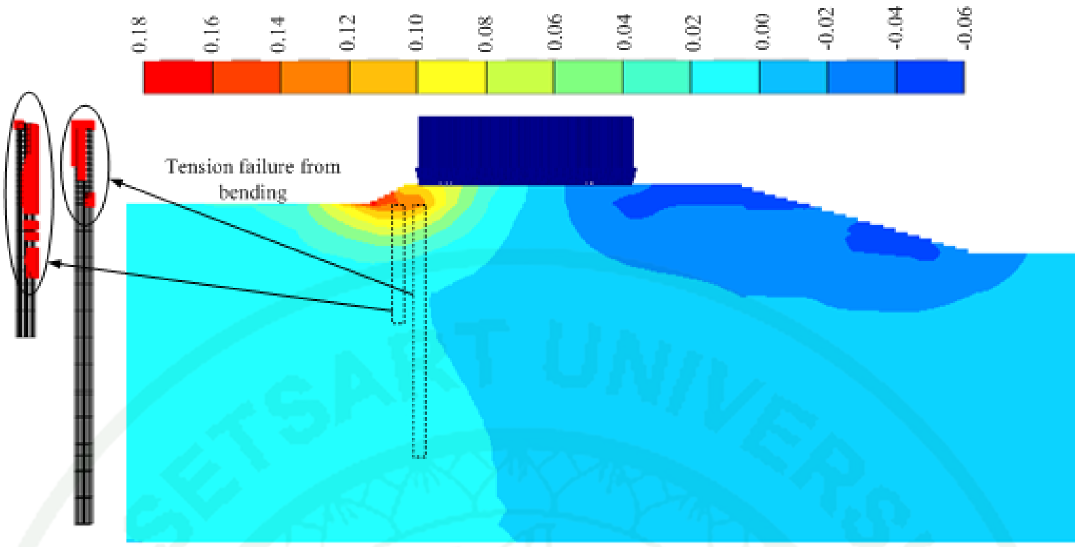

Figure 116 Contour shading of lateral movement and failure of DCM columns at the end of roadway construction

Numerical Analysis of a Stabilized Slope with One Row of DCM Columns: Parametric Analysis

Although, a number of success application of slope stabilization by mean of DCM column have been reported in the literature, in general there is a lack of clear knowledge of the exact behaviour and potential failure mechanisms of these columns. Current deign approaches of DCM columns are generally aimed at the stability of slope. Moreover, the stability analysis is still empirical in term of the composite strength and stiffness of the treated area. To develop an effective guideline for design, the behaviour and potential failure mechanisms of DCM columns should be studied in conjunction with the stability analysis.

Prior to study stability of a stabilized slope with multi-row of DCM columns, it is desired to examine stability of a stabilized slope with one row of columns. Three-dimensional shear strength reduction finite element method was adopted to solve the Factor of Safety (FS) value of stabilized slope. The behaviours of DCM columns at the slope failure were investigated. The parametric analysis was performed in order to clearly understand the influence of parameters on the stability of stabilized slope. The parameters examined are: location, embedded length and spacing of DCM columns.

Finite element modeling

Figure 117 shows the finite element mesh used in the parametric analysis. The excavated slope of 3.0 m deep with the grade of 1:3.5 (V:H) was used in analysis. The three-dimension mesh has a size of 4.5 m wide x 60 m long x 20.8 m deep. The soil profiles was similar to use in the numerical back-analysis. The boundary conditions are; restrained horizontal displacement and free vertical displacement on the side of boundaries. Both horizontal and vertical displacements are also restrained at the bottom of boundary. The DCM column of 0.6 m in a diameter, 1.5 m in a spacing (S/D = 2.5) was used as a basic configuration in the model.

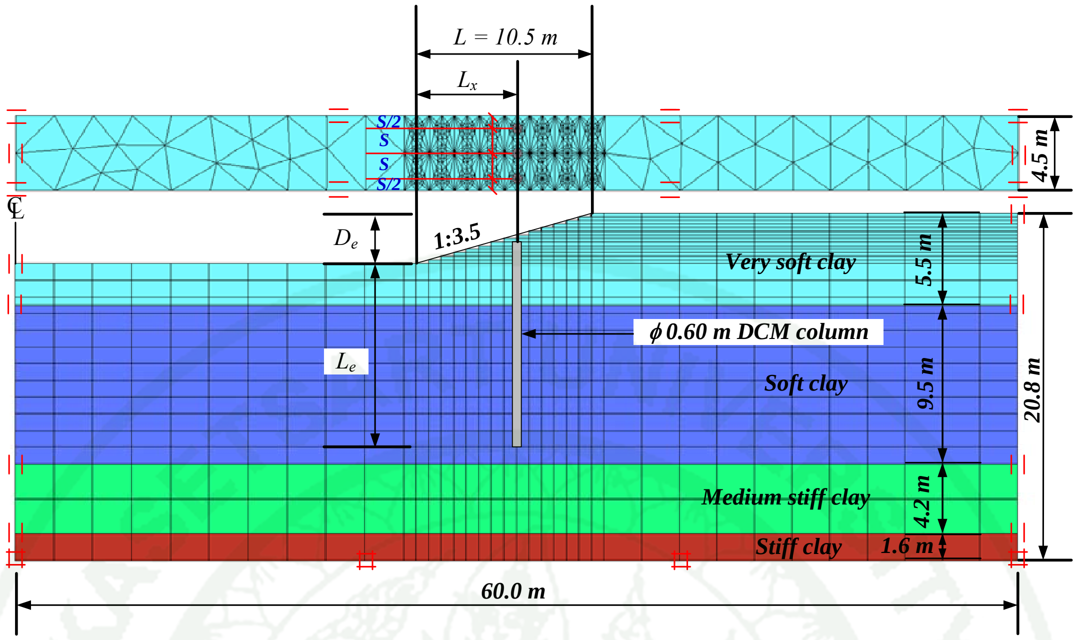

Note | | Restrained horizontal displacement

⌗ Fixed horizontal and vertical displacement

Figure 117 Finite element mesh for stabilized slope with one row of DCM columns

Constitutive model and parameters

The result from the numerical back-analysis in the previous section indicated that the Mohr-Coulomb (MC) model was reasonable to simulate the behavior of stabilized slope with DCM columns. Therefore, the in-situ soils were modeled as MC model. While a linear elastic material model is used for the DCM column in order to examine the ultimate resistance of column at the slope failure. This analysis applied the same set of parameters as numerical back-analysis. Table 21 shows the complete list of input parameters.

Table 21 List of parameters used in stabilized slope with one row of DCM columns

Materials	Very soft clay	Soft Clay	Medium stiff Clay	Stiff Clay	DCM column
Depth (m)	0.0- 5.5	5.5-15.0	15.0-19.2	19.2-20.8	-
Model	MC	MC	MC	MC	LE
Material behaviour	Undrained	Undrained	Undrained	Undrained	Undrained
E_u(kPa)	300	600Su	1000Su	1000Su	225000
γ (kN/m^3)	15.5	15.5	17	18	15
ν_u	0.495	0.495	0.495	0.495	0.33
ϕ (°)	-	-	-	-	-
S_u (kPa)	5	7	27	132.5	-

Note MCM = Mohr-Coulomb model

LEM = Lineal Elastic model

DCM = Deep Cement Mixing

S_u = Undrained shear strength

E_u = Undrained elastic modulus

ν_u = Undrained Poisson's ratio

Stability analysis of unstabilized slope

The geometry of slope in Figure 117 was used to investigate failure mechanism and find Factor of Safety (FS) of the unstabilized slope. Figure 118 shows potential failure mechanism of unstabilized slope represented by incremental total displacement contours. The FS of unstabilized slope was 1.04. The depth of potential failure surface was at 5.5 m to 6.0 m deep below the ground surface, and passed through the toe of slope.

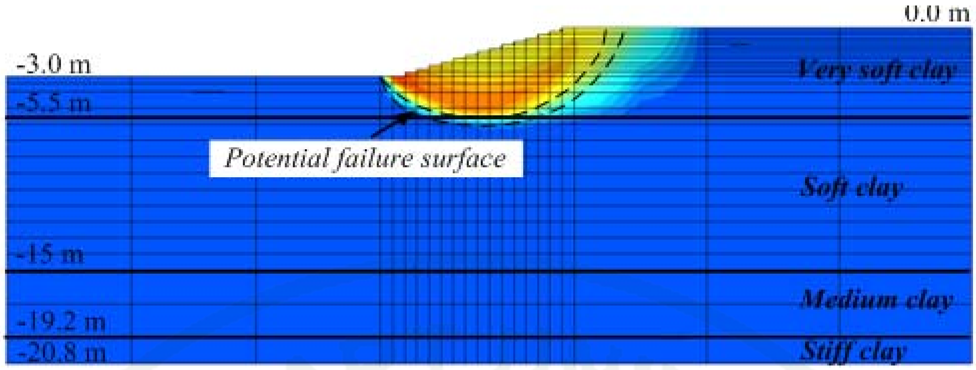

Figure 118 Estimated failure surface of unstabilized slope

Parametric analysis

1. Effect of position

The effect of DCM column position was carried out by moving the position of DCM column along the slope. The DCM column position in the slope are indicated by the ratio of the horizontal distance between the slope toe and the column position (L_x) to the horizontal distance between the slope toe and slope crest (L), as shown in Figure 117. The ratio of $L_x/L = 0$ means the position of DCM column is at the slope toe while the ratio of $L_x/L = 1$ indicates the column is placed at the slope crest. To provide a fixity condition, the lower tips of DCM columns were set at a depth of 14 m, which was deeper than the potential failure surface.

The influence of the DCM columns position on the FS of the slope is shown in Figure 119. The FS increases sharply with the increase of L_x/L from 0 to 0.29. It then slightly increases to the peak value of 1.29 at the $L_x/L = 0.58$. After that, the FS gradually decreases to the value of 1.21 at the $L_x/L = 1.0$. The effective zone is considered to be $L_x/L = 0.29$ to 0.86. This finding is very close to the result of Lee *et al*. (1995), Hassiotis *et al* (1997), Cai and Ugai (2000), Jeong *et al*. (2003), Won *et al*. (2005) and Ashour and Ardalan (2012).

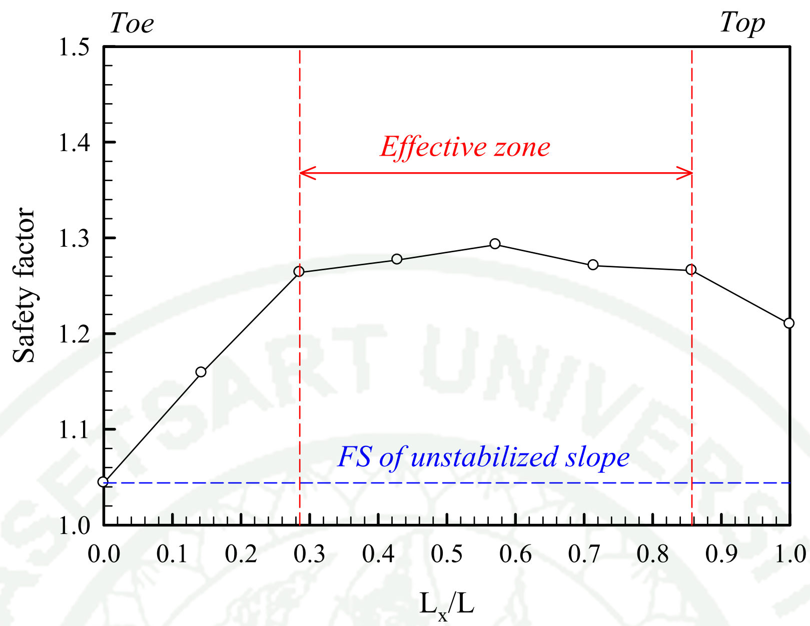

Figure 119 Effect of DCM column position on FS

Figure 120 presents the displacement, shear force and bending moment developed in DCM column at various positions. When the DCM columns are placed within the effective zone, the lateral pressure acting on the DCM columns is large. This can be indicated by DCM column displacement. Therefore, the resistance of DCM columns (i.e. shear force and bending moment) is sufficiently mobilized, and the large FS is obtained as on Figure 119. On the other hand, when the DCM columns were placed at the toe of slope, the resistance of DCM columns is not sufficiently mobilized due to small pressure acting on the DCM columns. It can be concluded that the developed resistance of DCM column is significantly influenced by the position.

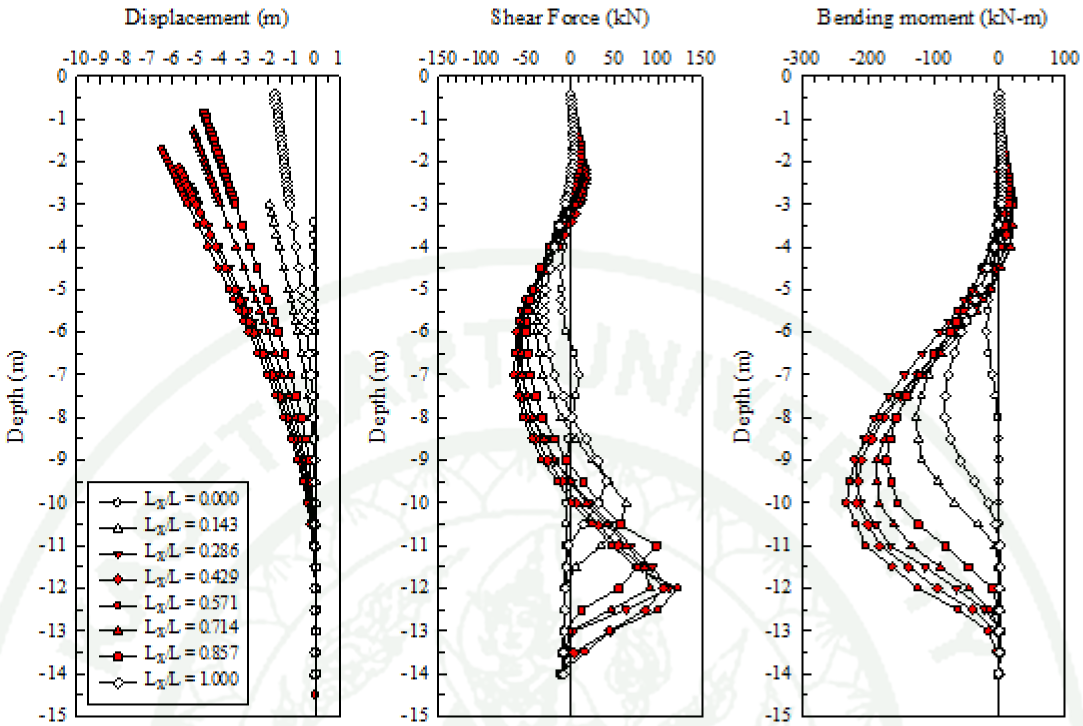

Figure 120 DCM column structural behaviour

2. Effect of embedded length

The embedded length (L_e) was expressed as a ratio of excavated depth (D_e). The various (L_e/D_e) were studied to see the effect of L_e and its corresponding behaviour. The values examined are: L_e/D_e = 0.33, 1.00, 1.67, 2.33, 3.00, 3.67, 4.70 and 5.93. Two positions of DCM columns within the effective position, i.e. L_x/L = 0.286 and 0.571, were used in this study.

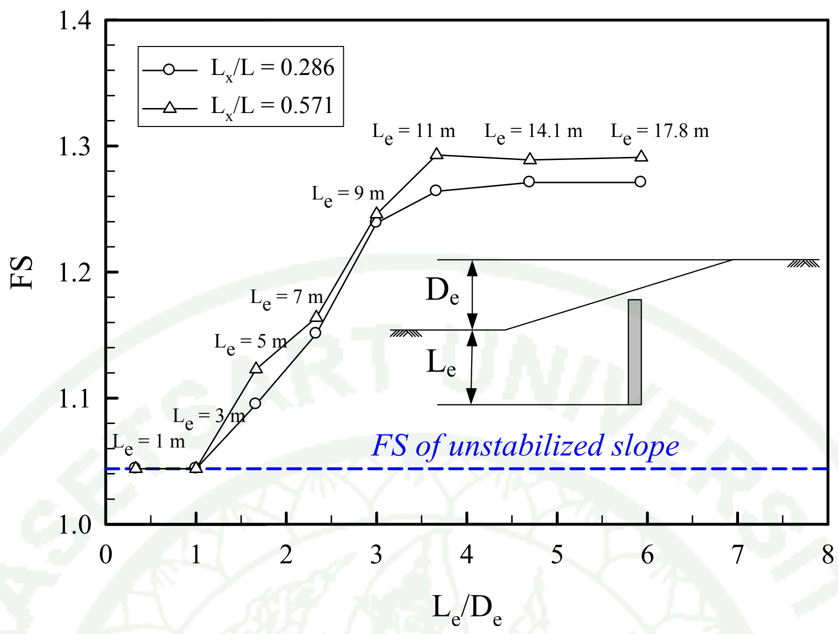

Figure 121 Effect of embedded length on FS

The effect of column depth on the Factor of Safety (FS) of slope is shown in Figure 121. When the $L_e/D_e > 1$ (i.e. the DCM column tip penetrates through the potential failure surface of unstabilized slope), the FS of both positions exhibits the increase with L_e/D_e. The relevant length is depended on the design requirement, but L_e/D_e more than 3.6 times will not benefit to the stability of slope.

The behaviour DCM column at the $L_x/L = 0.571$ was explained in to two cases as follows:

a. Short embedded length

The displacement, shear force, and bending moment developed in the DCM column for the $L_e = 1$ and 3 m are shown in Figure 122. When the embedded length is so short that it does no penetrate beyond the potential failure surface, the DCM columns displace with the sliding soil. This finding agrees with Poulos (1999) that described the failure mode of short pile, which involves failure of soil underneath the pile. Therefore, the resistances of DCM column (i.e. shear force and bending moment) are not adequately mobilized to improve stability of slope. When the lower tip of DCM columns penetrate beyond the potential failure surface, the column rotation rather than sliding was observed. The resistance of DCM columns is also more developed. It coincides with the increase of FS.

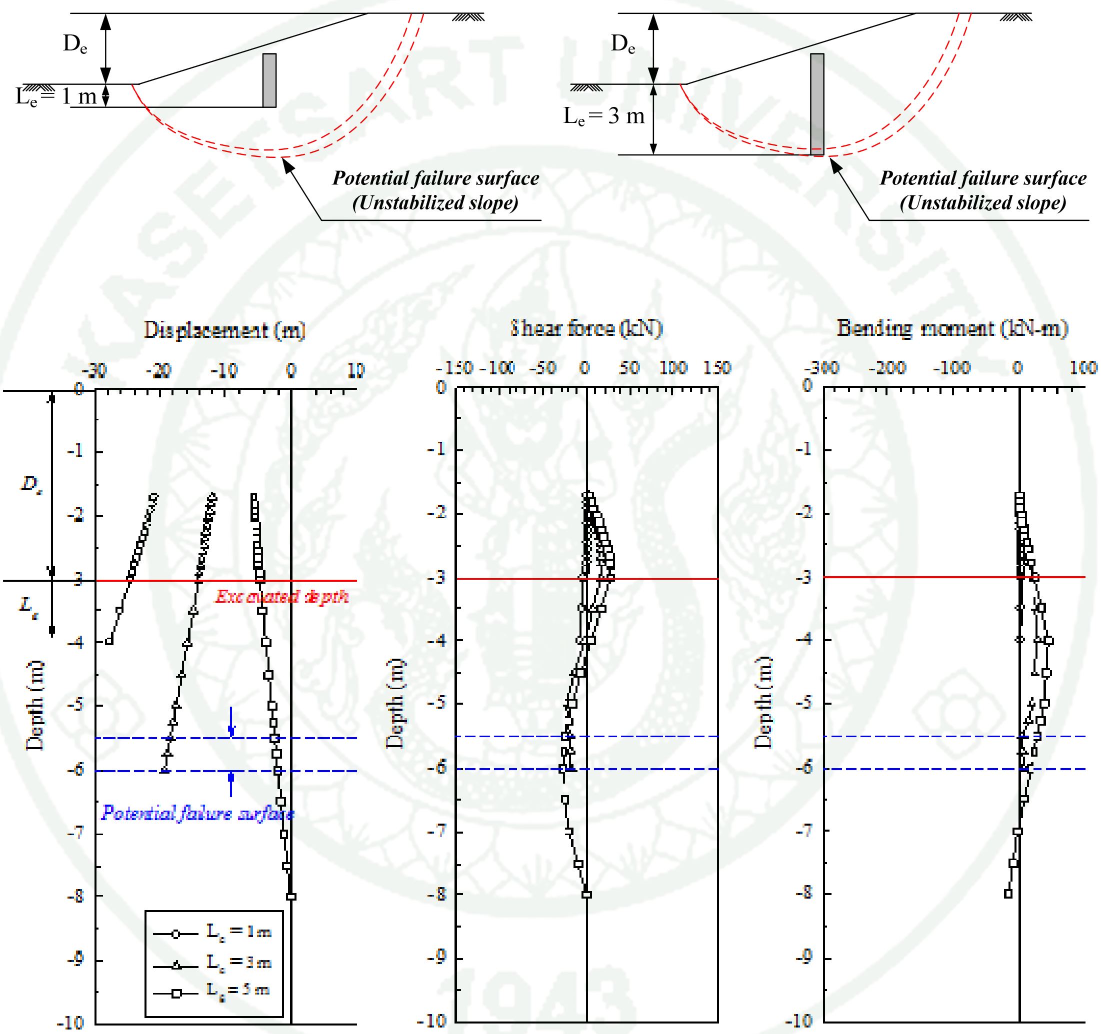

Figure 122 DCM column structural behavior for L_e = 1 m, 3 m and 5 m at L_x/L = 0.57

b. Intermediate and long embedded lengths

Figure 123 shows the displacement, shear force, and bending moment developed in the DCM column for the L_e = 5 m to 17.8 m. The potential failure behaviour were considered by the displacement behavior. The fixity condition at the lower tip of DCM column is pronounced when the L_e > 3 m. For the intermediate embedded length (L_e = 5 m and 7 m), the DCM columns behave as a rigid body rotation without substantial flexural. In this mechanism, the soil is assumed to be failure over the full length of DCM columns (Viggiani, 1981 and Poulos, 1995). For the long embedded length (L_e >7 m), the DCM columns flexure rather than rotation was observed. In this case, the failure of soil occurs around the upper portion of DCM columns (Viggiani, 1981 and Poulos, 1995). The failure mode of DCM columns involves with one plastic hinge, where maximum bending moment occurs.

The shear force increase with the increase of embedded length. The first extreme point of the shear force can be regarded as the level of potential failure surface described by Ito *et al.* (1981), Poulos (1995) and Hossiotis *et al.* (1997). The bending moment also increases with increasing embedded length. It is found that the point of maximum bending moves downward until stable even if the embedded length is larger. This is consistent with the constant of FS in Figure 121.

It is clear that the DCM column behaviours significantly influence on the FS of slope. To improve the FS of slope, the fixity condition at lower tip of DCM column should be provided. In this study, the FS reaches to the maximum value when the L_e/D_e = 3.6. The further increase of L_e does not benefit to increase the FS.

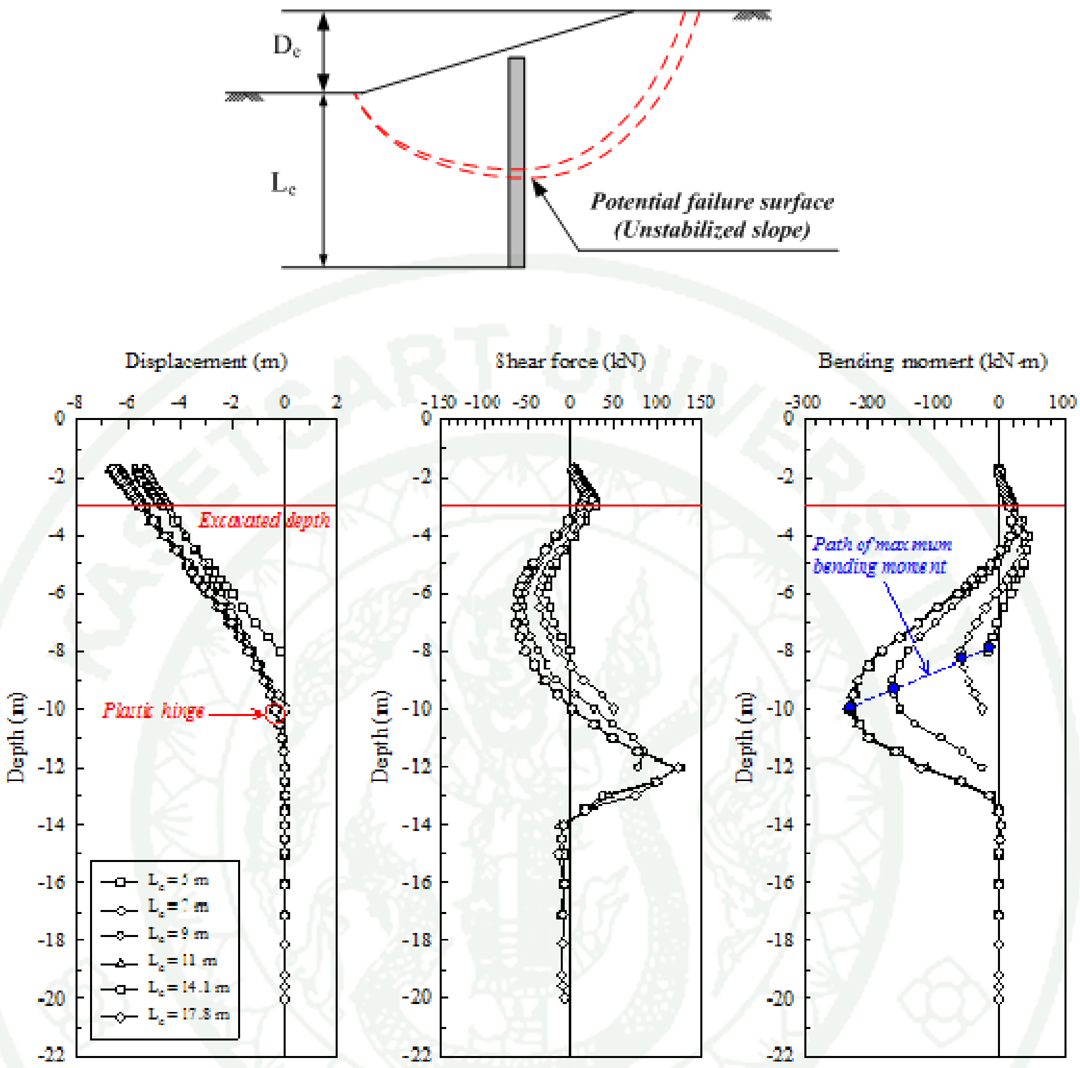

Figure 123 DCM column behavior for L_e = 5 m to 17.8 m (L_x/L = 0.57)

3. Effect of spacing

The purpose of this study is to investigate the effect of DCM column spacing on the stability of slope. To study the effect of the spacing, the ratios of S/D (S = center-to-center of column and D = diameter of the column) from 2 to 10 were investigated. Due to the previous analysis regarding the effective position and embedded length, the $L_x/L = 0.57$ and $L_e = 14$ m were determined. Therefore, the effect of spacing was only analyzed in the aforementioned position and embedded length.

The effect of DCM column spacing on the Factor of Safety (FS) is shown in Figure 124. The FS increased with the decrease of DCM columns spacing as found by Cai and Ugai (2000), Jeong *et al*. (2003), Won *et al*. (2005) and Ashour and Ardalan (2012). The optimum spacing cannot clearly identify in this analysis. This may be because the interface element model was not applied with DCM columns. Therefore, soil and DCM column move together. However, it is found that the rate of increase in the FS is shown obviously at the $S/D \leq 4$. This can be explained by the fact that the DCM column and surrounding soil start to act together as one soil mass (i.e. soil arching effect). The assumption is consistent with the finding of Prakash (1962), Cox *et al*. (1984), Reese *et al*. (1992), and Liang and Zeng (2002), who concluded that $S/D \leq 5$ is required to generate soil arching.

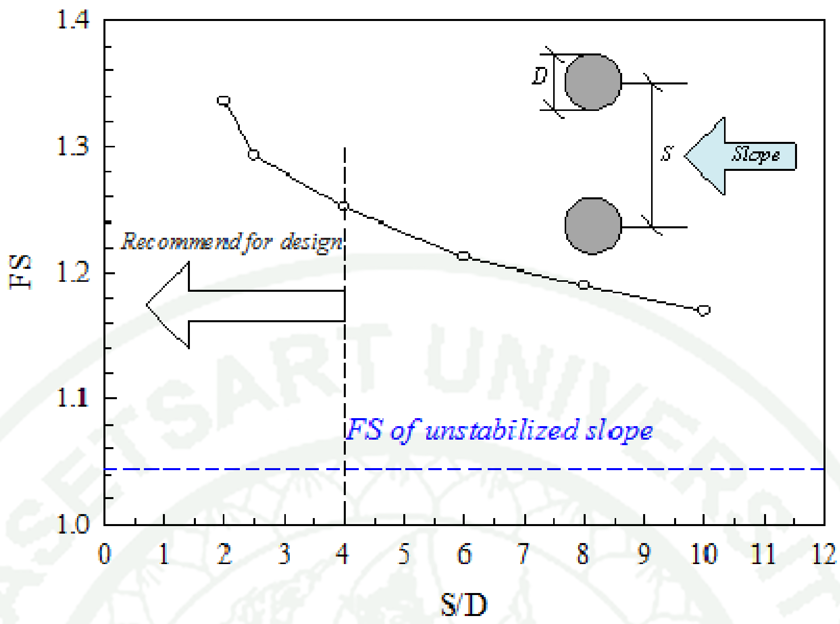

Figure 124 Effect of DCM column spacing on FS

Figure 125 illustrates the displacement, shear force, and bending moment developed in DCM columns for various spacings. It found that the displacement of DCM columns increase with the decrease in spacing as found by Cai and Ugai (2000) and Yang *et al.* (2011). This is because the DCM columns and soil in between act as a stronger mass. The stabilized slope does not reach the failure condition at small displacement until the DCM columns displace greatly. For the closer spacing, the large development of shear force and bending moment is noticeable at the lower portion of the DCM columns. It indicates that the resistance of DCM column is fully mobilized.

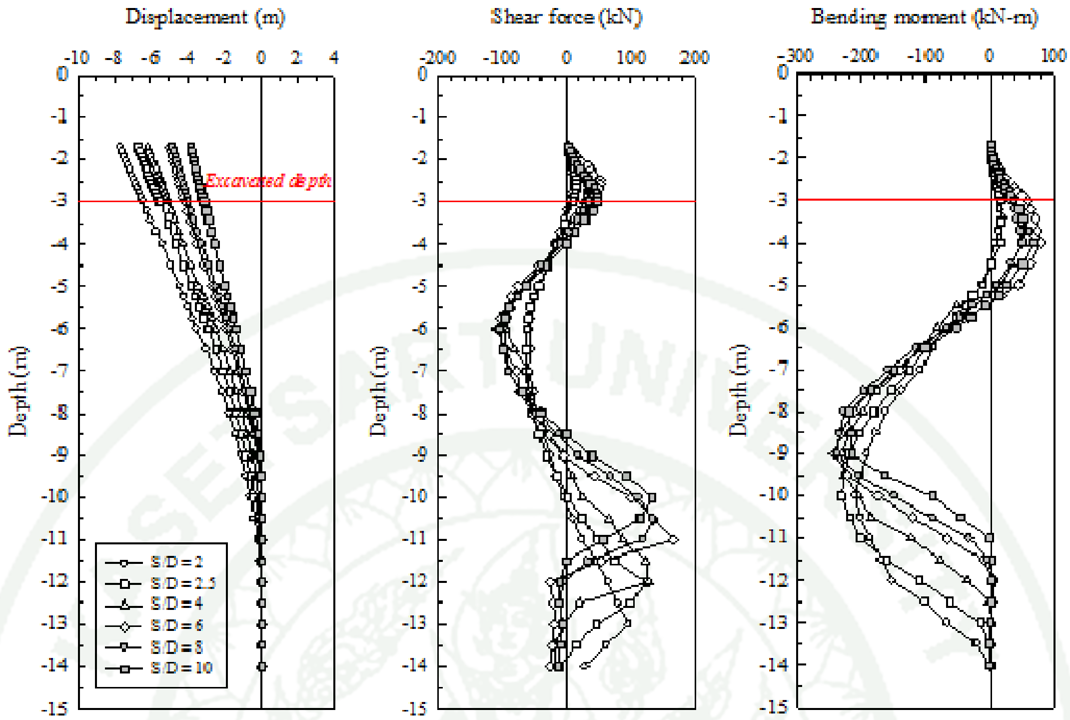

Figure 125 DCM columns structural behavior for various spacings ($L_x/L = 0.57$)

Numerical Analysis of Stabilized Slope with Multi-Rows of DCM Columns: Parametric Analysis

DCM column used for slope stabilization is generally designed as a row pattern of tangential or overlapping in order to improve its bending strength (Moseley and Kisach, 2004). However, the problem of alignment and contact of DCM columns can be encountered when the single mixing tool is used without sticky control. The poor construction of tangential DCM columns leads to lower bending strength than design. To avoid this problem, a group of individual DCM columns pattern can be utilized.

In the previous section, the influence of parameters on the stability of stabilized slope with one row of DCM column was investigated. The effective design parameters (i.e. position, embedded length and spacing) were addressed. When the DCM columns are grouped together, the column-soil interaction influences on the behaviour of each individual column. Therefore, this section study the effect of parameters on the stability of stabilized slope with a group of individual DCM column called as multi-rows of DCM columns. Three-dimensional shear strength reduction finite element method was adopted to solve the Factor of Safety (FS).

Finite element modeling

Figure 126 shows the finite element mesh of stabilized slope with rectangular or square and triangular of DCM columns. The DCM column spacing of 1.5 m in the cross-section of slope (S_S) and in the longitude of slope (S_L) was used as a basic configuration in the model. The three-dimensional mesh has a size of 4.5 m wide x 60 m long x 20.8 m deep. The boundary condition, constitutive models and parameters were the same as use in the analysis of one row of DCM columns.

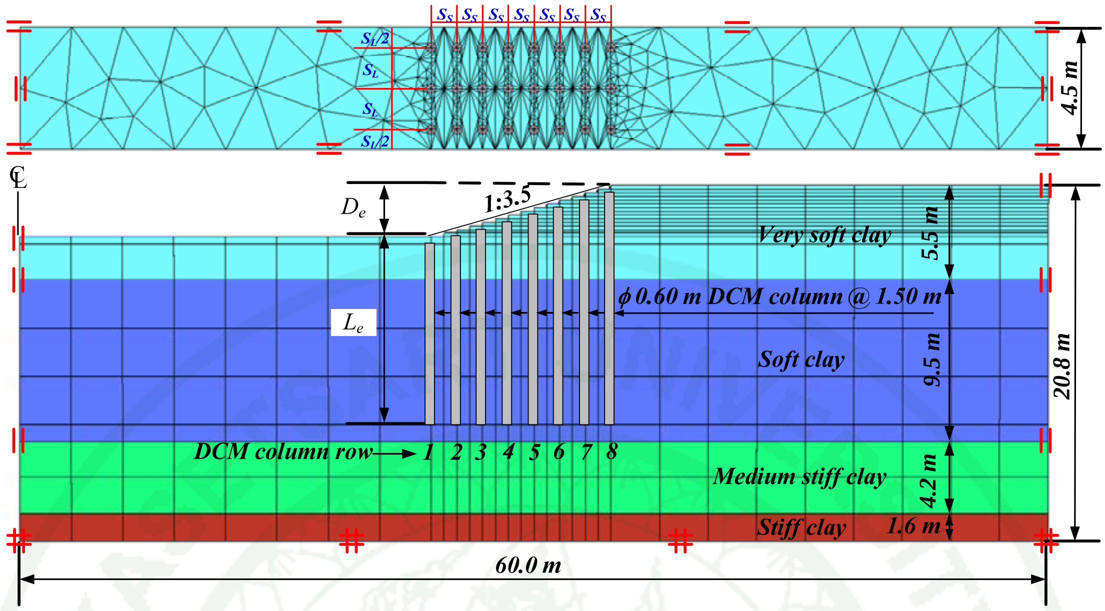

a) Rectangular and square patterns

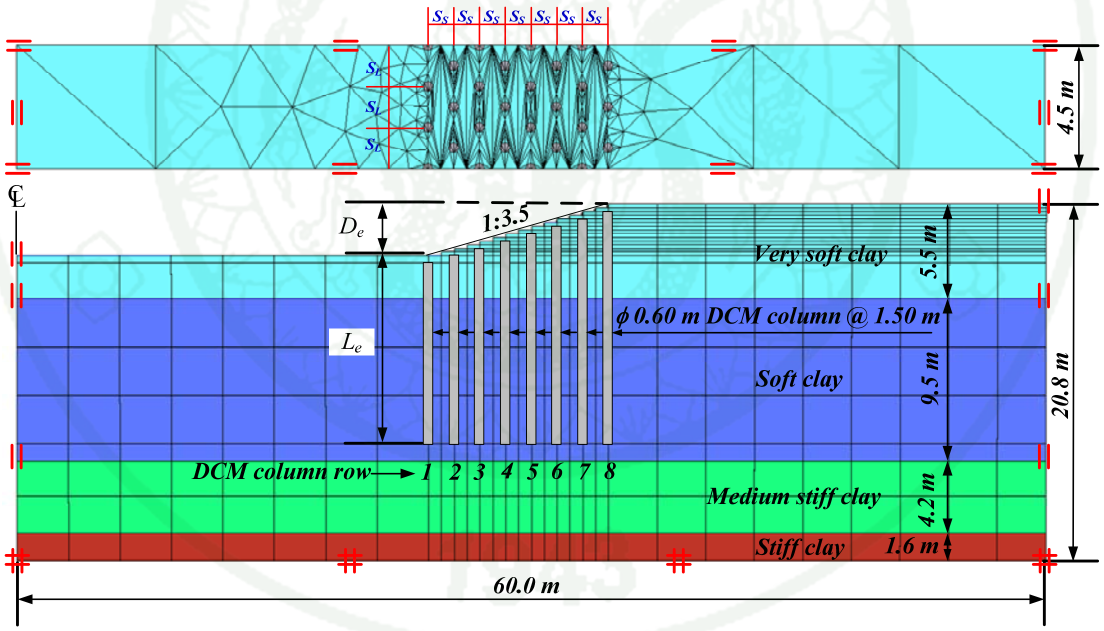

b) Triangular pattern

Note | | Restrained horizontal displacement

⌗ Fixed horizontal and vertical displacement

Figure 126 Finite element mesh for stabilized slope with multi-rows of DCM columns

Parametric analysis

1. Effect of embedded length

The embedded length of the DCM column below the excavation depth was varied parametrically. The embedded length (L_e) is expressed as a ratio of excavated depth (D_e). The values examined are: L_e/D_e = 0.33, 1.00, 1.67, 2.33, 3.00, 3.67, and 4.70. The effect of embedded length (L_e) on the Factor of Safety (FS) of slope is shown in Figure 127. The FS obtained from both patterns increases consistently with the L_e. There is no significant difference in the FS between rectangular and triangular patterns. It can be seen from the figure that the FS tends to approach a constant of 1.4 when the L_e/D_e is more than 2.33. Therefore, the further increase of L_e will not benefit to the slope stability. It can be seen from the figure that the L_e/D_e = 3 can be considered to be effective ratio.

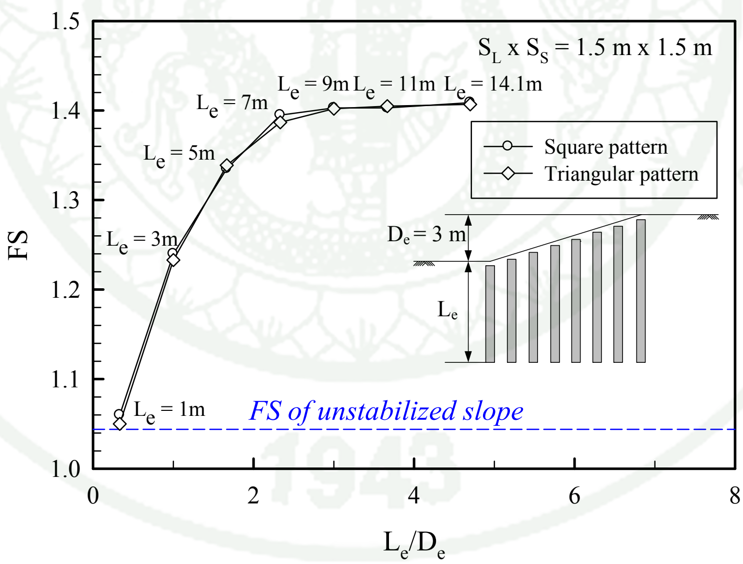

Figure 127 Effect of embedded length on FS

Figure 128 to 130 shows the behaviour of short embedded length of DCM columns (i.e. Le = 1 and 3 m). When the embedded length is so short that (L_e = 1 m) it does not penetrate beyond the potential failure surface, the potential failure mode of DCM columns is similar to short pile. The DCM columns move together with the sliding soil due to failure of soil underneath the column tip (Poulos, 1999). Therefore, the resistance of DCM columns is not adequately mobilized to improve stability of slope. The translation failure mode of DCM columns take place instead of sliding mode as the embedded length of DCM column reaches to 3 m (L_e = 3 m). The resistance of DCM columns can be sufficiently mobilized to escalate the FS.

Figure 131 to 134 illustrates the behavior of long embedded length of DCM columns (L_e = 5 to 14.1 m). The displacement of DCM columns shown in Figure 131 indicated that the fixity condition was pronounced at the embedded length of 9 m, that is consistent with the constant FS. This means a large embedded length is required to provide a fixity condition so that the highest FS is obtained. When the maximum bending moment within the DCM columns exceeds the moment capacity of columns, plastic hinges will develop at these locations, as illustrated in Figure 132. It can be seen from the figure that the two plastic hinges are almost formed within the DCM columns as the fix end condition is pronounced (i.e. L_e > 5 m). Figure 133 shows the development of shear force within the DCM columns. The negative shear force generally reaches the first extreme point approximately 5 m to 7 m from the original ground surface, depending on the DCM column position. This depth can be regarded as the level of the potential failure surface described by Ito *et al.* (1981), Poulos, 1995 and Hassiotis *et al*. (1997). Their analytical results of showed that the maximum shear force the pile was developed at the level of the slide plane. Figure 134 shows the development of bending moment within the DCM columns. The maximum bending moment occurs at the zero shear force. It is found that the positive bending moment caused by the lateral pressure from sliding soil was a function of the row position. The DCM column 8 located at the top of slope carried the greatest load whereas the DCM column 1 carried the lowest load. The negative bending moment increases with the increase of embedded length, and the point of maximum bending moment moves downward until it tends to be a stable. After reaching a maximum value, the negative bending movement decrease with a depth until approaches to be zero value at a depth from 12.5 to 13.0 m. This means that the further increase of DCM column length will not benefit to the stability of slope.

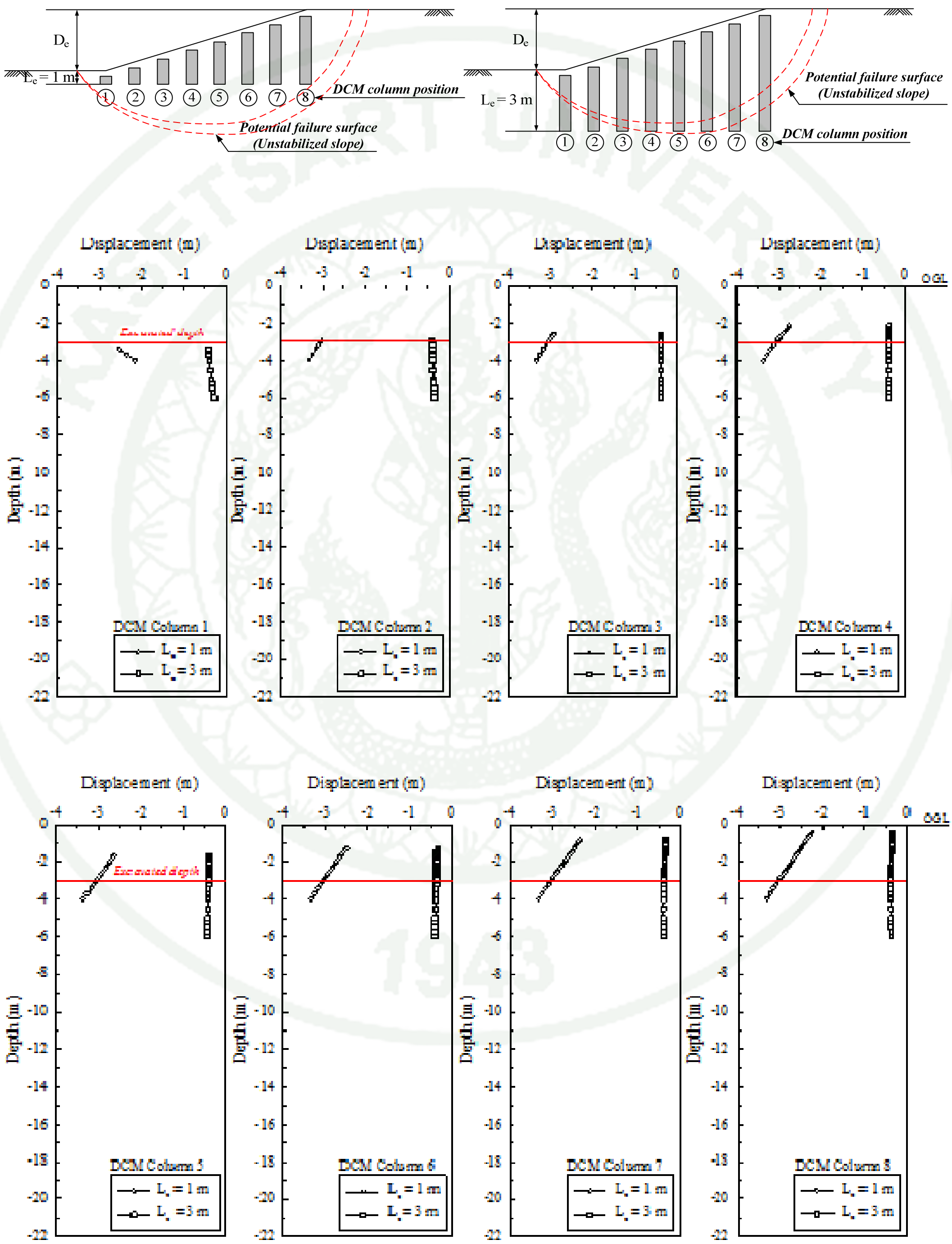

Figure 128 Displacement of multi-rows DCM columns for L_e = 1 m and 3 m

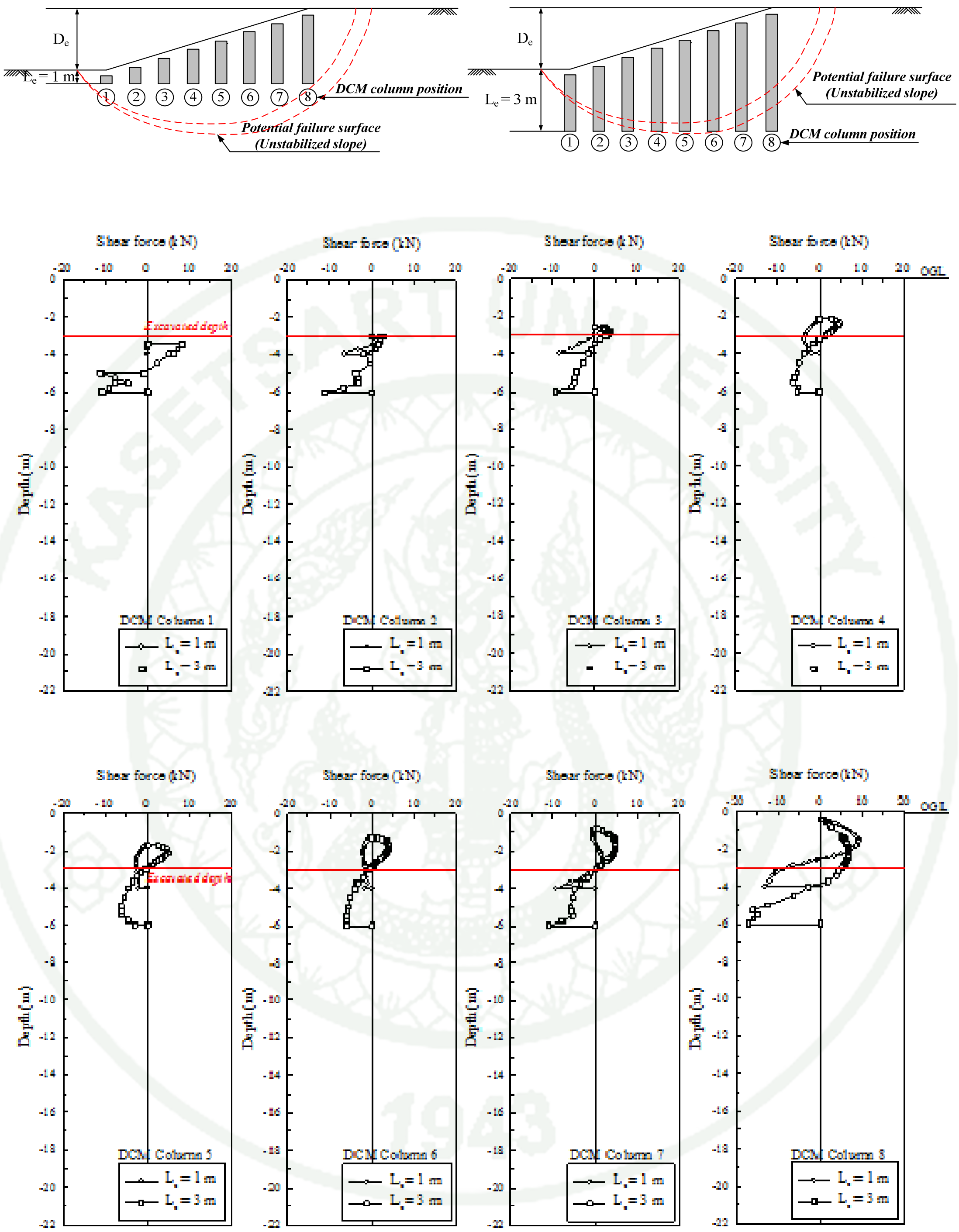

Figure 129 Shear force of multi-rows DCM columns for L_e = 1 m and 3 m

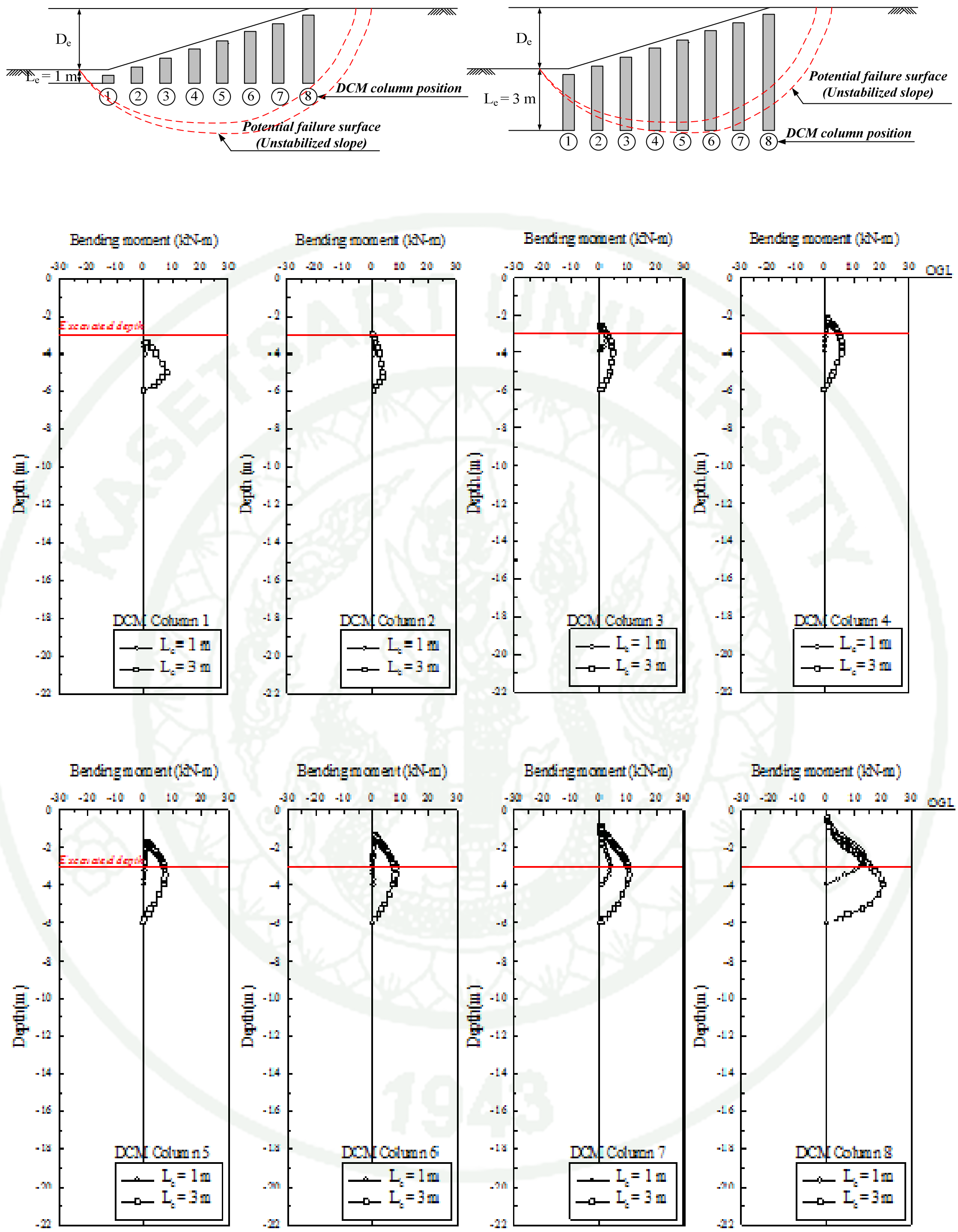

Figure 130 Bending moment of multi-rows DCM columns for L_e = 1 m and 3 m

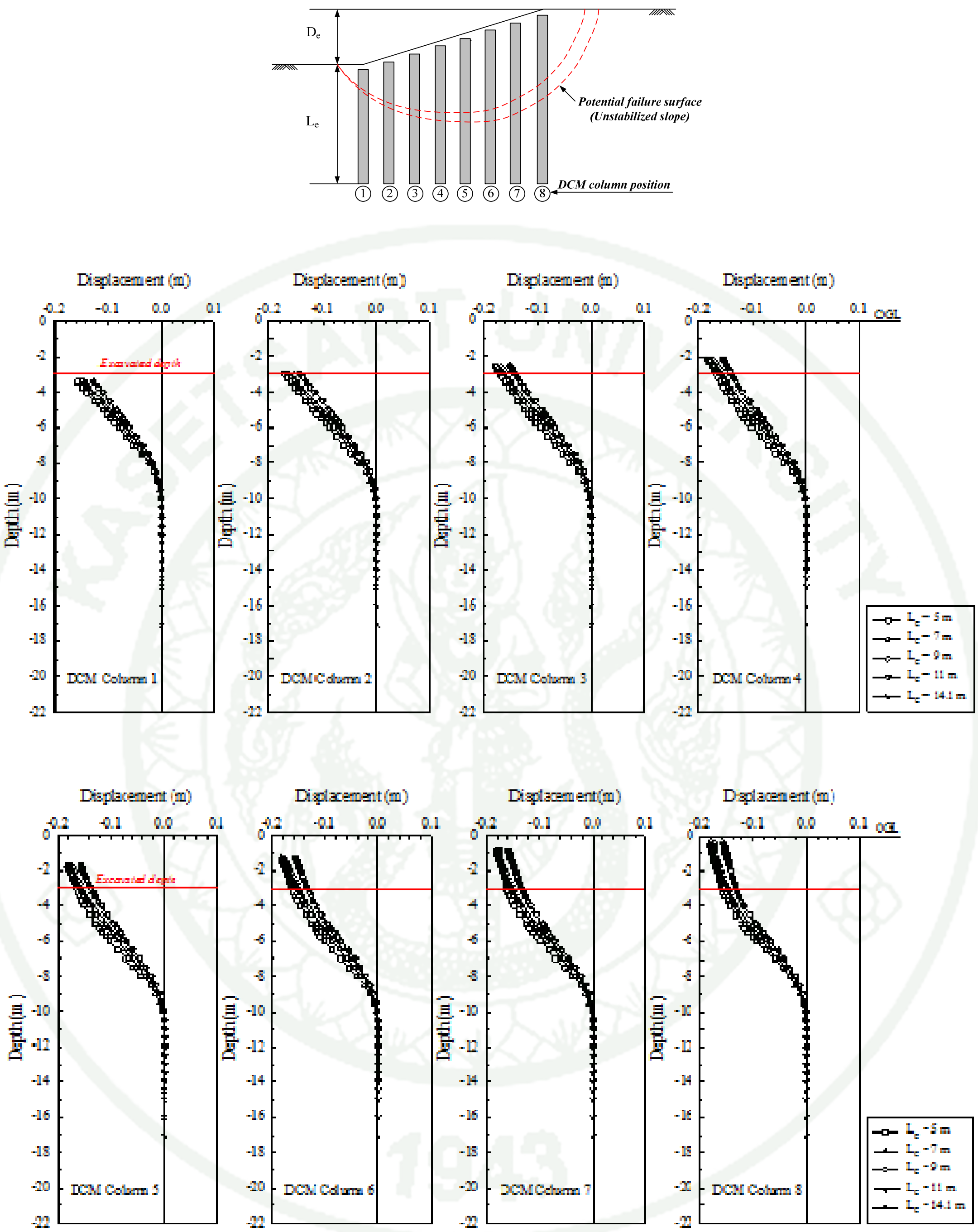

Figure 131 Displacement of multi-rows of DCM columns for L_e = 5 m to 14.1 m

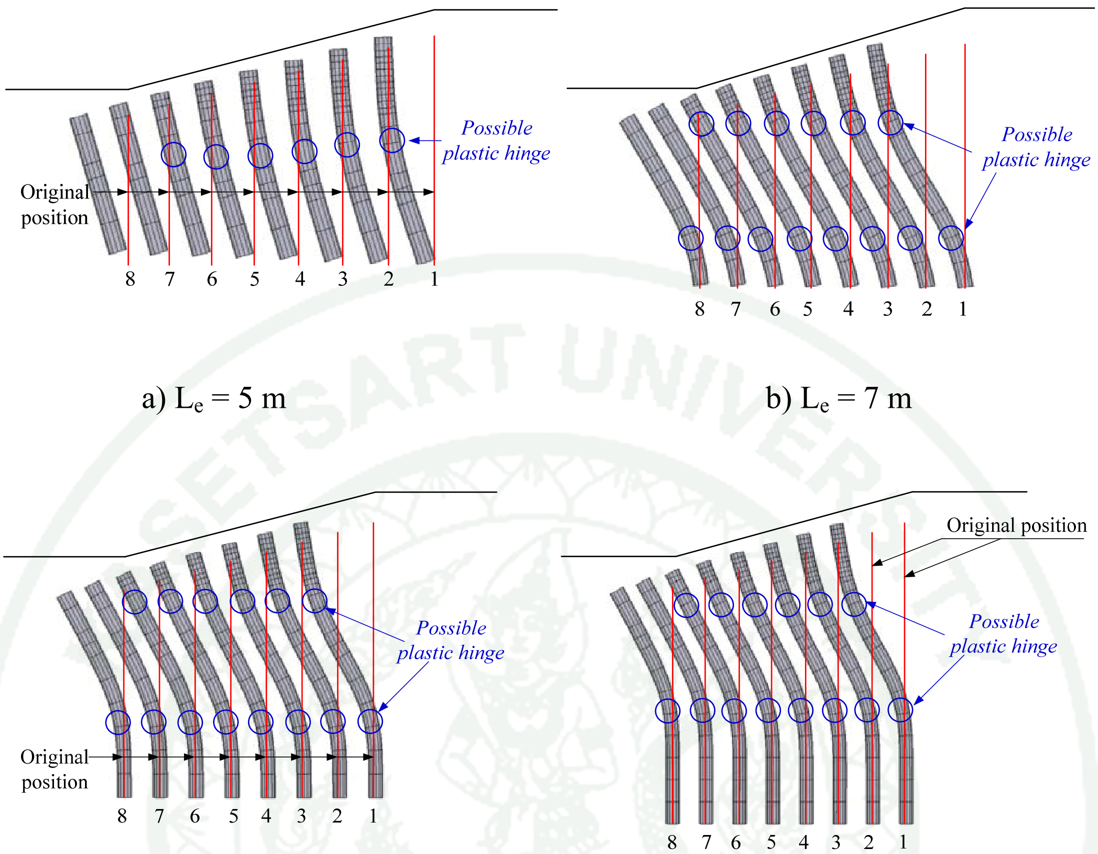

a) L_e = 5 m

b) L_e = 7 m

c) L_e = 9 m

d) L_e = 11 and 14 m

Figure 132 Formation of possible plastic hinge of multi-rows of DCM columns

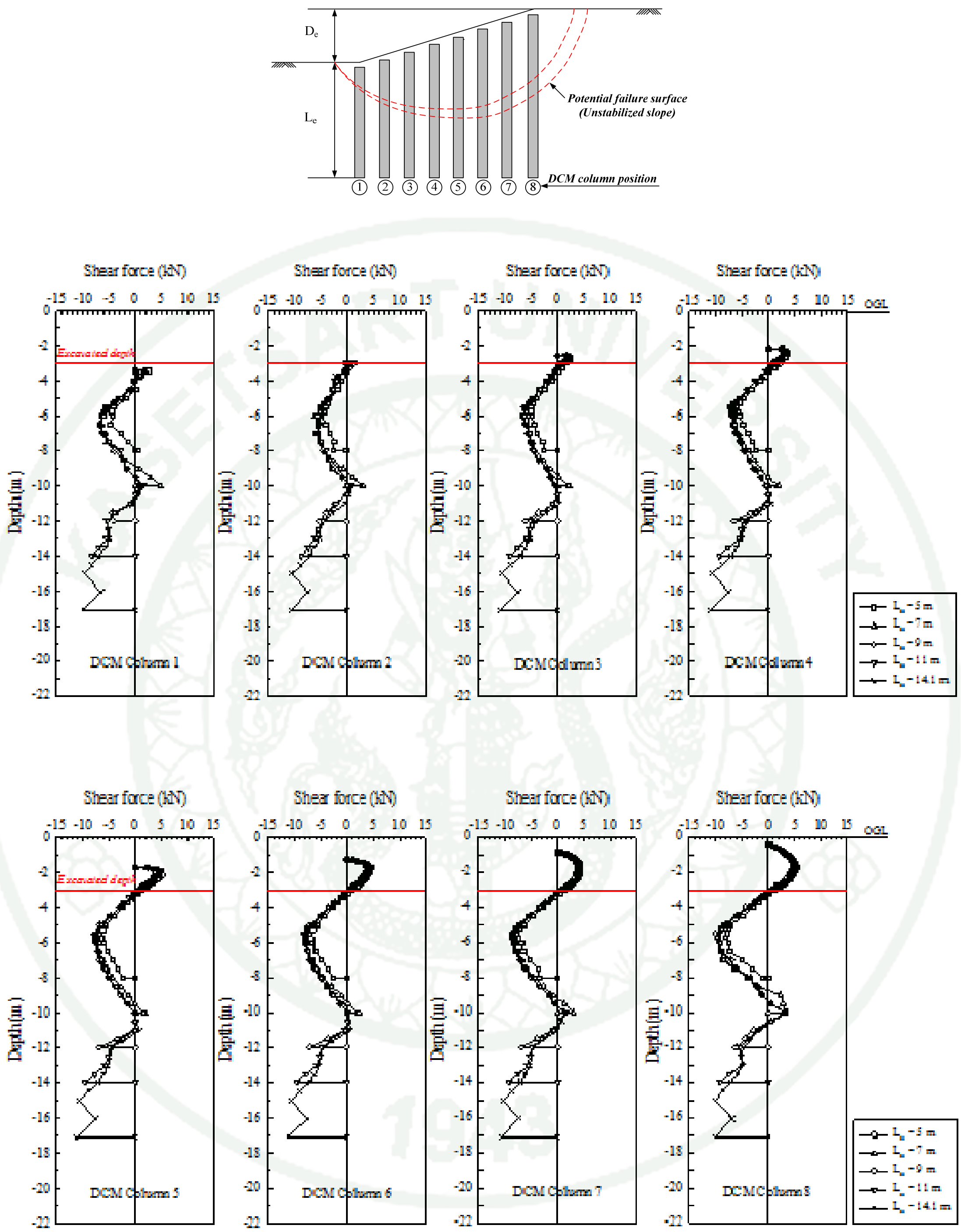

Figure 133 Shear force of multi-rows of DCM columns for L_e = 5 m to 14.1 m

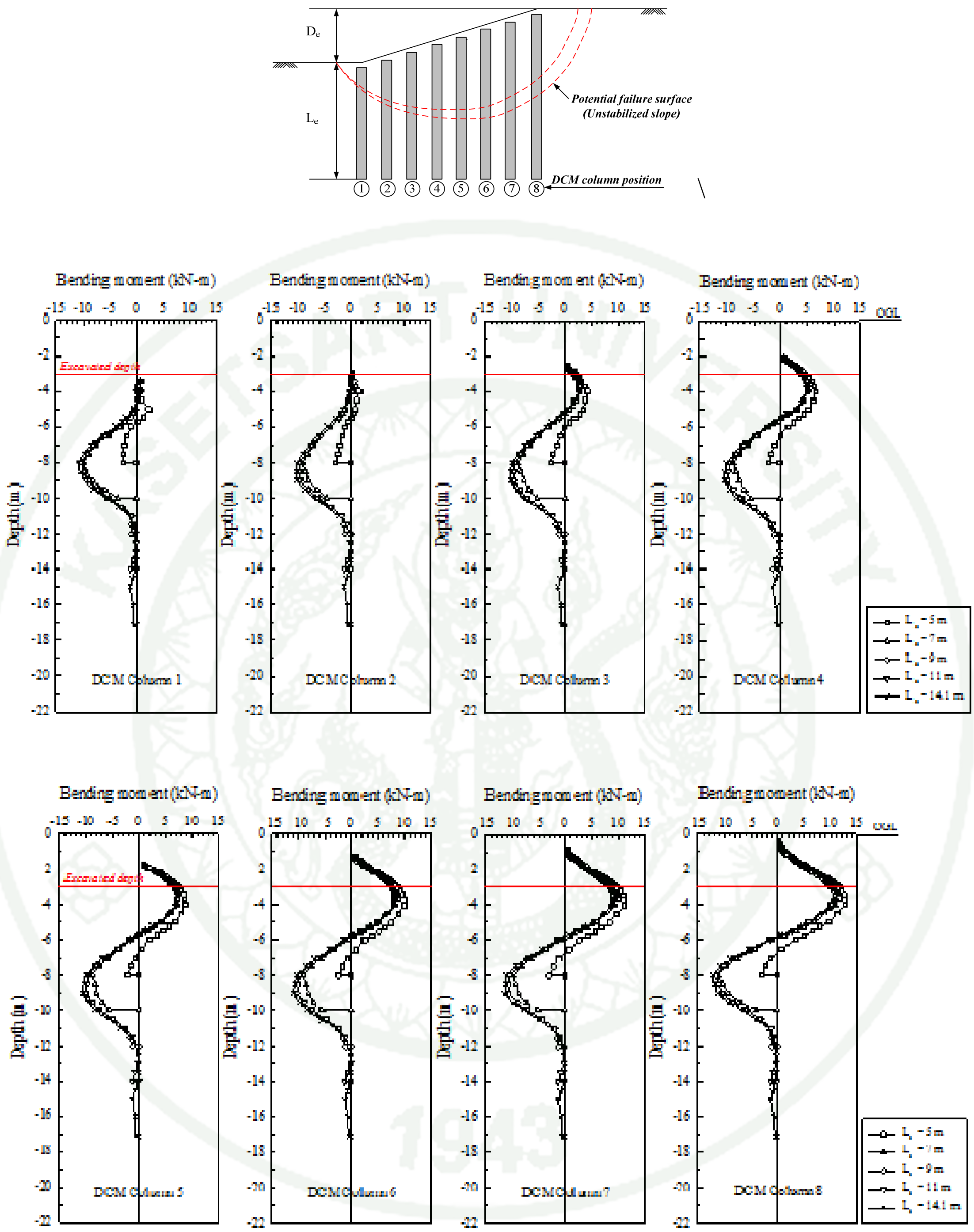

Figure 134 Bending moment of multi-rows of DCM columns for L_e = 5 m to 14.1 m

2. Effect of DCM column spacing

DCM column spacing must be sufficient for arching effect so that column and soil will act as one soil mass. Wang and Yen (1974) analytically studied the behaviour of piles in a rigid-plastic infinite soil slope. They concluded that both sandy and clayey slopes had the critical spacing beyond which almost no arching develops. This section investigated the effect of DCM column spacing on stability of slope. The spacing in the cross-section of slope (S_L) was varied while the spacing the longitude of slope (S_S) was kept constant. The effect of DCM column spacing (S_L) was expressed as a ratio of column diameter (D). The ratios of S_L/D varied were: 2, 2.5, 4, 6, 8 and 10. Due to previous analysis regarding the effect of embedded length (L_e), the L_e = 9 m was enough to provide the fixity condition and maximum Factor of Safety (FS). However, the L_e of 11 m was selected for the analysis to ensure the fixity condition of large spacing.

Figure 135 shows the effect of spacing on the FS of the slope. Similar to the one row DCM columns, the optimum spacing cannot identify in this analysis. However, it is observed that the rate of increase in the FS is significant at the $S_L/D < 8$. It can be interpreted that the interaction between DCM column and surrounding soil start to mobilize associated with arching effect. The effect of pattern is observed at the $S_L/D \leq 2.5$. The triangular pattern shows FS higher than the rectangular patter, especially at the $S_L/D = 2$. For $S_L/D = 2$, the DCM column in triangular pattern behave as a continuous large wall.

Figure 136 to 138 illustrate the displacement, shear force and bending moment within the multi-rows of DCM columns generally increase with increasing column spacing. This can be explained by the fact that each DCM column has to resist a wider strip of lateral soil movements at a high spacing. Figure 139 shows the maximum displacement of DCM columns for different column spacing. For $S_L/D \leq 4$, the DCM column in each row moves by nearly the same amount. It indicates that the DCM columns act as a continuous row associated arching effect in resisting lateral pressure from sliding soil. For the $S_L/D > 4$, the different movements of DCM column in each column are shown. The DCM columns behave like a individual column due to insufficient column-soil interaction. The maximum shear force and bending moment of DCM columns for different columns spacing are shown in Figure 140 and 141. The development of DCM column resistance in each row (i.e. negative shear force and bending moment) is approximately the same amount for the $S_L/D \leq 4$. While the significant difference of DCM column resistance development is found for the $S_L/D > 4$. As explained in more detail, $S_L/D = 4$ is largest ratio that is required to sufficiently mobilize arching effect and continuous row.

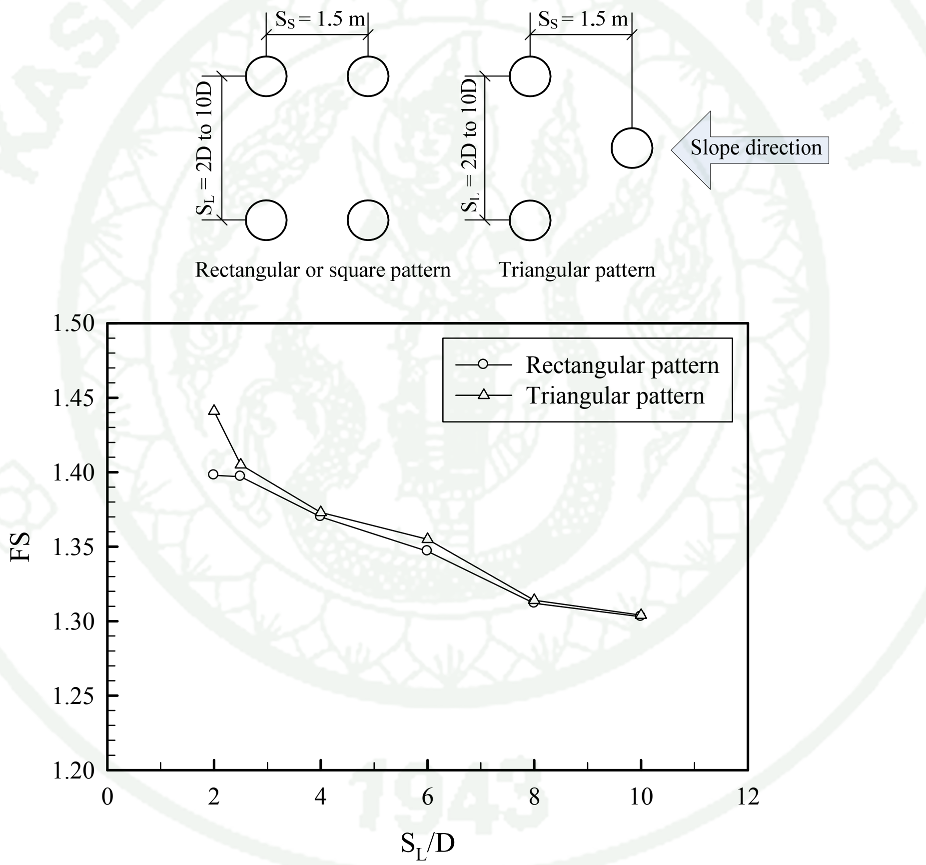

Figure 135 Effect of multi-rows DCM columns spacing on FS

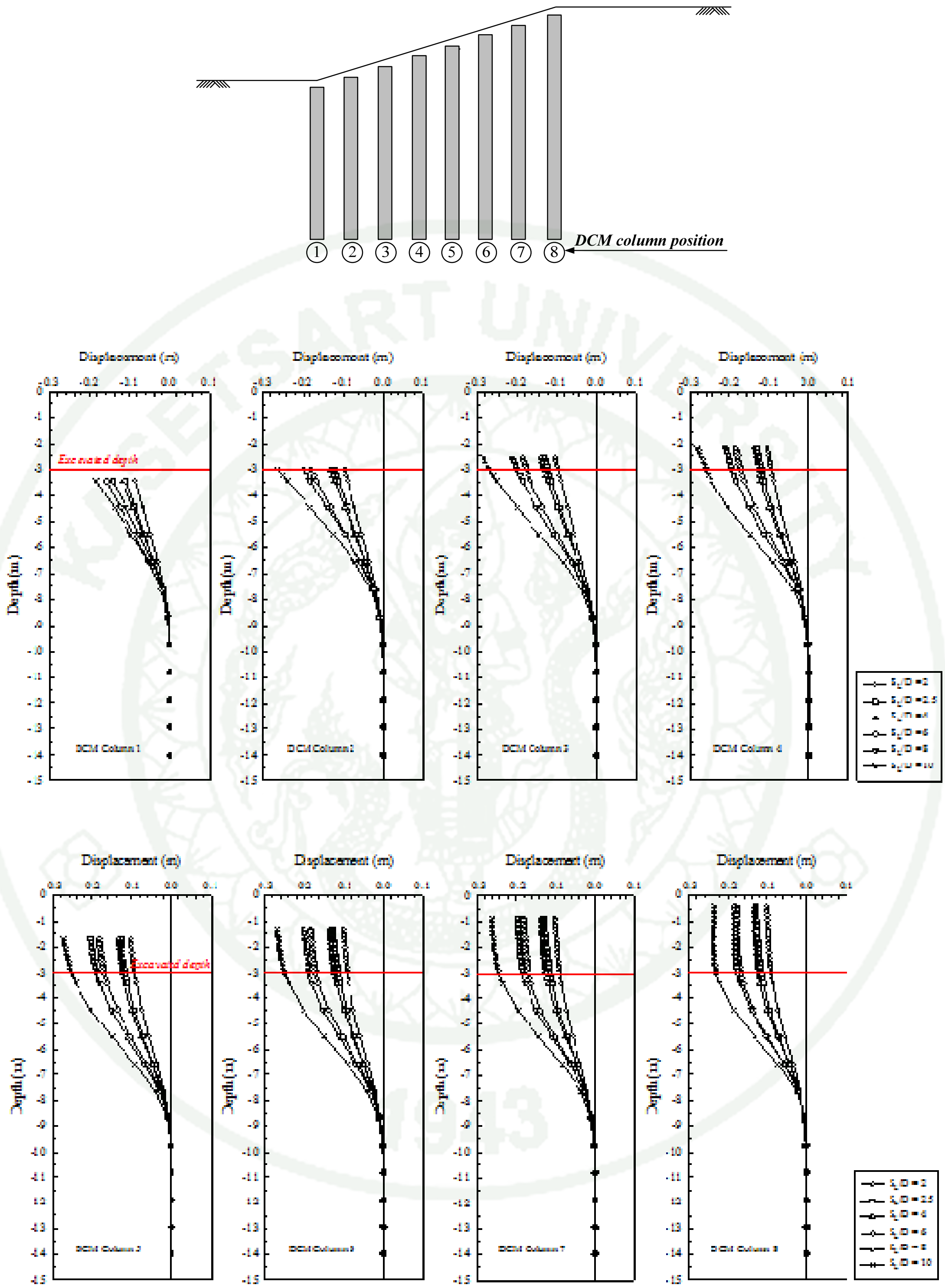

Figure 136 Displacement of multi-rows of DCM column for various spacings

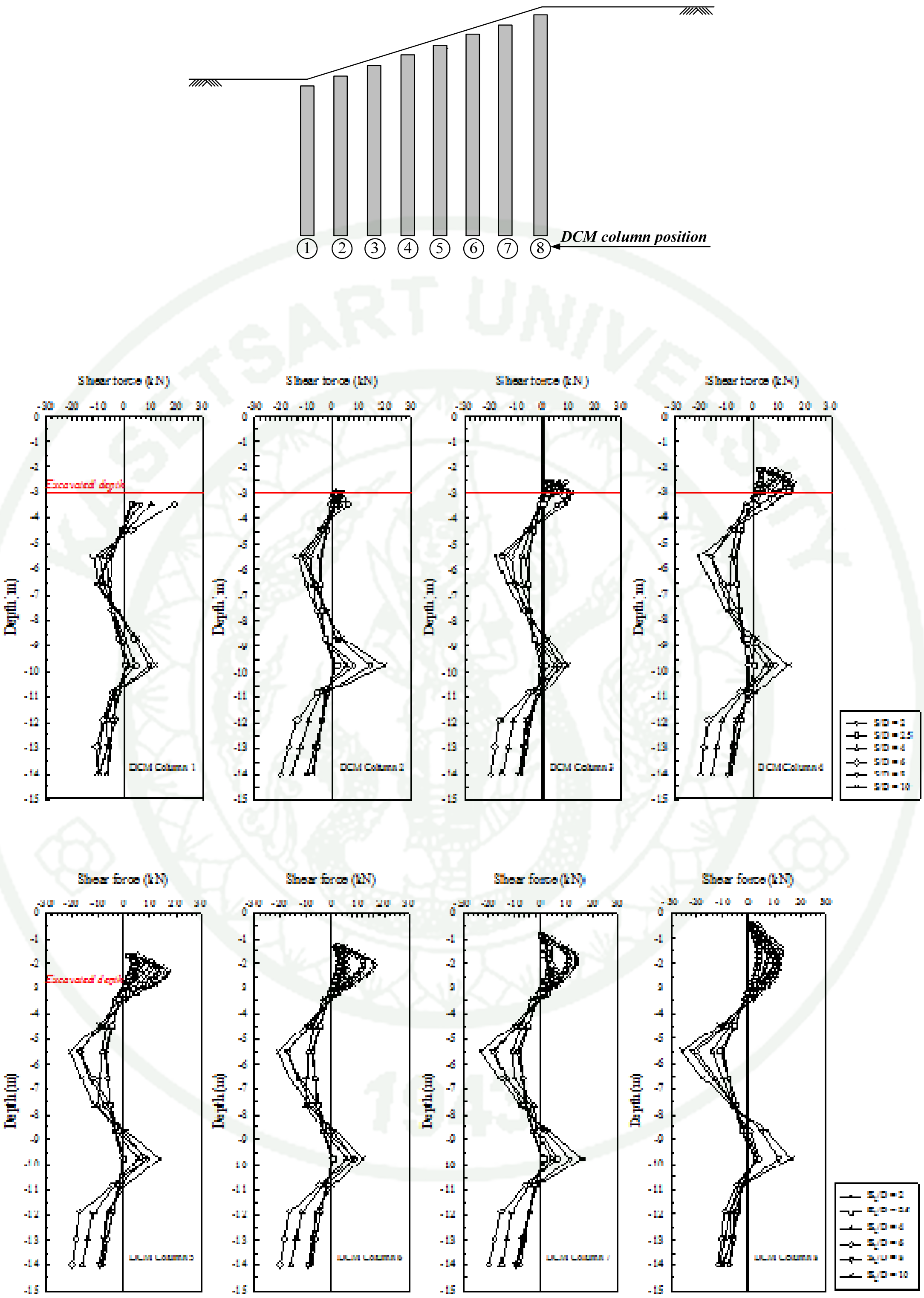

Figure 137 Shear force of multi rows of DCM column for various spacings

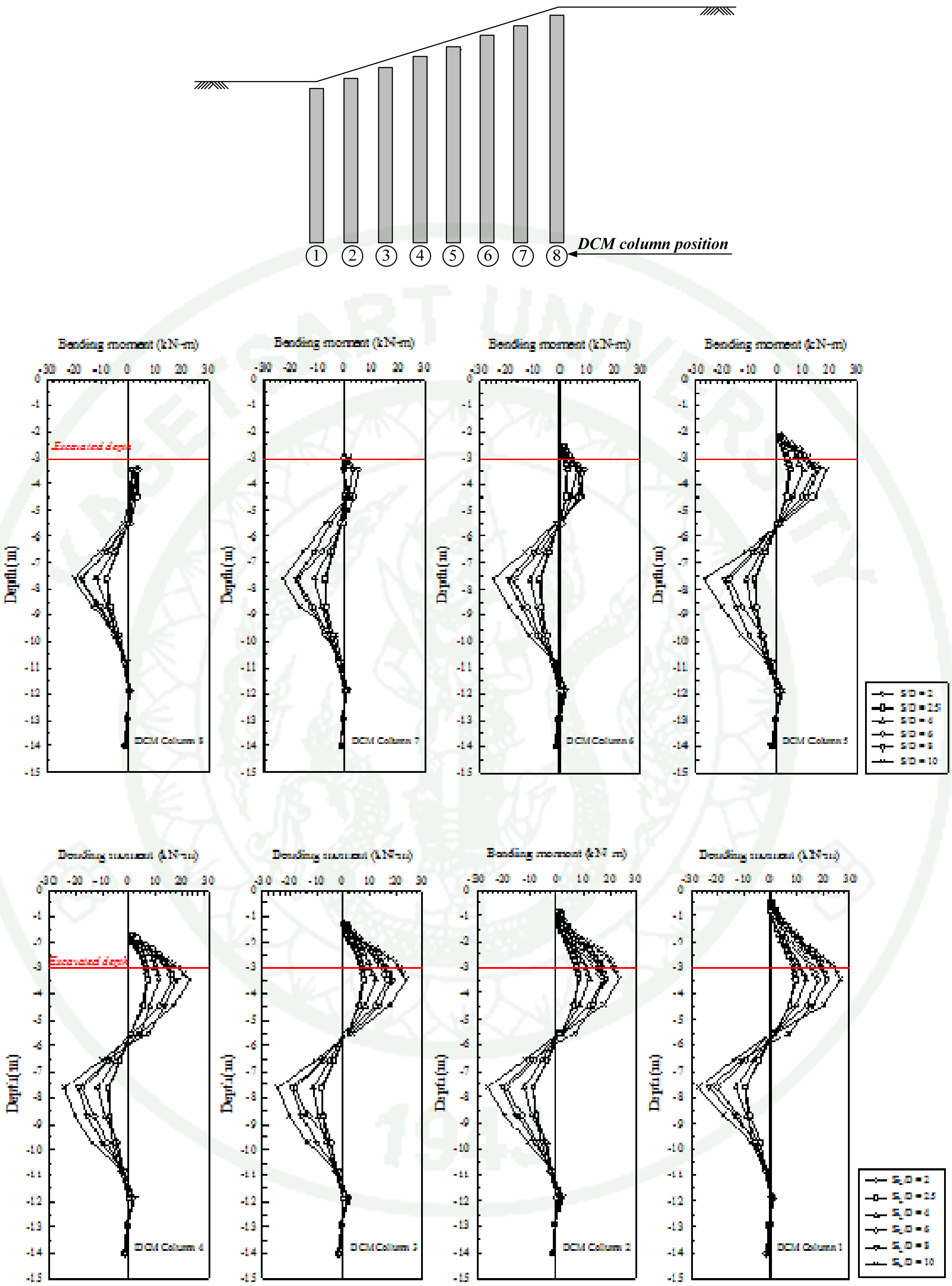

Figure 138 Bending moment of multi-row of DCM column for various spacings

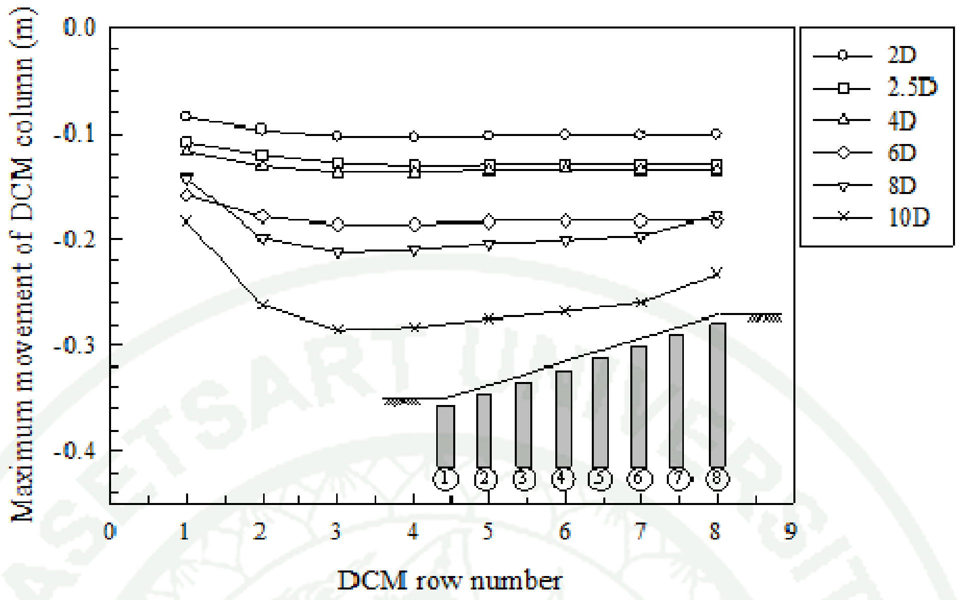

Figure 139 Maximum movement of DCM columns for various spacing

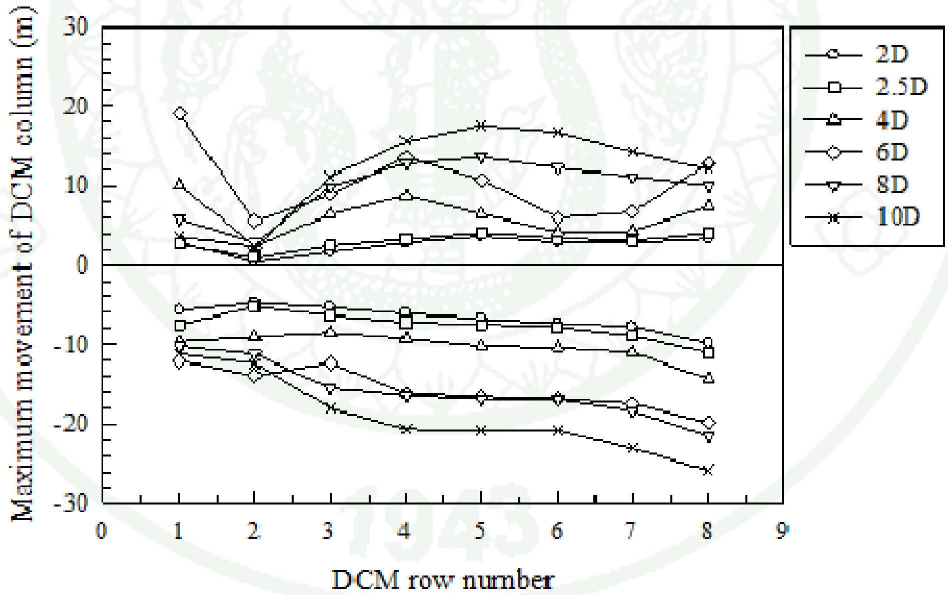

Figure 140 Maximum shear force of DCM columns for various spacing

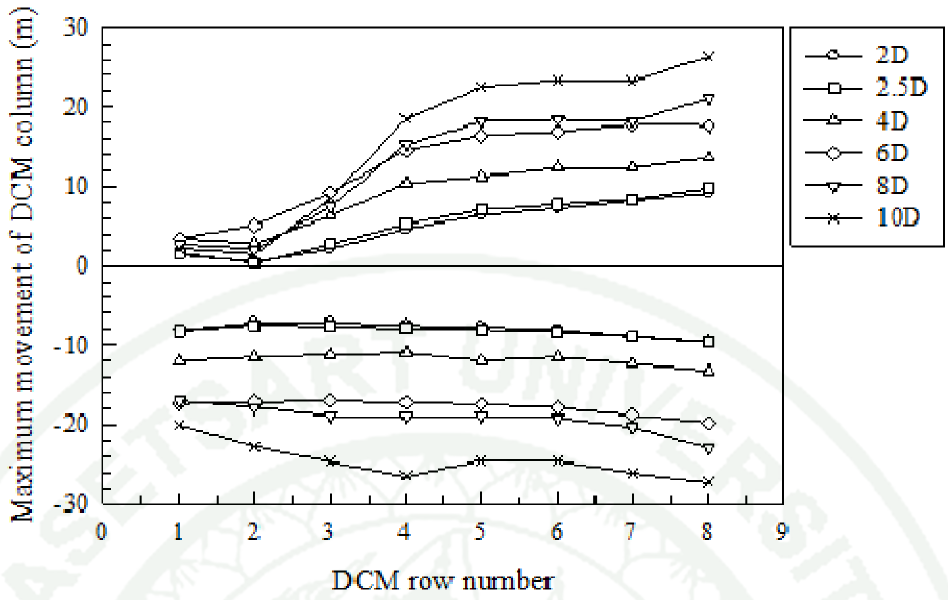

Figure 141 Maximum bending moment of DCM columns for various spacing

Alternative Design of Stabilized Canal and Roadway with DCM columns

Due to the increase of traffic volume, the construction of canal is often combined with the roadway. The guideline for selection DCM column patterns is still not addressed. In this section, four different DCM column patterns were analyzed. Three typical DCM column patterns from the Suvarnabhumi International Airport Drainage Canal project were taken. The other pattern called as the "alternative design" used the multi-rows of DCM columns for stabilization of canal slope. The lateral movement and Factor of Safety (FS) analyzed in each pattern were compared and discussed.

Finite element mesh, constitutive model and parameters

The finite element mesh of four difference patterns of DCM columns is shown in Figure 142. The analysis was focused on the patterns of DCM columns at the canal slope. The DCM column patterns A, B and C were taken from the Suvarnabhumi International Airport Drainage Canal project. The field behaviours were completely presented and discussed in the section of field trial tests. It found that the main problems of using tangential DCM column were alignment and contact of columns. Therefore, the multi-rows of DCM columns for stabilizing canal slope were proposed, as shown in pattern D. Embedded length and spacing of DCM columns were based on the results of previous analysis regarding to the effective value which gave the maximum FS. The embedded length (L_e) and spacing used in analyses were 9 m and 1.5 m, respectively. Soil, roadway and DCM columns were simulated by the Mohr-Coulomb (MC) model, linearly elastic-perfectly plastic model. The complete list of parameters used in the model is shown in Table 22. The boundary conditions are; restrained horizontal displacement and free vertical displacement on the side of boundaries. Both horizontal and vertical displacements are also restrained at the bottom of boundary.

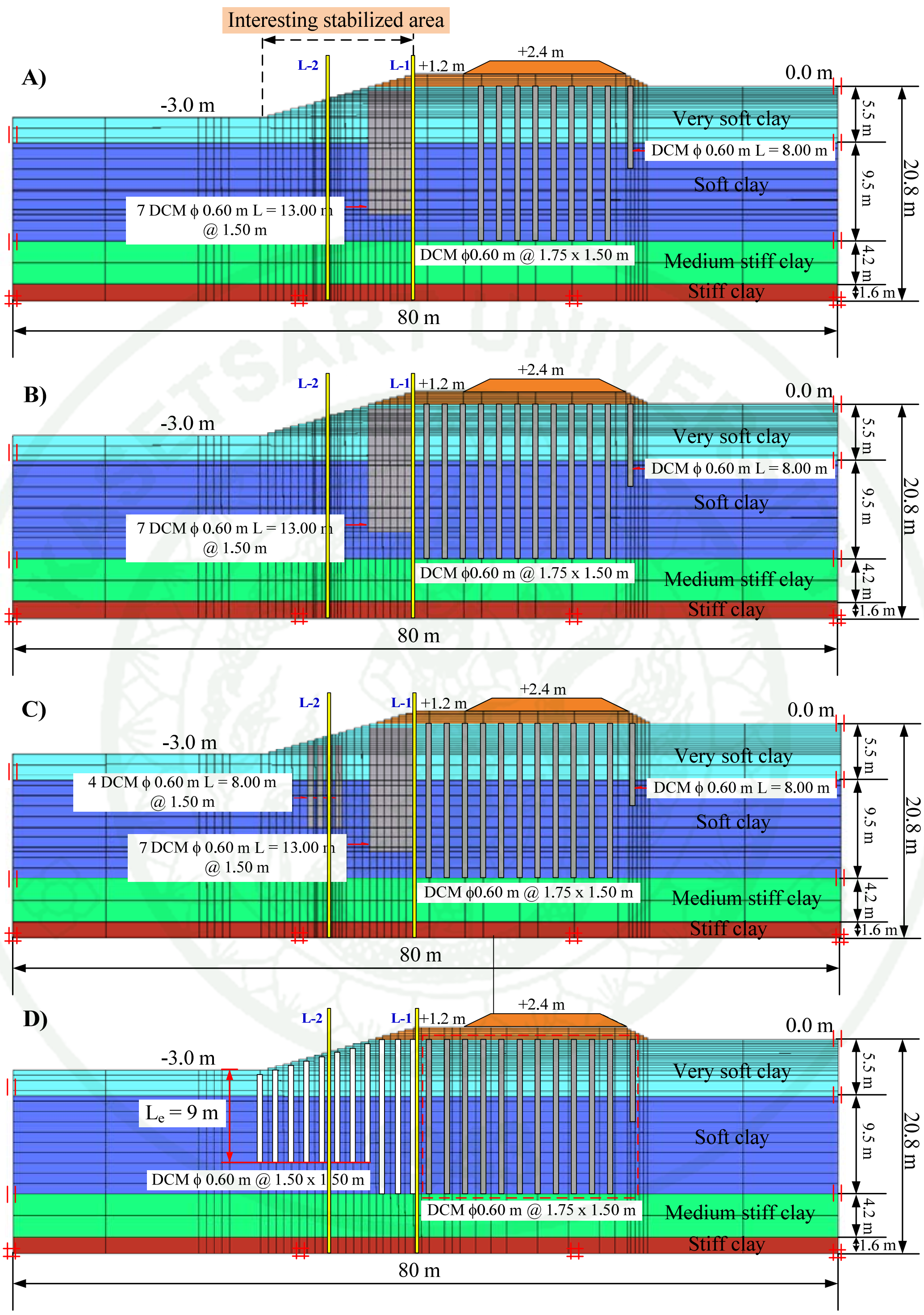

Figure 142 DCM column patterns: A) original design, B) normal soft clay, C) very soft clay, and D) alternative design

Table 22 List of parameters used in alternative design

Materials	Very soft clay	Soft Clay	Medium stiff Clay	Stiff Clay	DCM column
Depth (m)	0.0- 5.5	5.5-15.0	15.0-19.2	19.2-20.8	-
Model	MC	MC	MC	MC	MC
Material behaviour	Undrained	Undrained	Undrained	Undrained	Undrained
E_u(kPa)	300	600Su	1000Su	1000Su	225000
γ (kN/m^3)	15.5	15.5	17	18	15
ν_u	0.495	0.495	0.495	0.495	0.33
ϕ (°)	-	-	-	-	-
S_u (kPa)	5^*	7^*	27^*	132.5	500

Note MCM = Mohr-Coulomb model
DCM = Deep Cement Mixing
S_u = Undrained shear strength
E_u = Undrained elastic modulus
ν_u = Undrained Poisson's ratio
* = Strength increase with depth according to Figure 108

It is expected that the DCM columns under the roadway have effect on the lateral movement and FS. Therefore, the results were compared in term of DCM column volume per improvement area.

Lateral movement

The lateral movement at the top (L-1) and middle (L-2) of slope shown in Figure 142 was investigated to evaluate the performance of DCM column patterns. Figure 143 and 144 present the maximum lateral movement versus DCM column volume per area at the end of excavation and roadway, respectively. As show in the figure, the lateral movements tended to reduce with the increase of DCM column volume. However, the maximum lateral movement showed increase at the DCM column volume of 253.85 m^3 according to the pattern D (i.e. multi-rows of DCM column). It indicates that the decrease of maximum lateral movement depend not only the DCM columns volume but also the installation pattern. It is also found that the lateral movement significantly reduced as the additional DCM columns under the berm area were installed, as shown in pattern B. For the analyzed patterns, the tangential DCM columns are quite effective to minimize the lateral movement due to high stiffness of column.

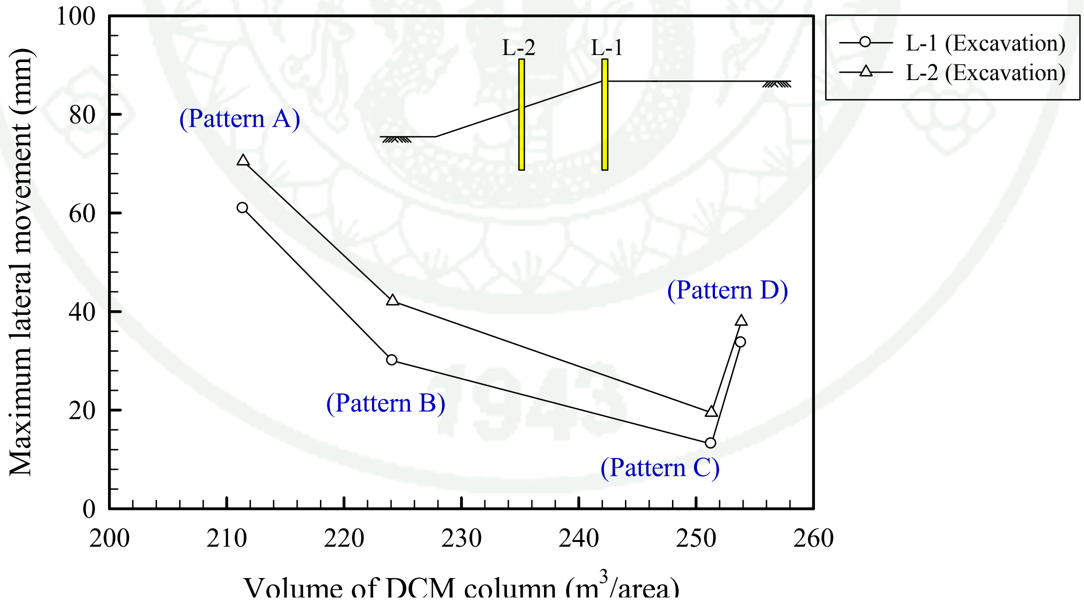

Figure 143 Maximum lateral movement at the end excavation

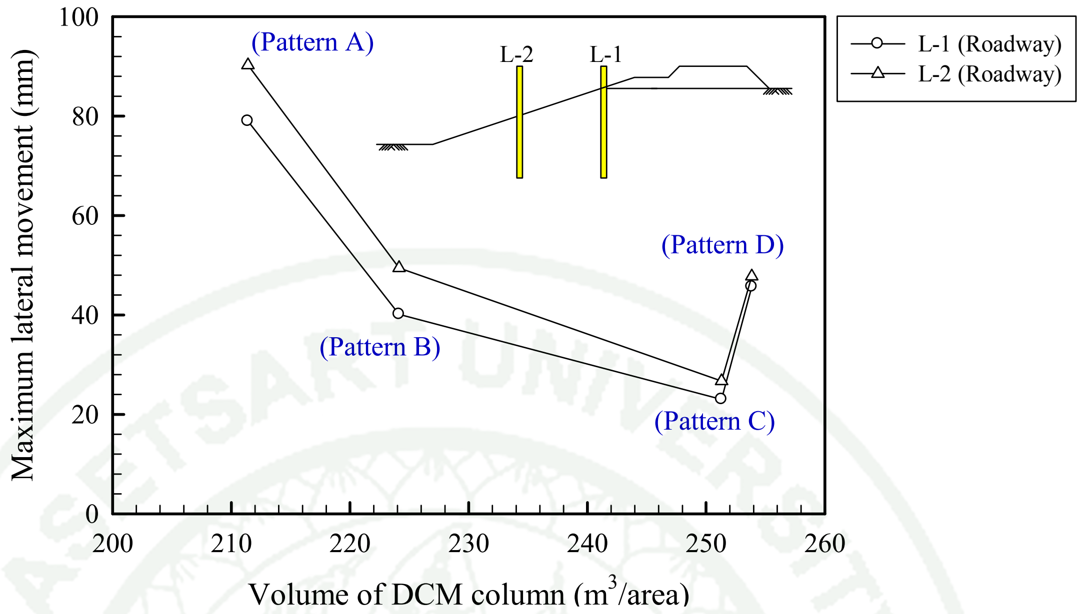

Figure 144 Maximum lateral movement at the end of roadway

Slope stability analysis

Figure 145 shows the variation of Factor of Safety (FS) versus the DCM column volume. The FS increased with the increase of DCM column volume and reached the maximum value at the column volume of 251.3 m^3 (pattern C). Beyond that, the reduction of FS was shown. It is clear that the installation pattern also affects on the FS. The significant increase of FS was shown as the additional DCM columns were installed ahead of tangential columns. To consider the effectiveness of DCM column patterns, the required Factor of Safety (FS) of 1.3 during the construction was set as criteria. Therefore, the DCM column pattern C and D can use for slope stabilization.

Figure 146 illustrates the potential failure surface for different DCM column patterns. The potential failure surface of DCM column pattern A extended top of slope throughout the berm are where no columns were installed. The potential failure surface is the same location as field failure behaviour. When the DCM columns were installed at the berm area (pattern B and C), the potential failure surface occurred at the slope top due to high stiffness of tangential columns. It is also found that two potential failure surfaces occurred with the DCM columns pattern C at the roadway stage. The potential failure surface of DCM column pattern D passes through the slope toe for both stages of construction due to low columns stiffness as compared with tangential column. However, if the alignment and contact of each DCM column are not sticky controlled, they will lead to lower bending strength than design.

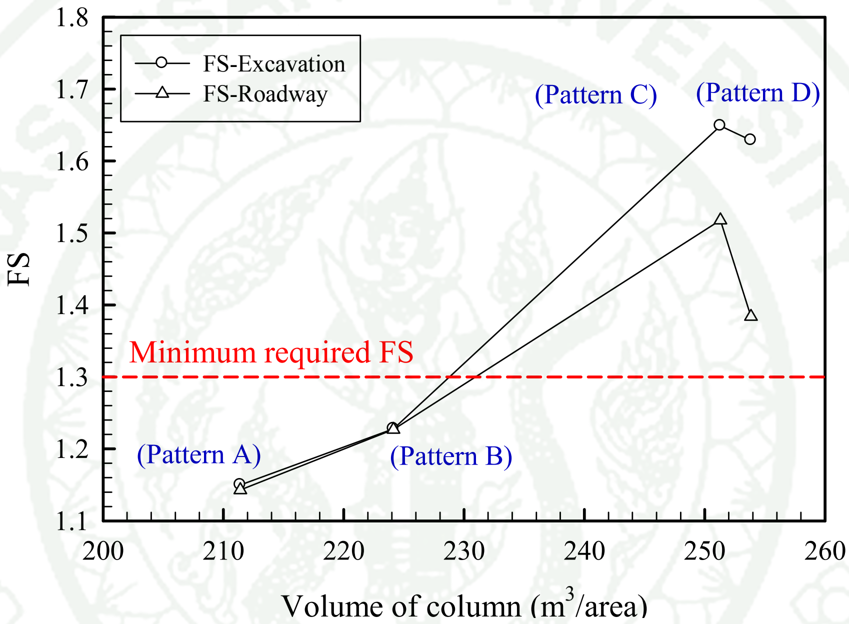

Figure 145 Factor of safety at end of excavation and roadway for various DCM columns patterns

Table 23 Summarize potential failure surface for different DCM column patterns

Pattern	Factor of safety	
	Excavation	Roadway
A	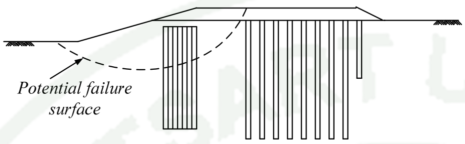 FS = 1.150	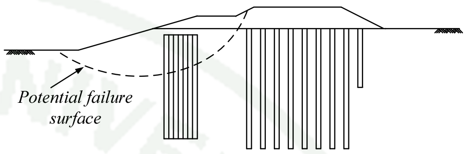 FS = 1.143
B	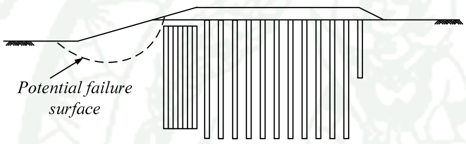 FS = 1.228	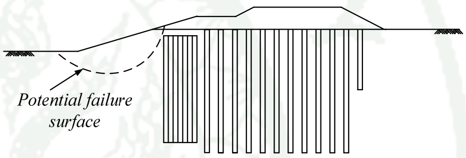 FS = 1.227
C	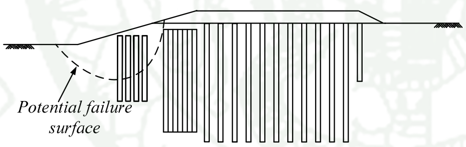 FS = 1.649	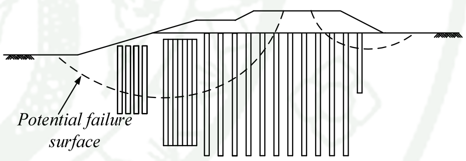 FS = 1.518
D	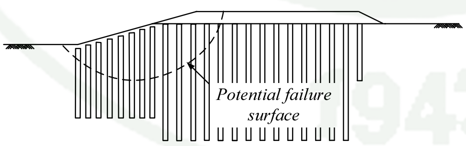 FS = 1.629	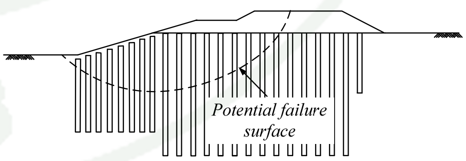 FS = 1.384

Figure 146 shows the failure mode of DCM columns of the pattern D. The figure indicated that the failure mode of DCM column using for stabilized slope and roadway was bending failure instead of shear failure. Therefore, the slope stability analyses by limit equilibrium method based on only shear failure may not represent the actual failure of DCM column leading overestimate FS.

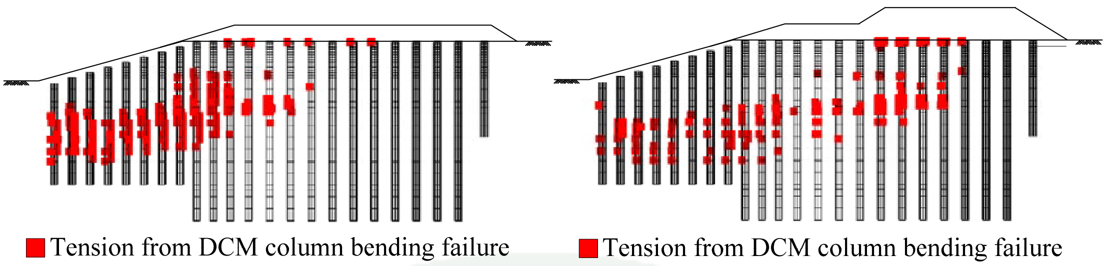

a) Excavation stage b) Roadway stage

Figure 146 Failure mode of DCM column for stabilized slope and roadway

Effect of water level during the construction of roadway

To increase the FS and decrease the lateral movement during the construction of roadway, the optimum water level in the canal was studied parametrically. Figure 147 presents the effect of water level on the FS. For the pattern B and D, the FS significantly increased with the increasing water level, and reached to the maximum value at the water level of 1.0 m high. On the other hand, the pattern C showed the slight reduction of FS as the increasing water level. The presence of water along the roadway relocates the potential failure surface to the outside edge of roadway for all patterns analyzed.

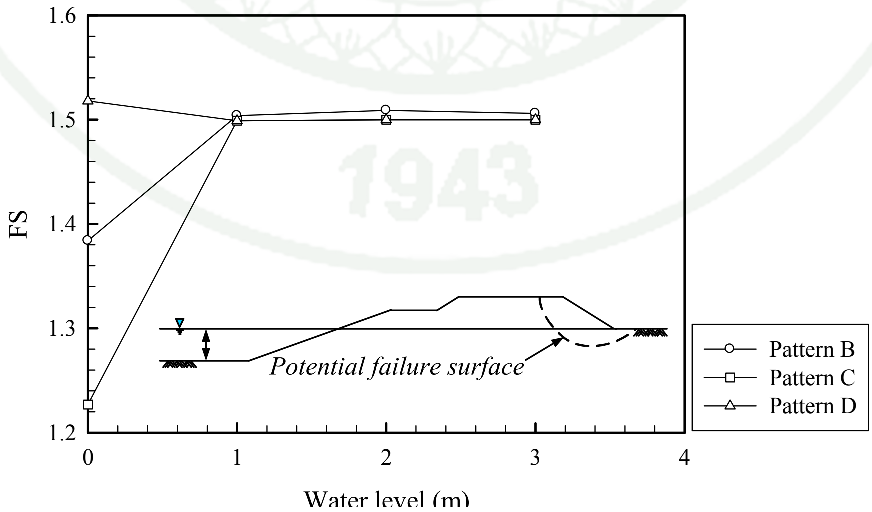

Figure 147 Effect of water level along the roadway on the FS

Based on the patterns of DCM columns analyzed, the conclusion can be tabulated in the Table 24.

Table 24 Recommendations for selection of DCM column patterns

Pattern	Recommendations
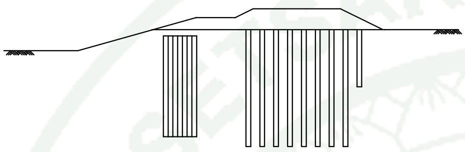	• Large lateral movement and low FS • Large active force acting on the tangential DCM columns • Slope stability based on only tangential DCM columns • Careful sequencing of construction • Sensitive with additional load on the roadway due to absent DCM column at the berm area.
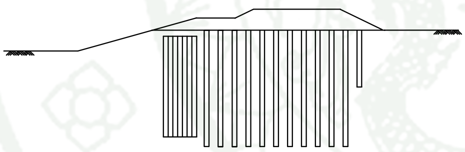	• Moderate lateral movement and FS with strictly control of construction of tangential DCM column • Small active force active on the tangential DCM column due to existing column under roadway • Unsuitable for very low soil strength • Local failure ahead of DCM column can be remedial by counterweight berm
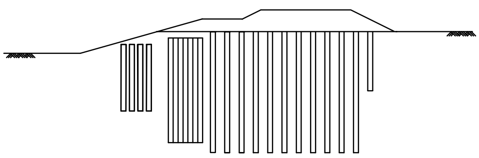	• Small lateral movement and high FS with strictly control of construction of tangential DCM column • Additional passive force is provided by additional DCM column ahead of tangential columns

Table 24 (Continued)

Pattern	Recommendations
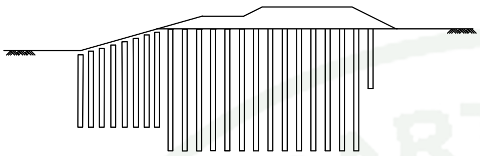	• Moderate lateral movement and FS • Less construction control of DCM columns • FS can be escalated by water level in the canal, but potential failure surface relocate to outside edge of roadway

Suggested Guideline for Design and Construction of DCM Columns on Excavated Slope and Roadway

One of the important objectives of this research was to provide a preliminary guide in design and construction of Deep Cement Mixing (DCM) columns using in stabilization of excavated slope and roadway. Based on the result of literature review, field trial tests, laboratory tests and numerical analysis in this research, following guideline is shown in Figure 148, which includes data compilation and testing, analysis and design, field trial test.

Data Compilation and Testing

The data compilation and testing includes determining the engineering properties of soil, and indentifying field investigation as well as laboratory tests. Prior experience for other DCM columns project may be obtained from published literature and from discussions with experience engineers. More details are described in the following section.

Soil investigation

1. Depth of investigation

The depth of investigation should be carried to such a depth that the net increase in soil stress under the weight of roadway is less than 10% of the applied load, or less than 5% of the effective stress in the soil at that depth. At the excavation side, the depth of investigation should be deeper than potential failure surface.

2. Spacing of borehole

The basic for determining the spacing of boreholes is based on variability of site conditions, performance requirement, experience, and judgment. The borehole spacing is usually performed at intervals of 50 to 200 m. In area where geological strata show considerable rises, additional boring is needed.

3. Soil strength properties

The shear strength testing of soil for slope stability analysis in a construction of canal and roadway should be performed both extension and compression tests (Buathong, *et al*. 2008). The strength parameters in term of undrained (S_u, $\phi= 0$) and drained strength (c', ϕ') are required for analyzing short term and long term condition, respectively. Field vane shear test and unconfined compression test are usually conducted to obtain the undrained shear strength. The drained shear strength is usually obtained from triaxial drained test or triaxial undrained test with measurements of pore water pressure during shear. The creep test may also need to be performed in order to determine standing time of canal which is left dry before filling canal water

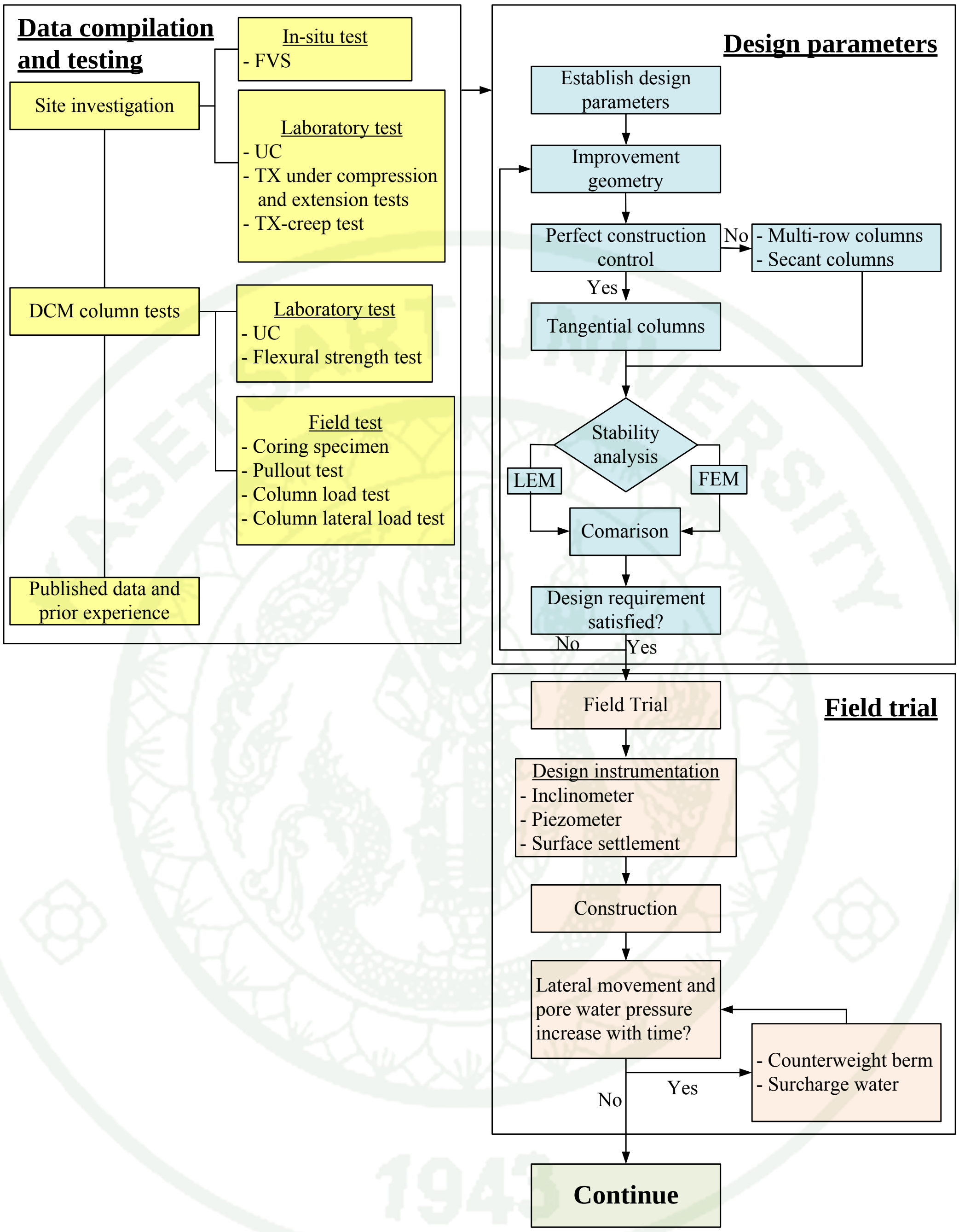

Figure 148 Flowchart for design and construction of DCM columns on stabilization of excavated slope and roadway

DCM column tests

1. Laboratory mixing test

The strength of DCM column depends on the binder material, in-situ soil condition, detail of mixing and curing condition. Therefore, a pre-construction, laboratory mixing test is required in order to determine appropriate cement content used in field mixing. It is also provided strength parameter and elastic modulus for preliminary analysis. Typical flowchart for mixing test procedure is shown in Figure 149.

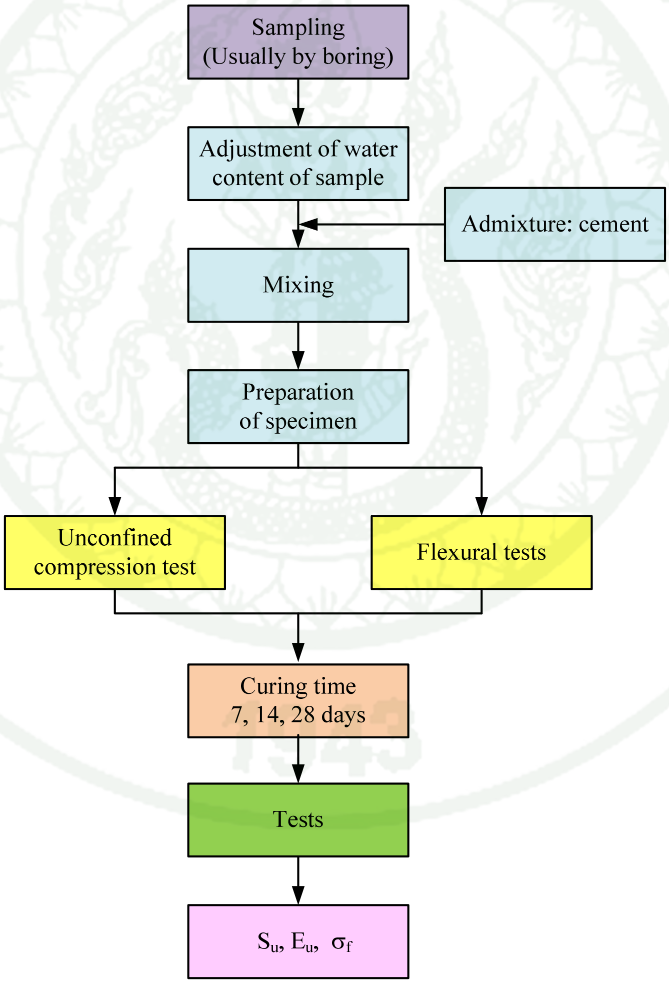

Figure 149 Flowchart for typical mix test procedure

Source: DOH and JICA (1998)

Samples taken during the soil investigation are also used as specimens for mixing test. For the trial mixing, cement content usually varies in rage of 125 kg/m^3 to 250 kg/m^3. The cement content can be expressed as follow:

$$A_w = \frac{\alpha}{\gamma_d}\ \% \qquad \text{(A1)}$$

Where:

A_w = cement content, %

α = cement content per cubic meter (kg/m^3)

γ_d = dry unit weight of soil

By dry mixing method, cement powder was added directly to the clay sample which has water content equal to in-situ. On the other hand, wet mixing method, clay sample was mixed with cement slurry determined by water-cement ratio (W/C). The water-cement ratio in trial mixing usually ranges from 0.8 to 1.2 in order to select an appropriate water-cement ratio and discharge capacity of stabilizer feeder (DOH and JICA, 1998). The mixing was done by using portable mechanical mixer for about 10 minute until a homogenous sample was attained.

The unconfined compression test (*ASTM D 2166-00*) is usually performed to determine undrained shear strength (S_u) and elastic modulus (E_u) of DCM column. Soil-cement mixture was placed into the mold when the mixing is completed. The mold usually made from PVC pipe which has 38 mm in diameter and 76 mm in height or 50 mm in diameter and 100 mm in height. Soil-cement mixture was pushed into the mold and shaking in order to remove the trapped air bubbles from specimen. When the mold was completely filled with soil-cement mixture, plastic sheets are wrapped at both ends of the mold. These specimens was placed in a humid room and cured before testing.

The flexural strength test (*ASTM D 1635-00*) is also required for evaluating flexural strength (σ_f) of DCM column due to the bending mode. The standard test specimens should be beam 76 x 76 x 290 mm. The total load of failure is recorded and calculation of flexural strength (or modulus of rupture).

2. Field tests

It is advisable to conduct the field tests adjacent to the construction site prior to actual construction. The required tests include coring of DCM column, column load test, column lateral load test and pullout test. At this stage, amount of stabilizing agent, rotation speed of mixing blade and penetration and withdraw speeds of shaft are calibrated.

The coring of DCM column is carried out throughout the column depth in order to verify the continuity. The ends of the cored specimen were trimmed and unconfined compression test was conducted.

DCM column load test is carried out to verify the design capacity of column. This test is performed in accordance with ASTM D1143-94, Standard Test Method for Piles Under Static Axial Compressive Load. The lateral load test on DCM column (ASTM D3966-95, Standard Lateral Loading Procedure) should be also conducted to evaluate lateral capacity of column used for stabilization of canal.

Pullout test was also conducted to extract the whole column for visual inspection, including homogeneity of material and DCM column size. The recovered DCM column was cut into several sections and split apart for investigating homogeneity and size. If the recovered DCM column has a perimeter smaller than 15% or larger than 20% of designed perimeter, then the construction process of DCM column is adjusted (i.e. mixing time, binder, injection energy, etc.)

Analysis and Design

Establish design parameters

Most strength and stiffness information about DCM column usually comes from unconfined compression tests. Numerous studies (Krishnakmnar, 1996; Hong, 1989; Soe, 1996; Uddin *et al.,* 1997 Yin and Lai, 1998; CDIT 2002; Horpibulsuk, 2005; Horpibulsuk, 2011) show that the unconfined compressive strength of DCM column increases with increasing stabilizer content, increasing mixing efficiency, increasing curing time, and increasing curing temperature. For Bangkok clay treated by cement, value of unconfined compressive strength obtained in laboratory test range from about 600 to1600 kPa, as shown in Figure 150.

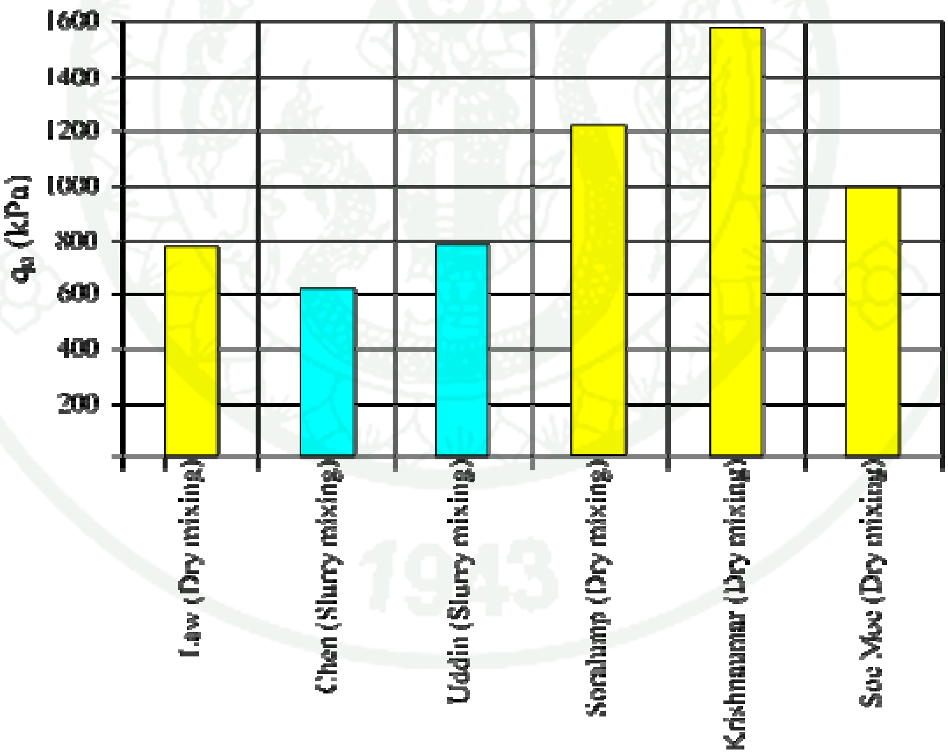

Figure 150 Comparison of unconfined compressive strength from AIT research, average cement content 150 kg, curing time 28 days

Source: Soe (1996)

Because of low quality of in-situ mixing, it is well known that the field unconfined compressive strength (q_{uf}) is usually lower than laboratory unconfined compressive strength (q_{ul}). Rojkansadarn (2009) study the q_{uf} from the Suvarnabhumi International Airport Drainage Canal project and found that the q_{uf} ranges from 600 to 1100 kPa. He also revealed that the q_{uf}/ q_{ul} ratios are about 0.7-0.9.

The elastic modulus of cement treated soil is generally correlated with the unconfined compressive strength (q_u). The E_{50} of cement treated Bangkok clay can be taken as 114 to150q_{ul} and 170 to 200q_{uf}. Rojkansadarn (2009) found that the E_{50} is about 159,160 and 140q_{uf} for low pressure mixing, jet grouting and modified dry mixing, respectively.

Terashi *et al.* (1980) reported that the flexural strength was 10% to 60% of unconfined compressive strength. Kitazume *et al*. (1996) reports that a value of 15% is used in Japan with wet mix methods. For soft Bangkok clay, the flexural strength of soft Bangkok clay was 0.16 of unconfined compressive strength (Jamswang *et al.*, 2011).

Improvement geometry

Square of triangular grid patterns of single DCM columns are usually applied under roadway to reduce settlement and increase bearing capacity of the foundation soil. Due to low flexural strength of DCM column, tangential or secant pattern is usually applied for stabilization of excavated canal. The field observation from Suvarnabhumi International Airport Drainage Canal project found that the perfect tangential pattern is difficult to construct if single mixing shaft is used. For this problem, the secant pattern can be used instead of tangential pattern. The multi-row of DCM column can also apply for stabilization of excavated canal. The main advantage of this pattern is easy to install and construction control.

Stability analysis

Stability analysis is performed to determine the critical failure surface and Factor of Safety (FS). Limit Equilibrium (LE) methods should be first performed for analyzing stability analysis due to simplicity. The LE methods usually overestimate in the FS, because they take into account only for shear failure mode of DCM column. Therefore, the numerical analyses by shear strength reduction method should be performed to evaluate the FS in concurrent with the LE methods.

If the canal is excavated rapidly enough to prevent dissipation of excess pore water pressures caused by unloading, such failure can be analyzed by total stress analysis with undrained shear strength (S_u, $\phi = 0$). The undrained shear strength is usually determined in laboratory from unconfined compression test (UC) or unconsolidated undrained (UU) triaxial test. In the field, it can be obtained from field shear vane test, pressuremeter, cone penetrometer, etc. The average relations of the undrained shear strength-effective stress ratio (S_u/σ'_{vo}) for soft Bangkok were 0.33-0.47 (Surarak, 2010; Amonkul 2010).

Over time, the negative excess pore water pressures dissipate; consequently, the effective stresses in soil around the excavation decrease. Therefore, the long condition is critical for an excavation. The drained shear strength (c', ϕ') is usually used in analysis of excavation in the long term condition. In engineering practice, drained shear strength parameters are often determined from triaxial tests. The ϕ' of soft Bangkok clay varied in range between 22.2° and 34.8° while the c' was zero.

Terashi (2005) indicated that the state of practice in Japan is to use a total stress, $\varphi = 0$ and $c = ½ q_u$ envelope for DCM column. Broms (2003) mentions use of total stress friction angles in the range of 25 to 30 degrees for deep-mixed materials. In Thailand, the S_u of DCM column is used for stability analysis. To indicate the failure criteria of the DCM columns due to the bending mode, the flexural strength should be applied in the numerical analyses.

Field trial

Prior to actual construction, field trial test with instrumentation should be conducted to verify design assumption and identify overall construction sequence of the project. The required instrumentation includes surface settlement inclinometer and piezometer. Results of measurements during construction can be used as a basis for modification of design assumption. Finite element analyses are often helpful in identifying critical locations of instruments. Structurally weak zone, most heavily loaded zones or highest pore pressures zones are an example.

During the excavation of canal, the lateral movement should be closely controlled and kept within allowable values. The experience from the Suvarnabhumi International Airport Drainage Canal project showed that the lateral movements of canal increased with time (i.e. creep behaviour) and led to eventually fail when the canal had left dry without water about 2 weeks. To prevent the failure due to creep behaviour, the counterweight berm and canal water may be applied.

CONCLUSION AND RECOMMENDATION

Conclusion

Field trial tests

1. The field integrity of tangential DCM columns showed that the alignment and contact of columns were not well. The excessive overlapping and gap between columns were observed. These problems lead to weakness on flexural resistance due to less section modulus.

2. The initial design of DCM columns showed that the slope failures occurred immediately as the excavation reached to its proposed level. The top of tangential DCM columns moved toward the canal side approximately 1.0 m.

3. Corrective design and second field trials were carried with limited numbers of field instrumentation. Construction Section I (F1-1 and F1-2), the failure was on Section F1-2 where the additional DCM columns were added on berm area only. On Construction Section II was carried out without failure with maximum lateral movement of 20 mm and some hairline crack on the roadway.

Numerical back-analysis of field trial test F1-1

1. The matching soil stiffness of the Hardening Soil (HS) and Mohr-Coulomb modes to the measured lateral movement are:

a. Mohr-Coulomb (MC) model

For very soft clay: $E_u = 300S_u$

For soft clay: $E_u = 600S_u$

For medium stiff clay: $E_u = 1000S_u$

For stiff clay: $E_u = 1000Su$

b. Hardening Soil (HS) model

For very soft clay: E^{ref}_{50} = 3,000 kPa, E_{oed} = 3,000 kPa, E_{ur} = 9,000 kPa

For soft clay: E^{ref}_{50} = 15,000 kPa, E_{oed} = 15,000 kPa, E_{ur} = 45,000 kPa

For medium stiff clay: E^{ref}_{50} = 30,000 kPa, E_{oed} = 30,000 kPa, E_{ur} = 90,000 kPa

For stiff clay: E^{ref}_{50} = 60,000 kPa, E_{oed} = 60,000 kPa, E_{ur} = 180,000 kPa

2. The excess pore water pressures were dissipated to a steady condition approximately 120 days. And rapid drawdown of water in the canal lower than 2 m contributed to slope failure.

Suitable arrangement with one row of DCM columns

1. The suitable position of DCM columns should be installed between L_x/L = 0.29 to 0.86 on the slope so that column resistances were sufficiently mobilized for maximum FS.

2. The ratio of embedded length (L_e) to excavated depth (D_e) of 3.67 was considered as effective ratio for maximum FS.

3. The FS of slope increases with decreasing DCM column spacing. As the spacing decreases, the DCM column and surrounding soil act as one soil mass (i.e. soil arching effect). The design spacing is depended on the required FS.

Modeling of full slope with multi-row of DCM columns

1. There was no significant difference in the FS between rectangular and triangular patterns.

2. The ratio of embedded length (L_e) to excavated depth (D_e) of 3 was considered as effective ratio for maximum FS.

3. The S/D = 4 is a largest ratio that is required for soil arching effect and one soil mass. The triangular pattern gave higher FS than rectangular pattern at the S/D = 2.

Alternative design of stabilized slope and roadway with DCM columns

1. The DCM columns should be distributed throughout the can slope to prevent the local failures.

2. The tangential DCM columns are quite effective to control lateral movement and provide high FS due to more section modulus.

3. The multi-rows DCM columns are possible alternative DCM column arrangement for slope stabilization.

4. The presence of water in the canal relocates the potential failure surface to the outside edge of roadway.

Recommendations

Based on thus research and literature reviews, some of the recommendation for further study on DCM stabilization on soft clay can be draw as follows:

1. Field shear strain during the excavation

2. Measure lateral movement of soil and DCM columns

3. Pore pressure dissipation during service period and long term consolidation

4. Effect of traffic loading on roadway and canal slope

5. Long-term stability and lateral movement due to creep effect

6. Risk base design for DCM stabilization slope

7. Soil-DCM interaction and lateral capacity of DCM

LITERATURE CITED

Abusharar, S.W., J.J. Zheng and B.G. Chen. 2009. Finite element modeling of the consolidation behavior of muti-column supported road embankment. **Computers and Geotechnics** 36 (4): 676-685.

Adams, T., G.M. Filz and M.P. Navin. 2009. Stability of embankments and levees on deep-mixed foundations, pp. 19-21. *In*. **Symp. Deep Mixing & Admixture Stabilization**. May 19-21, Okinawa, Japan.

Amonkul, C. 2010. **Engineering Subsoil Database of Lower Central Plain, Thailand.** M. Eng. Thesis, Kasetsart University.

Arnigo, J. V. 2002. **Effects of High Water Content on the Undrained Shear Strength and Compressibility of Bangkok Clay Treated with Cement.** M. Eng. Thesis, Asian Institute of Technology.

Ashour, M. and H. Ardalan. 2012. Analysis of Pile Stabilized Slopes Based on Soil-Pile Interaction. **Computers and Geotechnics** 39: 85-97.

ASTM D1143-94. 1994. **Standard Test Method for Piles Under Static Axial Compression Load**. Annual Book of ASTM Standards.

ASTM D3966-95. 1995. **Standard Test Method for Piles Under Lateral Loads**. Annual Book of ASTM Standards.

ASTM D1635-00. 2000. **Standard Test Method for Flexural Strength of Soil-Cement Using Simple Beam with Third-Point Loading**. Annual Book of ASTM Standards.

ASTM D2166-00. 2000. **Standard Test Method for Unconfined Compressive Strength of Cohesive Soil**. Annual Book of ASTM Standards.

Atkinson, J.H., D. Richardson and P.J. Robinson. 1987. Compression and extension of K_0 normally consolidated kaolin clay. **Journal of Geotechnical Engineering Division, ASCE**. 113: 1468-1482

Ausilio, E., E. Conte, and G. Dente. 2001. Stability analysis of slopes reinforced with piles. **Computers and Geotechnics** 28 (8): 591-611.

Arulanandan, K., C.K. Shen and R.B. Young. 1971. Undrained creep behavior of a coastal organic silty clay. **Goetechnique** 21 (4): 359-375.

Azman, Md., Md. Amin B. Ismail and A.F.L. Hyde. 1994. Deep foundations and ground improvement schemes, pp. 161-173. *In* **Proceedings on Geotexiles, Geomembranes and Other Geosynthetics in Ground Improvement**, Bangkok, Thailand.

Balasubramaniam, A.S. and A.R. Chaudhry. 1978. Deformation and Strength Characteristics of Soft Bangkok Clay. **Journal of Geotechnical Engineering Division, ASCE** 104: 1153-1167.

______, H. Zue-Ming, W. Uddin, A.R. Chaudhry and Y.G. Li. 1978. Critical state parameters and peak stress envelops for Bangkok clays. **Quaternary Journal of Engineering Geology** 11: 219-232.

______, A.H.M. Kamruzzaman, K. Uddin, D.G. Lin, N. Phienwij and D.T. Bergado. 1998. Chemical Stabilization of Bangkok Clay with Cement, Lime and Flyash Additives, pp. 253-258. *In* **Proc. 13th SEAGC**, Taipei.

Bergado, D.T., S. Ahmed, C.L. Sompaco and A.S. Balasubramaniam. 1990. Settlement of Bangna-Bangpakong highway on soft Bangkok clay. **Journal of Geotechnical Engineering Division, ASCE** 116: 136-155.

Bhadriraju, V., A.J. Puppala, R. Madhyannapu and R. Williammee. 2008. Laboratory procedure to obtain well-mixed soil binder samples of medium stiff to stiff expansive clayey soil for deep soil mixing simulation. **ASTM Geotechnical Testing Journal** 31 (3): 224-238.

Brinkgreve, R.B.J. and W.M. Swolfs. 2007. **PLAXIS 3D Foundation Finite Element Code for Soil and Rock Analyses**. Balkema, Rotterdam.

Broms, B. B. 1984. Stablisation of soft clay with lime columns, pp. 120-133. *In* **Proceedings, Seminar on Soil Improvement and Construction Techniques in Soft Ground**, NanYang Technological Institute, Singapore.

______. 1999. Can lime/cement columns be used in Singapore and Southeast Asia?. **3rd GRC Lecture**, Nov. 19, Nanyang Technological University and NTU-PWD Geotechnical research Centre, 214p.

______. 2003. **Royal Institute of Technology**. Stockholm, Sweden.

______. 2004. Lime and lime/cement column, pp. 254-330. *In* M.P. Moseley and K. Kirsch, eds**. Ch8 in Ground Improvement 2nd edition**. Spon Press, London and New York.

Buathong, P., W. Mairaing and S. Soralump. 2008. Stress Path Analysis of Road Embankment Adjacent to Drainage Canals. *In* **Regional Symposium on Infrastructure Development**. Bangkok, Thailand.

______. and ______. 2010. Failure behavior of large drainage canal reinforced by DCM piles. *In* **Proceedings EIT-JSCE Joint International Symposium**. Bangkok, Thailand.

Bulley, W.A. 1965. Cylindrical Pile Retaining Wall Construction-Seattle Freeway. **Paper presented at Roads and Streets Conference**. Seattle, Washington.

Cai, F. and K. Ugai. 2000. Numerical analysis of the stability of a slope reinforced with piles. **Soil and Foundations** 40 (1): 73-84.

Campanella, R.G. and Y.P. Vaid. 1974. Triaxial and Plane Strain Creep Rupture of an Undisturbed Clay. **Canadian Geotechnical Journal** 11 (1): 1-10.

CDIT (Coastal Development Institute of Technology). 2002. **The Deep Mixing Method: Principle, Design and Construction**. A.A. Balkema, The Netherlands.

Chaiyadhuma, W. 1974. **Undrained Shear Strength Characteristics of Soft Nong Ngoo Hao Clay.** M. Eng. Thesis, Asian Institute of Technology.

Chaudhry, A.R. 1975. **Effects of Applied Stress Path on the Stress-Strain Behavior and Strength Characteristics of Soft Nong Ngoo Hao Clay**. M. Eng. Thesis, Asian Institute of Technology.

Chen, L. 1994. **The Effect of Lateral Soil Movement on Pile Foundation.** Ph.D. Thesis, University of Sydney.

Chen R.P., Y.M. Chen and Z.Z. Xu. 2006. Interaction of rigid pile-supported embankment on soft soil. Advances in earth structures: research to practice (GSP 131). **ASCE**: 231-8.

Cox, J.B. 1968. A Review of the Geotechnical Characteristics of the Recent Marine Clay in Southeast Asia. **Asian Institute of Technology Research Report**. No. 6.

______. 1973. Trial embankment studies of Thonburi-Paktho Highway, Thailand. **LEA-GECO Int. Tech. Rep. R-5, Bangkok, Thailand**.

Cox, W. R., D.A. Dixon and B.S. Murphy. 1984. **Lateral load tests of 5.4 mm piles in very soft clay in side-side and in-line groups**. Laterally loaded deep foundations: Analysis and performance, ASTM, West Conshohocken, PA.

CPI. 1992. **Users Manual for Program ERCAP**, Coffey Partners International Pty Ltd, North Ryde, Australia.

Department of Highways. 1998. Ministry of Transport and Communications, Thailand and Japan International Cooperation Agency (JICA). **Manual for Design and Construction of Cement Column Method**. 75 pp.

Duncan, J.M. and H.B. Seed. 1966. Strength variation along failure surface in clay. **Journal of Soil and Foundation Division, ASCE** 96(5): 637-659.

______. and A.L. Buchignani. 1976. **An engineering manual for settlement studies**. Geotechnical Report of Civil Engineering Department, University of California at Berkeley.

Engineering Institute of Thailand. 2003. **Soil Data of Lower Chao Phraya Flood Plain**. E.I.T. Data (in Thai).

Eriksson, H., J. Gunther, and M. Ruin. 2005. MDM combines the advantages of Dry and Wet Mixing, pp. 509-520. *In* **Proceedings of the International Conference on Deep Mixing, Best Practice and Recent Advances, Stockholm**.

Esu, F. and B. D'Elia. 1974. Interazione terreno-struttura in un palo sollecitato dauna frana tip colata", Rev. **Ital di Geot.** III: 27-38.

Fukuoka, M. 1977. The Effects of Horizontal Loads on Piles due to Landslides, pp. 27-42. *In* **Proceeding 10th Specific Session, 9th International Conference Soil Mechanics and Foundation. Engineering.** Tokyo.

Goh A.T.C and K.S. Wong. 1997. Analysis of piles subjected to embankment induced lateral soil movements. **Journal of Geotechnical and Geoenvironmental Engineering, ASCE** 123: 312-323.

Griffiths, D.V., H. Lin, P. Cao. 2010. Optimization of stabilization of highway embankment slopes using driven piles-Phase I. COLORADO DEPARTMENT OF TRANSPORTATION DTD APPLIED RESEARCH AND INNOVATION BRANCH. **Report No. CDOT-2010-8**, Final Report.

Han, J., R.L. Parsons, J. Huang and A.R. Sheth. 2005. Factors of safety against deep-seated failure of embankments over deep mixed columns, vol. 1, pp. 231-236. *In* **Proceedings of the International Conference on Deep Mixing, Best Practice and Recent Advances.** Stockholm, Sweden.

Han J, J. Huang and A. Porbaha. 2005. **2D numerical modeling of a constructed geosynthetic-reinforced embankment over deep mixed columns**. Contemporary issues in foundation engineering (GSP 131), ASCE.

Hassan, Z. 1976. **Stress-Strain Behavior and Shear Strength Characteristics of Stiff Bangkok Clays.** M. Eng. Thesis, Asian Institute of Technology.

Hassiotis, S., J.L. Chameau and M. Gunaratne. 1997. Design method for stabilization of slopes with piles. **Journal of Geotechnical and Geoenvironmental Engineering** 123 (4): 314-23.

Hayward T, A. Lees, W. Powrie, D.J. Richards and J.A. Smethurst. 2000. Centrifuge modelling of a cutting slope stabilised by discrete piles, **TRL Report-471**, Transport Research Laboratory, Crowthorne, Berkshire, UK

Ho, I. H. 2009. **Optimization of Pile Reinforced Slopes using Finite Element Analyses.** Ph.D. Thesis, Iowa State University.

Hong, L. K. 1989. **Strength and deformation characteristics of cement-treated clay**, M. Eng., Thesis, Asian Institute of Technology.

Holzer, T.L., K. HEÖG and K. Arulanandan. 1973. Excess pore pressure during undrained clay creep. **Canadian Geotechnical Journal** 10: 12-24.

Horpibulsuk, S. 2005. Mechanism controlling undrained shear characteristics of induced cemented clays. **Lowland Technology International** 7(2): 9-18.

______, N. Miura, T.S. Nagaraj. 2005. Clay-water/cement ratio identity of cement admixed soft clay. **Journal of Geotechnical and Geoenvironmental Engineering**, **ASCE** 131 (2): 187-192.

______, R. Rachan, A. Suddeepong, A. Chinkulkijniwat. 2011. Strength development in cement admixed Bangkok clay: Laboratory and field investigations. **Soils and Foundations** 51(2): 239-251.

Hossain M.S., M.A. Haque, K.N. Rao. 2006. **Embankment over soft soil improved with chemico pile-a numerical study**. Advances in earth structures: research to practice (GSP 151), ASCE.

Huang J.T. and D.W. Airey. 1998. Properties of artificially cemented carbonate sand. **J. Geotech. Geoenviron. Eng** 124 (6): 492-499.

Huang J, J. Han and A. Porbaha. 2006**. Two and three-dimensional modeling of DM columns under embankments**. GeoCongress, ASCE.

______and J. Han. 2009. 3D coupled mechanical and hydraulic modeling of a geosynthetic-reinforced deep mixed column-supported embankment. **Geotextiles and Geomembrances** 27: 272-280.

Huang J and J. Han. 2010. Two-dimensional parametric study of geosynthetics-reinforced column-supported embankments by coupled hydraulic and mechanical modeling. **Computers and Geotechnics** 37(5): 638-648.

Hull, T.S., C.Y. Lee and H.G. Poulos, Mechanics of Pile Reinforcement for Unstable Slopes. **Research Report No. R636**, The University of Sydney, April 1991.

Ito, T. and T. Matsui. 1975. Methods to estimate lateral force acting on stabilizing piles. **Soils and Foundations** 18(4): 43-59.

______, T. Matsui and W.P. Hong. 1982. Extended design method for multi-row stabilizing piles against landslides. **Soils and Foundations** 22 (1): 1-13.

Japan International Cooperation Agency (JICA). 1999. **The study on integrated plan for flood mitigation in Chao Phraya River Basin**, Report submitted to Royal Irrigation Department, Kingdom of Thailand.

Jansawang P, D.T. Bergado and P. Voottipruex. 2010. Field behavior of stiffened deep cement mixing piles, p.33-49. *In* **Proceedings of the Institute of Civil Engineers-Ground Improvement** 164(1): 33-49.

Jeong, S., B. Kim, J. Won and J. Lee. 2003. Uncoupled analysis of stabilizing piles in weathered slopes. **Computers and Geotechnics** 30: 671-82.

Kanagasabai, S. 2010. **Three Dimensional Numerical Modeling of Rows of Discrete Piles Used to Stabilise Large Landslides.** Ph.D. Thesis, University of Southampton.

Kaushinger, J.L., E.B. Perry and R. Hankour. 1992. Jet grouting state of the practice, vol. 1, pp. 169-181. *In* **Proc. Grouting, soil improvement and geosynthetics**. ASCE, New York.

Kamruzzaman, A.H.M. 2002. **Physico-Chemical & Engineering Behavior of Cement Treated Singapore Marine Clay**. Ph.D. Thesis, National University of Singapore.

Kempfert, H.G. and B. Gebreselassie. 2006. **Excavation and Foundation in Soft Soils**. Springer Berlin Heidelberg, New York.

Kim, S.R. 1991. **Stress-Strain Behavior and Strength Characteristics of Lightly and Overconsolidated Clay.** D. Eng. Dissertation, Asian Institute of Technology.

Kitazume, M. and Karastanev, D. 1996. Bearing capacity of improved ground with column type DMM. Grouting and Deep Mixing. *In* **Proceedings of IS-Tokyo 96, 2nd International Conference on Ground Improvement,** Geosystems.

Kitazume, M. and K. Maruyama. 2005. Collapse failure of group column type deep mixing improved ground under embankment, vol. 1, pp. 245-254. *In* **Proceedings of the International Conference on Deep Mixing, Best Practice and Recent Advances, Stockholm**. สถานที่จัด **Stockholm, Sweden**

______. and ______. 2007. Internal stability of group column type deep mixing improved ground under embankment loading. **Soil and Foundations** 47 (1): 437-455.

KivelÖ, M. 1998. **Stabilization of Embankments on Soft Soil with Lime/Cement columns.** Doctoral Thesis, Royal Institute of Technology, Stockholm.

Kourkoulis, R., F. Gelagoti, I. Anastasopoulos and G. Gazetas. 2011. Slope stabilizing piles and pile-groups: Parametric study and design insights. **Journal of Geotechnical and Geoenvironmental Engineering**, **ASCE** 137 (7): 663-667.

Krishnakmnar. 1996. **Deep chemical mixing process as ground improvement in Bangkok subsoil**, M. Eng. Thesis, Asian Institute of Technology.

Lambe, T.W. and R.V. Whitman. 1979. **Soil Mechanics-SI Version**. Wiley, New York.

______. and W.A.Marr. 1979. Stress path method: second edition. **Journal of the Geotechnical Engineering Division** June 1979 (GT6):727-738.

Larsson, S. 1999. Shear box apparatus for modeling chemical stabilized soil - Introductory tests, pp. 115-121. *In* **Proceedings of the International Conference on Dry Mix Methods for Deep Soil Stabilization**. 13-15 October, Stockholm.

______, B.B. Broms. 2000. Shear box model tests with lime/cement columns - some observations of failure mechanisms. *In* **Proceedings of the International Conference on Dry Mix Methods**. 19-24 November, Melbourne,.

______. 2008. **Skjuvboxforsok pa jordforstarkt kaolinlera med kalkcementpelare (shear box tests on lime-cement column improved kaolin)**. Arbetsrapport, Swedish Deep Stabilization Research Centre (in Swedish).

Lee, C.Y., T.S. Hull and H.G. Poulos. 1995. Simplified pile-slope stability analysis. **Computers and Geotechnics** 17 (1): 1-16.

______. 1999. **A framework for the Design of Jet Grouting Piles in Singapore Marine Clay.** M. Eng. Thesis, National University of Singapore.

Li, Y.G. 1975. **Stress-Strain Behavior and Strength Characteristics of Soft Nong Ngoo Hao Clay under Extension Condition.** M. Eng. Thesis, Asian Institute of Technology.

Liang R and Zeng S. 2002. Numerical study of soil arching mechanism in drilled shafts for slope stabilization**.** **Soils and foundations** 42 (2): 83-92.

Lorenzo, G. and D.T. Bergado. 2006. Fundamental Characteristics of cement-admixed clay in deep mixing. **Journal of Materials in Civil Engineering**, **ASCE** 18: 161-174.

Madhyannapu R.S, A.J. Puppala, S. Hossain, J. Han and A. Porbaha. 2006. **Analysis of geotextile reinforced embankment over deep mixed columns: using numerical and analytical tools**. GeoCongress, ASCE.

Mairaing, W. and C. Amonkul. 2010. Soft Bangkok clay zoning. *In* **EIT-JSCE Joint International Symposium**. 6-7 September 2010. Bangkok, Thailand.

Mitchell, J.K. 1993. **Fundamentals of soil behaviour**. 2nd ed. John Wiley & Sons, Inc.

Moh, Z.C., J.O. Nelson and E.W. Brand. 1969. Strength and deformation behavior of Bangkok clay, vol. 1, pp. 303-307. *In* **International Conference of Soil Mechanics and Foundation Engineering**. Mexico city.

Moseley, M.P. and K. Kirsch. 2004. **Ground Improvement**. Second edition. Spon Press, London and New York.

NAVFAC. 1986. **Soil mechanics: Design Manual 7.01.** Naval Facilities Engineering Command, Alexandria: 355.

Nethero, M.F. 1982. Slide Control by Drilled Pier Walls, pp. 61-76. *In*. R.B. Reeves, ed. **Application of Walls to Landslide Control Problems**. ASCE.

Nian, T.K., G.Q Chen, M.T. Luan and D.F. Zheng. 2008. Limit analysis of the stability of slopes reinforced with piles against landslide in non-homogeneous and anisotropic soils. **Canadian Geotechnical Journal** 45: 1092-1103.

Offenberger, J.H. 1981. Hillside stabilized with concrete cylinder pile retaining wall. **Public Works** 112 (9): 82-86.

Ohtsubo, M., K. Egashira, T. Koumoto and D.T. Bergado. 2000. Mineralogy and chemistry, and their correlation with the geotechnical index properties of Bangkok clay: comparison with Ariake clay. **Soils and Foundations** 40 (1): 11-21.

Oliveira P.J.V., J.L.P. Pinheiro and A.A.S. Correia. 2011. Numerical analysis of an embankment built on soft soil reinforced with deep mixing columns: Parametric study. **Computers and Geotechnics** 38 (4):566-576.

Parnploy, U. 1985. **Deformation Analysis and Settlement Prediction of Bangna-Bangpakong Highwy (Section I).** M. Eng. Thesis, Asian Institute of Technology.

Parry, R.H.G. and V. Nadarajah. 1960. Triaxial compression and extension tests on remolded saturated clay. **Geotechnique** 10: 166-180.

______. and V. Nadarajah. 1973. Observation on laboratory prepared, lightly overconsolidated specimens of kaolin. **Geotechnique** 24: 345-358.

Petchgate, K., P. Jongpradist and S. Panmanajareonphol. 2003. Field pile load test of soil-cement column in soft clay, pp. 175-184. *In* **Proc. Int. Symp. 2003 on Soil/Ground Improvement and Geosynthetic in Waste Containment and Erosion Control Application**. Asian Institute of Technology, Thailand.

Petchgate, K and W. Petchgate. 2006. Songkhla combined cycle power plant, pp. 28-33. *In* **Proceeding of the 6th Symposium on Ground/Soil Improvement and Geosynthetics.** 7-8 December 2006, Bangkok, Thailand.

Phanumart K., P. Jongpradist, S. Youwai and P. Jamsawang. 2007. Excess pore water pressure distribution in surrounding soils during installation of cement column. *In* **12thNational Convention on Civil Engineering, 2-4 May 2007,** Phitsanulok, Thailand.

Porbaha, A. 1998a. State of the Art In Deep Mixing Technology. Part I: Basic concepts and overview. **Ground Improvement** 2:81-92.

______. 1998b. State of the Art In Deep Mixing Technology. Part II: Applications. **Ground Improvement** 2: 81-92.

______, S. Shibuya and T. Kishida. 2000. State of Art in Deep Mixing Technology. Part III: Geomaterial Characterization. **Ground Improvement** 3: 91-110.

Poulos, H. G. 1973. Analysis of piles in soil undergoing lateral movement. **Journal of Soil Mechanics and Foundation Engineering, ASCE** 99: 391-406.

______. 1995. Design of reinforcing piles to increase slope stability. **CanadianGeotechnical Journal** 32: 808-818.

______. 1999. Design of slope stabilizing piles, pp. 83-100. *In*, J.C. Jiang, N. Yagi, and T. Yamagami, eds. **Slope stability engineering.** Balkema, Rotterdam, Netherlands.

Pradel, D., J Garner, and A.O.L Kwok. 2010. Design of Drilled Shafts to Enhance Slope Stability. pp. 920-927. *In* **Proceeding of the 2010 Earth Retention Conference.** 1-4, August, 2010, Bellevue, Washington.

Prakash S. 1962. **Behavior of pile groups subjected to lateral load**. Ph.D. dissertation, Department of Civil Engineering, University of Illinois.

Priol, G., L. Grande and R. Aab∅e. 2007. Analytical and numerical analysis of slopes reinforced by deep mixing method. **Taylor & Francis Group**, London, UK.

Rahman, A. M. A. 1980. **Strength and Deformation Characteristics of Bangkok Subsoils under In-Situ Stress Condition.** M. Eng. Thesis, Asian Institute of Technology.

Reese, L.C., S.T. Wang, and J.L. Fouse. 1992. Use of Drilled Shafts in Stabilising a Slope, pp. 1318-1332. *In*. R.B. Seed and R.W. Boulanger, eds. **Stability and Performance of Slopes and Embankments-II**. ASCE

Rojkansadarn, S. 2009. **Soil Properties Effect on Construction of Soil-Cement Column: Case Study on Drainage System Suvarnabhumi International Airport Project.** M. Eng. Thesis, Kasetsart University.

Saitoh, S., Y. Suzuki and K. Shirai. 1985. Hardening of soil improved by the deep mixing method, 3, pp. 1745-1748. *In* **Proceeding of the 11th international conference on soil mechanics and foundation engineering**. San Francisco.

Seah, Tian Ho. 2000. Quality control of soil cement column along east outer Bangkok ring road, pp. 168-198. *In* **Third seminar on ground improvement in highways**. Thailand 16 August 2000, Bankok.

Skempton, A. W. 1954. The Pore Pressure Coefficients A and B. **Geotechnique** 4: 143-147.

SGF. 2000. Lime and lime cement columns. Guide for design, construction and control. **Report 2:2000**, Swedish Geotechnical Society, Linkoping, 111 pp. (in Swedish).

Sinsakul, S., N. Chaimanee and S. Tiyapairach. 2002. Quaternary geology of Thailand, pp. 170-180. *In* **The Symposium on Geology of Thailand**. 26-31 August 2002, Bangkok, Thailand.

Snead, D. 1970. **Creep Studies on an Undisturbed Sensitive Clay.** Forthcoming Ph.D. Thesis, University of British Columbia (U.B.C.).

Soe Moe Kyaw Win. 1996. **Curing time dependent properties of cement treated Bangkok clay**, M. Eng., Thesis Asian Institute of Technology.

Sommer, H. 1977. Creeping slope in a stiff clay, pp. 113-118. *In* **Proceeding 10th Specific Session 9th International Confonference Soil Mechanics and Foundation Engineering**. Tokyo.

Stroh D. 1974. **Berechnung verankerter Baugruben nach der Finite-Element-Methode**. Mitteilungen der Versuchsanstalt für Bodenmechanik und Grundbau der TH Darmstadt, Heft 13.

Surarak, C. 2010. **Geotechnical Aspects of the Bangkok MRT Blue Line Project.** Ph.D. Thesis, Griffith University.

Taesiri, Y. and P. Chantaranimi. 2001. Slope stabilizations of highway embankments adjacent to irrigation/drainage canal, pp. 211-227. *In* P**roceedings of Soft Ground Improvement and Geosynthetics Applications**, Thailand.

Tampubolon, M. 1981. **Behavior of Soft Bangkok Clay under Horizontal Loading.** M. Eng. Thesis, Asian Institute of Technology.

Tan, T.S., T.L. Goh and K.Y. Yong. 2002. Properties of Singapore marine clays improved by cement mixing. **Geotechnical Testing Journal** 25 (4):422-433.

Taniguichi, T. 1967. Landslides in Reservoirs, vol. 1, pp. 258-261. *In* **Proceeding 3rd Asian Regional Conference Soil Mechanics and Foundation Engineering**, Bangkok.

Tateyama, K., S.Ashida, R. Fukagawa and H. Takahashi. 2006. Geomechatronics-Interaction between ground and construction machinery and its application to construction robotis. **Journal of Terramechanics** 43: 341-353.

Terashi, M., H. Tanaka, T. Mitsumoto, Y. Niidome and S. Honma. 1980. Fundamental preoperties of lime and cement treated soil (2nd report). **Report of the Port and Harbour Research Institute** 19(1): 33-62 (in Japanese).

______, H. Tanaka, T. Mitsumoto, S. Honma and T. Ohhashi. 1983. Fundamental properties of lime and cement treated soil (3rd report). **Report of the Port and Harbour Research Institute** 22(1): 69-96 (in Japanese).

______. 1997. Theme Lecture: Deep Mixing Method-Brief State of the Art, vol.4, pp. 2475-2478. *In* **Proceeding of the 14th International Conference on Soil Mechanics and Foundation Engineering.**

Terzaghi, K. 1936. Stress distribution in dry and saturated sand above a yielding trap door, pp. 307-311. *In* **Proceedings of International Conference of Soil Mechanics**. Harvard University, Cambridge (USA).

Teparaksa, W., N. Thasnanipan and P. Tenseng. 1999. Analysis of lateral wall movement for deep braced excavation in Bangkok subsoils. **Civil and Environmental Engineering Conference**, Bangkok, Thailand.

Uddin, K., A. S. Balasubramaniam and D.T. Bergado. 1997. Engineering Behavior of Cement-Treated Bangkok Soft Clay. **Geotechnical Engineering** 28 (1): 89-119.

Vägverket. 2009. **Tekniska kravdokument Geo**. VV Publ. 2009:46. Vagverket, Borlange, (in Swedish).

Wang, W. 1969. **Effects of Anisotropic Consolidation on Shear Strength of Bangkok Clay.** M. Eng. Thesis, Asian Institute of Technology, Bangkok, Thailand.

Wang, W.L. and B.C. Yen. 1974. Soil arching in slope. **Journal of Geotechical Engineering Division, ASCE** 100 (1):61-78.

Wang, M.C., A.H. Wu and D.J. Scheessele. 1979. Stress and deformation in single piles due to lateral movement of surrounding soils., pp. 578-591. *In* R. Lunggren, ed. **Behavior of Deep Foundations, ASTM 670**. American Society for Testing and Materials.

Watn, A., S. Christensen, A. Emdal and S. Nordal. 1999. Lime-cement stabilization of slope-Experiences and a design approach, pp. 169-176. *In* Proceeding of the International **Conference on Dry Mix Methods for Deep Soil Stabilization**. Stockholm, Sweden, 13-15 October 1999.

Wei, W.B. and Cheng, Y.M. 2009. Strength reduction analysis for slope reinforced with one row of piles. **Computers and Geotechnics** 36: 1176-1185.

Win, S. M. K. 1997. **Engineering Properties of Cement Treated Bangkok Clay**. M. Eng. Thesis, Asian Institute of Technology.

Won, J., K. You, S. Jeong, and S. Kim. 2005. Coupled effect in stability analysis of pile-slope systems. **Computers and Geotechnics** 32: 304-315.

Xiao, H.W. and F.H. Lee. 2009. Curing time effect on behavior of cement treated marine clay. **International Journal of Engineering and Applied Sciences** 5: 7.

Yang, S., X. Ren and J. Zhang. 2011. Study on embedded length of piles for slope reinforced with one row of piles. J**ournal of Rock Mechanics and Geotechnical Engineering** 3(2): 167-178.

Yin, J.H., and Lai, C.K. 1998. Strength and Stiffness of Hong Kong Marine Deposits Mixed with Cement. **Geotechnical Engineering** 29 (1): 29-44.

APPENDIX

Result of Laboratory Tests

Laboratory tests were carried out to characterize undrained strength and deformation behavior of soft Bangkok clay related with an excavation. The testing program consists of undrained triaxial test under compression, extension and creep tests. The result from laboratory tests were analyzed and compared with the previous researches on Bangkok clay and others.

Undrained triaxial test under compression condition

1. Isotropically Consolidated Undrained (CIU) tests

The results from CIU test are summarized in Appendix Table 1.The deviator stress (σ_a) and axial strain (ε_a) relationship from CIU tests are shown in Appendix Figure 1.With an increase of consolidation pressure, the deviator stress presents hardening character. The strain at failure (ε_f) was found to be between 6% and 10%. Strain softening was observed after the deviator stress had reached its peak and reaching the residual stress at about 15% of peak. The undrained elastic modulus at 50% of maximum deviator stress ($E_{u,50}$) determined from the curves in Appendix Figure 1 for CIU I, II and III are 1803 kPa, 2477 kPa and 7238 kPa, respectively. It can be seen that $E_{u,50}$ increase with confining pressure.

The excess pore water pressures developed during the shear are shown in Appendix Figure 2. The excess pore water pressures increase steadily with the strain by positive value throughout the test. No sharp peaks are observed on the excess pore water pressure-strain relationship. Skempton (1954) pore pressure parameter at the failure (A_f) ranged from 0.4 to 0.9. The deviator stress and excess pore water pressure indicate typical behavior of normally to lightly overconsolidated clay, were the deviator stress and excess pore water pressure reaches their ultimate values at a relatively large strain.

Appendix Table 1 Results from CIU tests

Series	σ'_c (kPa)	γ (kN/m^3)	w_i(%)	w_f(%)	ε_f (%)	A_f (%)	ϕ_c	ϕ_c'
CIU I	50	1.45	79.89	73.58	6.18	0.60		
CIU II	80	1.45	92.04	73.36	8.47	0.84	16.6	26.4
CIU III	100	1.48	100.62	69.12	9.16	0.44		

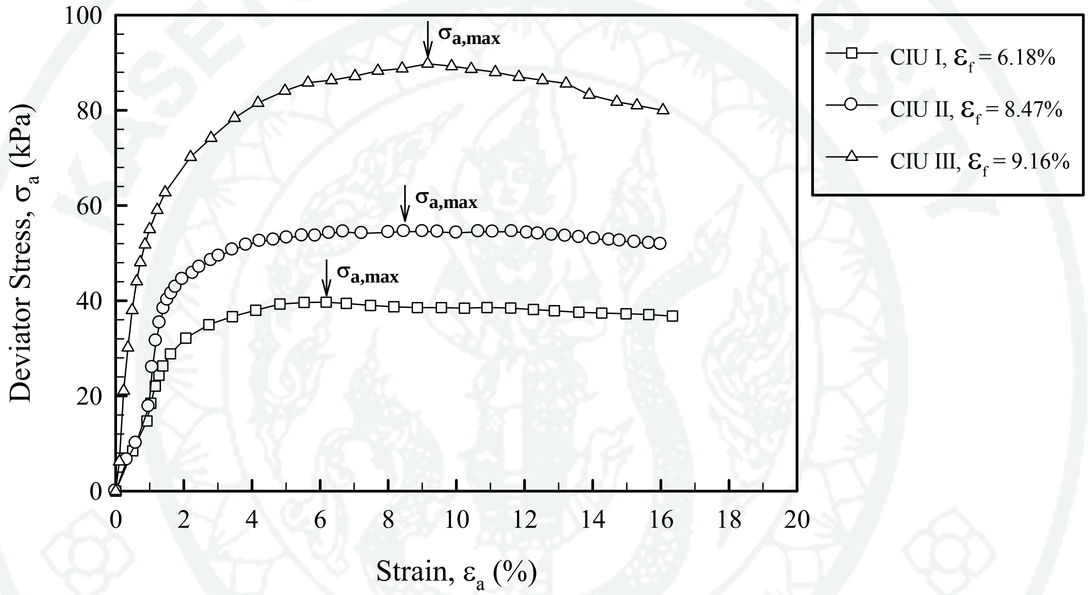

Appendix Figure 1 Deviator stress and strain relationships from CIU tests

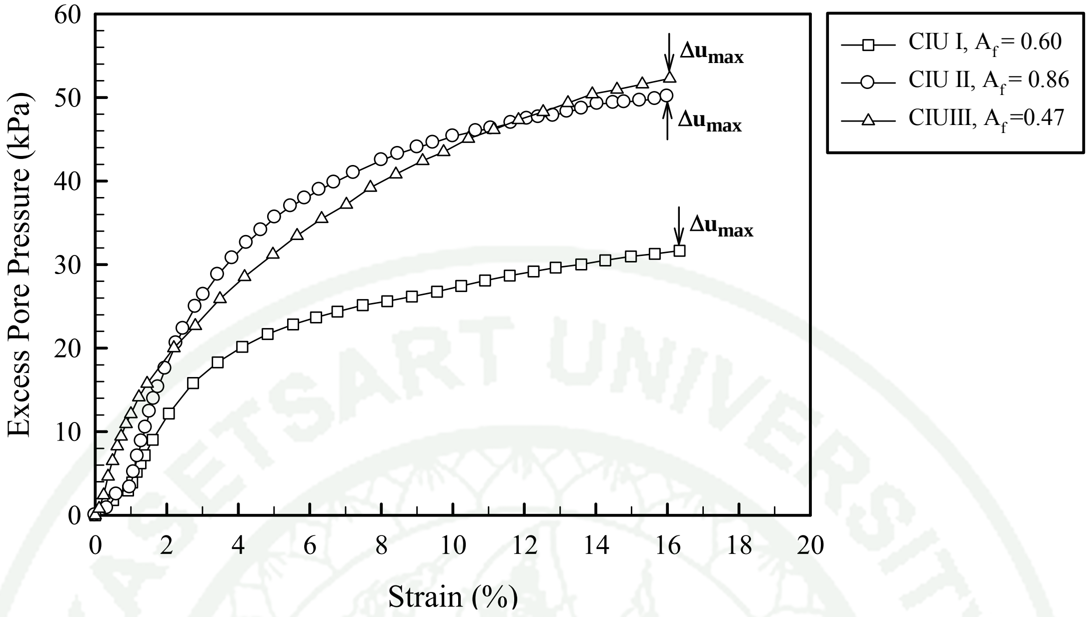

Appendix Figure 2 Excess pore water pressure and strain relationships from CIU tests

Total (p, q) and effective (p', q') stress paths for CIU tests are plotted in Appendix Figure 3 based on the data in Appendix Figure 1 and 2. The total stress paths rise at 45° to the right for the failure point (p_f, q_f) and end up at failure on a strength envelop with a slope α_c = 16° corresponding with Mohr Coulomb envelope ϕ_c = 16.6°. The equation relating strength and total stress is therefore given by:

$$q_f = p_f \tan 16° \tag{1}$$

The effective stress paths are different from the total stress paths due to excess pore pressure changes. They are displaced to the left equal by a value equal to the excess pore water pressure and end up at failure on a strength envelope with a slope α_c' = 24° corresponding with Mohr Coulomb envelope ϕ_c' = 26.4°. The relationship between strength and effective stress can be expressed by the equation:

$$q_f = p'_f \tan 26.4° \tag{2}$$

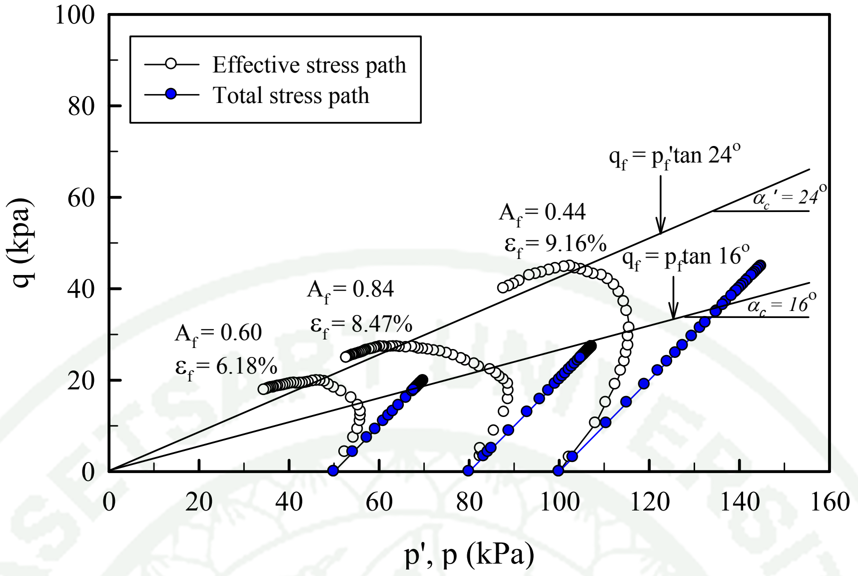

Appendix Figure 3 Total and effective stress paths from CIU tests

2. Anisotropically Consolidated Undrained (CAU) tests

The results from CAU tests are summarized in Appendix Table 2. The relationship between deviator stress (σ_a) and strain (ε_a) from CAU tests are shown in Appendix Figure 4. The strain at failure (ε_f) is approximately 2% to 4%, which are lower than the CIU tests. This corresponds to the investigation of Chaiyadhuma (1974) and concepts of strain contour by Lambe and Whitman (1969). Chaiyadhuma conducted the undrained triaxial tests on soft Bangkok clay consolidated under k_0 condition and found that the anisotropic consolidation caused the decrease in failure strain. The undrained elastic modulus at 50% of maximum deviator stress ($E_{u,50}$) determined from the stress-strain curves in Appendix Figure 4 for CAU I, II and III are 7450kPa, 15211 kPa and 34841kPa, respectively. Appendix Figure 5 shows positive excess pore water pressure generated during the shear. Skempon's (1954) pore pressure parameter at the failure (A_f) ranged from 0.3 to 0.5, lower than CIU tests. The results correspond with the conclusion made by Wang (1969) and Chaiyadhuma (1974). They concluded that anisotropic effects result in a decrease of A_f.

Appendix Table 2 Results from CAU tests

Series	σ'_3 (kPa)	σ'_1 (kPa)	k_0	γ (kN/m^3)	w_i (%)	w_f (%)	ε_f (%)	A_f (%)	ϕ_c	ϕ_c'
CAU I	37.5	62.5		1.42	104.4	88.1	2.51	0.38		
CAU II	75.0	125.0	0.6	1.43	107.4	67.7	2.50	0.44	25.1	30.6
CAU III	100.0	166.7		1.42	105.3	73.0	3.51	0.36		

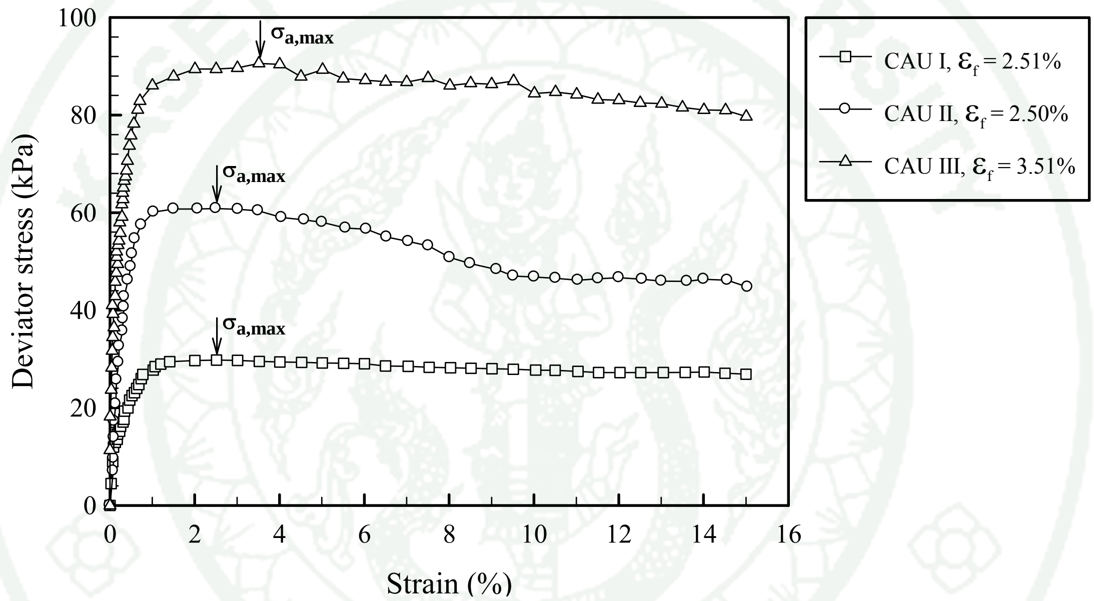

Appendix Figure 4 Deviator stress and strain relationships from CAU tests

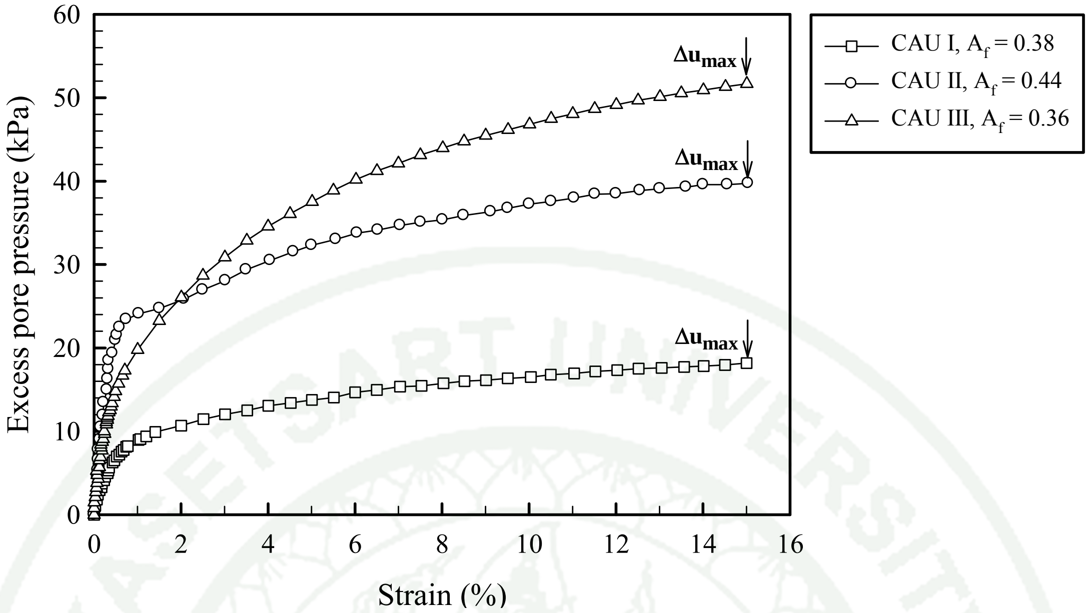

Appendix Figure 5 Excess pore water pressure and strain relationships from CAU tests

The total (p, q) and effective (p', q') stress paths from CAU tests are illustrated in Appendix Figure 6. The total stress paths end up at failure on a strength envelope with a slope α_c = 23.5°corresponding with Mohr Coulomb envelopeϕ_c = 25.1°. The relationship between strength and total stress at failure can be expressed by the equation:

$$q_f = p_f \tan 23.5° \tag{3}$$

The effective stress paths end up at failure on a strength envelope with a slope α_c' = 27° corresponding with Mohr Coulomb envelope ϕ_c' = 30.6°. The equation relating strength and effective stress is therefore given by:

$$q_f = p'_f \tan 27° \tag{4}$$

It can be seen that the total and effective strength parameters (α_c, ϕ_c, α_c', ϕ_c') from CAU test is higher than CIU test, which corresponds with the investigation of Chaiyadhuma (1974).

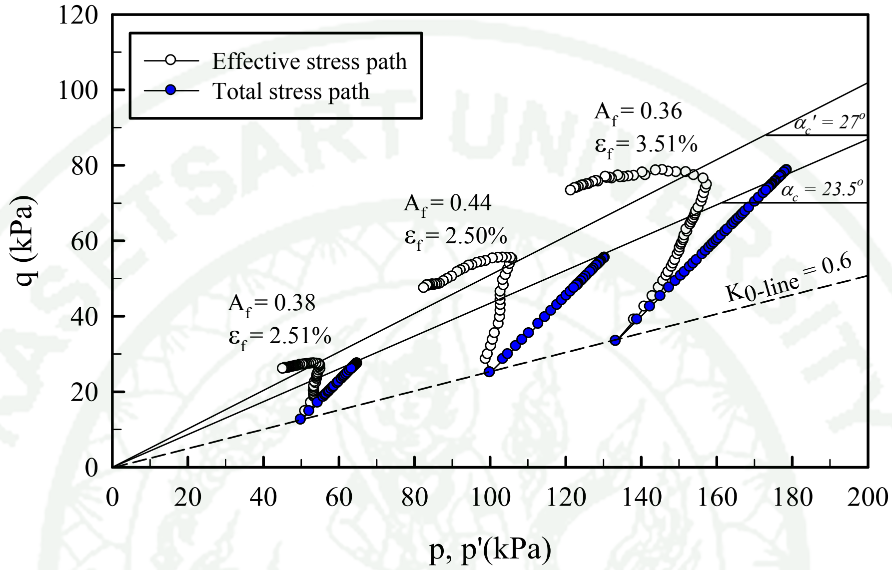

Appendix Figure 6 Total and effective stress paths from CAU tests

3. Comparison of the results with previous research

Appendix Table 3 summarizes the effective friction angle (ϕ_c') of soft Bangkok clay under compression condition, conducted at different consolidation stressed. The ϕ_c' was in range of 22.2° to 34.8°. While the ϕ_c' obtained from this research was 26.4 and 30.6 for CIU and CAU tests, respectively. They lie within the ranges reported in other studies. The variation in the ϕ_c' could be the result of personal judgement.

Appendix Table 3 Comparisons of effective friction angle on Bangkok clay with different consolidation stresses

Reference	Location	Depth (m)	Test type	ϕ_c'
Wang (1969)	NongNgooHao	8.83	CAU	34.8
Chaiyadhuma (1974)	AIT campus	5.5-6.0 7.0-7.4	CK_0U	27.1 28.3
Chaudhry (1975)	-	6.0	CIU	27.0
Balasubramaniam and Chaudhry (1978)	NongNgooHao	5.5-6.0	CIU	26.0
Balasubramaniam*et al.* (1978)	NongNgooHao	5.5-6.0	CIU	24.0
Rahman (1980)	AIT campus	4.5 5.5 6.5	CK_0U	25.5 23.6 23.2
Kim (1991)	AIT campus	3.0-4.0	CIU CK_0U	22.2 23.0
This research	Samutprakan	3.0-4.0	CIU CAU	26.4 30.6

Undrained triaxial test under extension condition

1. Isotropically Consolidation Undrained Extension ($CIUE_U$) tests under unloading condition

The results from CIUE tests are summarized in Appendix Table 4. The relationship between deviator stress (σ_a) and axial strain (ε_a) are shown in Appendix Figure 7. The deviator stresses exhibit strain softening after they reached a peak point. The strain at failure (ε_f) ranged from 11% to 18%.The undrained elastic modulus at 50% of maximum deviator stress ($E_{u,50}$) determined from the stress-strain curves in Appendix Figure 7 for $CIUE_U$ I, $CIUE_U$ II and $CIUE_U$ III are 1006 kPa, 1820 kPa and

2653 kPa. The negative excess pore water pressures shown in Appendix Figure 8 indicate decrease with the strain. After reaching a peak value, the excess pore water pressures increase with the strain. Skempon's (1954) pore pressure parameter at failure ($A_f = 1\text{-}\Delta u/\Delta\sigma_a$) varied from 0.7 to 1.0.

Appendix Table 4 Results from $CIUE_U$ tests

Series	σ'_c (kPa)	γ (kN/m^3)	w_i(%)	w_f(%)	ε_f (%)	A_f (%)	ϕ_e	ϕ_e'
CIUE I	50	1.48	107.89	82.153	12.12	0.91		
CIUE II	80	1.45	114.53	79.480	17.54	0.98	18.4	16.2
CIUE III	100	1.47	97.54	69.640	11.01	0.73		

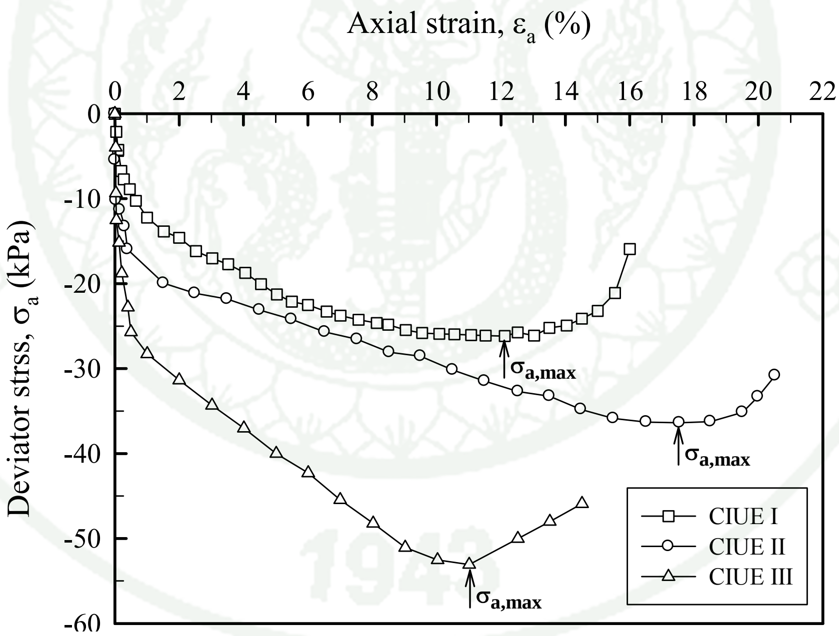

Appendix Figure 7 Deviator stress and strain relationship from CIUE tests

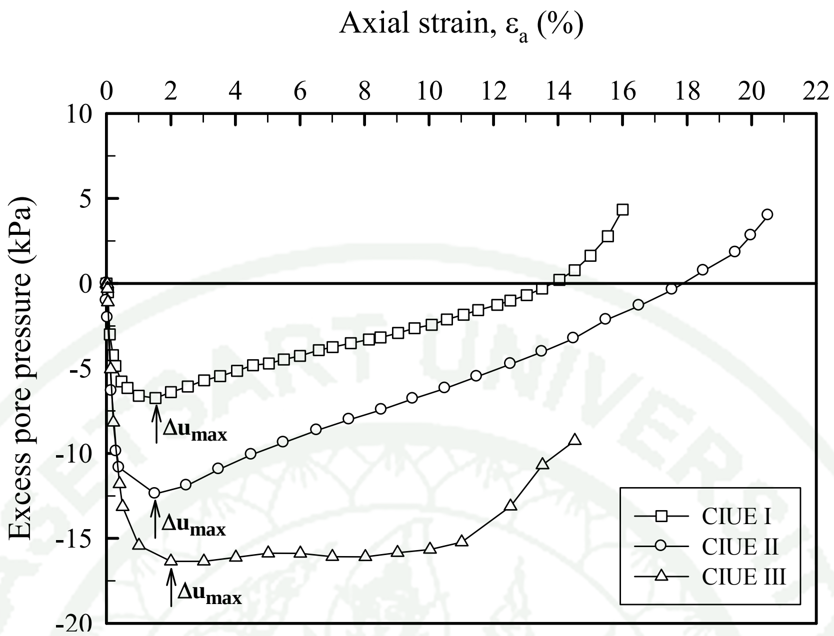

Appendix Figure 8 Excess pore water pressure and strain relationship from CIUE tests

Appendix Figure 9 shows the total (p, q) and effective (p', q) stress path based on the data in Appendix Figure 7 and 8. The total stress path follows a straight line inclined at 45° downward to the left and ends up at failure on a strength envelop with a slope α_e= 18.4° corresponding with Mohr Coulomb envelopeϕ_e=19.5°. The relationship between strength and total stress at failure can be expressed by the equation:

$$q_f = p_f \tan 18.4° \quad (5)$$

The effective stress path is different from the CIU and CAU tests (compression condition). It deviates from the total stress to the right due to negative excess pore water pressure generated during the shear. The effective stress path ends up at failure on a strength envelope with a slope α_e'=16.2° corresponding with Mohr Coulomb envelope ϕ_e'= 16.96. The relationship between strength and effective stress at failure can be expressed by the equation:

$$q_f = p'_f \tan 16.2° \quad (6)$$

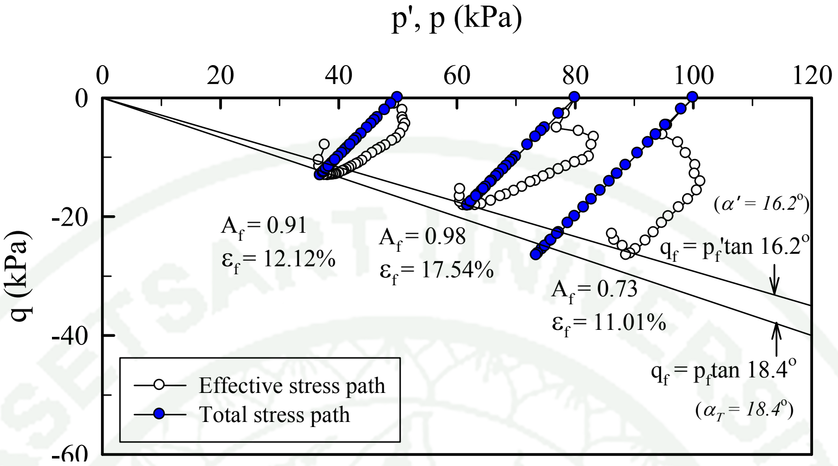

Appendix Figure 9 Total and effective stress paths from CIUE tests

2. Comparison of compression and extension tests

The comparison of effective stress path from CIU and CIUE tests is shown in Appendix Figure 10. The effective stress paths from the extension tests (CIUE) are found to be quite different from the compression tests (CIU) due to developed excess pore water pressure. The shapes of effective stress paths from the CIU test are found to be elliptical in nature. While the effective stress paths from the $CIUE_U$ are not smooth in curve, and are less rounded (Kim, 1991).

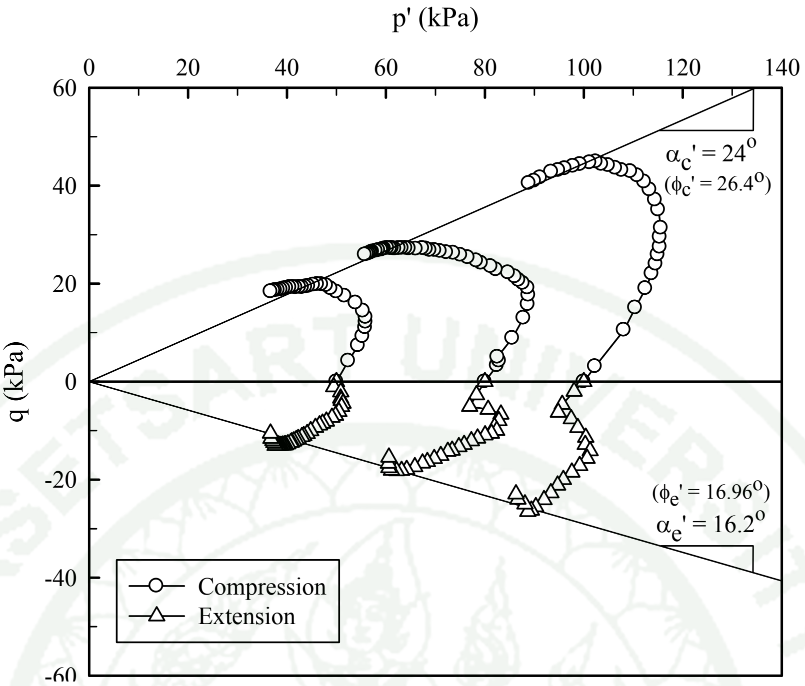

Appendix Figure 10 Effective stress path from CIU and CIUE tests

Appendix Figure 11 compares effective friction angle between Bangkok clay and other clays as isotropically consolidated. For Bangkok clay, the effective friction angle of the compression (ϕ'_c) and extension (ϕ'_e) were 22.2^o to 26.4^o and 14.1^o to 33.1^o, respectively. It is noted that the ϕ'_e varies in a larger range as comparing with theϕ'_c. Surarak 2010 stated that the possible reasons of this were incorrect value of membrane correction and occurring of pre-failure (i.e. necking failure) during the test.

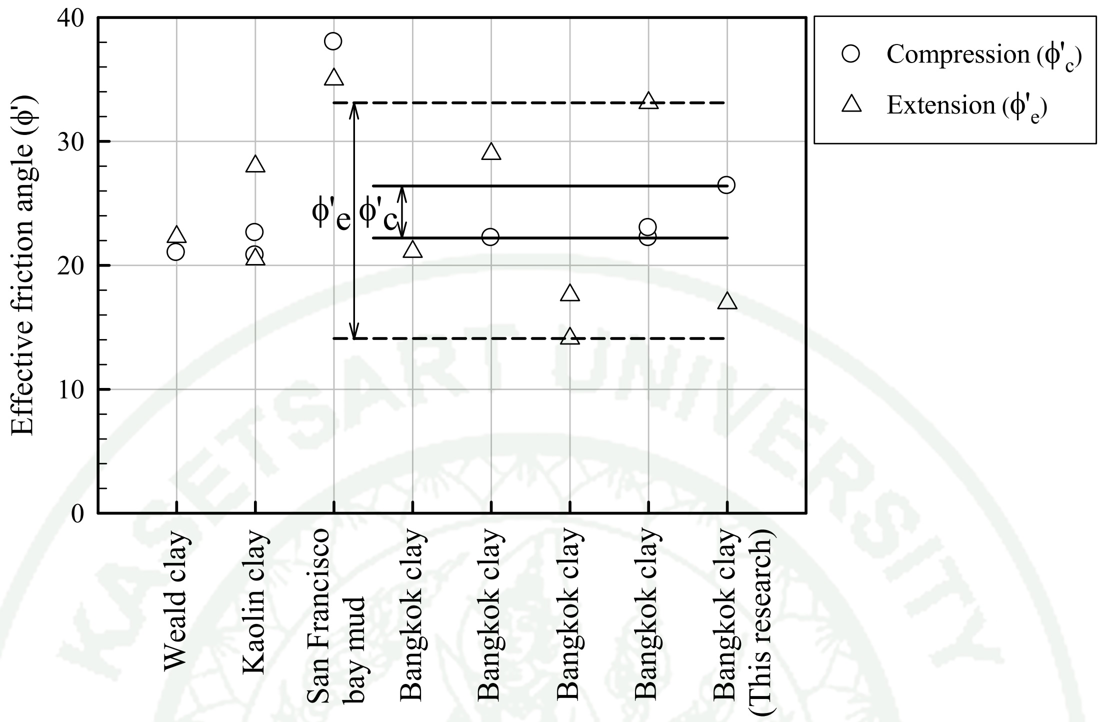

Appendix Figure 11 Comparison of effective friction angle between Bangkok clayand other clays

Undrained triaxial creep test

One of the failure modes of Suvannaphumi Drainage Canal is creep failure when the excavated canal was left dry without surcharge water for more than one month. Then the creep behavior of Bangkok Clay is needed to be verified. The axial loads for undrained creep tests were applied in single increment, and axial deformation versus time was recorded. Three different creep stress levels, 50%, 70% and 90% of the ultimate shear stress, were used for performing creep tests. The initial conditions of specimens used to conduct the isotropically and anisotropically consolidated undrained creep tests (CIUC and CAUC) are presented in Appendix Table 5 and 6, respectively.

Appendix Table 5 Initial condition for isotropically undrained creep tests

Creep stress level	γ (kN/m^3)	w_i (%)	σ'_3 kPa	Duration of test (month)
50%	14.8	99.69		
70%	14.9	94.08	50.00	1
85%	14.0	117.38		

Appendix Table 6 Initial condition for anisotropically undrained creep tests

Deviator stress	γ (kN/m^3)	w_i (%)	K_0	σ'_3 kPa	σ'_1 kPa	Duration of test (month)
40%	1.46	101.15				
60%	1.46	98.26	0.6	50.00	83.33	1
80%	1.46	103.77				

1. Selected ultimate deviator stress

The normal strength test is needed to perform in order to determine the ultimate deviator stress for calculation of stress levels. Appendix Figure 12 and 13 show the relationships between deviator stress (σ_a) and axial strain (ε_a)for CIU and CAU tests at the confining pressure (σ'_3) of 50 kPa. The ultimate deviator stress for the CIU and CAU test were 40 kPa and 54 kPa. It should be noted that the residual strength of 47 kPa is selected to calculate stress level for the anisotropic undrained creep tests.

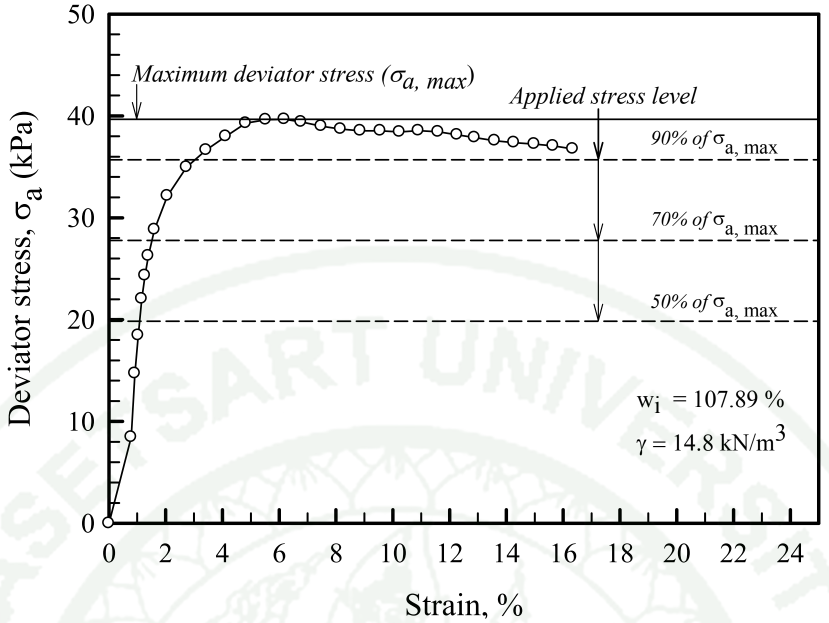

Appendix Figure 12 Ultimate deviator stress and applied stress levels for CIUC tests

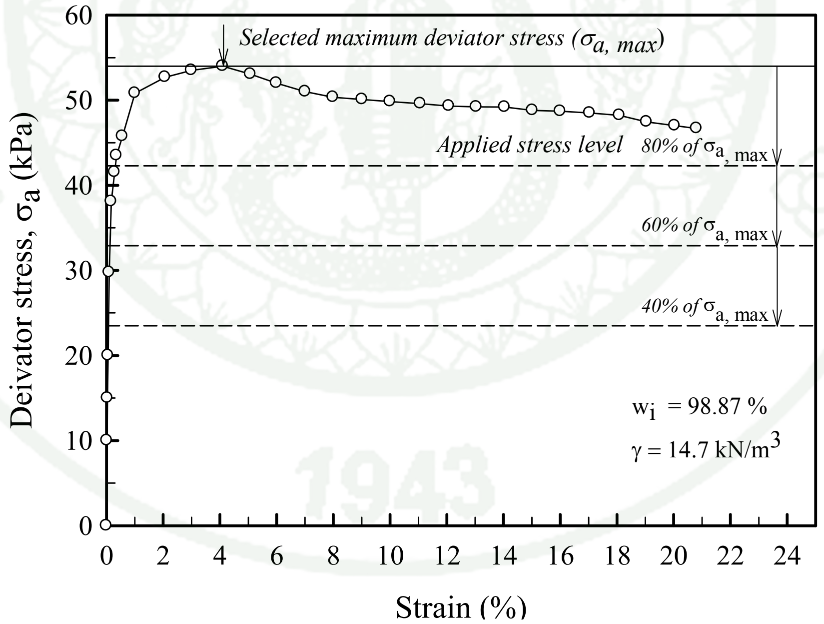

Appendix Figure 13 Ultimate deviator stress and applied stress levels for CAUC tests

2. Isotropically Consolidated Undrained Creep (CIUC) tests

The developments of axial strain with time at various creep stress levels for CIUC tests are shown in Appendix Figure 14. The specimen subjected to creep stress level of 50% show only a small increase in the strain after initial deformation, and no failure was detected within the time of testing. On the other hand, the specimens subjected to creep stress level of 70 and 90% progressively strained with time until eventually failure. Appendix Figure 15 and 16 illustrates the regions of creep curve for the creep stress level of 70% and 90%. Three regions are recognized for each curve, namely, the primary region of decreasing creep rate, the secondary region of essentially constant creep rate, and finally the tertiary region of accelerating creep rate (Campanella and Vaid, 1974).

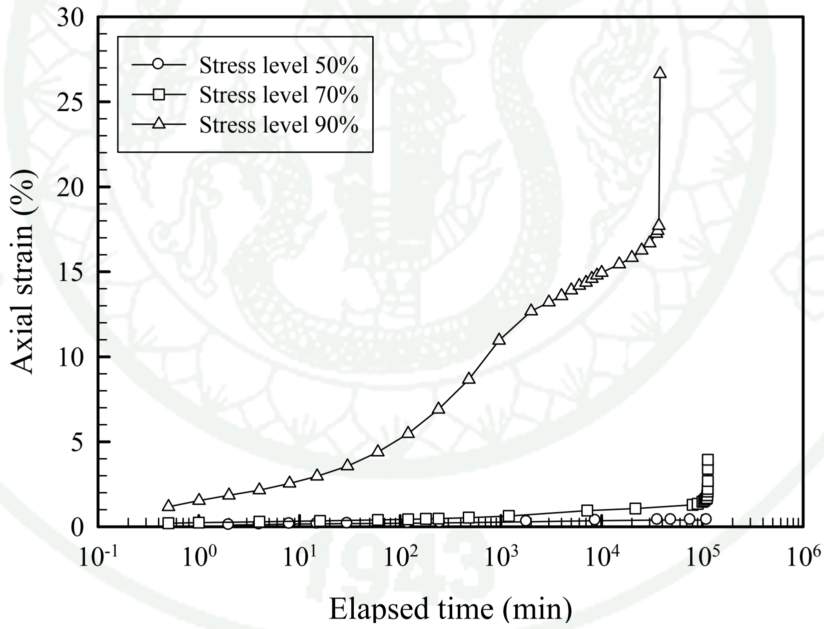

Appendix Figure 14 Axial strain behaviour for CIUC tests

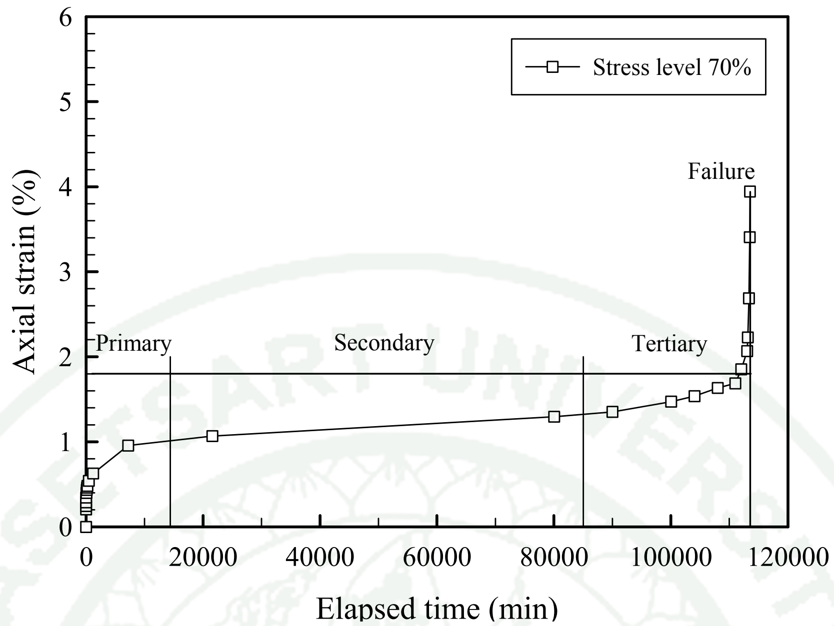

Appendix Figure 15 Regions of creep curve under creep stress level of 70% for CIUC test

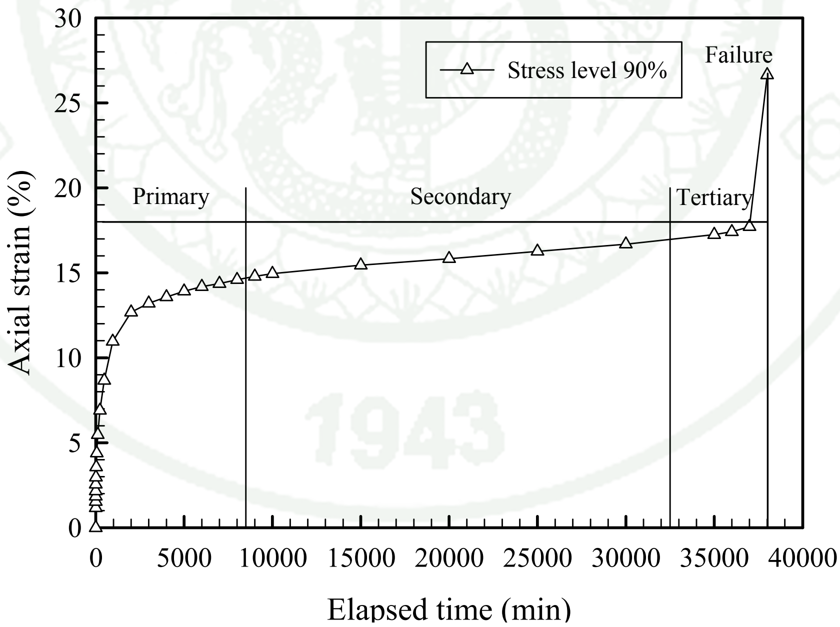

Appendix Figure 16 Regions of creep curve under creep stress level of 90% for CIUC test

Appendix Figure 17 shows the creep rate (axial strain rate) versus the time. For the specimens which eventually failed, the creep rate initially decreased until a minimum value was reached before its subsequent acceleration leading to failure. This phenomenon is similar to the observation of Snead (1970) and Campanella and Vaid (1974).The time to minimum creep rate is approximated to be 12 days and 35 days for stress level of 70% and 90%, respectively. While the specimens which did not fail (stress level of 50%) showed a continuous decreasing creep rate with time. It can be seen from the figure that the onset of an acceleration creep rate indicates the impending failure.

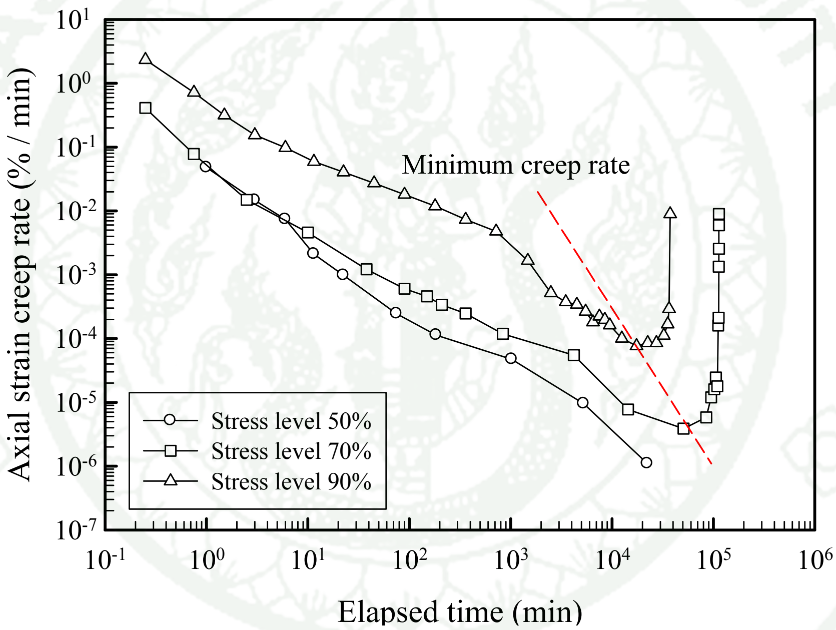

Appendix Figure 17 Creep rate behavior for CIUC tests

3. Anisotropically Consolidated Undrained Creep (CAUC) tests

Appendix Figure 18 presents the development of axial strain with time for anisotropically consolidated undrained creep test. The specimens progressively strained with time until eventually failure for all stress levels. The creep failure curves can be separated in three regions shown in Appendix Figure 19 to 21, namely, the primary region of decreasing creep rate, the secondary region of essentially constant creep rate, and finally the tertiary region of accelerating creep rate (Campanella and Vaid, 1974).It can be seen that the time to a tertiary region is faster than that of the isotropically consolidated undrained creep test.

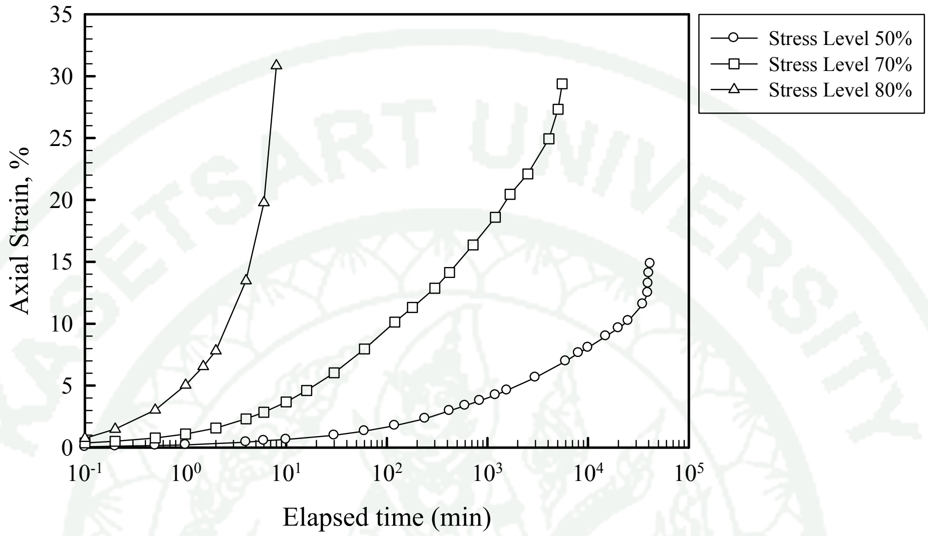

Appendix Figure 18 Axial strain behaviour for CAUC tests

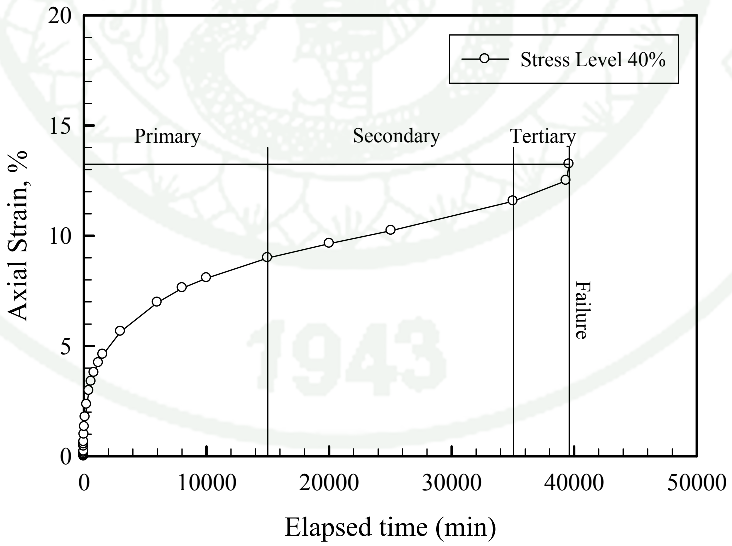

Appendix Figure 19 Regions of creep curve under creep stress level of 40% for CAUC test

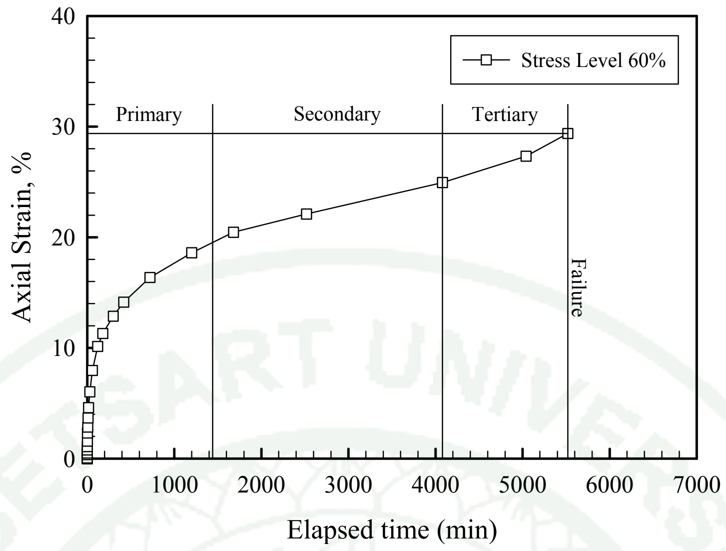

Appendix Figure 20 Regions of creep curve under creep stress level of 60% for CAUC test

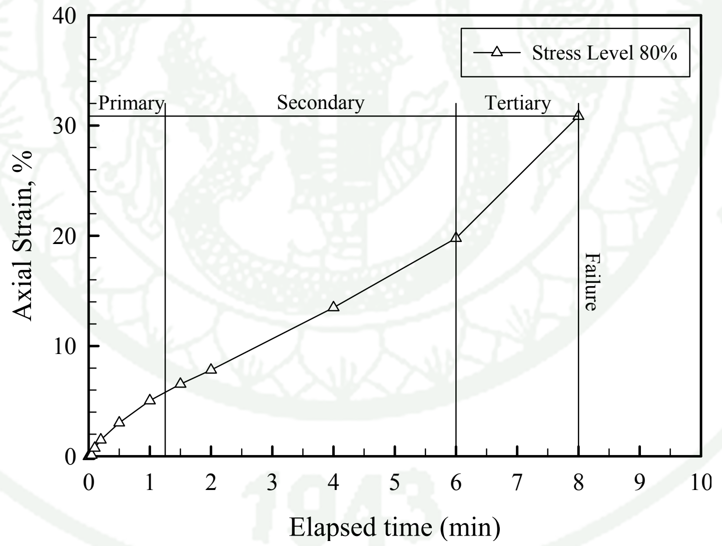

Appendix Figure 21 Regions of creep curve under creep stress level of 80% for CAUC test

Appendix Figure 22 shows the creep rate (axial strain rate) versus time for the CAUC tests. Under a given constant creep stress, the creep rate continuously decreased with elapsed time to a minimum value and thereafter increased until failure (Snead, 1970and Campanella and Vaid, 1974). The time to a minimum creep rate is foundat 1.75 minute, 3 days and 18 days for stress level of 80%, 60% and 40%, respectively. Similar to CIUC test, the onset of an accelerating creep rate indicates impeding failure.

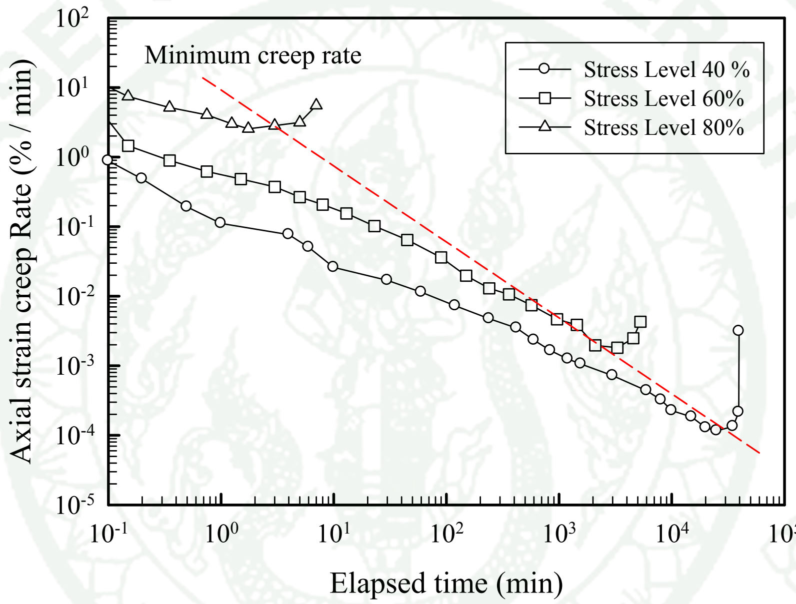

Appendix Figure 22 Creep rate behavior for anisotropic undrained creep test

CIRRICULUM VITAE

NAME : Mr. Phermphorn Buathong

BIRTH DATE : August 31, 1978

BIRTH PLACE : Bangkok, Thailand

EDUCATION :

YEAR	INSTITUTE	DEGREE/DIPLOMA
2001	Rajamangala Univ. of Tech..	B.Eng.(Civil Eng.)
2004	Rangsit Univ.	M.Eng.(Civil Eng.)

POSITION/TITLE : -

WORKPLACE : -

SCHOLARSHIP/AWARDS : -